Universidad de Huelva

Departamento de Ingeniería Química, Química Física y Ciencias de los Materiales

Electrospinning of lignin and ethyl cellulose nanofibers for structuring vegetable oils in lubricant applications

Memoria para optar al grado de doctora
presentada por:

María Borrego Algarra

Fecha de lectura: 8 de noviembre de 2024

Bajo la dirección de los doctores:

José María Franco Gómez

José Enrique Martín Alfonso

Huelva, 2024

Universidad de Huelva

Departamento de Ingeniería Química, Química Física y Ciencia de los Materiales

Electrospinning of lignin and ethyl cellulose nanofibers for structuring vegetable oils in lubricant applications

Tesis Doctoral

Programa de Doctorado en Ciencia y Tecnología Industrial y Ambiental

María Borrego Algarra

2024

Bajo la dirección de los doctores:

José María Franco Gómez

José Enrique Martín Alfonso

University of Huelva

Department of Chemical Engineering, Physical Chemistry and Materials Science

Electrospinning of lignin and ethyl cellulose nanofibers for structuring vegetable oils in lubricant applications

Ph. D. Thesis

Doctoral Program in Industrial and Environmental Science and Technology

María Borrego Algarra

2024

Supervisors:

José María Franco Gómez

José Enrique Martín Alfonso

Electrospinning of lignin and ethylcellulose nanofibers for structuring vegetable oils in lubricant applications

Research memory presented by María Borrego Algarra to apply for a Doctoral degree with International Mention at the University of Huelva.

María Borrego Algarra

The present Dissertation has been performed at the Department of Chemical Engineering, Physical Chemistry and Materials Science of the University of Huelva, under the auspices of Dr. José María Franco Gómez and Dr.José Enrique Martín Alfonso, which approve its defence:

Dr. José María Franco Gómez

Dr. José Enrique Martín Alfonso

Huelva, June 2024

AGRADECIMIENTOS

En primer lugar, dedicar la siguiente tesis doctoral a aquellas personas que han contribuido tanto personal como profesionalmente a su realización, por enseñarme y ayudarme en el camino, por dedicarme su tiempo y sus conocimientos, mi más sincero agradecimiento.

Por esto, dedicársela especialmente a mis dos directores, los pilares fundamentales de esta tesis, Dr. José María Franco Gómez y Dr. José Enrique Martin Alfonso, por guiarme por este camino, por su esfuerzo, por su paciencia y, lo más importante, por hacerme crecer profesionalmente durante estos años. Muchas gracias por todo vuestro tiempo dedicado y por confiar en mi desde el primer día.

A aquellos compañeros que hicieron mi paso por este proyecto fácil y divertido, que me enseñaron y nunca me negaron su ayuda, que me dieron todo su tiempo, aquellos que estaban día a día haciendo cada paso sencillo, jamás me perdonaría no agradeceros esto a Manolo, Esperanza, Clara, Adrián, Antonio, Rocío, Concha, Alba, Coraima, Rodrigo, Susana, Ortega, José Fernando, Ricardo, Isa, Samuel, Mauricio…En definitiva gracias a todo el centro de investigación en Tecnología de Productos y Procesos Químicos (Pro2Tecs) por su apoyo.

Gracias también al Dr. Erik Kuhn y a todo su equipo del laboratorio de tribología de la Universidad de Hamburgo por la maravillosa acogida recibida durante esos meses haciéndome sentir cómo una más en el complejo mundo de la tribología.

A mis padres y mi hermano por confiar en mí desde siempre, por enseñarme a ser siempre más, a querer dar lo mejor de mí, sin vosotros nunca habría sido imposible estar hoy aquí, gracias y siempre gracias. Gracias a mi compañero, a mi pareja, a mi pilar, David, por estar conmigo en este camino, por guiarme y darme fuerzas en todo momento, por estar y apoyarme por encima de todo, muchísimas gracias. Gracias a mis amigas porque sé que se alegran de este paso cómo si fuera suyo porque cuando yo pensaba que no sería capaz ellas siempre pensaban que sí.

Gracias a todos los que habéis formado parte de que esta Tesis Doctoral haya podido salir adelante, siempre tendré algo que agradeceros.

ACKNOWLEDGEMENTS

First of all, I would like to dedicate this PhD thesis to those people who have contributed both personally and professionally to its completion, for teaching me and helping me along the way, for dedicating their time and knowledge to me, my most sincere thanks.

For this, I would like to dedicate it especially to my two directors, the fundamental pillars of this thesis, Dr. José María Franco Gómez and Dr. José Enrique Martin Alfonso, for guiding me along this path, for their effort, their patience and, most importantly, for making me to grow professionally during these years. Thank you very much for all your time and for trusting me from the first day.

I would never forgive myself for not thanking Manolo, Esperanza, Clara, Adrián, Antonio, Concha, Rocio, Alba, Coraima, Rodrigo, Susana, Ortega, José Fernando, Ricardo, Isa, Antonio, Samuel... Thanks to all the research center in Technology of Chemical Products and Processes (Pro2Tecs) for their support.

Thanks also to Dr. Erik Kuhn and all his team at the tribology laboratory of the University of Hamburg for the wonderful welcome received during these months, making me feel like one more in the complex world of tribology.

To my parents and my brother for always trusting me, for teaching me to be always more, to want to give the best of me, without you it would have been impossible to be here today, thank you and always thank you. Thanks to my partner, my partner, my pillar, David, for being with me on this path, for guiding me and giving me strength at all times, for being and supporting me above all, thank you very much. Thanks to my friends because I know that they are happy with this step as if it were theirs because when I thought I would not be able to do it, they always thought I would.

Thanks to all of you who have been part of the success of this Doctoral Thesis, I will always have something to thank you for.

Contents

Chapter 1: Introduction **5**

Resumen 7

1. Summary 10

2. Justification 13

3. Objectives 15

4. Document Structure 16

Chapter 2: State-of-the-art **19**

1. Lignocellulosic materials 21

1.1. Main biomass components 22

1.1.1. Cellulose 22

1.1.2. Hemicellulose 23

1.1.3. Lignin 24

1.1.3.1. Solvents for lignin 27

2. Electrospinning 32

2.1. Basics of the technique 34

2.2. Parameters 36

2.2.1. Processing parameters 36

2.2.2. Solution parameters 40

2.2.3. Ambient parameters 42

2.3. Layout of the technique 42

2.4. Background on the electrospinning of biopolymers 45

3. Lubricating greases: a general overview 52

3.1. Bio-based or biodegradable lubricating greases 53

3.2. Biopolymers as thickening agents 55

3.3. Rheology of lubricating greases 58

3.4. Tribology of lubricating greases 60

4. References 65

Chapter 3: Materials & Methods 81

1. Materials 83

1.1. Polymers 83

1.1.1. Low sulfonate kraft lignin 83

1.1.2. Polvvinylpyrrolidone 83

1.1.3. Ethylcellulose 84

1.2. Surfactants 84

1.3. Solvents 86

1.4. Vegetable oil 86

2. Experimental procedures 87

2.1. Preparation of polymeric solution 87

2.2. Preparation of electrospun nanostructures 88

2.3. Preparation of oleo-dispersions 89

3. Characterization techniques 90

3.1. Characterization of polymeric solution 90

3.2. Characterization of oleo-dispersions 92

3.3. Characterization of electrospun nanofibers 97

4. References 99

Chapter 4: Results & Discussion 101

1. Compendium of publications 103

2. Electrospun lignin-PVP nanofibers and their ability for structuring oil 105

2.1. Resumen 107

2.2. Full article 111

3. Influence of surfactants on the electrospinnability of lignin-PVP solutions and subsequent oil structuring properties of nanofiber mats 121

3.1. Resumen 123

3.2. Full article 125

4. Developing electrospun ethylcellulose nanofibers webs: an alternative approach for structuring castor oil 145

4.1. Resumen 147

4.2. Full article 149

5. Impact of the morphology of electrospun lignin-ethyl cellulose nanostructure of their capacity to thicken castor oil 161

5.1. Resumen 163

5.2. Full article 167

6. Assessment of the tribological performance of electrospun lignin nanofribous web-thickened bio-based greases in a nanotribometer 181

6.1. Resumen 183

6.2. Full article 187

Chapter 5: Conclusions 201

List of figures & tables 209

Annex I **215**

1. List of articles that make up this doctoral thesis 217
2. Contributions to congresses and conferences derived from this doctoral thesis 218

Chapter 1: Introduction

Resumen

En la actualidad existe un gran interés en el uso de materias primas renovables y en el desarrollo de tecnologías y de nuevos productos que no resulten nocivos para el medio ambiente. En la industria de los lubricantes esto queda aún más latente debido al problema ocasionado por la pérdida de los mismos durante su vida útil y su consecuente liberación al medioambiente. En este trabajo se han utilizado aceites vegetales cómo alternativa a los aceites minerales tradicionalmente usados en los lubricantes comerciales, que ya han tenido resultados satisfactorios desde un punto de vista de la lubricación. Sin embargo, los actuales agentes espesantes comerciales, y los procesos de obtención asociados, no han podido ser aún reemplazados satisfactoriamente por productos y tecnologías medioambientalmente sostenibles. La búsqueda de agentes espesantes basados en sustancias naturales y renovables supone un gran reto debido a la alta eficiencia técnica que presentan los usados tradicionalmente y a las propiedades que le confieren al producto final. En este trabajo, se propone utilizar materias primas renovables, derivadas de materiales lignocelulósicos, como la lignina y la etilcelulosa. La principal dificultad para convertir estos biopolímeros en espesantes efectivos de medios oleosos reside en la compatibilidad con el aceite y la búsqueda de una tecnología que respete la línea medio ambiental de estos productos.

El electrohilado es una técnica simple, versátil y escalable capaz de desarrollar nanofibras continuas a partir de disoluciones poliméricas mediante la aplicación de un potencial eléctrico. Mediante esta técnica se pueden obtener fibras con diámetros nanométricos, así como una amplia variedad de nanoestructuras con distintas morfologías. De ahí que la simplicidad y versatilidad de esta técnica la convierte en una herramienta prometedora para el desarrollo de nuevos agentes espesantes. Por tanto, el

electrohilado se propone en este estudio cómo una alternativa real para obtener nanofibras de lignina y etilcelulosa con capacidad estructurante de aceites.

En esta tesis doctoral se estudian los siguientes sistemas para obtener nanofibras de lignina de bajo sulfonato (LSL) y/o etílcelulosa (EC) mediante electrospinning: LSL:PVP, LSL:PVP + tensioactivos, EC y LSL:EC.

En primer lugar, ya que la lignina por sí sola no es capaz de formar nanofibras, se usa el PVP cómo copolímero para mejorar la electrospinabilidad. Para los sistemas LSL:PVP se observa mediante SEM una transición morfológica que evidencia dicha mejora al aumentar el contenido en PVP. Las membranas desarrolladas se dispersaron en aceite de ricino obteniendo geles estables en los casos de membranas homogéneas predominantemente formadas por fibras, y no por partículas, resultando dispersiones que han mostrado funciones viscoelásticas típicas de geles y con un rendimiento tribológico similar, o incluso superior, al de grasas lubricantes convencionales.

Aquellas disoluciones con mayor relación LSL:PVP dieron lugar a membranas heterogéneas e irregulares, altamente particuladas, que se relacionan con sus propiedades reológicas y fisicoquímicas. Estas propiedades se ven condicionadas por la formación de complejos tensioactivo-polímero. Así, a las disoluciones se les adicionó diferentes proporciones de tensioactivos de carácter no iónico, aniónico o catiónico. La morfología de las membranas electrohiladas depende de la concentración de agregación crítica (CAC), ya que se observaron fibras finas y una reducción de las partículas presentes siempre que se trabaje por encima de dicha concentración. Del mismo modo, el desarrollo de los oleogeles dependió de la morfología de las membranas, mejorando con la presencia de tensioactivos por encima de la CAC, dando lugar a geles estables con un excelente rendimiento de lubricación, con bajos valores del coeficiente de

fricción y de desgaste de las superficies lubricadas, superior a los preparados sin tensioactivo.

Por otra parte, se examinó la capacidad de la EC para desarrollar nanofibras mediante electrospinning y su capacidad de oleogelación. La concentración de las disoluciones, el peso molecular de la EC y el papel de diferentes disolventes fueron los parámetros examinados. Se consiguieron fibras homogéneas sin defectos una vez se superó la concentración crítica de entrelazamiento, dicha concentración desciende con el aumento del peso molecular de la EC. En cuanto a los disolventes usados, aquellos con constantes dieléctricas más elevadas provocan mayores fuerzas de repulsión, dando lugar al estiramiento del jet y mayores fuerzas electrostáticas, disminuyendo los diámetros medios de las nanofibras. Las redes de EC se dispersaron en aceite de ricino dando lugar a dispersiones físicamente estables con una buena reversibilidad térmica y con una buena respuesta tribológica, excepto aquellas con estructuras predominantemente particuladas.

Una vez se observó la buena electrospinabilidad que presentaron las redes desarrolladas a partir de EC, se estudió la formulación de geles a partir de fibras de lignina/etilcelulosa. Los resultaron confirmaron que las nanoestructuras de fibras homogéneas mejoran la interacción fase continua-fase dispersa mientras que las oleo-dispersiones formadas por agregados de nanofibras con partículas dan lugar a dispersiones de más líquidas. En todos los casos se produjo un desgaste de las superficies lubricadas con surcos rugosos y profundos, lo cual sugiere un mecanismo de desgaste predominantemente por abrasión. No obstante, los tamaños de la huella de desgaste obtenidos fueron ligeramente menores que los obtenidos con grasas

comerciales, con valores del coeficiente de fricción similares, y muy inferiores a los obtenidos con aceite de ricino sin estructurar.

Por último, se estudió más profundamente el comportamiento tribológico de algunas oleo-dispersiones seleccionadas en un nanotribómetro. Se observó que la morfología de las fibras desarrolladas ejerce una gran influencia sobre la fricción y el desgaste. Un aumento de laa concentración de la nanoestructura en la dispersión aumenta significativamente el coeficiente de fricción. La presencia de un copolímero, junto a la lignina, hace disminuir el coeficiente de fricción lo cual sugiere que las nanoestructuras homogéneas, formadas mayormente por nanofibras, son capaces de liberar el aceite de forma más constante y sostenida en el tiempo. La lignina favorece la presencia de partículas, las cuales resultan ser más abrasivas y afectan al desgaste de las superficies de contacto, originando mayor fricción.

Tal y cómo se ha mencionado reiteradamente, la morfología de las nanoestructuras ejerce un papel crucial en el comportamiento reológico y tribológico de las oleo-dispersiones desarrolladas.

1. SUMMARY

Currently, there is a growing interest in the use of renewable raw materials and the development of environmentally friendly technologies to create new products. Within the lubricant industry, there is a heightened awareness of the significant problem caused by the loss of material during its service life and their subsequent release into the environment. Vegetable oils have been used as a substitute for mineral oils in commercial lubricants and have demonstrated highly satisfactory lubrication properties. However, existing commercial thickening agents and associated manufacturing processes have not yet been successfully replaced by environmentally sustainable

products and technologies, respectively. Finding alternative thickening agents based on natural and renewable resources to replace traditional ones is a challenging task due to their high efficiency and the exceptional properties they impart to the final product. In this work, some renewable feedstocks have been proposed, including lignin and cellulose derivatives, such as ethyl cellulose. The challenge in converting these biopolymers into effective thickeners for oily media lies in improving the compatibility with oil and finding a technology that aligns with the environmentally friendly nature of these products.

Electrospinning is a simple, versatile, cost-effective, scalable, and reliable technique that can produce continuous nanofibers from polymeric solutions through the application of an electrical potential. This technique can produce nanoscale fibers from a range of materials, with precise control over their morphology. The ease and versatility of the developed membranes, along with their low or zero environmental impact, make this technique very promising for the production of biodegradable lubricants. Therefore, electrospinning is proposed in this study as a real alternative to obtain lignin and ethyl cellulose nanofibers with oil structuring capacity.

In this PhD thesis the following systems have been studied to obtain low-sulfonate lignin (LSL) and/or ethyl cellulose (EC) nanofibers by electrospinning: LSL:PVP, LSL:PVP + surfactants, EC and LSL:EC.

Firstly, since lignin by itself is not able to form nanofibers, PVP was used as a copolymer to improve the electrospinnability. For the LSL:PVP systems, a morphological transition that evidences the improvement of the electrospinnability as PVP content increases was observed by SEM. The developed membranes were dispersed in castor oil thus obtaining stable gels in the cases of homogeneous

membranes dominated by fibers, and not by particles, which have shown a viscoelastic response typical of gels and a tribological performance similar, or even superior, to conventional lubricating greases.

Those solutions with higher LSL:PVP ratio gave rise to heterogeneous and highly particulate membranes, which was related to their rheological and physicochemical properties. These properties are conditioned by the formation of surfactant-polymer complexes. In this case, different proportions of nonionic, anionic or cationic surfactants were added to the solutions. The morphology of electrospun nanostructures depended on the critical aggregation concentration (CAC), since fine fibers and a reduction of the particles present were observed as long as the concentration increased. Similarly, the development of the oleogels depended on the morphology of the membranes, whereby the presence of surfactant above the CAC resulted in the development of stable gels with excellent lubrication performance, i.e. lower friction coefficient and wear, as compared with surfactant-free systems.

Furthermore, the ability of EC to develop nanofibers by electrospinning and its oleogelation capacity were explored. The solution concentration, EC molecular weight and the role of different solvents were the parameters examined. Homogeneous fibers without defects were obtained once the critical entanglement concentration was exceeded; this concentration decreases with increasing EC molecular weight. As for the solvents used, higher dielectric constants lead to higher repulsive forces, resulting in jet stretching and higher electrostatic forces, thus decreasing the average diameters of the nanofibers. The EC networks were dispersed in castor oil resulting in physically stable dispersions with good thermal reversibility and good tribological response, except those with predominant particulate structures.

Once confirmed the good electrospinnability of EC solutions, the formulation of oleogels from lignin/ethylcellulose fibers was studied. The results confirmed that homogeneous fiber nanostructures enhance the continuous phase-dispersed phase interaction while oleo-dispersions formed by particle aggregates or beaded nanofibers gave rise to liquid-like dispersions. In all cases, wear occurred in the lubricated surfaces showed rough and deep grooves, suggesting a predominantly abrasive wear mechanism. However, the wear track sizes obtained were slightly smaller than those obtained with commercial greases, with similar coefficient of friction values, and much smaller than those obtained with neat castor oil.

Finally, the tribological behaviour of selected oleo-dispersions was further studied in a nanotribometer. It was observed that the morphology of the developed fibers exert a strong influence on friction and wear. The concentration of the nanostructure significantly increases the friction coefficient. The presence of a copolymer, together with LSL, decreases the friction coefficient thus suggesting that homogeneous nanostructures, predominantly composed of nanofibers, are able to release oil more steadily over time. Lignin favours the presence of particles which are more abrasive and affect wear, also increasing friction.

As has been repeatedly mentioned, the morphology of the nanostructures plays a crucial role in the rheological and tribological behaviour of the developed oleo-dispersions.

2. JUSTIFICATION

The modernization and industrialization of contemporary society have resulted in a surge in global energy demand, leading to an increase in lubricant usage from 30 to 40 million tons. Approximately 55% of these lubricants end up in the environment.

Lubricating greases typically consist of a liquid phase, often mineral oil, and a dispersed phase, such as metallic soaps. The composition of 95% of the lubricating greases available on the market is harmful to the environment when released. This is a global concern due to the depletion of oil sources and increasing environmental risks. This concern has led to the development of methods and alternatives based on renewable resources and natural products.

The lubricant industry is increasingly interested in finding biodegradable lubricants due to environmental concerns. Bio-lubricants are lubricants that have been developed by replacing mineral oils with vegetable oils, such as castor oil, or their derivatives. This substitution results in lubricants that have good lubricity, a high flash point and high viscosity index. However, replacing mineral oil with vegetable oil does not make fully formulated and complex lubricants, such as lubricating greases, totally biodegradable.

Environmentally friendly alternatives to traditional thickening agents are natural polymers. Lignocellulosic biomass is the most promising biodegradable source, consisting mainly of cellulose (35-83%), hemicellulose (0-30%), lignin (1-43%) and other minor compounds. Among these, lignin is one of the main bio-resources. However, its use and exploitation are currently limited, and it is often considered a waste destined for energy production, despite being a renewable resource with significant industrial potential.

In view of the EU's commitment to a circular economy, one of the objectives of lignocellulose-based biorefineries is the revalorization of lignocellulosic materials. Thus, the main challenge is to achieve maximum value and utilization of all raw materials, products and waste, while promoting energy savings. Hence, the use of

lignocellulosic materials, such as lignin or other cellulose derivatives, as thickeners for the production of ecological lubricating greases is justified as a new revalorization pathway.

The primary challenge is to find a suitable technology that enables an efficient interaction between the biopolymer and the lubricating oil. One possible alternative is to obtain nanofibers using nanofabrication techniques, such as electrospinning. The high porosity, small size and high surface-to-volume ratio of nanofibers could induce the formation of a three-dimensional network that enhances the physical interactions between the lubricating oil and the thickener. Electrospinning is one of the most important techniques in the manufacture of polymeric nanofibers. Its great interest is due to the extraordinary possibilities offered by the engineered nanostructures. In this study, lignin and ethyl cellulose electrospun nanostructures are proposed for the first time as vegetable oil structuring agents. Lignin is one of the main by-products derived from the pulp industry, and other wood conversion processes, with great energy potential, low cost and very versatile. On the other hand, among the cellulose derivatives, ethyl cellulose is a highly attractive sustainable material due to their non-toxicity, hydrophobicity, and high flexibility. Both materials have been proposed as biodegradable thickening agents to replace traditional metallic soaps.

3. OBJECTIVES

The main objective of this doctoral thesis was to produce oleo-dispersions of electrospun lignin and ethyl cellulose nanofibers in vegetable oils aiming to replace traditional lubricating greases based on mineral oils and metallic soaps or polyureas.

To achieve this goal, in this study the interaction between the biopolymers, lignin and ethyl cellulose, and different organic solvents was examined. Additionally, the effect of adding dopant polymers and/or surfactants with varying properties to enhance their electrospinnability was evaluated. Moreover, aiming to propose the electrospun nanofibers as a versatile component in novel formulations of biodegradable lubricating greases, the optimal conditions for their preparation and implementation needed to be elucidated.

Finally, the functional properties of these oleo-dispersions as lubricants was evaluated through a comprehensive physicochemical, rheological, and tribological characterization, as a function of concentration, morphology and nature of the nanofibers. The biopolymer/co-spining polymer ratio was also taken into consideration in this analysis.

4. DOCUMENTS STRUCTURE

The doctoral thesis is divided into five chapters, including the current one. The chapter two introduces lignocellulosic materials, specifically focusing on lignin and cellulose and their derivatives. It also explores their various applications. Subsequently, it will discuss the electrospinning technique in more detail, including fundamentals, parameters, and effects on membrane morphology. It will also cover the technique's arrangements and compile the most relevant research on lignin electrospinning. Additionally, this chapter presents the basics of lubricants, with a focus on their biodegradability, as well as a general overview of the tribology and rheology of both traditional and biodegradable semi-solid lubricants. The latest research on the

development of biodegradable lubricants from vegetable oils and lignocellulosic materials is also discussed.

Afterwards, chapter 3 consists of the materials used and the description of the experimental methods for the development of the membranes by electrospinning, the characterization of the morphologies obtained and the dispersion of these in castor oil to formulate bio-based lubricating greases. The characterization techniques of these oleo-dispersions and the polymeric solutions used as feedstock in the electrospinning technique are also described.

Chapter 4 is the main part of this manuscript, which collects the results obtained in this research and their discussion, in the form of compendium of papers already published in scientific journals. The first block explores the development of membranes from lignin using a co-spinning polymer such as PVP by analyzing the effect of lignin:PVP ratio and the incorporation of surfactants, respectively, on the oil structuring ability. In the next block, the development of ethyl cellulose and lignin/ethyl cellulose nanofibers is discussed, as well as their incorporation of these membranes in castor oil to formulate bio-based semi-solid lubricants. Finally, in the last sub-section, the tribological performance of selected formulations developed in the previous sections was evaluated in a ball-on-three plates tribological contact.

Finally, chapter 5 includes the most relevant findings and conclusions drawn from the research carried out.

Chapter 2: State of the art

1. LIGNOCELLULOSIC MATERIALS

Biomass refers to all organic matter from trees, plants and animal waste that can be converted into energy. However, based on production data, biomass is narrowly defined as material derived from terrestrial plants, of which about 82% is lignocellulosic material found in forests. Wood is the most important component, but other lignocellulosic materials include natural residues, aquatic plants, grasses, and other plant materials.

The three main chemical constituent fractions of lignocellulosic material are cellulose (40-70%), hemicellulose (25-30%) and lignin (15-30%); these concentrations depending significantly on the type of biomass, the part and age of the plant, the part of the cellulose wall and the growing conditions. The main sources of lignocellulosic materials are listed in table 1.

Lignocellulosic material is characterized by products with a high level of diversity and variability in their properties conferring unique properties to the biomass due to this structure.

Table 1. Chemical composition of lignocellulosic materials

Lignocellulosic source	Cellulose	Hemicellulose	Lignin	Extract
Hardwood	43-47	25-35	16-24	2-8
Softwood	40-40	25-29	25-31	1-5
Abaa	63.72	5-10	21.83	1.6
Bagasse	40	30	20	10
Coir	32-43	10-20	43-49	4.5
Corn cobs	45	35	15	5
Corn stalks	35	25	35	5
Cotton	95	2	0.9	0.4
Flax (retted)	71.2	20.6	2.2	6.0
Flax (unretted)	62.8	12.3	2.8	13.1
Hemp	70.2	22.4	5.7	1.7
Henequen	77.6	4-8	13.1	3.6
Istle	73.48	4-8	17.37	1.9
Jute	71.5	13.6	13.1	1.8
Kenaf	36.0	21.5	17.8	2.2
Ramie	76.2	16.7	0.7	6.4
Sisal	73.1	14.2	11.0	1.7
Sunn	80.4	10.2	6.4	3.0
Wheat straw	30	50	15	5

1.1. Main biomass components

1.1.1. Cellulose

Cellulose is composed of repeating anhydrous glucose units (AGU) linked by covalent bonds connected by OH group units. The main OH group along the macromolecule chains are easily modified by interacting with functional groups giving

rise to a wide range of cellulose derivatives (1). It is considered a promising raw material for the production of sustainable materials due to its renewability and non-toxicity (2,3)(2,3). It is an organic compound with the formulation of a polysaccharide consisting of a linear chain of several hundred to many thousands of linked D-glucose units, its length depending on the plant source from which it originates. It is the most abundant polymer on earth. In addition to the already mentioned advantages such as biodegradability, it has other advantages, such as low density, high porosity, high specific surface area and reactivity as a consequence of the hydroxyl groups present in the structural chain (4–6). This means that it is available for a wide variety of fields (7,8).

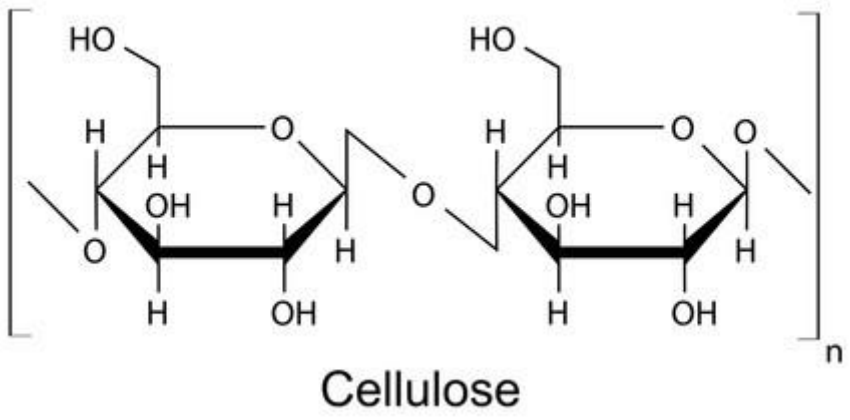

Figure 1. Chemical structure of cellulose.

1.1.2. Hemicellulose

Hemicelluloses are cell wall polysaccharides made up of various monomers such as xylose, arabinose, mannose, galactose, rhamonose and glucose. The monomer units are usually in the range of 500-3000 units, although the structure and abundance vary between different types of cellulose species and types of cellulose. (9,10). The combination of the various units usually generates four main hemicellulose structures, i.e.

xylan, xyloglucan, galactomannan and galactoglucomannan (11). The main function of hemicelluloses is to strengthen the cell wall by interacting with cellulose (9).

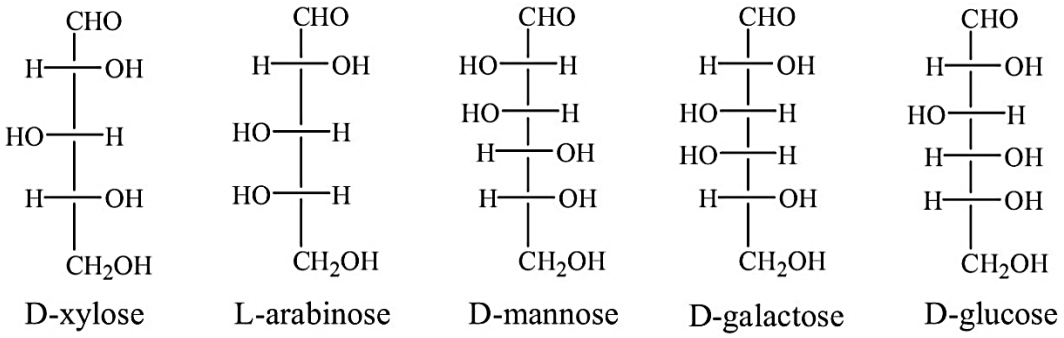

Figure 2. Main structural units that form hemicelluloses (12).

This biopolymer is classified as biodegradable and non-toxic, with a low molecular weight, low cost, good oxygen permeability, good flexibility, and high-water resistance (13). Its functional properties make it suitable for a wide variety of applications. Hemicelluloses find applications in gels, coatings, adhesives and gelling additives, stabilizers and viscosity enhancers in the food and pharmaceutical sectors, as well as in other industrial sectors (14).

1.1.3. Lignin

Lignin is an aromatic polymer mainly present in the thicker secondary wall of the cell wall, acting as a glue that holds cellulose and hemicellulose together in the cell fiber. It is the most abundant polymer after cellulose and is generally considered a by-product, or even a waste, of the paper industry. Approximately 50 million tonnes of lignin are produced annually (15), of which approximately 98-99% is incinerated in energy recovery processes within the pulp and paper industry. The remaining 1-2% of the lignin produced is extracted and used for commercial purposes (16,17).

It is a highly branched biomacromolecule with a variable composition depending on the plant source (18,19). The given structure can be rationalized into three main phenylpropanoid monomers: coniferyl alcohol (Figure 3a), sinapyl alcohol (Figure 3b), and p-coumaryl alcohol (Figure 3c).

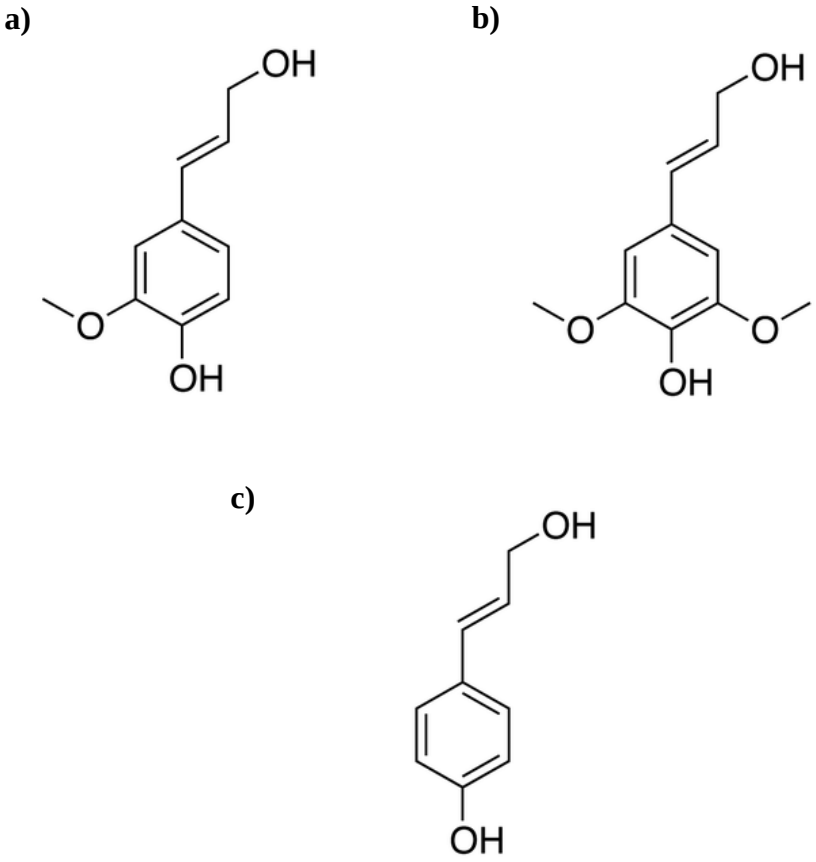

Figure 3. Lignin constituent monomers (a) conipheryl alcohol, (b) sinapyl alcohol and (c) p-coumaryl alcohol (20)

The composition of lignin varies depending on the type of plant, resulting in a wide range of monomer patterns that contribute to its complexity. The properties of commercial lignins depend substantially on the production process. Figure 4 provides a final representation of the lignin structure.

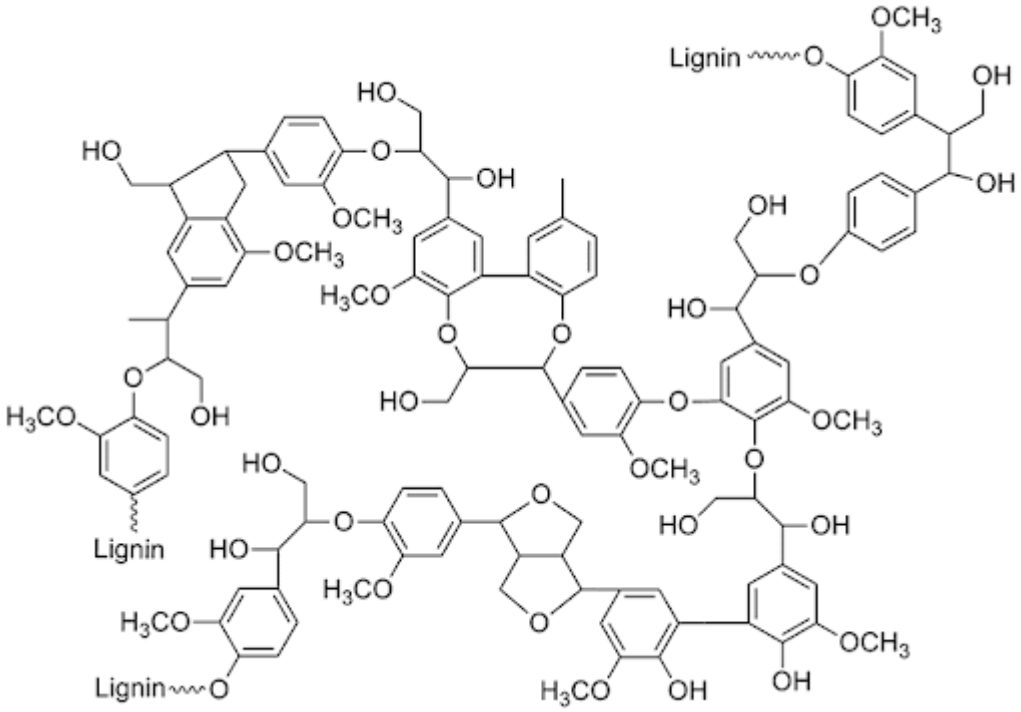

Figure 4. Lignin structure (21)

Despite its complex structure, lignin is known for its numerous advantages, including high carbon content, thermal stability, biodegradability, antioxidant activity, and favorable rigidity. These properties make it a product of great interest for the development of high added-value products.

For example, the use of lignin for the controlled release of slow-release fertilisers and herbicides in agriculture is of great interest (22,23), as well as in the field of bioplastics (24,25), dispersants (26–28), biofuel production (29), electrochemical applications (30–32) and on future biomass and biofuels applications (21). As previously stated, the structure of lignin and its properties vary depending on its origin and extraction method. The Table 2 displays the various molecular formulations of lignin monomers based on their origin and pre-treatment.

Table 2. Commercial lignin types according to origin (33)

TYPE	Monomer molecular formula	Monomer Mw	Ref
Kraft lignin	$C_9\ H_{8.5}\ O_{2.1}\ S_{0.1}\ (OCH_3)_{\ 0.8}\ (CO_2H)_{\ 0.2}$	180	(34)
Technical Kraft lignin	$C_9H_{7.98}\ O_{2.28}\ S_{0.08}\ (OCH_3)_{\ 0.77}$	176.52	(35)
Unreacted Kraft lignin	$C_9H_{8.97}\ O_{2.65}\ S_{0.08}\ (OCH_3)_{\ 0.89}$	189.73	(36)
Lignosulfonate lignin (softwood)	$C_9H_{8.5}\ O_{2.5}\ (OCH_3)_{\ 0.85}\ (SO_3H)_{\ 0.4}$	215-254	(34)
Lignosulfonate lignin (hardwood)	$C_9H_{7.5}\ O_{2.5}\ (OCH_3)_{\ 0.39}\ (SO_3H)_{\ 0.6}$	188	(34)
Organosolv lignin	$C_9H_{8.53}\ O_{2.45}\ (OCH_3)_{\ 1.04}$	nd	(34)
Pyrolisis lignin	$C_8\ H_{6.3\text{-}7.3}\ O_{0.6\text{-}1.4}\ (OCH_3)_{\ 0.3\text{-}0.8}\ (OH)_{\ 1\text{-}1.2}$	nd	(34)
Steam explosión lignin	$C_9H_{8.53}\ O_{2.45}\ (OCH_3)_{\ 1.04}$	~188	(34)
Dilute acid lignin	$C_9H_{8.53}\ O_{2.45}\ (OCH_3)_{\ 1.04}$	~188	(34)
Alkaline oxidation lignin	$C_9H_{8.53}\ O_{2.45}\ (OCH_3)_{\ 1.04}$	~188	(34)
Beech lignin	$C_9H_{8.83}\ O_{2.37}\ (OCH_3)_{\ 0.96}$	nd	(37)
Lignophenol (bamboo)	$C_9H_{8.27}\ O_{3.11}\ N_{0.088}\ S_{\ 0.0006}\ (OCH_3)_{\ 1.16}$	203.35	(38)
Soluble Kraft lignin (bamboo)	$C_9H_{8.77}\ O_{2.77}\ N_{0.093}\ S_{\ 0.16}\ (OCH_{\ 3})_{\ 0.75}$	187.76	(38)
Kraft lignophenol (bamboo)	$C_9H_{8.67}\ O_{3.36}\ N_{0.040}\ S_{\ 0.11}\ (OCH_{\ 3})_{\ 1.09}$	208.45	(38)
Milled bamboo lignin	$C_9H_{7.73}\ O_{3.81}\ (OCH_3)_{\ 1.2}$	215.13	76

1.1.3.1. Solvents for lignins

The solubility of lignins in solvents is affected by the extraction and purification methods. Lignosulphonate lignin is soluble in water, Kraft lignin is soluble in aqueous alkali, and organosolv lignin is soluble in a wide range of organic solvents. Table 3 lists the different organic solvents found in the literature for different lignins.

Table 3. Common organic solvents for lignin

	Organic solvent	Lignin solubility (g/Kg)	Lignin type	References
Alcohol	Methanol	6.1	From lignocellulosic bioethanol residues Kraft hardwood and sofwood Soda non-wood	(39)
	Ethanol	Unsoluble	Alkali	(40)
	1-propanol	Unsoluble	Alkali	(40)
	1-butanol	Unsoluble	Alkali	(40)
	Ethylene glycol	310	Alkali	(40)
	Glycerol	250	Alkali	(40)
Carboxylic acid	Formic acid	260	Kraft	(41)
	Acetic acid	7.2	Kraft	(42)
Ester	Ethyl acetate Ethylene carbonate Propylene carbonate	0.9 Unsoluble	Kraft From lignocellulosic bioethanol residues Kraft hardwood and softwood Soda non-wood	(41) (39)
Ester	Diethylether	0.1	Kraft	(41)
	Polyethylene glycol 200	20	From lignocellulosic bioethanol residues Kraft hardwood and softwood Soda non-wood	(39)
Heterocyclic compounds	1-methylimidazole Tetrahydrofuran	>500 0.8	From lignocellulosic bioethanol residues Kraft hardwood and softwood Soda non-wood	(39)
	Dioxane	7.3	Kraft	(42)

Ketones	Acetone	0.4	From lignocellulosic bioethanol residues Kraft hardwood and softwood Soda non-wood	(39)
Organochlorine compounds	Chloroform Dichloromethane	0.1 <0.1	From lignocellulosic bioethanol residues Kraft hardwood and softwood Soda non-wood	(39)
Organicsulphur compounds	Dimethylsulphoside	9.6	From lignocellulosic bioethanol residues Kraft hardwood and sofwood Soda non-wood	(39)
Water		0.8	From lignocellulosic bioethanol residues Kraft hardwood and softwood Soda non-wood	(39)

Eutectic systems have emerged as a 'green' alternative to the commonly used solvents for commercial lignins. Table 4 lists some eutectic mixtures employed as solvents for lignin

Table 4. Commercial lignin eutectic solvents

Eutectic solvents	Solubility lignin g/kg	Lignin type	References
Formic acid:choline chloride (2:1)	140	From lignocellulosic bioethanol residues Kraft hardwood Kraft softwood Soda non-wood	(39)
Acetic acid: Choline chloride (2:1)	120	From lignocellulosic bioethanol residues Kraft hardwood Kraft softwood Soda non-wood	(39)
Propanoic acid:Urea(2:1)	148.1	Kraft	(42)
	226.8	Kraft	(42)
Propanoic acid:urea (2:1)/water	598.5	Kraft	(42)
	745.8	Kraft	(42)
Lactic acid:alanine (9:1)	84.7	Alkali	(43)
Lactic acid:betaine (2:1)	90	Alkali	(44)
	120.3	Alkali	(43)
Lactic acid: choline chloride (1.3:1)	45-5	Alkali	(43)

Lactic acid: choline chloride (2:1)	53.8	Alkali	(43)
Lactic acid: choline chloride (5:1)	77.7	Alkali	(43)
lactic acid: choline chloride (10:1)	118.2	Alkali	(43)
Lactic acid: proline (2:1)	75.6	Alkali	(43)
Lactic acid: proline (3.3:1)	90	Alkali	(43)
Lactic acid: glycine (9:1)	87.7	Alkali	(44)
Lactic acid: histidine (9:1)	118.8	Alkali	(43)
Malic acid:alanine (1:1)	17.5	Alkali	(43)
Malic acid:betaine (1:1)	Unsoluble	Alkali	(43)
Malic acid:choline chloride (1:1)	34.0	Alkali	(43)
Malic acid:glycine (1:1)	14.6	Alkali	(43)
Malic acid:proline (1:1)	Unsoluble	Alkali	(43)
Malic acid:proline (1:2)	60.9	Alkali	(43)
Malic acid:proline (1:3)	149	Alkali	(43)
Malic acid:histidine (2:1)	Unsoluble	Alkali	(43)
Malic acid:nicotinic acid (9:1)	Unsoluble	Alkali	(43)

2. ELECTROSPINNING

Nanotechnology is the study and development of materials at the nanometric level. It has great potential for the development of new materials. Nanofibers, due to their high surface area and porosity, have important applications such as filter media and adsorption layers for protective clothing, among others.

Polymer nanofibers can be processed using several techniques, including drawing, template synthesis, phase separation, self-assembly, and electrospinning. Tables 5 and 6 provide a comparison of the different aspects related to these processing methods.

Table 5. Polymer nanofiber processing techniques

Process	Technological advances	Scalable	Repeatibility	Convenient to process?	Control to fiber on dimensions
Drawing	Laboratory	×	✓	✓	×
Template synthesis	Laboratory	×	✓	✓	✓
Phase separation	Laboratory	×	✓	✓	×
Self-Assembly	Laboratory	×	✓	×	×
Electrospinning	Laboratory & industrial processing	✓	✓	✓	✓

Table 6. Advantages and disadvantages of nanofiber processing techniques

Process	Advantages	Disavantages
Drawing	Minimum equipment requirement	Discontinuous process
Template synthesis	Fibers of different diameters can be easily achieved by using different templates	
Phase separation	Minimum equipment requirement. Process can directly fabricate a nanofiber matrix. Batch-to-batch consistency is achieved easily. Mechanical properties of the matrix can be tailored by adjusting polymer concentration	Limited to specific polymers
Self-Assembly	Good for obtaining smaller nanofibers	Complex process
Electrospinning	Cost effective. Long, continuous nanofibers can be produced	Jet instability

Electrospinning is the most advantageous processing technique for developing nanofibers. Electrospinning is a widely used process for preparing polymeric fibers with diameters ranging from 2 nm to several microns. This process is mainly used for polymers, but it can also be used for semiconductor composites and ceramic materials (45) Their high interest is due mainly to the control that can be exercised over the structure and size of the fibers, their polymer versatility and the unique characteristics offered by the material, i.e. high specific surface area, controllable and interconnected porosity, high mechanical performance, flexibility, etc. (46). These properties mean that the nanofibers developed have the potential to significantly improve current industrial process and find applications in new fields.

Important features of electrospinning are:

- A suitable solvent must be available to dissolve the polymer.

- The vapour pressure of the solvent must be adequate to evaporate fast enough for the fiber integrity to be achieved when it reaches the target, but not too fast for the fiber to harden before reaching the nanometer range.
- The viscosity and surface tension of the solvent must not be too high to prevent the formation of the jet nor too low to allow the polymer solution to escape freely from the needle.
- The energy supply must be adequate to overcome the viscosity and surface tension of the polymer solution to form and maintain the jet.
- The space between the needle and the grounded surface must be sufficient for the solvent to evaporate in time for the fibers to form.

2.1. Basics of the technique

The formation of nanofibers by electrospinning is based on the uniaxial stretching of a viscoelastic solution. Unlike conventional methods, the electrospinning technique uses electrostatic forces to stretch the solution as it solidifies. The basic execution of this technique (see Figure 5) consists of a capillary through which the polymer solution must be expelled, a high voltage source that has two electrodes which must be connected one to the outlet of the solution and the other to the collector plate, which usually consists of a sheet of conductive metal, where the fibers will be deposited (47). The main scheme of the electrospinning process is based on the connection of three main components: the current generator, the metal needle, and the collector. The needle is mounted in a syringe containing the polymer solution, the flow of which is controlled by a pump. When a voltage is applied (typically in the range 3-30 kV), the droplet exiting the needle is electrified and the charges are distributed on the surface, so that the droplet experiences two types of electrostatic forces: the repulsion between the surface charges and the

Coulomb forces exerted by the external electric field. The surface of the droplet, under the effect of the exerted force, begins to elongate and form a cone, known as a Taylor cone. The elongation process reaches a limit where the charge concentration is so high that it exceeds the surface tension of the solution and results in the creation of a current at the tip of the cone. During the process, the solution is stretched, and the solvent evaporates. Attracted by the charged collector, the fiber is deposited and distributed randomly to form an interconnected membrane of polymeric fibers, like the one shown in Figure 6 (2).

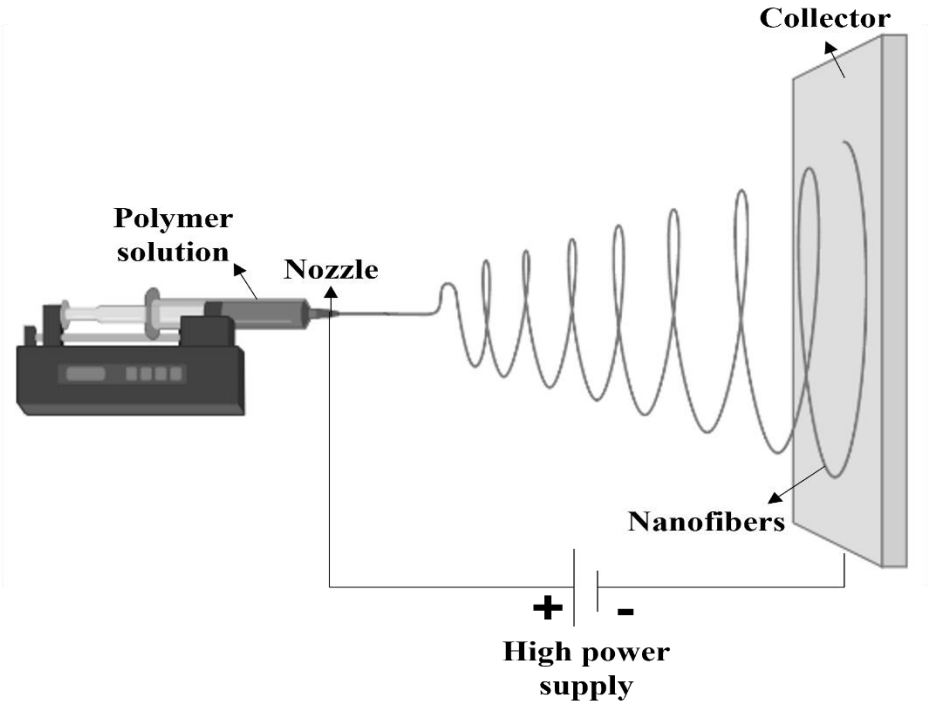

Figure 5. Schematic diagram of electrospinning equipment assembly

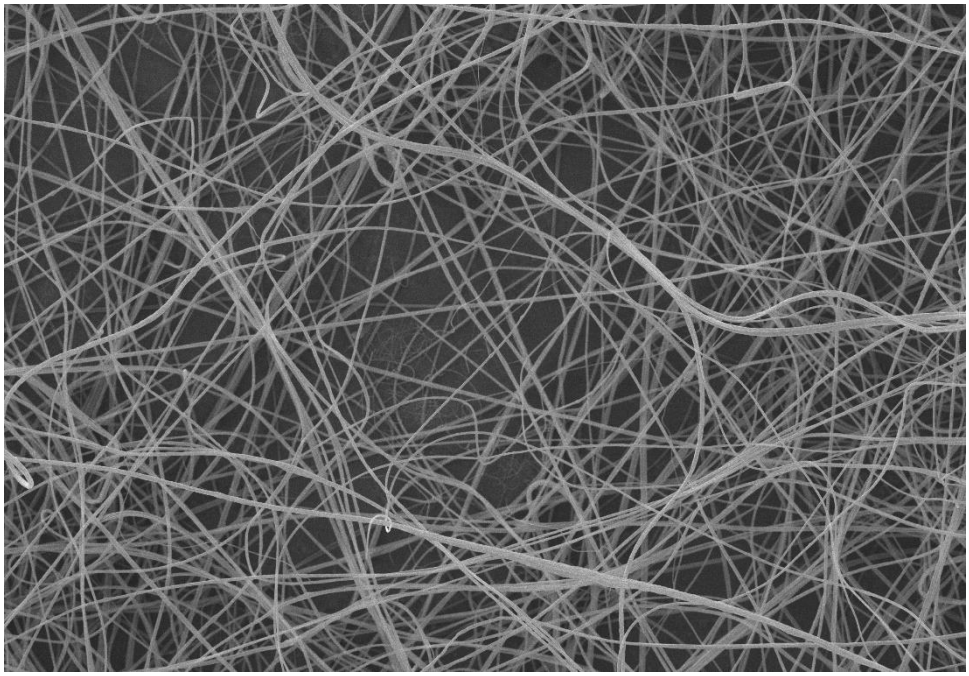

Figure 6. Nanofibers of polymeric material developed by electrospinning.

2.2. Parameters

The electrospinning process is governed by a wide variety of parameters, classified into process parameters, solution parameters and environmental parameters. These parameters significantly affect the morphology of the nanostructures obtained in the electrospinning process of the polymer solution and, therefore, its electrospinnability. The correct choice and manipulation of these parameters allows to control and fine-tune the required characteristics of the developed membranes to be obtained.

2.2.1. Processing Parameters

Process parameters affecting the morphology and fiber diameter of the developed membranes include the following:

- ✓ Voltage: In general, an increase in voltage causes a stretching of the current favoring the narrowing of the fibers but also a too high voltage can cause accumulations of the material (see Figure 7). Therefore, a higher stretching of the

jet induces a decrease in fiber diameter as demonstrated by Bogdan et al.(48) (see Figure 8), i.e. an increase in voltage leads to a decrease in diameter. The influence of the voltage also depends on the viscoelastic properties of the material.

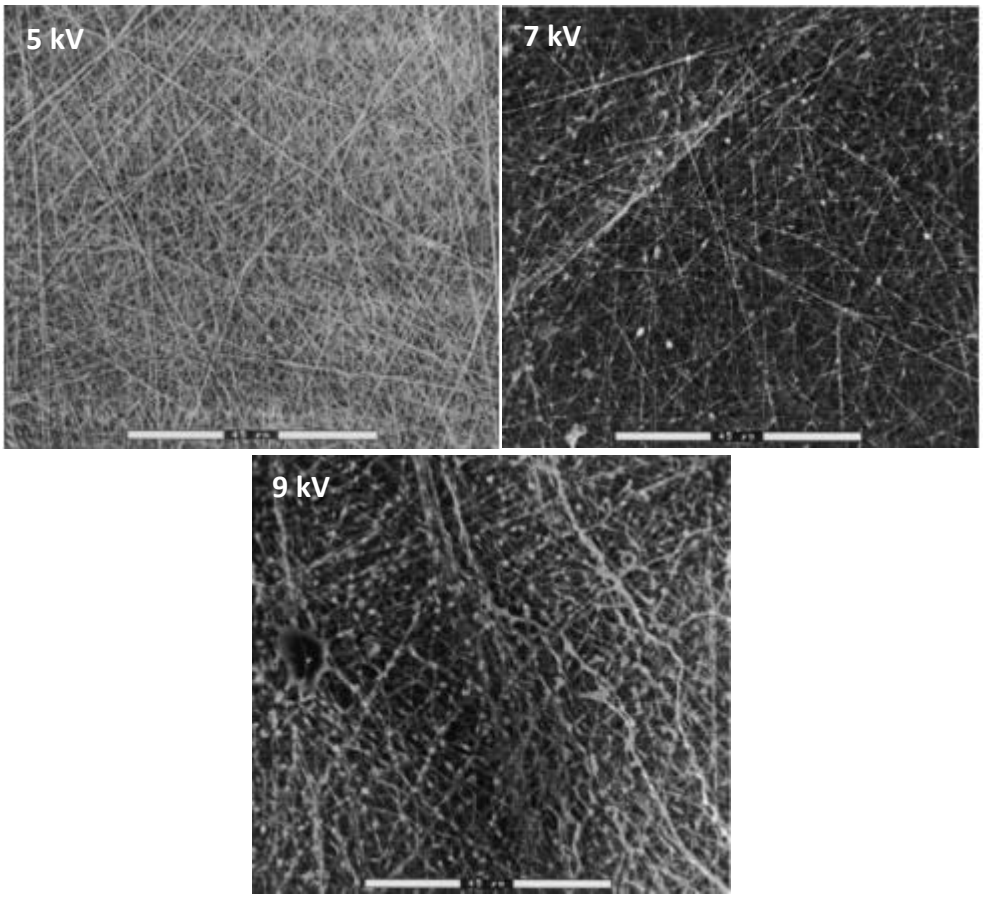

Figure 7. SEM photographs nanofibers electrospun under different electrical potentials (49)

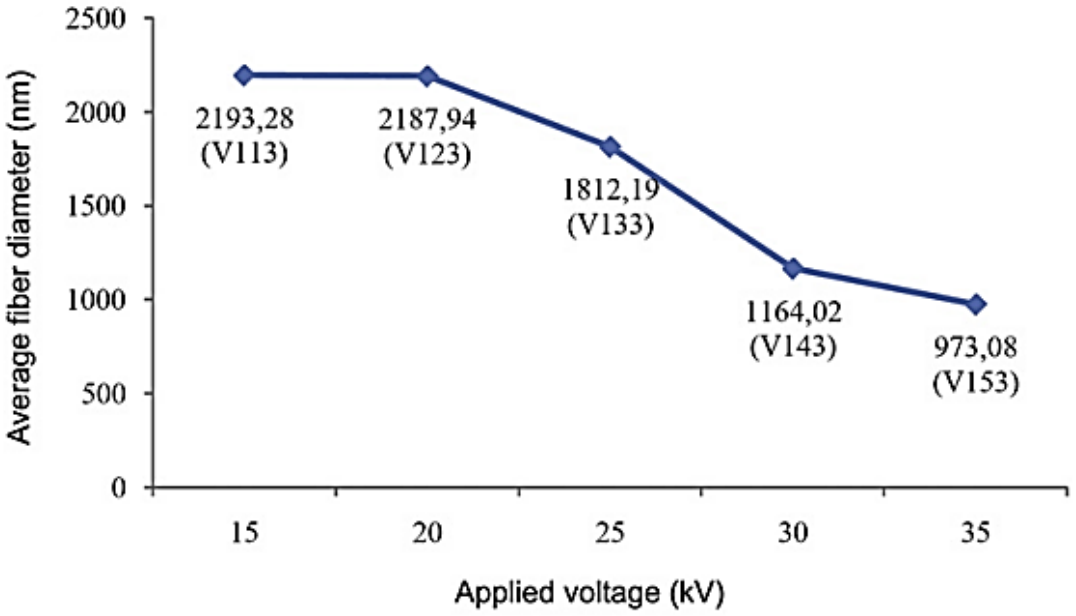

Figure 8. Average fiber diameter vs Applied voltage (48)

- ✓ Feed flow: Regarding the outflow of the solution, a flow that allows the complete evaporation of the solvent is considered the most suitable, it is necessary to overcome a minimum feed flow that manages to stabilize the current, the appearance of the Taylor cone determines a correct stabilization of the jet (see Figure 9). As the flux increases, the amount of material in the membrane increases and, consequently, the fiber diameter increases. However, too high values cause imperfections due to the inability to evaporate the solvent completely (see Figure 10).

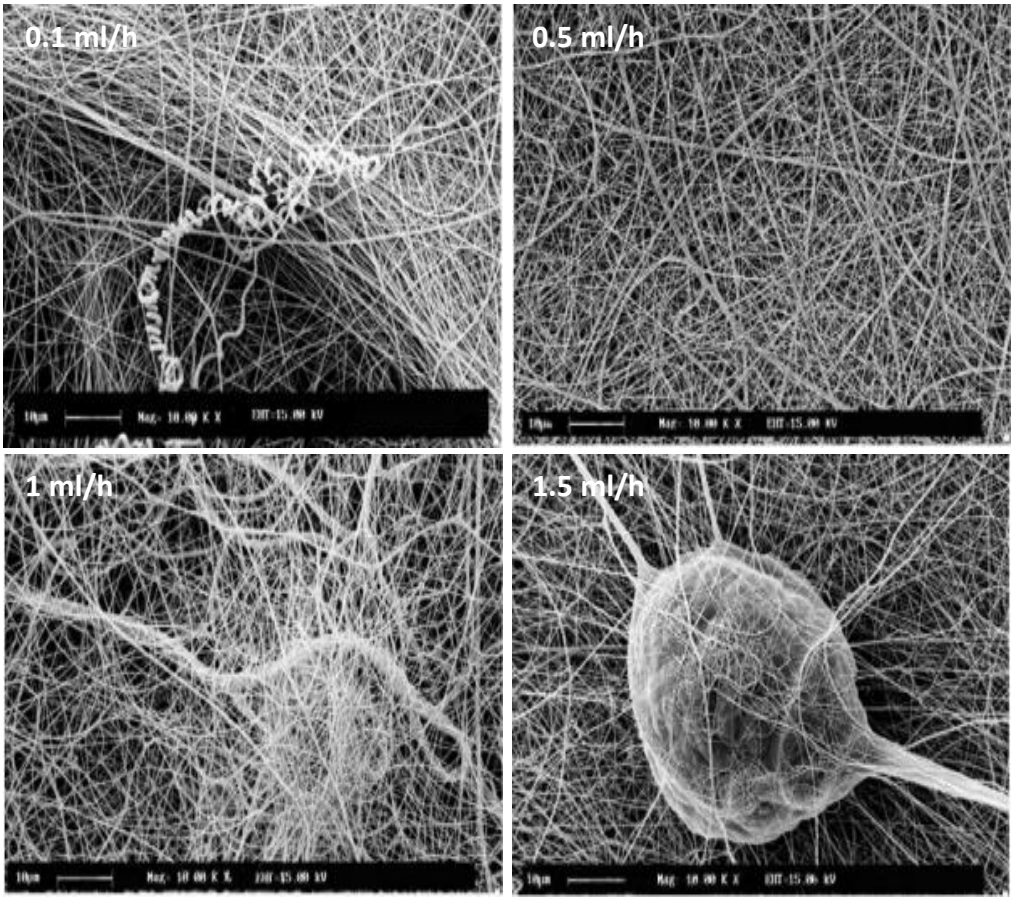

Figure 9. SEM images of the electrospun nanofibers at various flow rates (50).

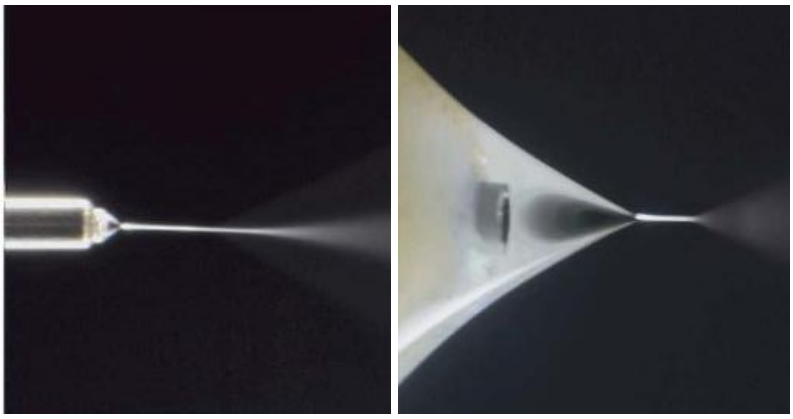

Figure 10. Taylor cone formation (51).

✓ Needle-collector distance: The required distance for total solvent evaporation depends on the properties of the feed solution used. Short distances may result in

the formation of larger filament diameter and even the presence of beads in the membranes, while distances that are too large may cause the fibers to break.

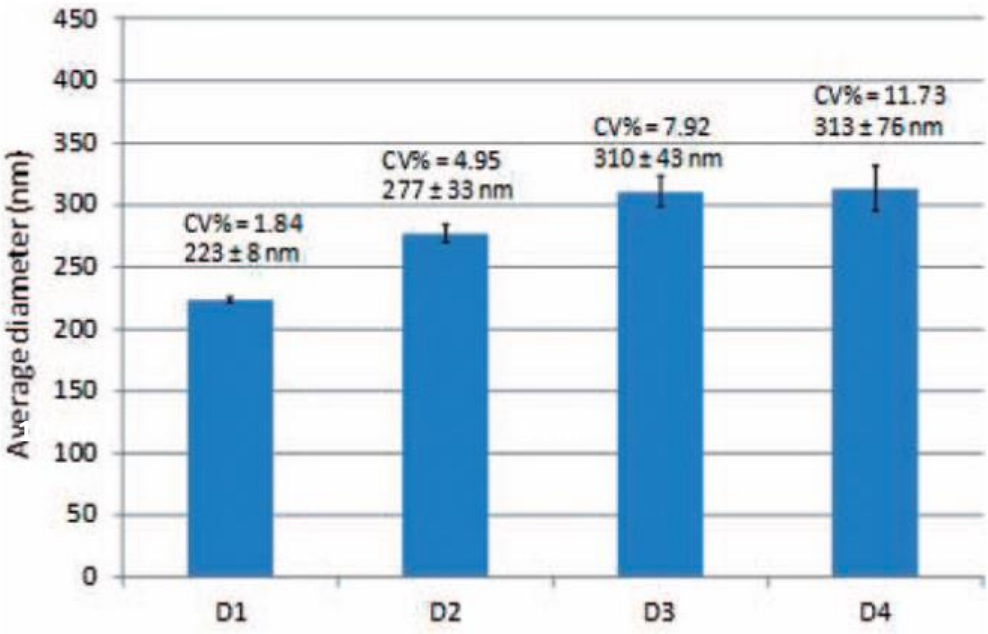

Figure 11. Average diameter of nanofibers for different needle-tip-to-collector distances: D1:20 cm; D2:15 cm; D3:10 cm; and D4:5 cm. (52).

2.2.2. Solution Parameters

Controlling the feed solution parameters is as crucial as the processing ones. The following parameters are the most relevant:

- Viscosity (related to polymer molecular weight and solution concentration): This is one of the most determining parameter of fiber morphology, diameter, and porosity. High viscosities, determined by high molecular weights and/or high solution concentrations, induce the formation of larger diameters. On the other hand, too low viscosity values lead to smaller diameters and can even cause

irregularities in the membrane, such as bead formation or even electrospraying of isolate particles.

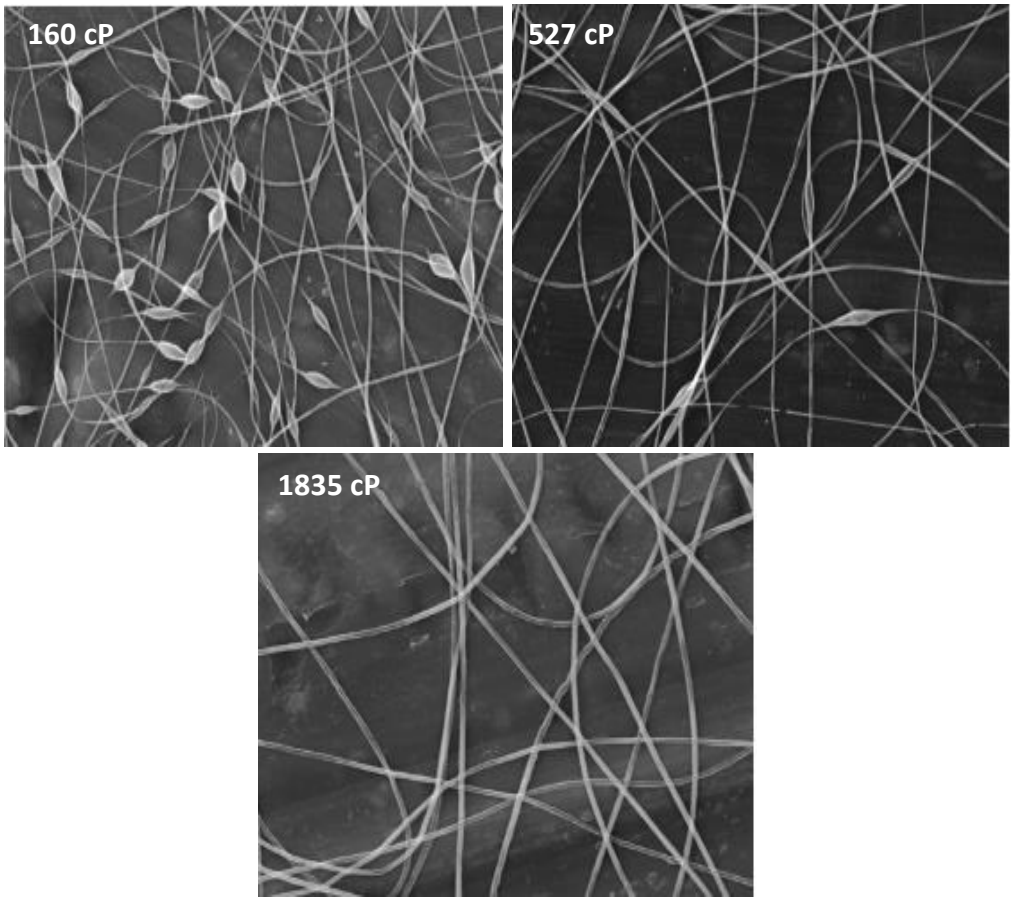

Figure 12. SEM images of nanofiber morphology depending on viscosity (53).

- Surface tension: Surface tension is a property that makes to resist rapid changes in shape and attempts to reduce the surface area per unit mass. By applying high voltage, it seeks to increase the surface area by opposing the formation of beads and favouring the formation of thinner jets. According to the literature, reducing surface tension predominantly results in bead-free fibers(54)
- Electrical conductivity is a crucial factor in the fiber generation process. If the conductivity is too low, there will not be enough current stretching to generate fibers. On the other hand, a high conductivity indicates increased charge transport,

resulting in greater stretching of the solution and, consequently, thinner fibers (55–57).

2.2.3. Ambient Parameters

In addition to the above-mentioned parameters, environmental parameters such as temperature and humidity must be taken into account. Lia et al (58) conclude that the formation of pores in membranes is affected by the vapour pressure of the solvent and the humidity. It was suggested that the effect of rapid evaporation of a solvent due to its high volatility could induce the separation of the polymer into different phases in the liquid stream and together with high humidity an increase in density and pore size occurs.

2.3. Layout of the technique

The conventional arrangements for the electrospinning technique are shown in Figure 12. While it is possible to develop the technique vertically, this can result in dripping from the capillary to the collector plate, leading to defective fibers.

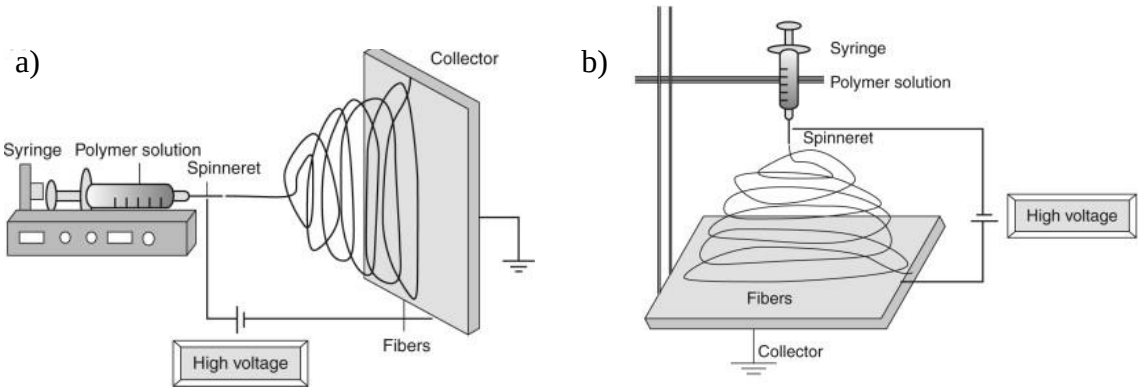

Figure 13: a) traditional horizontal layout of the technique b) vertical layout of the technique.(47)

Moreover, there are nowdaysn other alternative techniques such as coaxial electrospinning and forcespinning. Coaxial electrospinning (as shown in Figure 14) is a process that involves the simultaneous co-spinning of two polymeric liquids. The system uses two coaxially positioned needles to form composite polymeric droplets. The inner needle pumps a solution while the outer needle supplies the coating material. After applying a strong electric field, fibers composed of the polymeric solution and a 'shell' with the selected shielding material are formed. The main requirement for this process is that the polymer shell is a solution that can be electrospun and that it produces stable fibers. The inner polymeric solution may not be suitable for electrospinning.

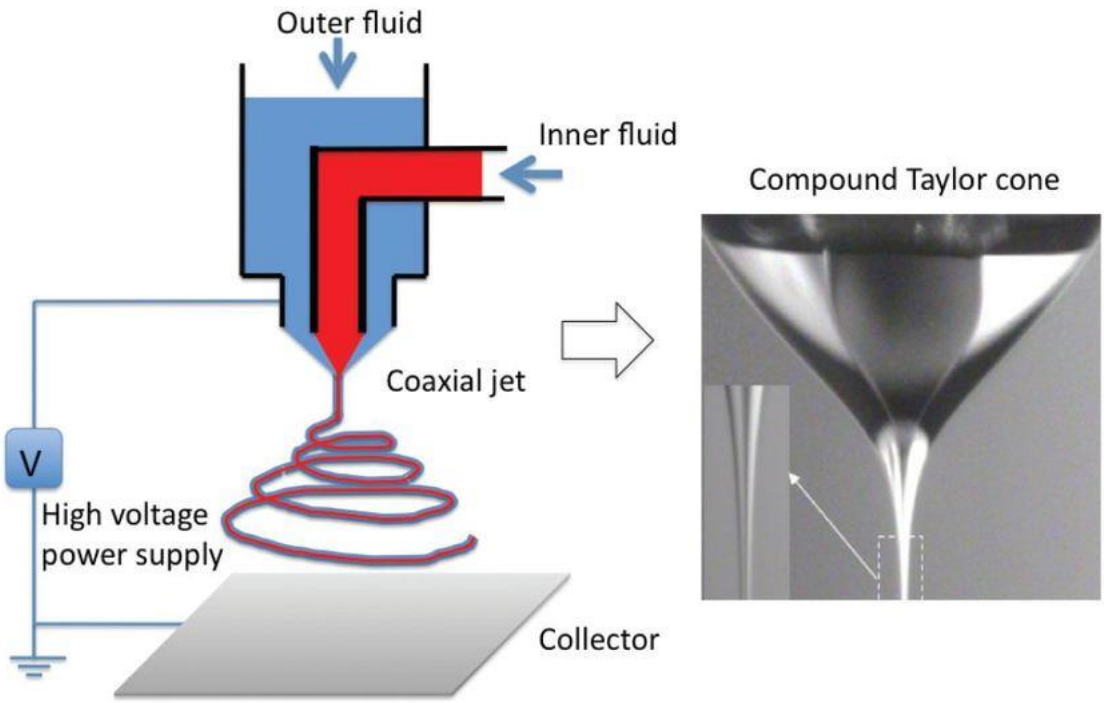

Figure 14. Coaxial electrospinning system (59)

Moreover, a centrifugal force-based method can be used as an alternative to electrostatic forces for developing polymer nanofibers. This method drives the material

through a set of holes designed within a spinneret. A polymeric solution or a polymer melt is placed in a spinneret and as the angular velocity increases, a critical value is reached at which the centrifugal force overcomes the surface tension and the fibers emerge from the tip of the needles into an outer collector, as shown in Figure 15. Friction with air causes the fibers to be deposited in an outer collector. The friction with the air causes the fibers to stretch and thin while the solvent evaporates (60). The advantage of this technique lies in its efficiency in developing nanofibers from materials of low dielectric constant.

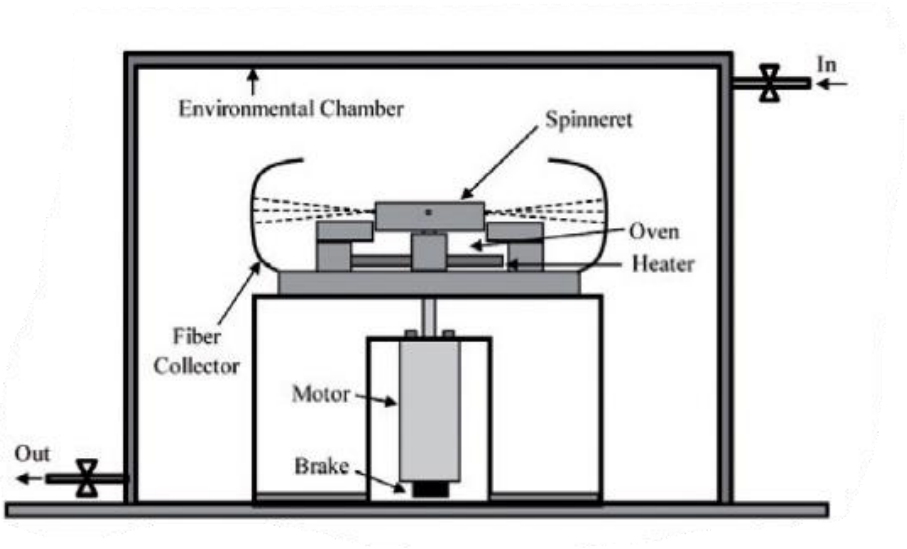

Figure 15. Traditional layout of the forcespinning method (61)

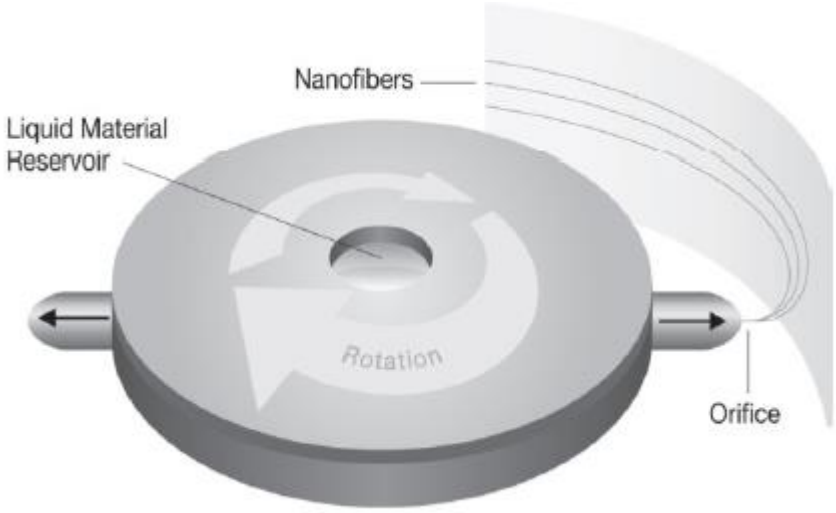

Figure 16. Mechanism of fiber formation by means of forcespinning. (62)

2.4. Background on the electrospinning of biopolymers

The electrospinning technique is widely recognized as highly efficient for fabricating polymer nanofibers. In recent years, numerous studies have been conducted on the electrospinning of biopolymers, including cellulose derivatives and lignin, and other biocompatible polymers of interest such as PVP. In general, the challenges when biopolymers or natural and/or biocompatible polymers are subjected to electrospinning are *i)* to achieve consistent and controllable fiber diameters and *ii)* to obtain uniform and defect-free surfaces or structures, which depend on the nature of the polymer and the chosen processing parameters previously discussed. The most relevant studies for our research are briefly discussed below.

Dallmeyer et al. (63) studied the effect of lignin structure on the formation of nanofibers by electrospinning, with seven different types of lignin dissolved in DMF. The addition of a copolymer, PEO, was necessary to improve the electrospinnability of the solutions because lignin alone formed BOAS membranes. A clear transition between electrospraying and electrospinning was evident with the significant increase of the solution concentration favoring the uniformity of the fibers. It was concluded that the

lignin structure and molecular interactions, such as hydrogen bonds or association complexes, influence the properties of the solution and thus the electrospinnability of the systems. Viscosity was shown to be a key parameter in the formation of homogeneous, pearl-free fibers.

Jia et al. (64) synthesized a nanocarbon network material from electrospun Kraft lignin (KL) and cellulose acetate (CA) fibers. It was observed that LK is not electrospinnable by itself due to the lack of chain structures and/or molecular entanglements caused by its relatively low molecular weight and high polydispersity index. However, it successfully electrospins after mixing with CA presenting fibrous structures in its electrospun membranes.

Aslanzadeh et al. (65), in the same way as Dallmeyer (63), studied the morphology of lignin softwood (LSK) with the effect of polyethylene oxide (PEO) addition. PEO proved to be a successful co-helper in the electrospinning process achieving uniform and bead-free fibers. The increase in molecular weight caused a transition from BOAS to bead-free fibers due to the density of entanglements in the polymer chain.

Klossner et al. (66) fabricated defect-free nanofibers by electrospinning from solutions of chitosan and polyethylene oxide (PEO) in acetic acid. The degree of deacetylation proved to be crucial. Electrospun fibers were only formed when there were sufficient intertwined chains despite increasing the solution concentration may excessively increase viscosity for electrospinning. It was observed that polymer concentration must be at least 2-2.5 times higher than the entanglement concentration in order to form a continuous fiber. This concentration is the one at which the solution passes from the semi-dilute non-entangled regime to the semi-dilute entangled regime. Chitosan alone was not capable of forming continuous fibers, it was mixed with PEO to produce

fibers without microspheres. The addition of PEO reduced the overall solution viscosity making it a more electrospinnable. It was observed that, as the polymer concentration increases, the number of microspheres decreases, while increasing the chitosan concentration decreases the fiber diameter. It is hypothesized that this behavior is due to the fact that chitosan is a polyelectrolyte and the positively charged chain behaves differently in the electric chain than a neutral chain.

In order to neutralize the beads developed in the electrospun lignin-PVA fibers Fang et al. (67) anionic, cationic and non-ionic surfactants (SDS, DTAB and Triton X-100) are added. Depending on the nature of the surfactant the impact on viscosity is different. SDS binds to PVA and lignin forming a complex once the critical micellar concentration is exceeded. Triton X-100, on the other hand, does not carry out cooperative binding due to the non-ionic character. And yet, DTAB interacts with alkali lignin through electrostatic forces when reaching its critical micellar concentration and this is why viscosity decreases with DTAB concentration. As for the surface tension, when the surfactant concentration exceeds the critical micellar concentration, the molecules form micelles and align at the gas-liquid interface causing a reduction of the surface free energy and surface tension. The addition of surfactants removed the beads from the fibers and reduced the average diameter of the fibers obtained, as long as the critical micellar concentration was exceeded.

Wang et al. (68) added Triton X-100 to PVP polymeric solutions to study the influence on the electrospinnability of the solutions. The Triton X-100 addition considerably improved the electrospinnability of this biocompatible polymer, resulting in homogeneous membranes due to a decrease in surface tension in the presence of the surfactant. This also led to a decrease in fiber diameter.

Crabbe-Mann et al (69) subjected three cellulose derivatives (ethyl cellulose, cellulose acetate and carboxymethyl cellulose) to an electrohydrodynamic process by dissolving these derivatives in environmentally friendly solvents: ethanol, acetone, and water. Ethyl cellulose together with ethanol and water showed a transitional regime from particles to fibers at a concentration of 17 to 25% by weight, finally providing continuous and homogeneous fibers. Cellulose acetate electrospinning with acetone also led to a transition as the solution concentration was increased from 10% to 20% and smooth fibers were obtained by increasing the solution concentration and reducing the evaporation rate. The use of carboxymethyl cellulose led to larger fibers compared to the other polymers due to the increased molecular weight. All three cellulose derivatives proved to be more than valid options for use in electrohydrodynamic processes together with environmentally friendly solvents with the ability to control both fiber diameter and fiber morphology.

Mariko et al. (70) produced fibers by electrospinning aqueous dispersions of lignin, poly(vinyl alcohol) (PVA) and cellulose nanocrystals (CNC). This solution produced defect-free fibers with up to 90% lignin and 15% CNC. They observed an improvement in the morphology of the membranes with increasing viscosity, by increasing the total concentration of the solution. They distinguished three different composition regions, beaded fibers, non-beaded fibers, and phase separation. In the latter case, very high viscosity solutions were obtained, and electrospinning did not take place. Non-beaded fibers were observed in a concentration range of 0-32% lignin, 2-19% PVA and 66-86% water. Fiber diameter was observed to increase with total polymer concentration. Here it was observed that the formation of non-beaded fibers occurred at low lignin contents.

In short, there is a wide variety of research defining the wide range of polymers that have been found to be satisfactorily processed using electrohydrodynamic techniques. Table 7 collects additional studies on this matter.

Table 7. Studies on the processing of biopolymers and biocompatible polymers using electrohydrodynamic techniques, including solvents and range of solution concentration.

Polymer	Solvent	Concentration	Applications
PVA	Distilled water (71-73)	7 to 33 wt%	Carbon nanofibers
PLA	Dichloromethane (74) Dimethylformamide (75) Dichloromethane (76)	5-15 wt% 30 wt% 5-15 wt%	Filtration, biomedical material and membrane.
PEO	Chloroform, ethanol, DMaC, Water(77) Distilled water (78)	3-7 wt%	Biomedical applications
PVP	Ethanol (79) DMF/Ethanol (80)	8-12 wt% 10-18 wt%	Films for sensor, filtration, drug delivery
CA, cellulose acetate	Acetone (81) Chloroform DMF Dichloromethane (DCM) Methanol (MeOH) Formic acid Pyridine Acetone (69)	5 wt% 2-12 wt% 10 wt%	Biomedical applications
PCL	THF:DMF (82) Chloroform (83) Formic acid	15 wt% 12.5-20 wt%	Biomedical applications

Regarding the electrospinning of lignocellulosic materials, and specifically lignin, due to its potential for revalorization, Table 8 collects other relevant studies, in addition to those previously mentioned.

Table 8. Electrospun lignin together with their copolymer.

Polymer	Ratio	Solvent	Concentration
Lignin:PEO (SKL, HKL, HOL, SOL, PL)	99:1- 95:5	DMF (63)	10-50 wt%
Kraft lignin:PEO	95:5-97:3	DMF (84) Water	5-11 wt%
Softwood Kraft lignin:PVA/CNCs	0:100/0-20:80/15	Water (70)	5-17.5 wt%
Sulfur-free softwood lignin:PEO	99:1-95:5	DMF (65,85)	1.1-0.03 wt%
Kraft lignin:PEO	0:100-100:0	Water (86)	4 vol%
Alkali lignin:PVA - SDS, DTAB and TX-100	70:30 (0.2-1 wt%)	Water (67)	10 wt%
Softwood Kraft lignin:PEO	99:1-98:2	DMF (87)	25-50 wt%
Alkali lignin:PVA	70.30-50:50-30:70	Distilled water (88)	9-12 wt%
Softwood Kraft lignin:PEO	98:2	DMF (89)	30 wt%
Alkali lignin:PHB	5:95	HFP (90)	3 wt%
Lignin:PCL	95:5-90:10-85:15	HFP (91)	10 wt%
Lignin:PCLLA	90:10	HFP (92)	10 wt%
Lignin:PLA/PLLA	1/2	HFP (93)	6 wt%

3. LUBRICATING GREASES: A GENERAL OVERVIEW

According to the American Society for Testing and Materials (ASTM), a lubricating grease is a solid or semi-fluid material that contains a thickening agent dispersed in a lubricating liquid. It is considered that these are colloidal suspensions in which a solid thickening agent, typically a metallic soap, is dispersed in a liquid matrix, traditionally a mineral oil, forming a three-dimensional gel-like network. This network gives rise to a fibrous structure where the oil is trapped (Figure 17). The physical properties of lubricating greases are determined by their microstructure. Therefore, it is crucial to select the right ingredients and processing variables to ensure optimal performance (94,95).

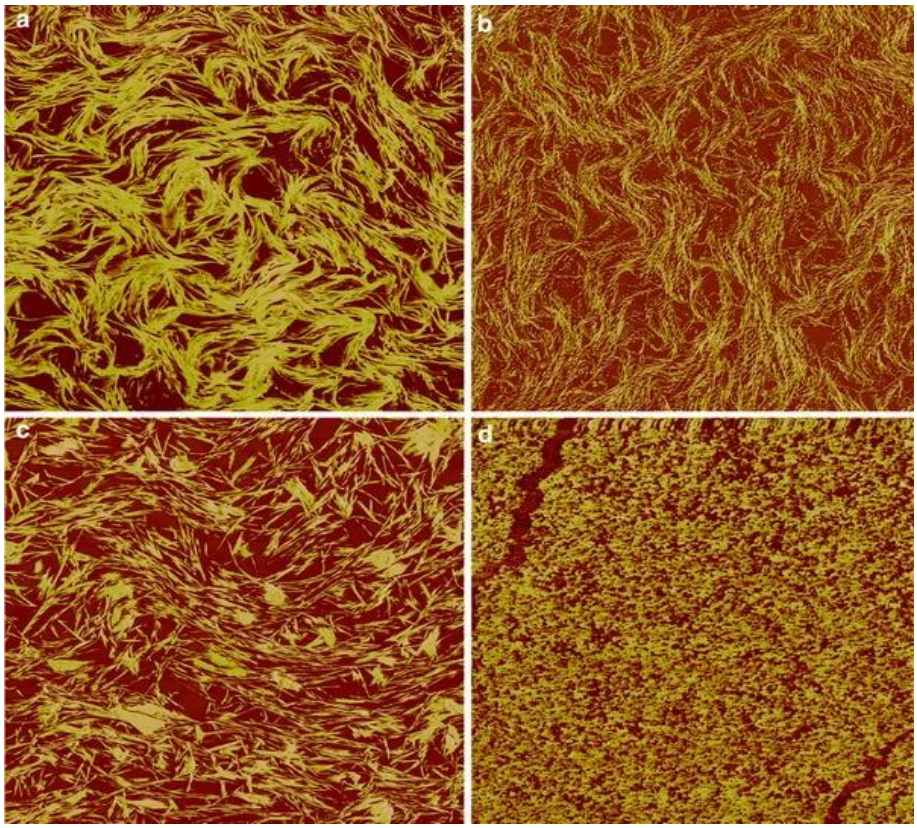

Figure 17 AFM micrographs for selected commercial lubricating greases.(96)

The typical composition and percentage of the most common components in lubricating greases are listed in Table 9:

Table 9: Typical composition of traditional lubricants

Component	***Composition (%)***	***Basic function***
Oil (mineral/sintetic)	65-95	Lubricant
Thickening agen	5-35	Oil carrier/additive
Additives	0-10	Improvement of specific properties

3.1. Bio-based or biodegradable lubricating greases

From 2010 to 2030 energy demand has increased by 33.5% (97) due to the industrialization, modernization, and societal development. The annual use of lubricants has increased, resulting in a consumption of 30 to 40 million tonnes. Unfortunately, around 55% of these lubricants end up in the environment, and 95% of them are derived from fossil fuels, posing a significant threat to the environment.

The concern about environmental risks has increased due to the threat posed by them. This has led to a rise in the development of renewable resources and natural alternatives (98,99). Along these lines, bio-lubricants arise as an ecological alternative to traditional lubricants, which are derived from vegetable oils, animal fats or any other environmentally friendly hydrocarbon (100). These materials offer satisfactory technical performance with good lubrication, a high flash point, a high viscosity index, and good shear strength (101,102).

The development of bio-lubricants poses a challenge in terms of applying suitable, sustainable, and cost-effective technologies, as well as achieving complete biodegradability. The literature contains numerous studies that explore the development

of biodegradable lubricants through the substitution of mineral oils with vegetable oils, such as soybean, castor, and rapeseed oils. (103–106). Moreover, there is an increasing demand for eco-friendly bio-lubricants that substitute mineral oils with vegetable oils and conventional thickening agents with natural polymers. This approach avoids the use of non-biodegradable polymers or those that require highly toxic production processes. Lubricating greases that are currently considered biodegradable may have the following composition:

Table 10. Composition of biodegradable lubricating greases

Component	Composition (%)	Basic function
Base fluid (vegetables oils, synthetic esters, glycols)	75-95	Lubricant
Thickening agent (calcium soaps, bentonite/silica/clays, aluminium complex soaps, polyureas)	5-20	Oil Carrier/additive
Additives	1-8	Improvement of specific properties

Vegetable oils have an excellent affinity with metal surfaces, providing intrinsic anti-corrosion properties. Therefore, the use of anti-corrosion additives is uncommon. If necessary, the amount of additive required to achieve anti-corrosion properties is quite low. However, there are certain limitations concerning the optimum working temperature (-20°C-80°C) (107).

Regarding biodegradable lubricating greases, as previously mentioned, replacing the oil has been successfully addressed. However, substituting the thickener remains a challenge in this area of research due to the high efficiency of traditional metal soaps, which provide suitable rheological, thermal, and tribological properties. In the following

section, we will provide a more comprehensive review of the available biodegradable options.

3.2. Biopolymers as thickening agents

Currently, greases manufactured with vegetable oils or their derivatives but including metallic soaps or polyureas as thickeners cannot be considered fully biodegradable since these components are not environmentally friendly. To achieve full biodegradability, it is necessary to disperse biodegradable materials in vegetable oils. For this reason, the scientific community is increasingly searching for new ways to replace traditional gelling agents. These agents must be environmentally friendly, non-toxic, and derived from natural resources. In addition to continuously searching for new gelling agents, it is necessary to achieve a proper interaction between the oil and thickener matrix. Chemical modifications are often made to facilitate this compatibility. Previous research at our Research Centre (Pro2TecS) has focused on using lignocellulosic materials as bio-thickeners. Delgado et al. (108) and Cortés et al. (109) developed biological fats formulated by dispersions of epoxy-functionalised alkaline lignins (EAL) in castor oil. PEGDE-modified alkaline lignin showed similar behaviour to traditional greases. In addition, increasing T to 150ºC decreased the storage and loss modulus in contrast to the thermoreological behaviour of commercial greases (see Figure 18).

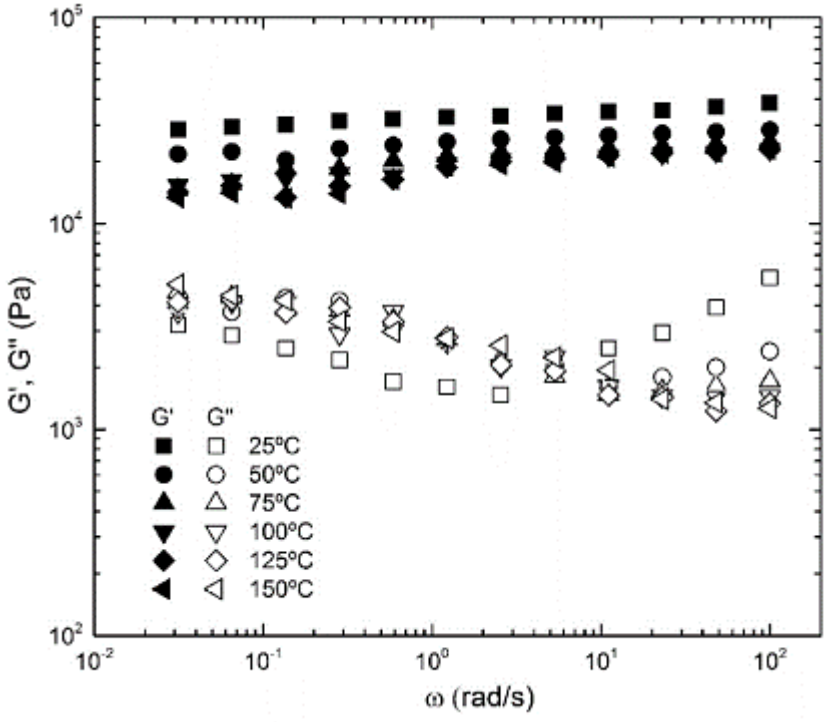

Figure 18. Thermorheological behaviour of commercial fats

Gallego et al. (107) functionalised various commercial cellulose and methyl cellulose pulps with isocyanate groups. They then characterised the resulting lubricating greases both rheologically and tribologically.

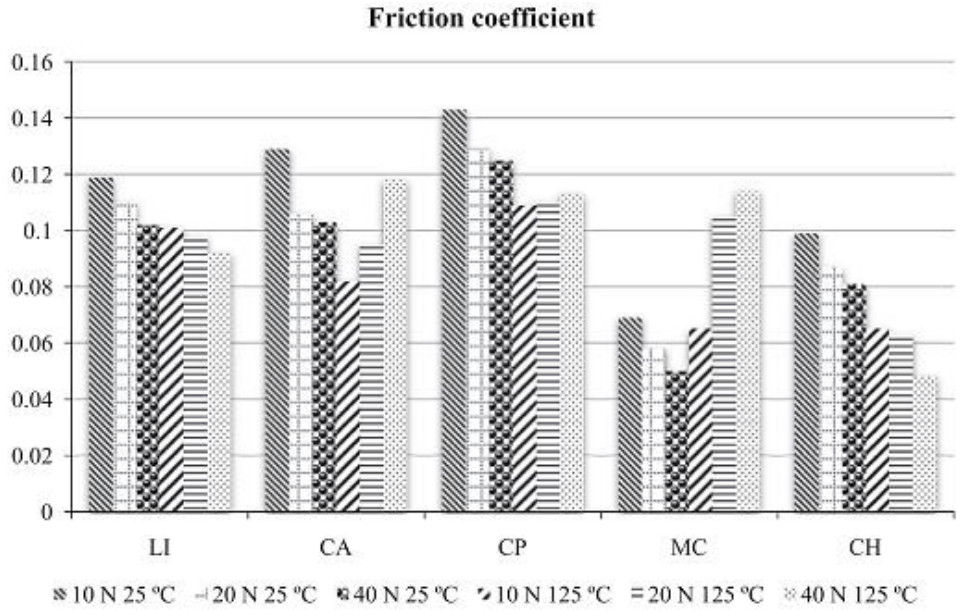

Figure 19. Coefficients of friction of functionalised greases

Sánchez et al. (102,110–112) dispersed cellulose derivatives in castor oil. EC significantly reduced phase separation and, like methyl cellulose, showed mechanical stability comparable to that of commercial greases. The nature of the oil also had a significant influence, with better results being obtained in those formulations where castor oil was used.

Nuñez et al. (113) developed biodegradable lubricating greases by dispersing eucalyptus kraft cellulose pulp in an ethyl cellulose/castor oil medium. Through rheological, tribological, thermal analysis, and mechanical stability studies, it was determined that these greases have a stable evolution similar to traditional greases and a higher decomposition temperature than the standard.

Table 11. Results of thermogravimetric analysis of biodegradable lubricating greases

Samples	T_{onset} (°C)	Decomposition temperature range (°C)	T_{max} (°C)	Residue (%)
Kraft cellulose pulp	333	333–391	375	10.4
Methylcellulose	199	199–210/210–324	204/260	33.1
B	365	365–415	395	1.2
C	360	360–417	390	2.4
E	364	364–419	392	1.8
F	352	352–417	386	3.7
G	350	350–414	384	4.6
H	342	342–408	374	12.0
I	338	338–409	372	13.5
COLi	329	329–403	362	0.3
Standard naphthenic oil-based grease	223	223–323	296	1.3

Gallego et al. (114,115) incorporated chitin and chitosan functionalized with isocyanate groups as thickening agents in castor oil. Regarding their rheological behaviour, viscoelastic functions very similar to those found in standard lubricants were observed; similar results were observed by Sanchez et al (116) using chitin, chitosan and acylated derivatives (see Figure 20). They prepared physically stable oleogels or gel-like

dispersions with a higher thermal resistance than traditional greases, i.e. with higher degradation temperature (Table 12).

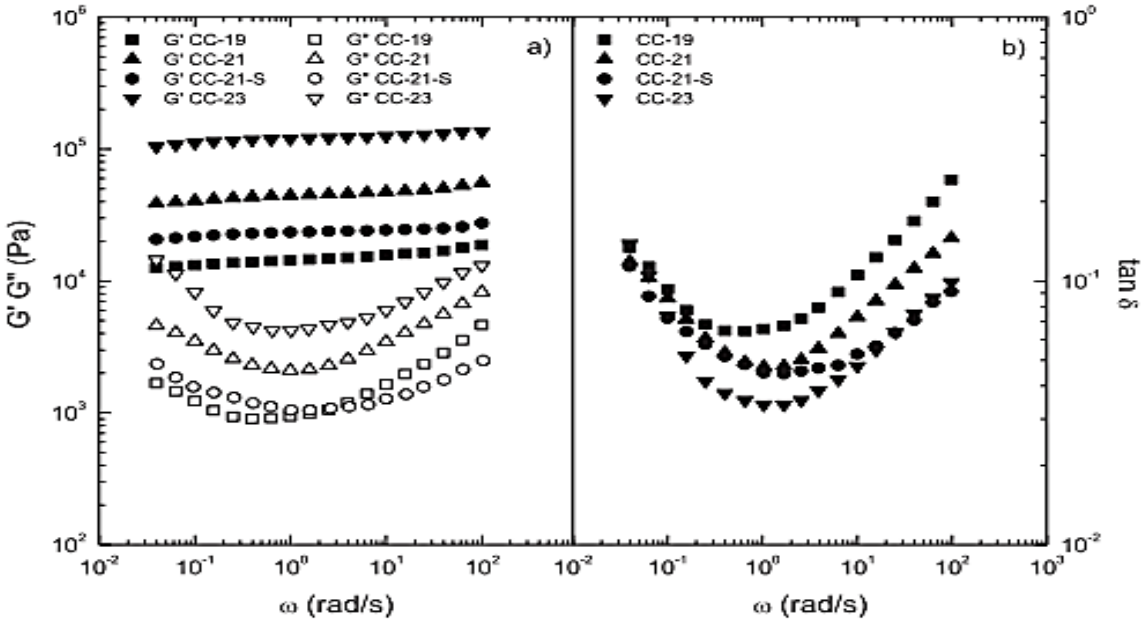

Figure 20. Evolution of SAOS functions with frequency for chitin-based oleogel formulations, at 25 ◦C (116).

Table 12. Characteristic TGA parameters of the studied oleogel formulations based on isocyanate-functionalized chitin and chitosan (115).

Sample	T_{onset} (°C)	T_{max} (°C)	T_{final} (°C)	Residue (%)	ΔW (%)
CSAN-1-30	297	344/386/452	481	7.40	92
CSAN-2-30	301	339/389/451	481	9.97	90
CTIN-1-30	327/444	376/450	410/485	5.07	95
CSAN-30	278/357	302/389/449	319/482	3.89	96
CTIN-30	342/425	381/459	409/595	10.46	89

3.3. Rheology of lubricating greases

Rheology is the science that studies the relationship between the external forces acting on a given material and the deformation they produce. Determining the rheological properties of lubricating greases is gaining importance due to the increasing interest in grease manufacturing and expanding their applications. Determining the rheological

behaviour of greases is also useful for understanding evolution of the microstructure with shear and essential for predicting their response under specific operating conditions. The rheological behaviour, and other functional properties, of lubricating greases is basically determined by the thickener used but also depend on both other composition variables (oil viscosity, additives, thickener-oil interactions…) and the manufacturing process (102,117,118).

In general, lubricating greases exhibit a highly pronounced shear-thinning behaviour, resulting in a decrease in apparent viscosity with shear rate (Figure 21).

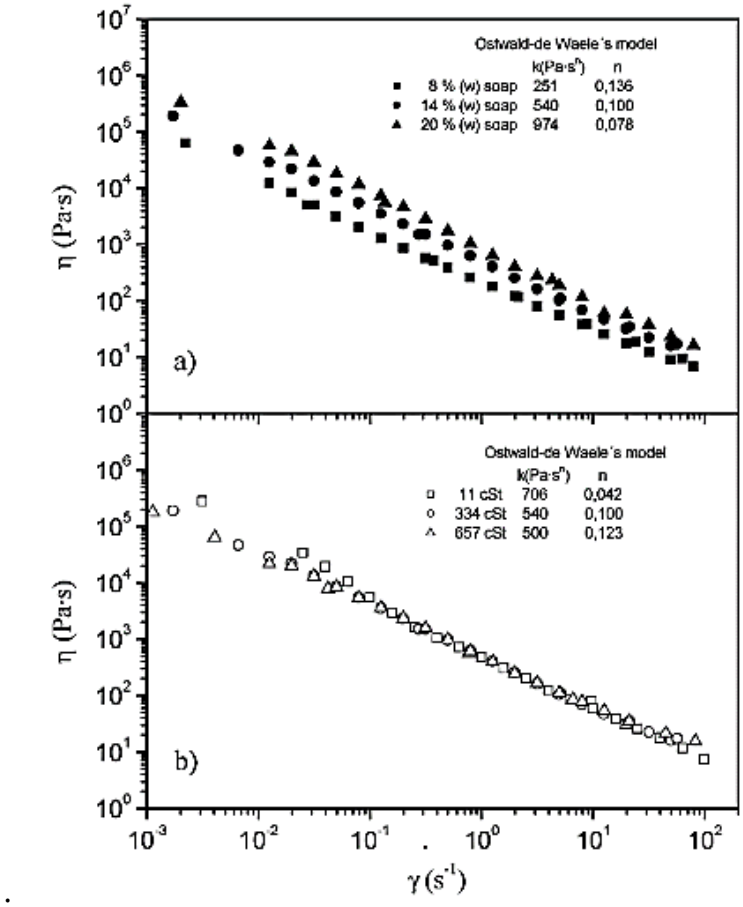

Figure 21. Shear-thinning behaviour in lubricating greases: a) effect of thickener concentration b) effect of oil viscosity (118)

Furthermore, the viscoelastic character of lubricating greases has been mostly studied through small amplitude oscillatory shear (SAOS) tests that use frequency sweeps at a constant amplitude within the linear viscoelastic region.

Figure 22 shows the typical evolution of the storage modulus (G') and loss modulus (G") with frequency within the linear viscoelastic range for lubricating greases. The moduli typically increase with the concentration of the thickener, which conforms a continuous three-dimensional network. This mechanical spectrum typically observed in lubricating greases is the characteristic of structured gel-like colloidal suspensions (119,120).

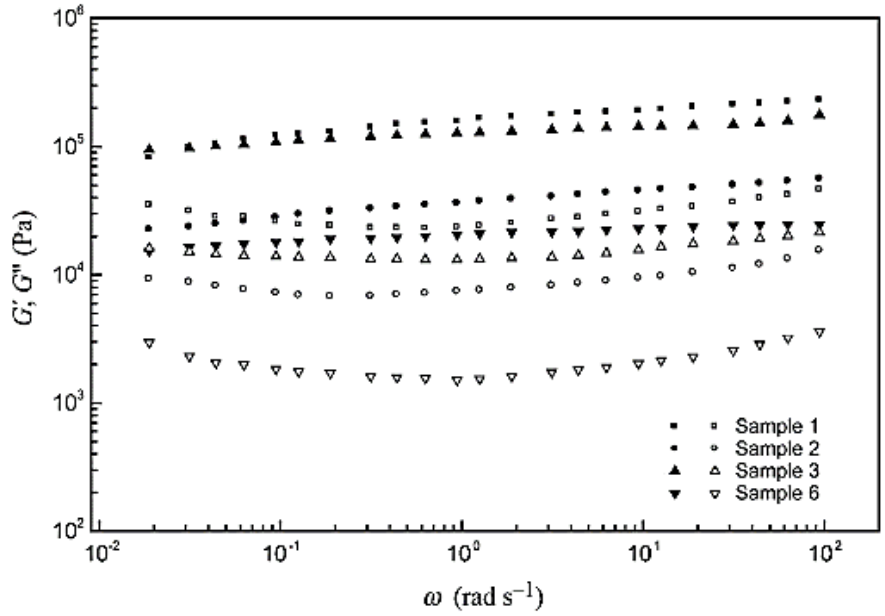

Figure 22. Frequency dependence of the storage (G') and loss (G'') moduli of selected lubricating grease samples.(117)

3.4. Tribology of lubricating greases

Tribology is the science of wear, friction, and lubrication, and it encompasses the behavior of interacting surfaces. These are not material properties but responses to a tribological system consisting of a bearing, a shaft and a lubricant combination, as shown

in Figure 23. When one surface moves across another, there is always a resistance to movement. This force is known as “friction”. Lubrication is thus the use of a material to improve the sliding of one material over another. In order to achieve a sliding action that is not so aggressive, it is not so important to achieve low friction factors but to achieve constant friction.

In addition to reducing and controlling friction, lubricants aim to reduce wear and prevent overheating and corrosion, thereby increasing the lifetime of equipment.

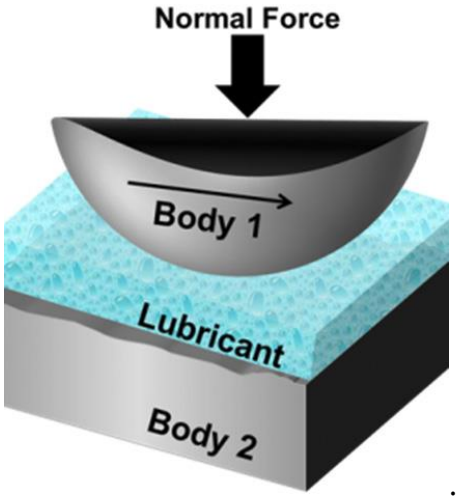

Figure 23. Schematic of a tribological system.

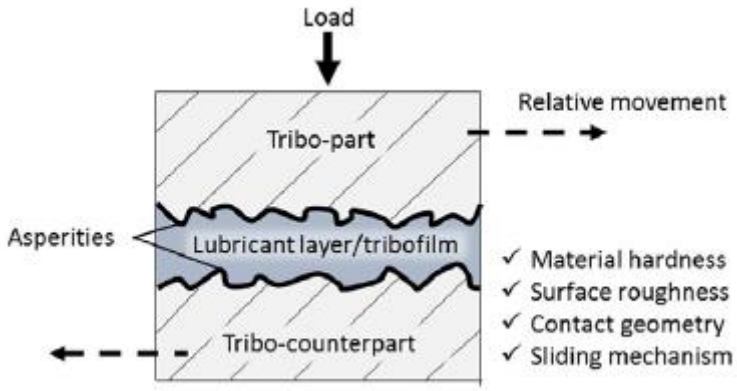

Figure 24. Mechanical properties of a tribological system (121).

The tribological properties of lubricating greases generally depend on the film formation between the two sliding surfaces and its corresponding thickness. This is usually affected by the NLGI grade (or grease consistency), the type of thickener, the viscosity of the base oil, and the mechanical stability of the greases, i.e. loss of consistency under operating conditions. (122). The tribological behaviour of lubricants is often characterized by the Stribeck curve (Figure 25), in which the coefficient of friction, speed, viscosity and applied load are related.

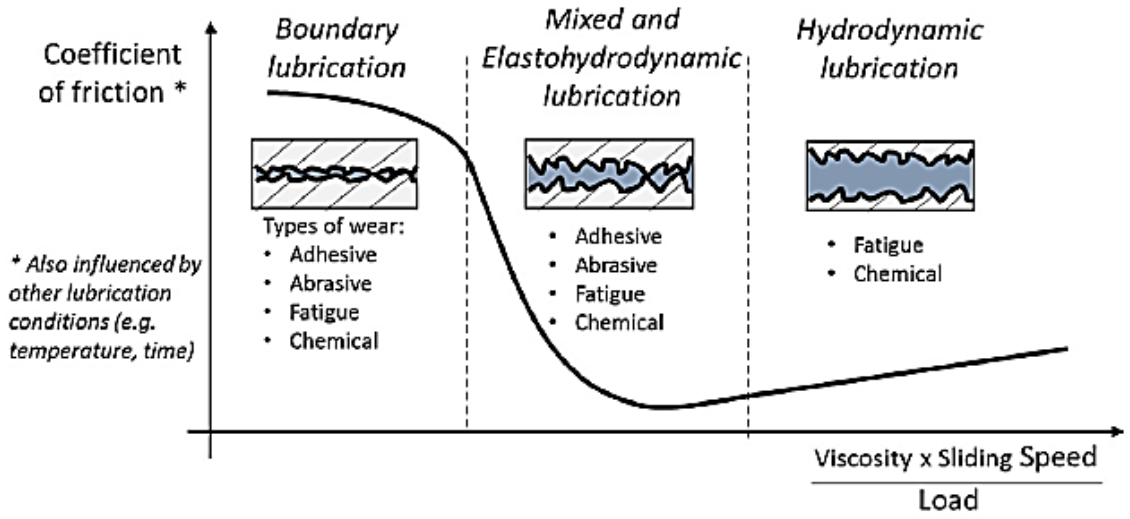

Figure 25. Stribeck curve of a lubricated contact (121)

In the Stribeck curve there are three clearly differentiated zones. From right to left we find the hydrodynamic lubrication zone, in which the oil film is sufficient to ensure that there is no contact between the shaft seals and the bearings, of just between two sliding surfaces. In the hydrodynamic lubrication regime, the friction is generally lower than in the other regimes, and basically depends on the lubricant internal friction, i.e. its viscosity. The hydrodynamic pressure generated in the lubricating film due to the relative motion and internal friction of the film is too low to cause surface deformation. In the mixed lubrication zone in which there is contact between the sliding surfaces to some

extent but other zones in which the film is sufficient so that there is no such contact, being a mixture of hydrodynamic and boundary regimes. Friction losses vary over a wide range according to the two regimes involved. And, finally, for low viscosity and/or speeds, the boundary lubrication regime arises, in which the lubricant film has been greatly reduced and the load makes the surfaces to come into contact. It is characterized by much higher friction losses than the other regimes. It can occur during start-up and shutdown of equipment, when the equipment operates in extreme conditions, dented gears, or in oscillating movements.

Generally, the tribological behaviour of greases is affected by the physicochemical properties of the base oil, such as polarity and viscosity, as well as the concentration of the thickener and the the resulting thickener-oil interactions.

Couronne et al (123) found a significant influence of the interaction between soap and oil and proposed an intriguing correlation between the storage modulus, film thickness in the elastohydrodynamic regime, and friction coefficient. Delgado et al (124) investigated the impact of soap concentration and oil viscosity on the viscoelastic properties and transient flow of lubricating greases concluding that the density of entanglements and fibers, responsible for the structural skeleton, is directly linked to the rheological response. The shear-induced evolution of the microstructure was analyzed using the Leider-bird model.

4. References

1. **George J, Sabapathi SN.** Cellulose nanocrystals: Synthesis, functional properties, and applications. Nanotechnol Sci Appl. 2015 Nov 4;8:45–54.

2. **Aziz T, Ullah A, Ali A, Shabeer M, Shah MN, Haq F, et al.** Manufactures of bio-degradable and bio-based polymers for bio-materials in the pharmaceutical field. Vol. 139, Journal of Applied Polymer Science. John Wiley and Sons Inc; 2022.

3. **Aziz T, Fan H, Zhang X, Khan FU**. Synergistic impact of cellulose nanocrystals and calcium sulfate fillers on adhesion behavior of epoxy resin. Mater Res Express. 2019 Oct 23;6(11).

4. **Gallego Calvo R**. Functionalization of biopolymers with reactive groups to be used as thickeners in oil media. 2015.

5. **Kobayashi S, Sakamoto J, Kimura S.** In vitro synthesis of cellulose and related polysaccharides Prog. Polym. Sci. 2001:26;1525-1560

6. **Klemm D, Heublein B, Fink HP, Bohn A.** Cellulose: Fascinating biopolymer and sustainable raw material. Angewandte Chemie - International Edition. 2005:44;3358–93.

7. **Marchessault RH, Sundararajan PR**. Cellulose. 1983.

8. **Aziz T, Farid A, Haq F, Kiran M, Ullah A, Zhang K, et al**. A Review on the Modification of Cellulose and Its Applications. Polymers. MDPI; 2022:14;3206

9. **Scheller HV, Ulvskov P.** Hemicelluloses. Annu Rev Plant Biol. 2010 Jun 2;61:263–89.

10. **Yang H, Yan R, Chen H, Lee DH, Zheng C**. Characteristics of hemicellulose, cellulose and lignin pyrolysis. Fuel. 2007 Aug;86(12–13):1781–8.

11. **Borrero-López AM, Valencia C, Franco JM**. Lignocellulosic Materials for the Production of Biofuels, Biochemicals and Biomaterials and Applications of Lignocellulose-Based Polyurethanes: A Review. Polymers. MDPI; 2022:14;881

12. **Lu Y, He Q, Fan G, Cheng Q, Song G**. Extraction and modification of hemicellulose from lignocellulosic biomass: A review. Green Processing and Synthesis. De Gruyter Open Ltd; 2021:10;779–804.

13. **Weerasooriya PRD, Nadhilah R, Owolabi FAT, Hashim R, Abdul Khalil HPS, Syahariza ZA, et al.** Exploring the properties of hemicellulose based carboxymethyl cellulose film as a potential green packaging. Current Research in Green and Sustainable Chemistry. 2020:1;1–2:20–8.

14. **Ebringerová A.** Structural diversity and application potential of hemicelluloses. In: Macromolecular Symposia. Wiley-VCH Verlag; 2005:232;1–12.

15. **Demuner IF, Colodette JL, Demuner AJ, Jardim CM**. Biorefinery Review: Wide-Reaching Products Through Kraft Lignin. BioResources. 2019:14(3);7543-7581.

16. **Zakzeski J, Bruijnincx PCA, Jongerius AL, Weckhuysen BM.** The catalytic valorization of lignin for the production of renewable chemicals. Chem Rev. 2010 Jun 9;110(6):3552–99.

17. **Mahmood N, Yuan Z, Schmidt J, Xu C**. Depolymerization of lignins and their applications for the preparation of polyols and rigid polyurethane foams: A review. Renewable and Sustainable Energy Reviews. Elsevier Ltd; 2016:60;317–29.

18. **Bussemaker M, Trokanas N, Koo L, Cecelja F.** Ontology Modelling for Lignocellulosic Biomass: Composition and Conversion. In: Computer Aided Chemical Engineering. Elsevier B.V.; 2018;1565–70.

19. **Mosier N, Wyman C, Dale B, Elander R, Lee YY, Holtzapple M, et al**. Features of promising technologies for pretreatment of lignocellulosic biomass. Bioresour Technol. 2005;96(6):673–86.

20. **Stuart E. Lebo Jr., Jerry D. Gargulak, Timothy J. McNally**. Lignin. Encyclopedia of Polymer Science and Technology.2001;3:100-124.

21. **Crestini C, Crucianelli M, Orlandi M, Saladino R**. Oxidative strategies in lignin chemistry: A new environmental friendly approach for the functionalisation of lignin and lignocellulosic fibers. Catal Today. 2010 Oct 25;156(1–2):8–22.

22. **Du X, Li J, Lindström ME**. Modification of industrial softwood kraft lignin using Mannich reaction with and without phenolation pretreatment. Ind Crops Prod. 2014 Jan;52:729–35.

23. **Wang X, Zhao J**. Encapsulation of the herbicide picloram by using polyelectrolyte biopolymers as layer-by-layer materials. J Agric Food Chem. 2013 Apr 24;61(16):3789–96.

24. **Chung YL, Olsson J V., Li RJ, Frank CW, Waymouth RM, Billington SL, et al.** A renewable lignin-lactide copolymer and application in biobased composites. ACS Sustain Chem Eng. 2013 Oct 7;1(10):1231–8.

25. **Stewart D.** Lignin as a base material for materials applications: Chemistry, application and economics. Ind Crops Prod. 2008 Mar;27(2):202–7.

26. **Yang D, Qiu X, Zhou M, Lou H**. Properties of sodium lignosulfonate as dispersant of coal water slurry. Energy Convers Manag. 2007 Sep;48(9):2433–8.

27. **Yang D, Qiu X, Pang Y, Zhou M.** Physicochemical properties of calcium lignosulfonate with different molecular weights as dispersant in aqueous suspension. J Dispers Sci Technol. 2008 Oct;29(9):1296–303.

28. **Nadányi R, Ház A, Lisý A, Jablonský M, Šurina I, Majová V, et al**. Lignin Modifications, Applications, and Possible Market Prices. Vol. 15, Energies. MDPI; 2022.

29. **Wu W, Li P, Huang L, Wei Y, Li J, Zhang L, et al**. The Role of Lignin Structure on Cellulase Adsorption and Enzymatic Hydrolysis. Biomass. 2023 Mar 1;3(1):96–107.

30. **Milczarek G, Inganäs O.** Renewable cathode materials from biopolymer/conjugated polymer interpenetrating networks. Science (1979). 2012 Mar 23;335(6075):1468–71.

31. **Nagaraju DH, Rebis T, Gabrielsson R, Elfwing A, Milczarek G, Inganäs O.** Charge storage capacity of renewable biopolymer/conjugated polymer interpenetrating networks enhanced by electroactive dopants. Adv Energy Mater. 2014 Jan;4(1).

32. **Caballero-Calero O, Díaz-Chao P, Abad B, Manzano C V., Ynsa MD, Romero JJ, et al**. Improvement of Bismuth Telluride electrodeposited films by the addition of Sodium Lignosulfonate. Electrochim Acta. 2014 Mar 20;123:117–26.

33. **Zakzeski J, Bruijnincx PCA, Jongerius AL, Weckhuysen BM.** The catalytic valorization of lignin for the production of renewable chemicals. Chem Rev. 2010 Jun 9;110(6):3552–99.

34. **Holladay JE, Bozell JJ, White JF, Johnson D.** Top Value-Added Chemicals from Biomass - Volume II—Results of Screening for Potential Candidates from Biorefinery Lignin. 2007.

35. **Chen C.L**. Methods in Lignin Chemistry. 1992:466-472.

36. **John F. Kadla, Hou-min Chang and Hasan Jameel.** The Reactions of Lignins with High Temperature Hydrogen Peroxide. Holzforschung. 1999:53;277–284

37. **Nimz H**. Beech Lignin-Proposal of a Constitutional Scheme. Angrw. Chrm. internat. Edit.1974:13(5);313-321.

38. **Ren H, Dai X, Zhai H, Liu Z, Omori S**. Comparison of bamboo native lignin and alkaline lignin modified by phase-separation method. Cellulose Chem. Technol. 2015:49 (5-6);429-438.

39. **Sameni J, Krigstin S, Sain M.** Acetylation & lignin solubility. Bioresources. 2017;12(1):1548–65.

40. **Sun J, Dutta T, Parthasarathi R, Kim KH, Tolic N, Chu RK, et al**. Rapid room temperature solubilization and depolymerization of polymeric lignin at high loadings. Green Chemistry. 2016;18(22):6012–20.

41. **Rashid T, Kait CF, Murugesan T**. Effect of Temperature on Molecular Weight Distribution of Pyridinium Acetate Treated Kraft Lignin. Procedia Eng . 2016;148:1363–8.

42. **Melro E, Alves L, Antunes FE, Medronho B.** A brief overview on lignin dissolution. J Mol Liq. 2018;265:578–84.

43. **Francisco M, Van Den Bruinhorst A, Kroon MC.** New natural and renewable low transition temperature mixtures (LTTMs): Screening as solvents for lignocellulosic biomass processing. Green Chemistry. 2012;14(8):2153–7.

44. **Lynam JG, Kumar N, Wong MJ**. Deep eutectic solvents' ability to solubilize lignin, cellulose, and hemicellulose; thermal stability; and density. Bioresour Technol. 2017;238:684–9.

45. **Teo WE, Ramakrishna S.** A review on electrospinning design and nanofibre assemblies. Nanotechnology. 2006;17(14).

46. **Garcia. Garcia. N.** Electrospinning: una técnica fascinante para la obtención de nanofibras poliméricas. Revista de plásticos modernos 2013:105;677.

47. **Duque Sánchez LM, Rodriguez L, López M**.. Electrospinning, Revista Iberoamericana de Polímeros Volumen. 2014;14:10.

48. **Cramariuc B, Cramariuc R, Scarlet R, Manea LR, Lupu IG, Cramariuc O**. Fiber diameter in electrospinning process. J Electrostat. 2013 Jun;71(3):189–98.

49. **Deitzel JM, Kleinmeyer J, Harris D, Tan NCB.** The effect of processing variables on the morphology of electrospun nanofibers and textiles Polymer 42 (2001) 261–272

50. **Zargham S, Bazgir S, Tavakoli A, Rashidi AS, Damerchely R.** The Effect of Flow Rate on Morphology and Deposition Area of Electrospun Nylon 6 Nanofiber. 2012;7(4):42-49.

51. **Morad MR, Rajabi A, Razavi M, Pejman Sereshkeh SR**. A Very Stable High Throughput Taylor Cone-jet in Electrohydrodynamics. Sci Rep. 2016 Dec 5;6.

52. **Hekmati AH, Rashidi A, Ghazisaeidi R,** Drean JY. Effect of needle length, electrospinning distance, and solution concentration on morphological properties of polyamide-6 electrospun nanowebs. Textile Research Journal. 2013;83(14):1452–66.

53. **Fong H, Chun I, Reneker DH.** Beaded nanofibers formed during electrospinning. Polymer 40 (1999) 4585–4592.

54. **Valizadeh A, Farkhani SM.** Electrospinning and electrospun nanofibres. IET Nanobiotechnol. 2014;8(2):83–92.

55. **Uyar T, Besenbacher F.** Electrospinning of uniform polystyrene fibers: The effect of solvent conductivity. Polymer (Guildf). 2008 Nov 10;49(24):5336–43.

57. **Wang SC, Wei TC, Chen W Bin, Tsao HK**. Effects of surfactant micelles on viscosity and conductivity of poly(ethylene glycol) solutions. Journal of Chemical Physics. 2004;120(10):4980–8.

58. **Li D, Xia Y**. Electrospinning of nanofibers: Reinventing the wheel? Vol. 16, Advanced Materials. 2004. p. 1151–70.

59. **Amariei N, Manea LR, Bertea AP, Cramariuc R, Bertea A, Cramariuc O.** Electrospinning Polyaniline for Sensors. Materials Science and Engineering 2017;209.

60. **Padilla-Gainza V, Morales G, Rodríguez-Tobías H, Lozano K**. Forcespinning technique for the production of poly(d,l-lactic acid) submicrometer fibers: Process–morphology–properties relationship. J Appl Polym Sci. 2019 Jun 10;136(22).

61. **Sarkar K, Gomez C, Zambrano S, Ramirez M, De Hoyos E, Vasquez H, et al.** Electrospinning to Forcespinning TM Open access under CC BY-NC-ND license. 2010;13.

62. **Raghavan B, Soto H, Lozano K.** Fabrication of Melt Spun Polypropylene Nanofibers by Forcespinning. Journal of Engineered Fibers and Fabrics.2013;8(1):52-60.

63. **Dallmeyer I, Ko F, Kadla JF.** Electrospinning of technical lignins for the production of fibrous networks. Journal of Wood Chemistry and Technology. 2010;30(4):315–29.

64. **Jia H, Sun N, Dirican M, Li Y, Chen C, Zhu P, et al**. Electrospun Kraft Lignin/Cellulose Acetate-Derived Nanocarbon Network as an Anode for High-Performance Sodium-Ion Batteries. ACS Appl Mater Interfaces. 2018;10(51):44368–75.

65. **Aslanzadeh S, Zhu Z, Luo Q, Ahvazi B, Boluk Y, Ayranci C.** Electrospinning of Colloidal Lignin in Poly(ethylene oxide) N,N-Dimethylformamide Solutions. Macromol Mater Eng. 2016;301(4):401–13.

66. **Klossner RR, Queen HA, Coughlin AJ, Krause WE**. Correlation of Chitosan's rheological properties and its ability to electrospin. Biomacromolecules. 2008 Oct;9(10):2947–53.

67. **Fang W, Yang S, Yuan TQ, Charlton A, Sun RC.** Effects of Various Surfactants on Alkali Lignin Electrospinning Ability and Spun Fibers. Ind Eng Chem Res. 2017;56(34):9551–9.

68. **Wang, S.-Q., He, J.-H., & Xu L.** Non-ionic surfactants for enhacing electrospinability and for the preparation of electrospun nanofibers. Polym Int. 2008;57(Jul):1079–82.

69. **Crabbe-Mann M, Tsaoulidis D, Parhizkar M, Edirisinghe M**. Ethyl cellulose, cellulose acetate and carboxymethyl cellulose microstructures prepared using electrohydrodynamics and green solvents. Cellulose. 2018;25(3):1687–703.

70. **Ago M, Okajima K, Jakes JE, Park S, Rojas OJ**. Lignin-based electrospun nanofibers reinforced with cellulose nanocrystals. Biomacromolecules. 2012 Mar 12;13(3):918–26.

71. **Ding B, Kim HY, Lee SC, Shao CL, Lee DR, Park SJ, et al.** Preparation and characterization of a nanoscale poly(vinyl alcohol) fiber aggregate produced by an electrospinning method. J Polym Sci B Polym Phys. 2002 Jul 1;40(13):1261–8.

72. **Koski A, Yim K, Shivkumar S.** Effect of molecular weight on fibrous PVA produced by electrospinning. Mater Lett. 2004 Jan;58(3–4):493–7.

73. **Tao J, Shivkumar S**. Molecular weight dependent structural regimes during the electrospinning of PVA. Mater Lett. 2007 May;61(11–12):2325–8.

74. **Setayesh S, Marsitzky D, Müllen K.** Nanostructured Fibers via Electrospinning** for additional scanning electron micro-scopy investigations. PLLA fibers. Macromolecules. 2000;13.

75. **Zong X, Kim K, Fang D, Ran S, Hsiao BS, Chu B**. Structure and process relationship of electrospun bioabsorbable nanofiber membranes. Polymer. 2002;43:4403–4412.

76. **Yamada H, Satoh M, Asoh H, Nakao M, Tamamura T, Rachel Caruso BA, et al.** Titanium Dioxide Tubes from Sol-Gel Coating of Electrospun Polymer Fibers. Phys. Status Solidi A. Plenum Press; 1997;79.

77. **Son WK, Youk JH, Lee TS, Park WH.** The effects of solution properties and polyelectrolyte on electrospinning of ultrafine poly(ethylene oxide) fibers. Polymer (Guildf). 2004;45(9):2959–66.

78. **Jacobs V, Anandjiwala RD, Maaza M**. The influence of electrospinning parameters on the structural morphology and diameter of electrospun nanofibers. J Appl Polym Sci. 2010 Mar 5;115(5):3130–6.

79. **Utkarsh, Hegab H, Tariq M, Syed NA, Rizvi G, Pop-Iliev R**. Towards Analysis and Optimization of Electrospun PVP (Polyvinylpyrrolidone) Nanofibers. Advances in Polymer Technology. 2020 May 4;2020:1–9.

80. **Nasouri K, Shoushtari AM, Mojtahedi MRM.** Evaluation of effective electrospinning parameters controlling polyvinylpyrrolidone nanofibers surface morphology via response surface methodology. Fibers and Polymers. 2015 Sep 1;16(9):1941–54.

81. **Tungprapa S, Puangparn T, Weerasombut M, Jangchud I, Fakum P, Semongkhol S, et al.** Electrospun cellulose acetate fibers: Effect of solvent system on morphology and fiber diameter. Cellulose. 2007 Dec;14(6):563–75.

82. **Croisier F, Duwez AS, Jérôme C, Léonard AF, Van Der Werf KO, Dijkstra PJ, et al**. Mechanical testing of electrospun PCL fibers. Acta Biomater. 2012;8(1):218–24.

83. **Mochane MJ, Motsoeneng TS, Sadiku ER, Mokhena TC, Sefadi JS.** Morphology and properties of electrospun PCL and its composites for medical applications: A mini review. Applied Sciences (Switzerland). MDPI AG; 2019;9.

84. **Poursorkhabi V, Mohanty AK, Misra M.** Electrospinning of aqueous lignin/poly(ethylene oxide) complexes. J Appl Polym Sci. 2015;132(2):1–9.

85. **Aslanzadeh S, Ahvazi B, Boluk Y, Ayranci C.** Morphologies of electrospun fibers of lignin in poly(ethylene oxide)/N,N-dimethylformamide. J Appl Polym Sci. 2016;133(44).

86. **Schreiber M, Vivekanandhan S, Mohanty AK, Misra M.** A study on the electrospinning behaviour and nanofibre morphology of anionically charged lignin. Adv Mater Lett. 2012;3(6):476–80.

87. **Dallmeyer I, Ko F, Kadla JF**. Correlation of elongational fluid properties to fiber diameter in electrospinning of softwood kraft lignin solutions. Ind Eng Chem Res. 2014 Feb 19;53(7):2697–705.

88. **Lai C, Zhou Z, Zhang L, Wang X, Zhou Q, Zhao Y, et al.** Free-standing and mechanically flexible mats consisting of electrospun carbon nanofibers made from a natural product of alkali lignin as binder-free electrodes for high-performance supercapacitors. J Power Sources. 2014;247:134–41.

89. **Gao G, Dallmeyer JI, Kadla JF.** Synthesis of lignin nanofibers with ionic-responsive shells: Water-expandable lignin-based nanofibrous mats. Biomacromolecules. 2012 Nov 13;13(11):3602–10.

90. **Kai D, Chong HM, Chow LP, Jiang L, Lin Q, Zhang K, et al**. Strong and biocompatible lignin /poly (3-hydroxybutyrate) composite nanofibers. Compos Sci Technol. 2018 Apr 12;158:26–33.

91. **Wang J, Tian L, Luo B, Ramakrishna S, Kai D, Loh XJ, et al.** Engineering PCL/lignin nanofibers as an antioxidant scaffold for the growth of neuron and Schwann cell. Colloids Surf B Biointerfaces. 2018 Sep 1;169:356–65.

92. **Kai D, Zhang K, Jiang L, Wong HZ, Li Z, Zhang Z, et al.** Sustainable and Antioxidant Lignin-Polyester Copolymers and Nanofibers for Potential Healthcare Applications. ACS Sustain Chem Eng. 2017;5(7):6016–25.

93. **Kai D, Ren W, Tian L, Chee PL, Liu Y, Ramakrishna S, et al**. Engineering Poly(lactide)-Lignin Nanofibers with Antioxidant Activity for Biomedical Application. ACS Sustain Chem Eng. 2016 Oct 3;4(10):5268–76.

94. **Adhvaryu A, Erhan SZ**. Epoxidized soybean oil as a potential source of high-temperature lubricants. Ind Crops Prod. 2002;15(3):247–54.

95. **Franco JM, Delgado MA, Valencia C, Sánchez MC, Gallegos C.** Mixing rheometry for studying the manufacture of lubricating greases. Chem Eng Sci. 2005;60(8-9 SPEC. ISS.):2409–18.

96. **Sánchez MC, Franco JM, Valencia C, Gallegos C, Urquiola F, Urchegui R**. Atomic force microscopy and thermo-rheological characterisation of lubricating greases. Tribol Lett. 2011 Feb;41(2):463–70.

97. **Saidur R, Abdelaziz EA, Demirbas A, Hossain MS, Mekhilef S.** A review on biomass as a fuel for boilers. Vol. 15, Renewable and Sustainable Energy Reviews. 2011. p. 2262–89.

98. **Soni S, Agarwal M.** Lubricants from renewable energy sources – a review. Green Chem Lett Rev. 2014;7(4):359–82.

99. **Panchal TM, Patel A, Chauhan DD, Thomas M, Patel J V.** A methodological review on bio-lubricants from vegetable oil based resources. Renewable and Sustainable Energy Reviews. 2017;70(August 2016):65–70.

100. **Salimon J, Salih N, Yousif E.** Biolubricants: Raw materials, chemical modifications and environmental benefits. European Journal of Lipid Science and Technology. 2010:112;519–30.

101. **Gallego R, Cidade T, Sánchez R, Valencia C, Franco JM.** Tribological behaviour of novel chemically modified biopolymer-thickened lubricating greases investigated in a steel-steel rotating ball-on-three plates tribology cell. Tribol Int. 2016 Feb 1;94:652–60.

102. **Sánchez R, Franco JM, Delgado MA, Valencia C, Gallegos C**. Rheological and mechanical properties of oleogels based on castor oil and cellulosic derivatives potentially applicable as bio-lubricating greases: Influence of cellulosic derivatives concentration ratio. Journal of Industrial and Engineering Chemistry. 2011 Jul 25;17(4):705–11.

103. **Martín-alfonso JE, Valencia C.** Tribology International of oleogels based on EVA copolymer and vegetables oils for lubricant applications. Tribiology International. 2015;90:426–34.

104. **Franco JM**. Applied Clay Science Tunable rheological-tribological performance of " green " gel-like dispersions based on sepiolite and castor oil for lubricant applications. Appl Clay Sci. 2020;192(April):105632.

105. **Delgado MA, Quinchia LA, Spikes HA, Gallegos C**. Suitability of ethyl cellulose as multifunctional additive for blends of vegetable oil-based lubricants.

106. **González M, Gallego R, Romero MA, González-delgado JA, Arteaga JF, Valencia C, et al.** Impact of natural sources-derived antioxidants on the oxidative stability and rheological properties of castor oil based-lubricating greases. Ind Crops Prod. 2016;87:297–303.

107. **Adhvaryu A, Sung C, Erhan SZ.** Fatty acids and antioxidant effects on grease microstructures. Ind Crops Prod. 2005 May;21(3):285–91.

108. **Delgado MA, Cortés-Triviño E, Valencia C, Franco JM**. Tribological study of epoxide-functionalized alkali lignin-based gel-like biogreases. Tribol Int. 2020;146(January).

109. **Cortés-Triviño E, Valencia C, Delgado MA, Franco JM.** Thermo-rheological and tribological properties of novel bio-lubricating greases thickened with epoxidized lignocellulosic materials. Journal of Industrial and Engineering Chemistry. 2019 Dec 25;80:626–32.

110. **Sánchez R, Franco JM, Delgado MA, Valencia C, Gallegos C.** Development of new green lubricating grease formulations based on cellulosic derivatives and castor oil. Green Chemistry. 2009;11(5):686–69.

111. **Sánchez R, Fiedler M, Kuhn E, Franco JM**. Tribological characterization of green lubricating greases formulated with castor oil and different biogenic thickener agents: A comparative experimental study. Industrial Lubrication and Tribology. 2011;63(6):446–52.

112. **Sánchez R, Franco JM, Delgado MA, Valencia C, Gallegos C**. Effect of thermo-mechanical processing on the rheology of oleogels potentially applicable as biodegradable lubricating greases. Chemical Engineering Research and Design. 2008;86(10):1073–82.

113. **Núñez N, Martín-Alfonso JE, Valencia C, Sánchez MC, Franco JM**. Rheology of new green lubricating grease formulations containing cellulose pulp and its methylated derivative as thickener agents. Ind Crops Prod. 2012;37(1):500–7.

114. **Gallego R, González M, Arteaga JF, Valencia C, Franco JM**. Influence of functionalization degree on the rheological properties of isocyanate-functionalized chitin- and chitosan-based chemical oleogels for lubricant applications. Polymers (Basel). 2014;6(7):1929–47.

115. **Gallego R, Arteaga JF, Valencia C, Franco JM.** Isocyanate-functionalized chitin and chitosan as gelling agents of castor oil. Molecules. 2013 Jun;18(6):6532–49.

116. **Sánchez R, Stringari GB, Franco JM, Valencia C, Gallegos C**. Use of chitin, chitosan and acylated derivatives as thickener agents of vegetable oils for bio-lubricant applications. Carbohydr Polym. 2011;85(3):705–14.

117. **Delgado MA, Sánchez MC, Valencia C, Franco JM, Gallegos C**. Relationship among microstructure, rheology and processing of a lithium lubricating grease. Chemical Engineering Research and Design. 2005;83(9 A):1085–92.

118. **Delgado MA, Valencia C, Sánchez MC, Franco JM, Gallegos C.** Influence of soap concentration and oil viscosity on the rheology and microstructure of lubricating greases. Ind Eng Chem Res. 2006;45(6):1902–10.

119. **Madiedo JM, Franco JM, Valencia C, Gallegos C.** Modeling of the non-linear rheological bahavior of a lubricating grease at low-shear rates. J Tribol. 2000;122(3):590–6.

120. **Sánchez R, Franco JM, Delgado MA, Valencia C, Gallegos C**. Thermal and mechanical characterization of cellulosic derivatives-based oleogels potentially applicable as bio-lubricating greases: Influence of ethyl cellulose molecular weight. Carbohydr Polym. 2011;83(1):151–8.

121. **Chan CH, Tang SW, Mohd NK, Lim WH, Yeong SK, Idris Z**. Tribological behavior of biolubricant base stocks and additives. Renewable and Sustainable Energy Reviews. Elsevier Ltd; 2018:93;145–57.

122. **D. Dowson et al.** Understanding grease lubrication. The Third Body Concept. 1996; 573-581.

123. **Couronné I, Vergne P, Mazuyer D, Truong-Dinh N, Girodin D**. Effects of grease composition and structure on film thickness in rolling contact. Tribology Transactions. 2003 Jan 1;46(1):31–6.

124. **Delgado MA, Franco JM, Valencia C, Kuhn E, Gallegos C**. Transient shear flow of model lithium lubricating greases. Mech Time Depend Mater. 2009 Mar;13(1):63–80.

Chapter 3: Material and Methods

1. MATERIALS

1.1. Polymers

1.1.1. Low sulfonate kraft lignin

A commercial low sulfonate alkali lignin from the Kraft process was used as raw material in the production of electrospun nanostructures. The generic chemical structure of this compound, which was provided by Sigma Aldrich in powder form, is shown in Figure 26.

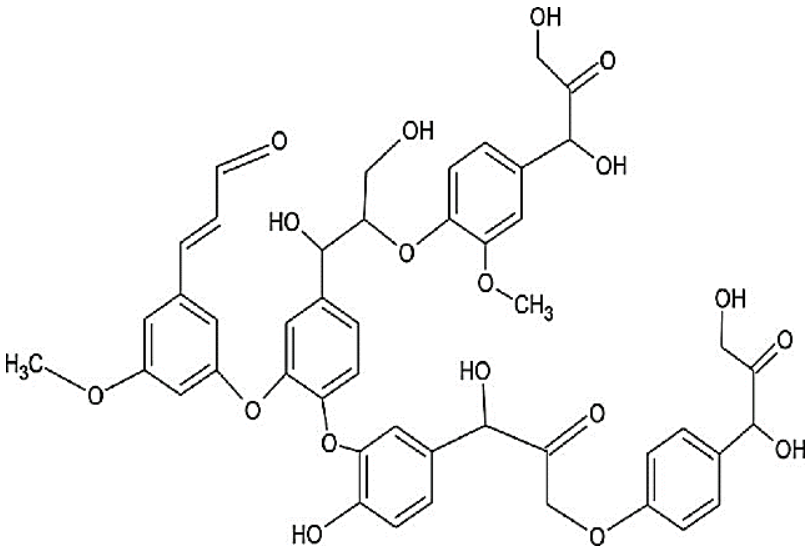

Figure 26. A structural model of a technical kraft lignin fragment (1)

1.1.2. Polyvinylpyrrolidone

Polyvinylpyrrolidone (PVP) is a stable, bulky, non-ionic, non-toxic and biocompatible polymer. It is dissolved together with lignin, as co-spinning polymer, to facilitate the production of nanofibers through electrospinning. Its chemical structure can be observed in Figure 27.

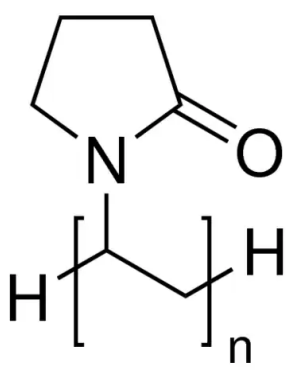

Figure 27. Structure of polyvinylpyrrolidone (Sigma-Adrich)

1.1.3. Ethyl cellulose

Ethyl cellulose (EC) is a linear polysaccharide derived from cellulose. It was used in this study singly to produce EC nanofibers and as a co-spinning polymer to improve the electrospinnability of lignin. The chemical structure of this biopolymer, supplied by Sigma Aldrich, is shown in Figure 28.

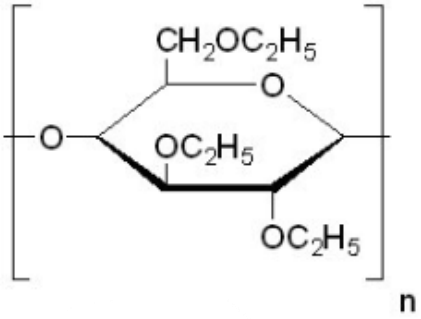

Figure 28. Structure of ethylcellulose (2)

1.2. Surfactants

Surfactants are amphiphilic organic compounds consisting of two parts, a hydrophilic head part with affinity to polar phases and a hydrophobic group attracted to non-polar phases. Due to their unique structure they can be used to reduce the surface

tension in solutions and the interfacial tension between two phases. The main classification is based on the charge of the polar head group, which divide surfactants into anionic, cationic, nonionic and zwitterionic. The latter contain both ionic and cationic charges under normal conditions.

In this work, they have been used as co-assistants to help to reduce the surface tension of the polymeric solutions. The following surfactants were employed, all of them obtained from Sigma Aldrich:

- Sodium dodecylsulphate or sodium lauryl sulphate (SDS), anionic surfactant.

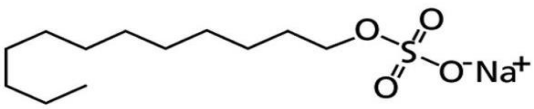

Figure 29. SDS structure

- Hexadecyltrimethylammonium bromide (CTAB), which is a quaternary ammonium salt and a cationic surfactant.

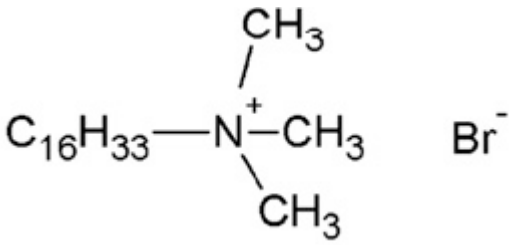

Figure 30. CTAB structure

- Tween-20 or polysorbate 20 or polyoxyethylene(20)sorbitan monolaurate, non-ionic surfactant.

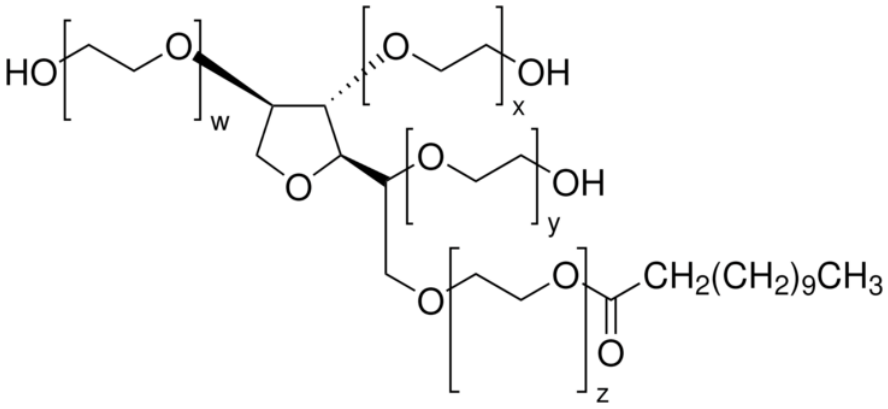

Figure 31. Tween-20 structure.

1.3. Solvents

The organic solvents used to prepare the polymeric solutions used as feed flow in the electrospinning device were dimethylformamide (DMF) (purity ≥ 99.8%), acetone (purity 99.5%), dimethylacetamide (DMAc) (purity 99.8%), tetrahydrofuran (THF) (purity 99.0%) and acetic acid (purity ≥ 99.0%).

1.4. Vegetable oil

Castor oil, supplied by Guinama (Valencia, Spain), was selected as biodegradable lubricating base oil. It is mainly composed of glycerol triricinoleate, i.e., esters of 12-hydroxy-9-octadecenoic (ricinoleic acid) and other minority fatty acids. The predominant chemical structure and fatty acid profile can be seen in Table 13, respectively. Castor oil is characterized by the existence of three different functionality points, such as carboxyl groups, the single point of unsaturation and the hydroxyl groups, making it suitable for many chemical reactions and modifications (3). Moreover, the presence of hydroxyl groups with their corresponding hydrogen bridges, provides it exceptional viscosity

properties thus favouring the reduction of friction in a tribological contact, in comparison with other vegetable oils (3,4).

Table 13. Fatty acids compositions of castor oil (5)

Fatty Acid	***Concentration (%)***
Mystiric C14:0	Trace
Palmitic C16:9	1.70
Palmitoleic C16:1	Trace
Stearic C18:0	1.96
Oleic C18:1	5.34
Ricinoleic C18:1:OH	82.48
Linoleic C18:2	7.01
Linoleic C18:3	1.51
Arachidic C20:0	Trace
Lignoceric C24:0	Trace
Saturated	3.66
Monounsaturated	87.82
Polyunsaturated	8.52

2. EXPERIMENTAL METHODS

A general description of the experimental methods followed is given below. More detailed information on the specific procedures is given in chapter 4, in each of the articles included.

2.1. Preparation of polymer solutions

The polymer was added to the selected solvent and stirred magnetically (Heidolph), for a period between 2 and 24 hours at room temperature or at 50ºC. Solutions then underwent centrifugation at 3000 rpm for 10 minutes and filtration to remove any solids.

2.2. Preparation of electrospun nanostructures

The Star-Up Lab Device V2.1 (Star-Up Advanced) from Doxa Microfluids is used as an electrospinning device to obtain the nanofibers from the different polymeric solutions. The electrospinning chamber includes:

- A high voltage power supply (-30 kV to 30 kV)
- A 200x200 mm stainless steel flat-plate collector. This can be placed either vertically or horizontally.
- Two feeding pumps with B-D 10 cc syringes and the corresponding capillary tubes in order to inject the solution.
- Taylor cone visualisation system.
- Gas extraction system.

The following process parameters were applied:

Table 14. Process Parameters

Layout	Flow rate	Voltage	Collector-needle distance	Needle
Vertical Horizontal	0.5-3 ml/h	5-21 kV	12-20 cm	Syringe: 5ml, 11.99 mm internal diameter, 20G flat-tip needle

Figure 32. Doxa Microfluids electrospinning equipment

2.3. Preparation of oleo-dispersions

The electrospun polymer nanofibers were dispersed in castor oil in an open vessel using a controlled rotational speed mixing device (RW 20, Ika) equipped with an anchor impeller. The mixture was stirred at 70 rpm for at least 24 hours at room temperature.

3. Characterization techniques

3.1. Characterization of polymer solutions

Physico-chemical characterization:

The physicochemical characterization of the lignin-co-spinning polymer solutions included electrical conductivity, surface tension and shear and extensional viscosity measurements.

The electrical conductivity measurements were conducted using two conductivity meters, a Crison multi-frequency (1000-5000 Hz) conductivity meter (GLP 31), and a Laqua PC-110 conductivity meter with a LAQUA 3553-10D cell (Horiba Scientific). Prior to use, both conductivity meters were calibrated with standard KCL solutions (1413 μS/cm and 12.88 μS/cm).

Surface tension data were obtained with a Sigma 703D tensiometer (Biolin Scientific) using a Wilhelmy platinum plate with a measuring range of 1-1000 mN/m, all measurements at 25°C.

Figure 33. Sigma 703D tensiometer.

Flow curves of the spinning solutions were obtained in a shear range of 1-500 s^{-1}, using an ARES (Rheometric Scientific) controlled shear rate rheometer with a Couette geometry (inner radius 16 mm, outer radius 17 mm, cylinder height 33.35 mm).

Figure 34. Controlled shear rate rheometer ARES

The extensional viscosity of spinning solutions was evaluated in a capillary breakup extensional rheometer (CaBER, ThermoHaake). The filament was created by placing the solution between two parallel plates (6 mm diameter) and causing a sudden plate-to-plate separation from 1.5 to 15 mm in 10 ms. The extensional rheological properties were obtained from the evolution of the filament diameter, *D*, over time. The extensional viscosity can be quantified as follows:

$$\mu_{ext} = \frac{\sigma}{\left(-\frac{dD(t)}{dt}\right)} \quad (1)$$

being σ the surface tension.

Figure 35. CaBER rheometer

3.2. Characterization of oleo-dispersions

Rheological characterization

In order to obtain the viscoelastic response of the processed lubricating greases, oscillatory shear (SAOS) tests were performed using a RheoScope controlled stress

rheometer (ThermoHaake, Germany) equipped with a thermostatic bath at 25 °C, using roughened plate-plate geometries (25 and 35 mm diameter) to avoid slip effects. First, a stress sweep was performed at 1 Hz to determine the linear viscoelastic range. Once the extension of the viscoelastic zone was determined, frequency sweeps were carried out to determine the evolution of the viscoelastic functions with frequency, in a range from 10^{-3} to 10^{3} rad/s.

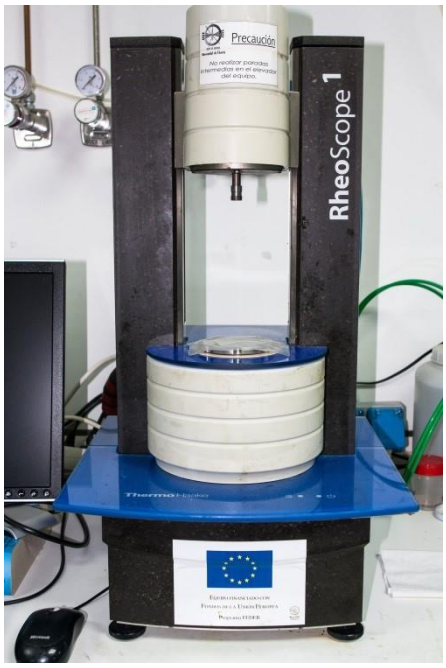

Figure 36. Rheoscope Controlled Strain Rheometer (ThermoHaake).

Temperature sweep tests were carried out in order to analyze the thermorheological response of selected samples, using ARES (Rheometrics Scientific, Great Britain) and Physica MCR 501 (Anton Paar, Austria) rheometers, in a temperature range between 25ºC and 125ºC. A forced air convection oven and a Peltier temperature controller were used for controlling temperature, respectively. A first heating stage from 25ºC to 125ºC, a second cooling stage and another heating stage were carried out to evaluate the thermo-reversibility of the microstructural networks.

Figure 37. ARES II Controlled Deformation Rheometer

Tribological characterization

Tribological measurements were carried out in the Physica MCR-501 rheometer (Anton Para, Austria) equipped with a tribological cell, consisting of a 6.35 mm diameter metal ball rotating on three 45° rectangular steel plates on which the oleo-dispersions were spread acting as lubricants. A constant normal load and a rotational speed of 30 N and 10 min^{-1}, respectively, were applied. The wear marks produced on the steel plates were analyzed by Olympus BX51 optical microscopy.

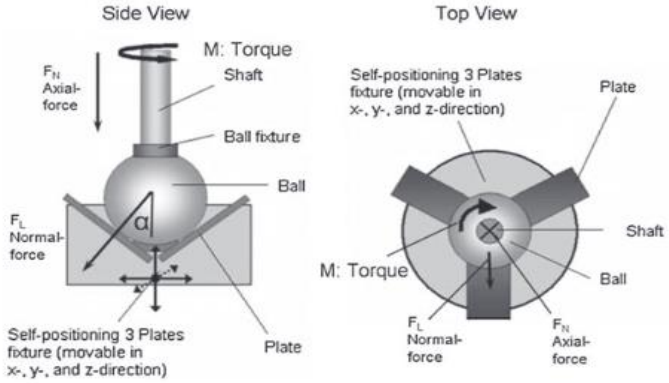

Figure. 38.Schematic set-up tribology accessory in side and top views. Torque and normal force applied by the rheometer are indicated by arrows

An Olympus BX51 optical microscope was used, with different magnification lenses: 10x, 20x and 50x, coupled to an Olympus Camedia C-5050ZOOM digital camera, a JVC TKC1281B colour video camera and the Linkam Cryo-CSS450 and Linkam LTS350 systems. The steel plates were placed on the sample holder and photographs were taken at different magnifications, which allowed us to observe the wear marks caused in the tribological tests.

Figure 39. Interferometer Zygo neoview

Figure 40. Olympus BX51 Optical Microscope

On the other hand, the tribological performance of some greases was investigated on a ball-on-disk CSM nanotribometer (Peseux, Switzerland). The equipment basically consists of a static ball, fixed to a cantilever to prevent it from rolling, and a moving disc which is put under tension by applying a normal force. A fiber optic sensor measures the deflection of the cantilever in the radial direction to determine the friction force. Tests were performed in rotational mode by applying a speed of 40 mm-s-1 on steel-steel (115CrV3 hardness 22.72 HRC) ball-on-disc, using a 1 mm diameter ball. Three normal loads (400, 700 and 900 mN, corresponding to Hertzian pressures 1.60, 1.93 and 2.10 GPa, respectively) were applied for 20 minutes. Each test was repeated ten times on the same track at room temperature (21 ± 1ºC). The dimensions of the wear grooves of the steel discs created after the ten tests were quantified using the white light interferometry technique, using a Zygo Nexview device (Middlefield, OH, USA) and Zygo Mx software. The wear volume values given below correspond to a groove length of 100 μm.

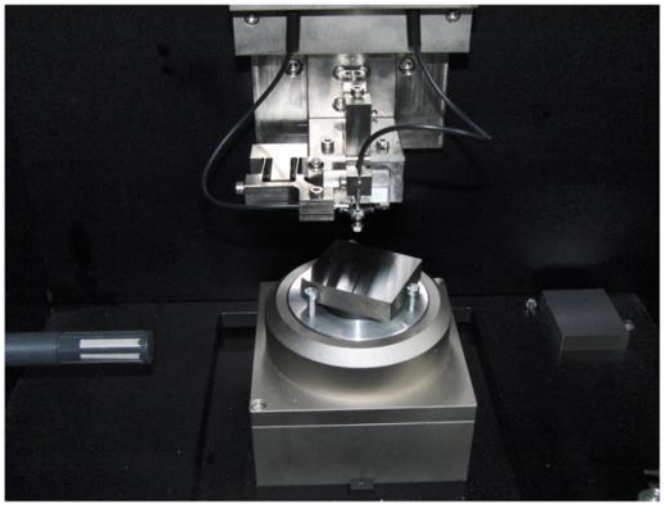

Figure 41. CSM nanotribometer.

3.3. Characterization of electrospun nanofibers.

Scanning electron microscopy SEM

Scanning electron microscopy (SEM) was used to study the morphology of the electrospun nanostructures, using a scanning electron microscope, model JSM-5410 (Jeol, Japan). Porosity and diameter measurements were analyzed with the help of the ImageJ software.

Figure 42. Scanning Electron Microscope JSM-5410

Thermogravimetry analysis (TGA).

TGA was used to characterize the composition and thermal stability of selected electrospun nanostructures. Measurements were performed with a thermogravimetric balance model TGA-Q50 (TA Instrument Waters, USA). 10-15 mg of samples was weighted, and the heating rate applied in each experiment was 10°C/min, in a temperature range from 35 to 600°C, using a nitrogen atmosphere with a total flow rate of 100 ml min^{-1}.

Figure 43. Thermogravimetric balance TGA model Q50

4. References

1. **Mahmood Z, Yameen M, Jahangeer M, Riaz M, Ghaffar A, Javid I.** Lignin as natural antioxidant capacity. Lignin-Trends and Applications; 2018:8;181-206.

2. **Khan SA, Ahmad M, Aamir MN.** Study of Nimesulide Release From Ethylcellulose Microparticles and Drug-Polymer Compatibility Analysis. Latin american journal of pharmacy. 2010.

3. **Ogunniyi DS**. Castor oil: A vital industrial raw material. Bioresource Technology. 2006:97;1086–91.

4. **Boyde S**. Green lubricants. Environmental benefits and impacts of lubrication. Green Chemistry. Royal Society of Chemistry; 2002:4;293–307.

5. **Quinchia LA, Delgado MA, Valencia C, Franco JM, Gallegos C**. Viscosity modification of different vegetable oils with EVA copolymer for lubricant applications. Ind Crops Prod. 2010 Nov;32(3):607–12.

Chapter 4: Results and discussion

Chapter 4. Results & discussions. Compendium of publications.

Debido a restricciones relativas a derechos de autor, el artículo "Electrospun lignin-PVP nanofibers and their ability for structuring oil" ha sido retirado de la tesis. En sustitución del mismo ofrecemos la siguiente información: referencia bibliográfica, enlace a la revista y resumen.

-Borrego, M., Martín-Alfonso, J. E., Sánchez, M. C., Valencia, C., & Franco, J. M. (2021). Electrospun lignin-PVP nanofibers and their ability for structuring oil. In International Journal of Biological Macromolecules (Vol. 180, pp. 212–221). Elsevier BV. https://doi.org/10.1016/j.ijbiomac.2021.03.069

Enlace al texto completo: https://doi.org/10.1016/j.ijbiomac.2021.03.069

RESUMEN:

This work explores the electrospinnability of low-sulfonate Kraft lignin (LSL)/polyvinylpyrrolidone (PVP) solutions in *N*,*N*-dimethylformamide (DMF) and the ability of the different micro- and nano-architectures generated to structure castor oil. LSL/PVP solutions were prepared at different concentrations (8–15 wt%) and LSL:PVP ratios (90:10–0:100) and physico-chemically and rheologically characterized. The morphology of electrospun nanostructures mainly depends on the rheological properties of the solution. Electrosprayed nanoparticles or micro-sized particles connected by thin filaments were obtained from solutions with low LSL/PVP concentrations and/or high LSL:PVP ratios, whereas beaded or bead-free nanofibers were produced by increasing concentration and/or decreasing LSL:PVP ratio, due to enhanced extensional viscoelastic properties and non-Newtonian characteristics. Electrospun LSL/PVP nanofibers are able to form oleogels by simply dispersing them into castor oil at concentrations between 10 and 30 wt%. The rheological properties of the oleogels may be tailored by modifying the LSL:PVP ratio and nanofibers content. The potential application of these oleogels as bio-based lubricants was also explored in a tribological cell. Satisfactory friction and wear results are achieved when using oleogels structured by nanofibers mats with enhanced gel-like properties as lubricants. Overall, electrospinning of lignin/PVP solutions can be proposed as a simple and effective method to produce nanofibers for oil structuring.

1. COMPENDIUM OF PUBLICATIONS

Block 1: Development of lignin-PVP nanofibers by electrospinning and their ability for structuring oil.

- Article 1. Electrospun lignin-PVP nanofibers and their ability for structuring oil.
- Article 2. Influence of surfactants on the electrospinnability of lignin-PVP solutions and subsequent oil structuring properties of nanofiber mats.

Block 2: Development of ethyl cellulose and ethyl cellulose-lignin nanofibers by electrospinning and their ability for structuring oil.

- Article 3. Developing electrospun ethyl cellulose nanofibrous webs: an alternative approach for structuring castor oil.
- Article 4. Impact of the morphology of electrospun lignin ethyl cellulose nanostructures of their capacity to thicken castor oil.

Block 3: Tribological characterization of bio-based lubricating greases thickened with electrospun nanofibers.

- Article 5. Experimental investigation on the friction and wear performance of model bio-based lubricating greases thickened with electrospun lignin nanofibrous webs.

2. ARTICLE 1

Electrospun lignin-PVP nanofibers and their ability for structuring oil

María Borrego, José E. Martín-Alfonso, M. Carmen Sánchez, Concepción Valencia, José M. Franco *

* Pro2TecS – Chemical Product and Process Technology Research Center, Department of Chemical Engineering and Materials Science, Universidad de Huelva, ETSI, Campus de "El Carmen", 21071, Huelva, Spain.

Published in:

Publishing company: Elsevier

Editor-in-Chief: John F. Kennedy

Volume 180, Issue 1, pp 212-221

Year: 2021

ISSN: 0141-8130

DOI: 10.1016/j.ijbiomac.2021.03.069

Impact factor (2022): 8.2

JCR Journal rank: 7/73 in Applied Chemistry; 5/86 in Polymer Science

Chapter 4. Results & discussions. Compendium of publications.

Debido a restricciones relativas a derechos de autor, el artículo "Electrospun lignin-PVP nanofibers and their ability for structuring oil" ha sido retirado de la tesis. En sustitución del mismo ofrecemos la siguiente información: referencia bibliográfica, enlace a la revista y resumen.

-Borrego, M., Martín-Alfonso, J. E., Sánchez, M. C., Valencia, C., & Franco, J. M. (2021). Electrospun lignin-PVP nanofibers and their ability for structuring oil. In International Journal of Biological Macromolecules (Vol. 180, pp. 212–221). Elsevier BV. https://doi.org/10.1016/j.ijbiomac.2021.03.069

Enlace al texto completo: https://doi.org/10.1016/j.ijbiomac.2021.03.069

RESUMEN:

This work explores the electrospinnability of low-sulfonate Kraft lignin (LSL)/polyvinylpyrrolidone (PVP) solutions in *N*,*N*-dimethylformamide (DMF) and the ability of the different micro- and nano-architectures generated to structure castor oil. LSL/PVP solutions were prepared at different concentrations (8–15 wt%) and LSL:PVP ratios (90:10–0:100) and physico-chemically and rheologically characterized. The morphology of electrospun nanostructures mainly depends on the rheological properties of the solution. Electrosprayed nanoparticles or micro-sized particles connected by thin filaments were obtained from solutions with low LSL/PVP concentrations and/or high LSL:PVP ratios, whereas beaded or bead-free nanofibers were produced by increasing concentration and/or decreasing LSL:PVP ratio, due to enhanced extensional viscoelastic properties and non-Newtonian characteristics. Electrospun LSL/PVP nanofibers are able to form oleogels by simply dispersing them into castor oil at concentrations between 10 and 30 wt%. The rheological properties of the oleogels may be tailored by modifying the LSL:PVP ratio and nanofibers content. The potential application of these oleogels as bio-based lubricants was also explored in a tribological cell. Satisfactory friction and wear results are achieved when using oleogels structured by nanofibers mats with enhanced gel-like properties as lubricants. Overall, electrospinning of lignin/PVP solutions can be proposed as a simple and effective method to produce nanofibers for oil structuring.

2.1. Resumen

En este trabajo se explora la electrospinabilidad de disoluciones de lignina de bajo contenido en sulfonato (LSL) dopadas con polinivilpirrolidona (PVP). Las disoluciones utilizadas cómo alimentación se caracterizaron reológica y fisicoquímicamente con el fin de encontrar una relación con su electrospinabilidad.

Las membranas desarrolladas se dispersaron en aceite de ricino con el fin de observar su capacidad cómo agente espesante de medios oleosos para desarrollar lubricantes biodegradables, y se estudiaron sus propiedades reológicas y tribológicas.

Se prepararon disoluciones poliméricas LSL:PVP de relaciones en peso comprendidas entre 90:10 y 0:100 (p/p), a diferentes concentraciones (8-15 %). La inclusión de lignina aumenta la tensión superficial de las disoluciones y confiere una mayor conductividad eléctrica debido al carácter polar de la lignina. En cuanto a las propiedades reológicas, tanto las disoluciones al 8 cómo al 10% exhiben un comportamiento Newtoniano con menor viscosidad a medida que aumenta el contenido de LSL. Esto se debe a la presencia de monolignoles aromáticos presentes en la estructura de la lignina que forman estructuras compactas y rígidas que complican el desarrollo de enlaces físicos. Por el contrario, un aumento de concentración de la disolución (15 %wt) y la disminución de la relación en peso LSL:PVP producen una respuesta no-Newtoniana descrita por el modelo Williamson.

En cuanto a la reología extensional las disoluciones de menor viscosidad (8% y 90:10 LSL:PVP relación en peso del 10%) no presentaron características extensionales. En los demás sistemas se observó una evolución lineal de adelgazamiento del filamento similar a los fluidos newtonianos y un decaimiento exponencial del diámetro del filamento, típico de fluidos viscoelásticos, cuanto mayor era la presencia de PVP. Por otra

parte, mayores tiempos de relajación y de viscosidad extensional se encontraron al incrementar la concentración de la disolución, lo cual coincide con los sistemas de comportamiento no-newtoniano.

Se analizó la morfología de las membranas desarrolladas mediante SEM. Se pudo observar una transición morfológica desde micro-partículas conectadas por filamentos a membranas homogéneas de nanofibras con la disminución de la relación en peso LSL:PVP y el aumento de la concentración, aumentando a su vez el diámetro de las nanofibras.

Las diferentes nanofibras se dispersaron en aceite de ricino desde el 10 al 30 % p/p de espesante. Las membranas formadas predominantemente por partículas dieron lugar a dispersiones inestables en las que se separaron las fases inmediatamente. Por el contrario, membranas homogéneas con nanofibras uniformes dieron lugar a oleogeles estables capaces de atrapar el aceite favorablemente, mejorando la interacción aceite-espesante. En cuanto a sus propiedades reológicas, éstas dieron lugar a oleogeles más consistentes, con funciones viscoelásticas dinámicas que varían con la frecuencia conforme a un comportamiento típico de geles. Por otra parte, las funciones viscoelásticas pudieron modularse en función del tipo de nanoestructura.

Con el fin de determinar una posible aplicación industrial se evaluó el rendimiento tribológico. Se obtuvieron valores satisfactorios de fricción y desgaste, similares o inferiores a los de las grasas convencionales. Las diferencias encontradas en las propiedades tribológicas dependen claramente de la morfología de las nanofibras. Nanofibras bien desarrolladas y uniformes favorecen la retención del aceite y son capaces de penetrar en el lubricante. En cambio, oleogeles más blandos constituidos por partículas

tienen más dificultades para penetrar en el contacto, favoreciendo el desgaste de las superficies lubricadas y la fricción.

3. ARTICLE 2

Influence of surfactants on the electrospinnability of lignin-PVP solutions and subsequent oil structuring properties of nanofiber mats

María Borrego, José E. Martín-Alfonso, M. Carmen Sánchez, Concepción Valencia, José M. Franco *

* Pro2TecS – Chemical Product and Process Technology Research Center, Department of Chemical Engineering and Materials Science, Universidad de Huelva, ETSI, Campus de "El Carmen", 21071, Huelva, Spain.

Published in:

Publishing company: Springer

Editor-in-Chief: Daewon Sohn

Volume 80, Issue 9, pp 6885-6904

Year: 2021

ISSN: 0170-0839

DOI: https://doi.org/10.1007/s00289-022-04382-0

Impact factor (2022): 3.2

JCR Journal rank: 36/86 in Polymer Science

3.1. Resumen

Los polímeros neutros cómo el PVP son capaces de formar distintos tipos de asociaciones con tensioactivos en función de la concentración. Estas asociaciones están impulsadas por interacciones eléctricas e hidrofóbicas, lo que produce un aumento de la viscosidad, sobre todo en los casos de los tensioactivos iónicos. Para los no iónicos, la interacción polímero-tensioactivo está más limitada. Por otra parte, en el caso de la lignina, los grupos hidroxilo y carboxilo de su estructura interactúan electrostáticamente con tensioactivos iónicos. En general, el aumento de la viscosidad se ve especialmente favorecido por la formación de complejos tensioactivo-polímero por encima de la llamada concentración crítica de agregación (CAC), la cual determina el inicio de la interacción entre los tensioactivos y el polímero. Estas interacciones pueden condicionar la electrospinabilidad de las disoluciones.

En cuanto a las propiedades viscosas, la adición de una pequeña cantidad de tensioactivo aumenta significativamente el carácter pseudoplástico. Además del impacto en la viscosidad, la adición de tensioactivos influye en propiedades fisicoquímicas cómo la conductividad eléctrica y la tensión superficial. Cómo es de esperar, la adición de tensioactivos aniónicos y catiónicos aumentó significativamente la conductividad eléctrica, junto a la esperada disminución de la tensión superficial. Por el contrario, la conductividad eléctrica no se encuentra afectada por la adición de tensioactivos no iónicos (Tween-20). Estos cambios en las propiedades fisicoquímicas tienen un gran impacto en el proceso de electrospinning.

Cómo es bien sabido, la tensión superficial disminuye con la concentración de tensioactivo hasta alcanzar la concentración micelar crítica. En el caso de las disoluciones poliméricas, dicha CAC se alcanza antes, cuando la tensión se reduce debido a las

interacciones polímero-tensioactivo. Así pues, la CAC a la que el polímero comienza a interactuar con el tensioactivo determinará el punto crítico de la actividad superficial, siendo muy similar entre todos los tensioactivos evaluados.

Las morfologías obtenidas no se vieron muy afectadas siempre que se trabaje por encima de la CAC de la disolución. La adición de tensioactivos por encima de la CAC produjo fibras finas con una mayor cantidad de interconexiones, en comparación con las disoluciones libres de tensioactivos, y se redujo también la aparición de partículas.

Las nanofibras obtenidas al añadir de tensioactivos a disoluciones con una relación LSL:PVP del 90:10 formaron geles blandos, sin embargo, las nanofibras de disoluciones a partir de relaciones 70:30 generaron geles fuertes, a una concentración 20 %wt. Las funciones viscoelásticas dinámicas de los oleogeles aumentaron ligeramente con la concentración de tensioactivo. En cuanto a las propiedades tribológicas, mostraron un excelente rendimiento de lubricación, con valores bajos de fricción y desgaste en comparación con las grasas lubricantes tradicionales analizadas, reduciéndose los valores del coeficiente de fricción y desgaste respecto de los oleogeles preparados con nanofibras obtenidas sin adición de tensioactivos.

Polymer Bulletin (2023) 80:6885–6904
https://doi.org/10.1007/s00289-022-04382-0

ORIGINAL PAPER

Influence of surfactants on the electrospinnability of lignin-PVP solutions and subsequent oil structuring properties of nanofiber mats

M. Borrego[1] · J. E. Martín-Alfonso[1] · C. Valencia[1] · M. C. Sánchez[1] · J. M. Franco[1]

Received: 20 April 2022 / Revised: 27 June 2022 / Accepted: 13 July 2022 /
Published online: 29 July 2022

Abstract

This work focuses on the improvement of the electrospinnability of low-sulfonate lignin (LSL)/polyvinylpyrrolidone (PVP) solutions by the addition of surfactants (SDS, CTAB and Tween-20) as well as on the ability of resulting nanofibers to structure castor oil. Solutions with two LSL/PVP weight ratios (70:30 and 90:10) in DMF were prepared by adding variable surfactant concentrations (0–1 wt.%), and physicochemically characterized. Electrical conductivity, surface tension and rheological measurements were performed. Variations of these physicochemical properties were explained on the basis of surfactant-polymer interactions. The addition of surfactants to LSL/PVP solutions improves electrospinnability, producing more compact and uniform fiber mats in 70:30 LSL/PVP systems, generally reducing the average diameter of the nanofibers and the number of beads. In contrast, nanofiber mats were not obtained with 90:10 LSL/PVP solutions, but different nanostructures composed of particle clusters. Dispersions of nanofiber mats obtained by electrospinning from 70:30 LSL/PVP solutions in castor oil were able to generate physically stable strong oleogels. In general, linear viscoelastic functions of oleogels increased with surfactant concentration. In addition, these oleogels exhibited excellent lubrication performance in a tribological contact, with extremely low values of the friction coefficient and wear diameters, which may lead to potential applications as lubricants.

Keywords Electrospinning · Lignin · Lubricant · Oil structuring · Surfactant

✉ J. M. Franco
franco@uhu.es

[1] Pro2TecS – Chemical Process and Product Technology Research Center, Department of Chemical Engineering and Materials Science. ETSI, Universidad de Huelva, Campus de "El Carmen". 21071, Huelva, Spain

Introduction

Nowadays, there is a growing interest in exploiting waste materials and by-products to manufacture end-use products and thus reduce resource depletion and/or expensive disposal treatments [1–4]. This is the case of lignin, which is produced in huge amounts in the paper industry where is considered a waste or low valuable by-product, and whose main use consists of direct incineration to recover some of the energy spent during the process [5, 6]. So far, the valorization of lignin as raw material in added-value products is scarcely explored, probably due to its complex chemical nature and the variability of its composition and structure. However, this issue has recently been a matter of intensive research [7, 8] and, nowadays, lignin is considered a renewable resource with great potential for different industrial applications [9].

On the other hand, the development of bio-based oleogels from renewable raw materials represents a target for the lubricant industry to mitigate the well-known environmental problems associated with lubricant spillage [10]. In previous research, the Chemical Process and Product Technology Research Center (Pro-2TecS, University of Huelva) has dedicated great efforts to develop eco-friendly oleogels, attempting to mimic the functional properties of traditional lubricating greases [11, 12]. Among the different biopolymers tested as oil thickening agents, lignins were found to be a promising alternative upon chemical modifications, such as epoxidation [13, 14] or isocyanate functionalization [15–17], that promote the formation of chemical gels by generating covalent bonds between lignin and vegetable oil. However, despite the fact that these final formulations may be considered bio-based, inert, and non-toxic materials, some of these chemical modifications involve the use of non-green chemicals and solvents and, therefore, alternative cleaner processes and methodologies must be further explored. In a previous work [18], the electrospinning technique was employed to produce lignin nanofibers with the ability to physically structure vegetable oils by simply dispersing the electrospun nanofiber mats in the oil, thus avoiding previous complex chemical functionalization. This procedure results in a much simpler and green strategy to produce oleogels. However, to obtain appropriate nanofiber morphologies, lignin must be doped with a readily electrospinnable polymer such as PVP. Besides, in general, the lignin electrospinning process still has room for improvement, for instance by optimizing the physicochemical properties of the solution to be electrospun.

The addition of surfactants to polymer solutions has been a common practice to improve electrospinnability, mainly due to a drastic reduction of the surface tension, but also to the modification of other important physicochemical properties such as viscosity and electrical conductivity. The change in these properties depends on the nature of the polymer and the surfactant that govern the interactions between them. For instance, Kumar and Tyagi [19] studied the interactions between PVP and anionic surfactants, such as SDS and a carboxylate-based dimeric surfactant. Different conformations of the PVP-surfactant complexes were proposed depending on the surfactant concentration ranges, delimited by

the critical aggregation concentration (CAC) and the critical micellar concentration (CMC), respectively. The CAC was defined as the surfactant concentration required for the onset of the interaction between the surfactant and the polymer. These authors also proposed simple experimental methods to determine these critical concentrations through conductometric and surface tensiometric measurements. On the other hand, Wang et al. [20] observed a considerable increment in the viscosity of PEG/surfactant solutions which they associated with the formation of transient polymer networks crosslinked by surfactant micelles.

In direct relation with the improvement of electrospinnability, Jia et al. [21] and Fang et al. [22] studied polymer-surfactant interactions in PVA and lignin/PVA solutions, respectively, and how these interactions influence the physicochemical properties of the solution depending on the nature of both the polymer and the surfactant. Jia et al. [21] concluded that, apart from the beneficial effect of decreasing the surface tension, the solution viscosity steadily increased with the concentration of ionic surfactants, which was attributed to the formation of PVA-surfactant complexes, while non-ionic or amphoteric surfactants did not significantly affect the solution viscosity. In the presence of lignin, Fang et al. [22] also attributed the increase in viscosity to the formation of complexes after exceeding a critical surfactant concentration, depending on the type of surfactant. This increase was especially relevant in the case of SDS. However, they obtained a decrease in viscosity with cationic and non-ionic surfactants due to favorable electrostatic forces or the absence of cooperative binding among the complexes. Araujo et al. [23] investigated the improvement of the electrospinnability of PVA solutions by reducing the surface tension upon the addition of a non-ionic surfactant, reporting an important reduction of beads in the nanofiber mats as surfactant concentration increased, finally yielding almost bead-free nanofibers at high surfactant concentration. Similarly, Kriegel et al. [24] concluded that the addition of surfactants to PEO/chitosan solutions induced an improvement in membrane morphology, decreasing the bead content. The solution properties were especially affected by the interaction of ionic surfactants and chitosan, which is a polycationic polymer. In the same line, Wang et al. [25] reported a significant decrease in the nanofiber width by adding a non-ionic surfactant to electrospun PVP solutions.

In this work, the addition of surfactants to lignin/PVP solutions was studied aiming to improve electrospinnability and reduce heterogeneity and the appearance of defects and beads in the morphology of nanofibers. Further, how this morphology affects the ability of nanofiber mats to structure castor oil was investigated as well as the potential use of resulting oleogels as lubricants by analyzing their rheological and tribological properties.

Experimental

Materials

Low sulfonate Kraft lignin (LSL, M_w: ~ 10,000 g/mol) and polyvinylpyrrolidone (PVP, M_w: ~ 360,000 g/mol) were obtained from Merck Sigma-Aldrich. *N*,

N-Dimethylformamide (DMF, purity ≥ 99.8%) was used as solvent to prepare LSL/PVP solutions. Sodium dodecyl sulfate (SDS), hexadecyltrimethylammonium bromide (CTAB) and polyethylene glycol sorbitan monolaurate (Tween-20) were used as anionic, cationic and non-ionic surfactants, respectively, in LSL/PVP solutions, all of them also purchased from Merck Sigma-Aldrich. Castor oil was supplied by Guinama (Spain), whose main physical properties and fatty acid composition can be found elsewhere [26].

Preparation and physicochemical characterization of LSL/PVP solutions

LSL/PVP solutions in DMF were prepared at a 15 wt.% total concentration and two different LSL/PVP weight ratios (70:30 and 90:10). SDS, CTAB or Tween-20 was also added at small concentrations in the range 0–1 wt.% The surfactant was dissolved for two hours at 50 °C in DMF under agitation. The corresponding amounts of LSL and PVP were then added while maintaining magnetic stirring for 24 h. The final solution was then centrifuged for 10 min at 3000 rpm and filtered to verify the complete dissolution.

Rheological characterization was carried out in a controlled-strain rheometer (ARES, Rheometric Scientific), in a shear rate range of 0.03–300 s^{-1}, at 25 °C, using a Couette geometry (inner radius 16 mm, outer radius 17 mm, height 33.35 mm). LSL/PVP solutions are Newtonian for a 90:10 LSLS/PVP weight ratio, whereas at a 70:30 LSLS/PVP weight ratio they showed a non-Newtonian flow response which was satisfactorily fitted ($R^2 > 0.995$) to the Williamson model:

$$\eta = \frac{\eta_0}{1 + (K\dot{\gamma})^m} \tag{1}$$

where η is the apparent viscosity, $\dot{\gamma}$ is the shear rate, η_0 is the zero-shear-rate-limiting viscosity, and m and K are fitting parameters.

Electrical conductivity was measured using a LAQUA PC-110 conductivity meter (Horiba Scientific) at room temperature. Surface tension was measured in a Sigma 703D tensiometer (Biolin Scientific) using a Wilhelmy platinum plate with a measuring range of 1–1000 mN/m. All measurements were replicated at least twice.

Electrospinning process and morphological characterization of electrospun nanostructures

LSL/PVP solutions in DMF were submitted to electrospinning in a Doxa Microfluids equipment using a 10-ml BD syringe of 11.99 mm internal diameter and a flat 20G needle connected to a high voltage power source, where the negative terminal was connected to an aluminum collector plate and the positive terminal to the needle, in a horizontal configuration. The distance between needle and collector was set at 10 cm, and the feed flow and voltage applied were varied in the 0.5–1 ml/h and 17–21 kV ranges, respectively. A camera coupled to the electrospinning chamber was used to control the correct formation of the Taylor cone and detect flow instabilities. All experiments were carried out at room temperature (22 ± 1 °C).

The morphology of the nanostructures obtained by electrospinning was assessed by scanning electron microscopy (SEM) observations carried out on both the JEOL, model JXA-8200 SuperProbe, and the Hitachi, model FlexSEM 1000 II, microscopes, operating at 10–20 kV accelerating voltages and different magnifications. The open-source FIJI ImageJ analysis program was used to analyze the SEM images.

Preparation and characterization of oleogels

LSL/PVP nanofiber templates obtained by electrospinning were dispersed in castor oil by applying agitation with an anchor geometry, at room temperature, for 24 h. The concentration of electrospun mats was fixed at 20% wt. The homogeneity of oleogel microstructure was verified with an Olympus BX51 optical microscope.

Resulting oleogels were rheologically characterized using a Rheoscope (ThermoHaake) controlled-stress rheometer and an ARES (Rheometric Scientific) controlled-strain rheometer, at 25 °C, using plate-plate geometries (25 and 35 mm diameter, respectively, and 1 mm gap). Small-amplitude oscillatory shear (SAOS) tests were performed inside the linear viscoelastic regime in a frequency range of 0.08–100 rad/s. At least two replicates of each test were performed.

Oleogels were also tribologically characterized to explore potential applications as lubricants. The tribological characterization was carried out in a tribological cell coupled to a Physica MCR-501 (Anton-Paar) controlled-stress rheometer, using a 1/2"-diameter steel ball-on-three 45°-inclined steel plates configuration. Constant axial normal load and a rotational speed of 30 N and 20 min^{-1}, respectively, were applied for 10 min, while recording the friction coefficient values. The effective normal force on plates and friction coefficient were calculated from the applied axial normal force, the friction force measured by the rheometer and the ball radius according to Heyer and Läuger [27]. At least four replicates of each test were carried out at ambient temperature.

Results and discussion

Influence of surfactants on the physicochemical properties of LSL/PVP solutions.

All LSL/PVP solutions are Newtonian for a 90:10 LSLS/PVP ratio, independently of the type and concentration of the surfactant. The viscosity values at 25 °C are shown in Table 1. As can be seen, the viscosity of LSL/PVP solutions initially decreased with surfactant addition and then increased from a critical concentration (~0.1 wt.%), in the case of ionic surfactants (SDS and CTAB). However, viscosity slightly decreased initially and remained almost constant when adding a non-ionic surfactant (Tween-20). Similar effects have been reported for lignin/PVA solutions in water [22], which were attributed to the different surfactant–lignin and surfactant–neutral polymer interactions. On the one hand, neutral polymers such as PVP and surfactants are able to form different kinds of associations depending on the concentration, which in turn may entail interactions between polymer chains

Table 1 Physicochemical properties of LSL/PVP 90:10 solutions containing different types and concentrations of surfactants

Solution	Viscosity (μ) (Pa·s)	Electrical conductivity (k) (μS/cm)	Surface tension (σ) (mN/m)
90:10 LSL/PVP (surfactant-free)	$0.07 \pm 2.8 \cdot 10^{-3}$	523.7 ± 4.7	37.12 ± 0.02
90:10 LSL/PVP + SDS			
0.01%	$0.07 \pm 3.3 \cdot 10^{-2}$	540.7 ± 2.0	36.37 ± 0.32
0.05%	$0.06 \pm 4.8 \cdot 10^{-3}$	549.7 ± 2.1	34.95 ± 0.12
0.1%	$0.02 \pm 5.1 \cdot 10^{-2}$	665.3 ± 2.5	33.21 ± 0.09
0.5%	$0.06 \pm 2.7 \cdot 10^{-2}$	984.6 ± 2.7	32.75 ± 0.11
1%	$0.26 \pm 1.5 \cdot 10^{-1}$	1063.6 ± 2.3	30.27 ± 0.21
90:10 LSL/PVP + Tween-20			
0.01%	$0.06 \pm 2.1 \cdot 10^{-2}$	516.1 ± 1.6	37.19 ± 0.08
0.05%	$0.05 \pm 5.3 \cdot 10^{-3}$	545.1 ± 9.5	36.11 ± 0.11
0.1%	$0.05 \pm 1.3 \cdot 10^{-2}$	519.3 ± 4.04	32.29 ± 0.23
0.5%	$0.03 \pm 1.2 \cdot 10^{-2}$	504.3 ± 5.7	30.95 ± 0.88
1%	$0.04 \pm 6.7 \cdot 10^{-3}$	536.4 ± 6.8	30.08 ± 1.45
90:10 LSL/PVP + CTAB			
0.01%	$0.07 \pm 1.5 \cdot 10^{-3}$	544.6 ± 1.2	36.42 ± 1.91
0.05%	$0.06 \pm 9.3 \cdot 10^{-3}$	548.0 ± 4.6	34.67 ± 0.15
0.1%	$0.05 \pm 1.4 \cdot 10^{-2}$	573.3 ± 2.5	32.02 ± 0.76
0.5%	$0.08 \pm 6.4 \cdot 10^{-2}$	672.1 ± 1.0	29.49 ± 0.31
1%	$0.11 \pm 3.3 \cdot 10^{-3}$	892.3 ± 3.6	29.12 ± 0.19

and single surfactants molecules, or more complex assemblies involving surfactant aggregations and micelles [19, 20]. These associations are driven by electrical and hydrophobic interactions yielding an increase in viscosity especially in the case of ionic surfactants. For non-ionic surfactants, the cooperative binding between the surfactant and polymer is much more constrained [21]. On the other hand, the polar hydroxyl and carboxyl groups of lignin are able to interact electrostatically with ionic surfactants. Fang et al. [22] argued that the cationic surfactant interacts with lignin forming binary complexes and reducing the interaction between a neutral polymer (PVA) and both lignin and surfactant, at least up to a critical aggregation concentration, whereas the electrostatic repulsion between SDS and lignin prevents the formation of such complex but reinforces the entanglement among SDS, lignin and PVA. In general, the increase in viscosity is especially favored by the formation of surfactant–polymer complexes above a critical concentration known as critical aggregation concentration (CAC), which determine the onset of the interaction between the surfactant and the polymer.

For a lower LSL/PVP weight ratio (70:30), the solutions showed a non-Newtonian response and the viscosity always increased with surfactant concentration above 0.01 wt. %, regardless of the type of surfactant. This means that the cooperative associations among lignin, PVP and surfactants are dominated by

Table 2 Physicochemical properties and Williamson fitting parameters of 70:30 LSL/PVP solutions containing different types and concentrations of surfactants

Sample	η_o (Pa·s)	K (10^3) (s)	m	Electrical conductivity (k) (μS/cm)	Surface tension (σ) (mN/m)
70:30 LSL:PVP (surfactant-free)	0.54	3.3	0.53	470.7 ± *1.9*	36.91 ± *0.04*
70:30 LSL:PVP+SDS					
0.01%	0.39	9.7	0.86	777.3 ± *3.5*	35.13 ± *0.12*
0.05%	0.88	4.1	0.54	787.1 ± *1.4*	27.87 ± *0.15*
0.1%	1.02	3.8	0.52	801.3 ± *7.1*	24.36 ± *0.11*
0.25%	1.29	5.3	0.51	830.1 ± *7.1*	23.31 ± *0.17*
0.5%	1.79	4.4	0.61	850.1 ± *1.2*	23.88 ± *0.05*
0.75%	2.15	5.4	0.73	858.1 ± *2.1*	22.78 ± *0.08*
1%	2.67	7.3	0.82	919.2 ± *4.1*	22.71 ± *0.03*
70:30 LSL:PVP+Tween-20					
0.01%	0.42	9.7	0.96	499.1 ± *2.1*	35.48 ± *0.07*
0.05%	0.95	2.9	0.64	464.3 ± *3.1*	31.01 ± *0.06*
0.1%	1.14	3.3	0.84	438.1 ± *3.1*	25.63 ± *0.09*
0.5%	1.44	4.4	0.77	467.1 ± *3.1*	23.04 ± *0.13*
1%	2.05	4.9	0.85	482.7 ± *0.6*	22.27 ± *0.11*
70:30 LSL:PVP+CTAB					
0.01%	0.38	9.9	0.95	579.7 ± *2.1*	35.11 ± *0.06*
0.05%	0.43	9.7	0.83	671.3 ± *4.5*	30.79 ± *0.09*
0.1%	0.98	2.8	0.73	778.3 ± *2.5*	23.09 ± *0.02*
0.5%	1.34	3.9	0.58	841.3 ± *2.1*	20.55 ± *0.12*
1%	1.88	7.1	0.67	846.7 ± *2.3*	20.66 ± *0.18*

the PVP-surfactant interactions [19]. The non-Newtonian flow response comprises almost constant values of viscosity over 2–3 decades and a subsequent shear-thinning region at relatively high shear rates, which can be described by the Williamson model, as shown for selected systems in Fig. 1. The corresponding fitting parameters for each solution are included in Table 2. A shear-thinning response was already evinced in the surfactant-free solution, thus PVP being the main responsible for the increased level of entanglements, which has been reported to be fundamental for the correct formation of fibers during the electrospinning [24, 28]. In general, the addition of surfactants may enhance, or not, the shear-thinning character of these complex solutions, depending on the predominant associations among the neutral polymer, lignin and the surfactant, as well as on surfactant concentration [22, 24]. In these systems, a small addition of surfactant, i.e. 0.01 wt. %, significantly enhanced the shear-thinning character (see higher values of parameter m in Table 2), suggesting the formation of new associations where the surfactants are involved. However, the addition of higher amounts of surfactants seems to dampen this effect but mainly to delay the onset

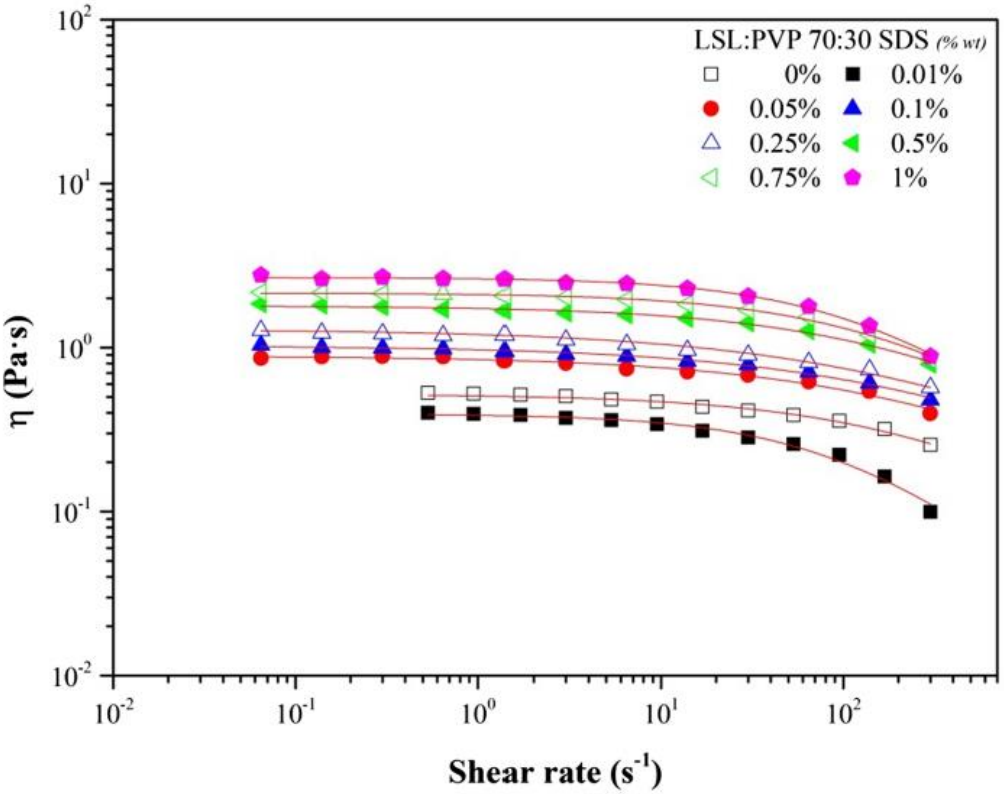

Fig. 1 Viscous flow curves of LSL/PVP 70:30 solutions in DMF as a function of SDS concentration. Solid lines refer to the Williamson model fits (Eq. 1)

of shear thinning to higher shear rates (lower K values). More important, the values of the zero-shear-rate-limiting viscosity noticeably increased above a very low level of surfactant addition, i.e. 0.01 wt.%.

Apart from the impact on viscosity, surfactant addition influences other physicochemical properties of relevance for electrospinning such as electrical conductivity and surface tension. Surface tension and electrical conductivity values can be found in Tables 1 and 2 for all the LSL/PVP solutions studied. As expected, the addition of anionic and cationic surfactants significantly increased the electrical conductivity, yielding increments of around 90–100% with respect to the surfactant-free solutions when adding 1 wt.%. On the contrary, electrical conductivity is not much affected when adding the non-ionic surfactant (Tween-20). Moreover, as has been widely reported in the literature [21–25, 29], the addition of surfactants considerably decreases the surface tension of polymer solutions, with huge impact on the electrospinning process. This decrease in surface tension was especially relevant for the 70:30 LSL/PVP weight ratio, for which a reduction down to 20–23 mN/m was obtained. This means that the PVP-driven polymer–surfactant complexes have a superior surface activity than those dominated by LSL-surfactant interactions. In addition, the surface tension reduction was similar for all the surfactants studied although slightly larger for CTAB. The surface tension sharply decreased with a small addition

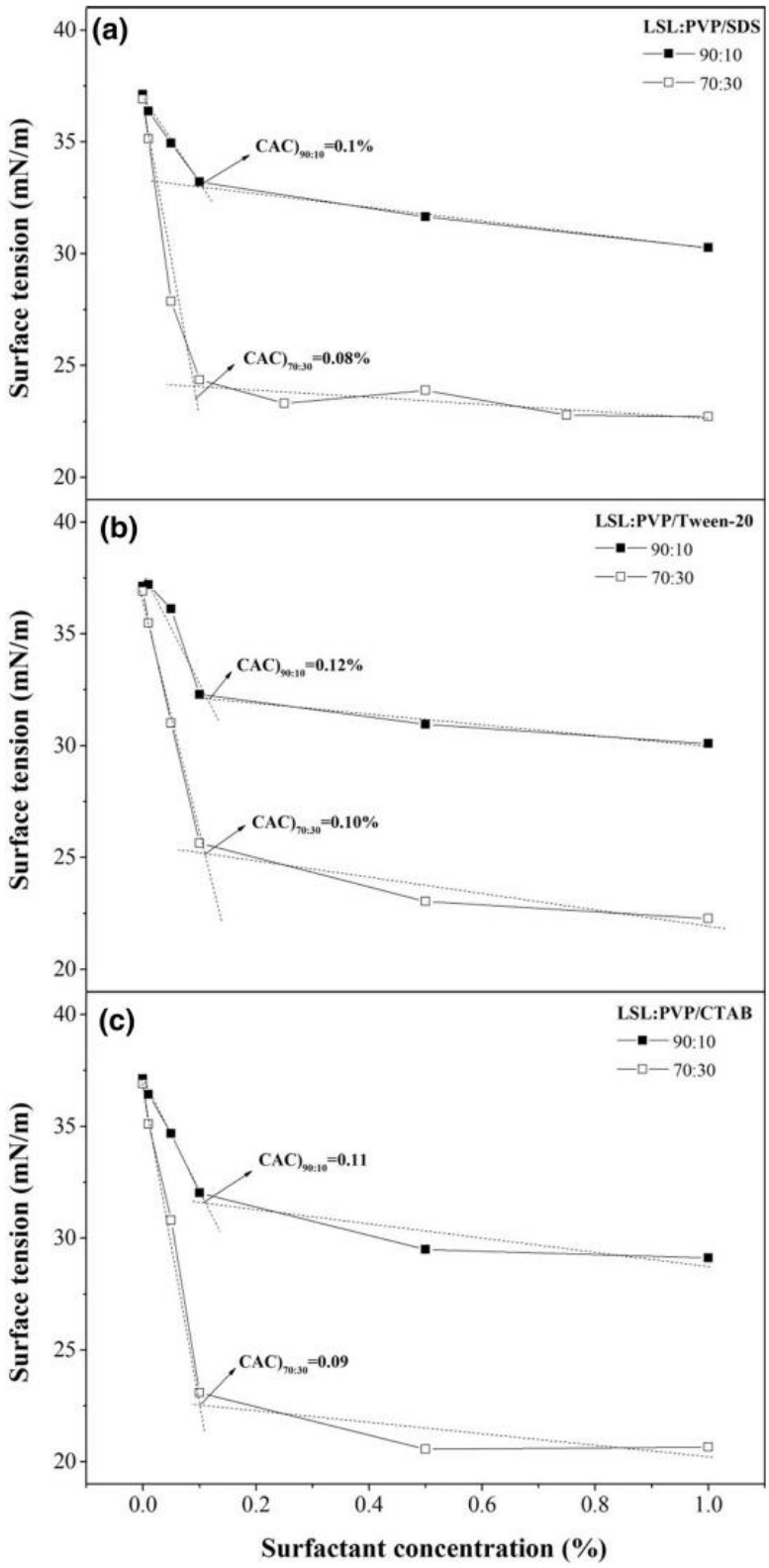

Fig. 2 Evolution of surface tension with surfactant concentration and determination of the critical aggregation concentration (CAC) for **a** LSL/PVP/SDS **b** LSL/PVP/ Tween-20, and **c** LSL/ PVP/CTAB solutions

of surfactant and then reached an almost plateau value. This behavior is related to the presence and mobility of single surfactant molecules, and it is very well known for polymer-free surfactant solutions, where the surface tension significantly decreases up to reach the critical micelle concentration. In the case of polymer solutions, this plateau was reached earlier, at around CAC, when the surfactant mobility is reduced because of the polymer-surfactant interactions, as reported for PVP-surfactant solutions [19]. In fact, one of the methods proposed to determine the value of the critical aggregation concentration (CAC) is based on the variation of the surface tension with surfactant concentration [19, 30], as illustrated in Fig. 2. Thus, the CAC at which the polymer starts to interact with the surfactant determines the critical point for a reduction in surface activity. In the LSL/PVP solutions studied, the CAC is very similar for all the surfactants studied and varies between 0.08 and 0.12 wt.%. Slightly higher CACs than those obtained in this study for LSL-PVP-SDS solutions were reported for PVP-SDS solutions [19].

Effect of surfactant addition on the electrospinnability of LSLS/PVP solutions and morphology of electrospun nanostructures

For a 70:30 LSL/PVP weight ratio, all the solutions were electrospinnable and nanofiber mats were obtained regardless of the type and concentration of surfactants, including the surfactant-free solution. This is due to a convenient combination of electrical conductivity, surface tension and rheological characteristics. As well known [31], both an increase in conductivity and a decrease in surface tension favor the stretching of nanofibers, whereas viscosity retards the stretching, thus reducing the filament rupture and/or increasing fiber diameter. On the other hand, a marked shear-thinning behavior favors filament stretching at high spinning flow rates and enhances jet formation.

As can be observed in Fig. 3, the addition of surfactant at concentrations around or above CAC produced more compact and uniform fiber mats with a higher amount of junctions and interconnected thin fibers due to improved electrospinnability, as a result of the increased level of entanglements in polymer solutions. However, the morphology of the nanofibers depends only slightly on the type and concentration of surfactant when added above this CAC. The presence of embedded particles and/or formation of large lumps eventually detected in nanofibers obtained from the surfactant-free solution (see Fig. 3a) were reduced with surfactant addition although not completely eliminated. Instead, morphologies very similar to those obtained from surfactant-free solutions were found at surfactant concentrations below CAC (results not shown). Moreover, typical beads appearing in lignin nanofibers [32] are scarcely present when adding surfactants and tend to disappear at high SDS and Tween-20 concentrations. However, some beaded nanofibers are apparent when adding CTAB, even at 1 wt.% (Fig. 3j). This fact can be explained on the basis of the more favorable interaction between CTAB and lignin, excluding PVP to some extent from the complexes, which also is associated to a lower shear-thinning character in comparison with SDS and Tween-20 (see *m* values in Table 2). On the other hand, thicker fibers and/or bundles

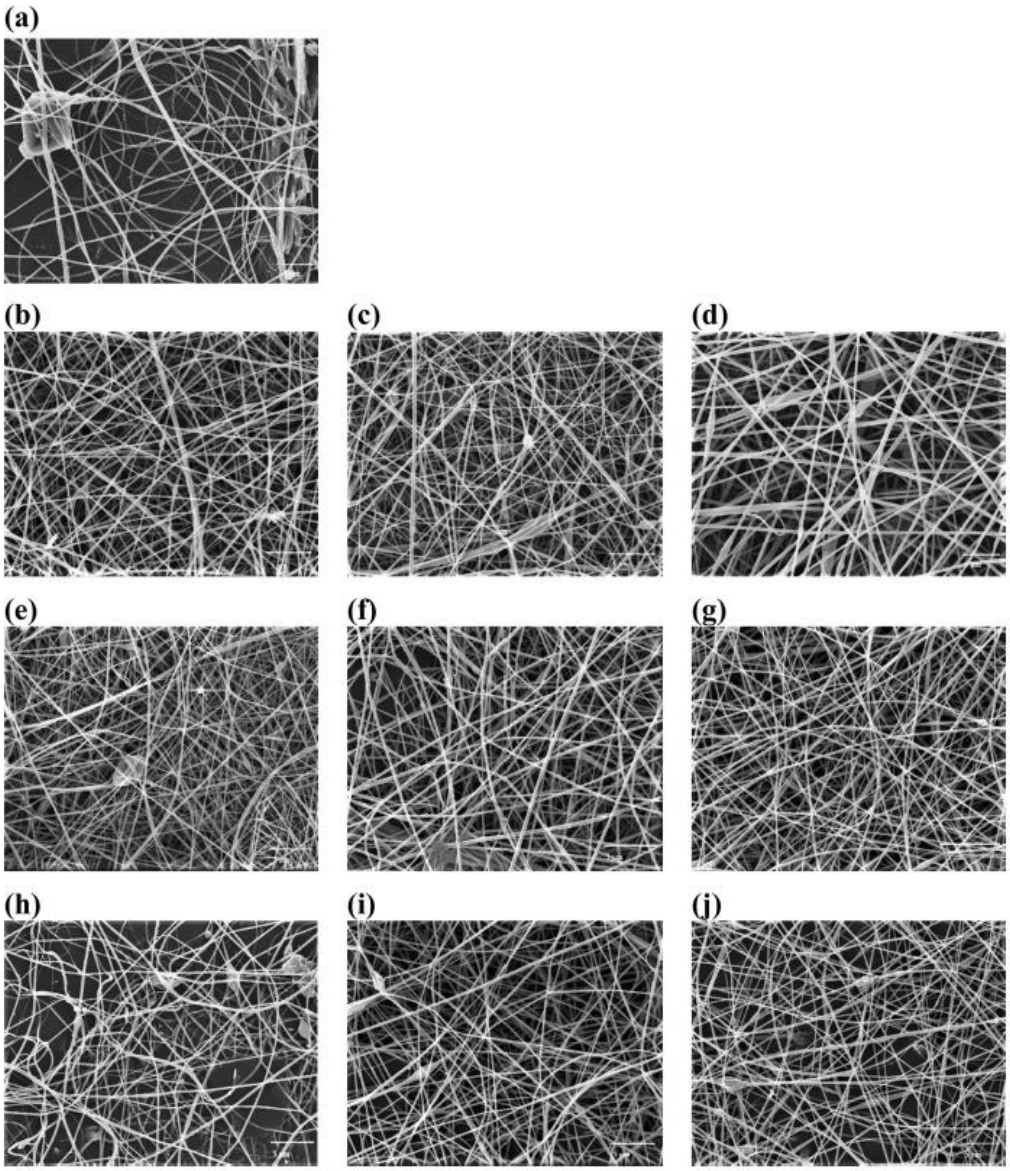

Fig. 3 SEM Images of 70:30 LSL/PVP nanofibers mats obtained with different types and concentrations of surfactants: **a** surfactant-free, **b** 0.1 wt.% SDS, **c** 0.5 wt.% SDS, **d** 1 wt.% SDS, **e** 0.1 wt.% Tween-20, **f** 0.5 wt.% Tween-20, **g** 1 wt.% Tween-20, **h** 0.1 wt.% CTAB, **i** 0.5 wt.% CTAB and **j** 1 wt.% CTAB. (Magnification 4000x, scale bars correspond to 5 μm)

of fibers were found in nanofiber mats containing 1 wt.% SDS (see Fig. 3d), which may be related to the particularly high viscosity of the spinning solution (see Table 2). In contrast, highly homogeneous and almost bead-free thin fiber mats were especially obtained from solutions containing high contents of Tween-20 (see Fig. 3g). This fact suggests that surfactant-polymer complexes favored by ionic surfactants cause a certain degree of agglomeration producing beaded fibers and/or bundles to some extent. Average fiber diameter generally decreased with surfactant concentration, as shown in

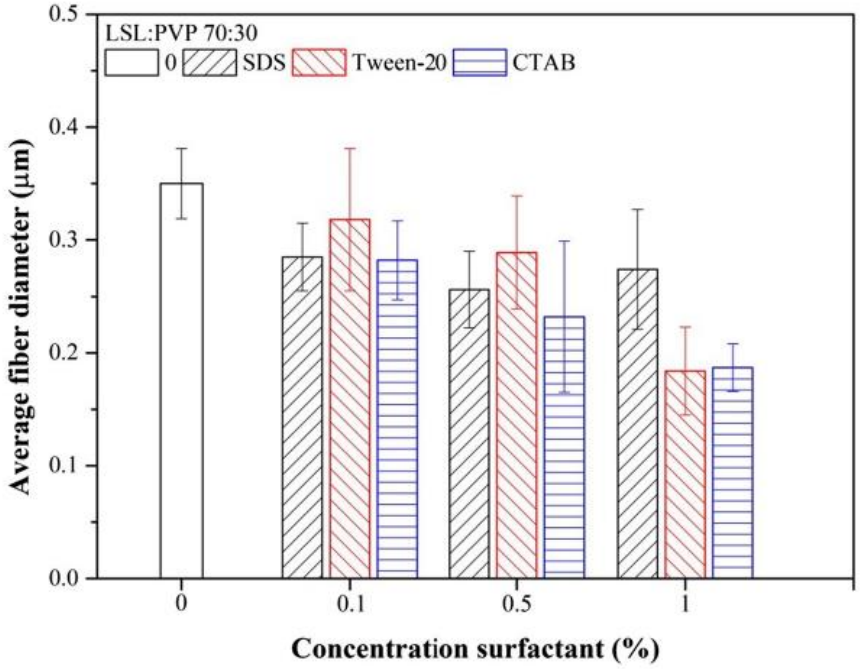

Fig. 4 Average fiber diameter of LSL/PVP 70:30 solutions containing different types and concentrations of surfactants

Fig. 4. This phenomenon is mainly due to the surfactant-induced reduction in surface tension and enhanced shear-thinning character, making easier the stretching of the jet in the Taylor cone, and has been widely reported for instance for PVP, PVA and lignin/PVA nanofibers [21, 25, 33]. Fiber diameter was especially reduced by adding 1 wt.% Tween-20 or CTAB to the electrospun LSL/PVP solution. In contrast, as discussed above, the more entangled LSL-PVP-SDS complexes generally imparting higher viscosity to the solution seem to promote the formation of thicker fibers or fiber bundles, slightly increasing the average fiber diameter at high SDS concentration.

For a higher LSL/PVP weight ratio, i.e. 90:10, nanofibers were not obtained but electrosprayed particles connected by thin filaments, probably as a result of not high enough levels of entanglements in the polymeric solutions. Moreover, the addition of surfactant is not advantageous for obtaining fibers, although some unusual nanostructures were produced, and particle size was significantly reduced. As can be seen in Fig. 5, the addition of small amounts of SDS or CTAB leads to the appearance of uniform structures composed of clusters of small (nanosized) particles. In the particular case of Tween-20, some networks of such small particles and agglomerates are apparent.

Oil structuring ability

The different electrospun nanostructures obtained from LSL/PVP/surfactant solutions were mixed with castor oil, at 20% wt. concentration, to examine the ability

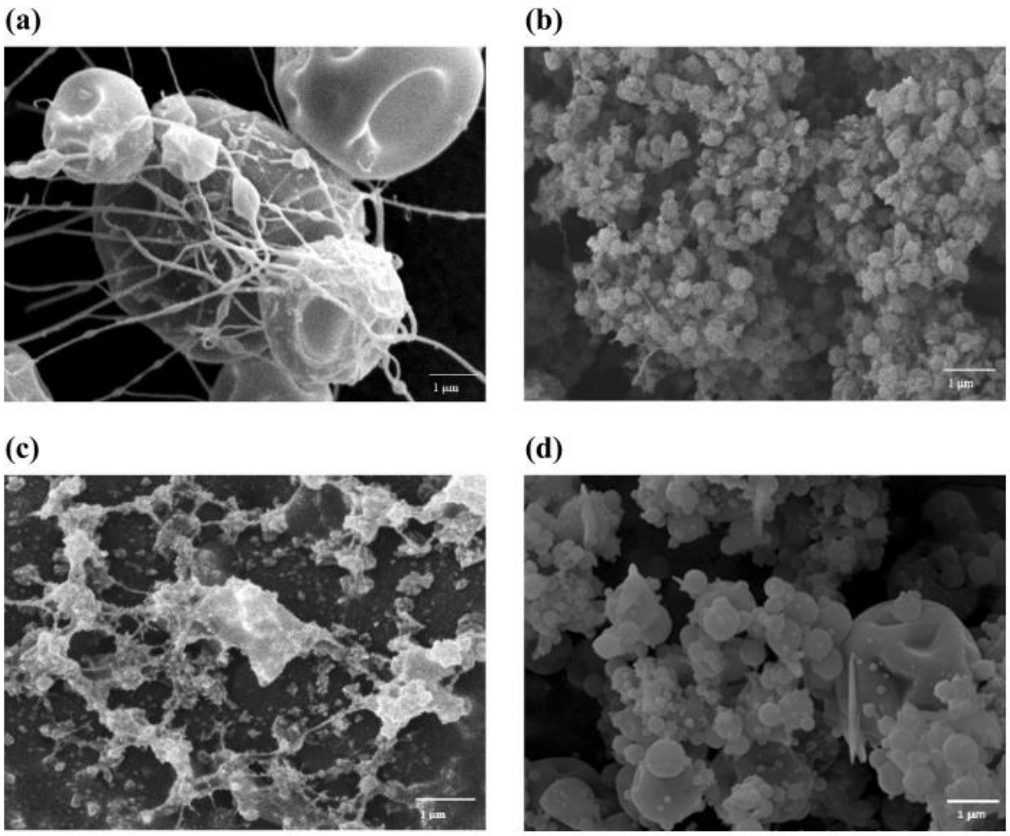

Fig. 5 SEM Images of 90:10 LSL/PVP nanostructures obtained with different types of surfactants: **a** surfactant-free, **b** 0.1 wt.% SDS, **c** 0.1 wt.% Tween-20 and **d** 0.1 wt.% CTAB. (Magnification 10,000x, scale bars correspond to 1 μm)

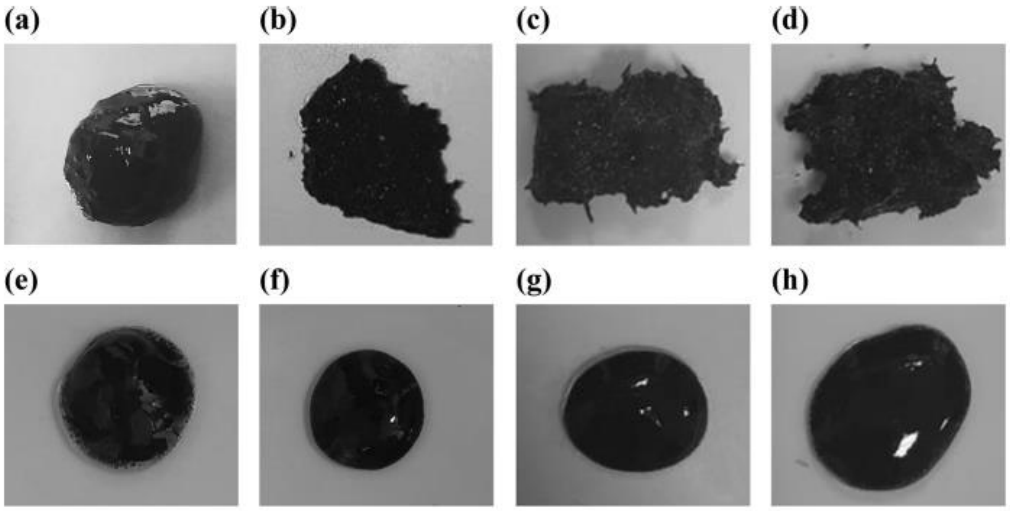

Fig. 6 Blends of castor oil and LSL/PVP nanostructures at 20 wt.% concentration. Upper row, 70:30 LSL/PVP nanofibers, **a** surfactant-free, **b** 0.5 wt.% SDS, **c** 0.5 wt.% Tween-20 and **d** 0.5 wt.% CTAB. Lower row, 90:10 LSL/PVP nanostructures, **e** surfactant-free, **f** 0.5 wt.% SDS, **g** 0.5 wt.% Tween-20 and **h** 0.5 wt.% CTAB

Fig. 7 Evolution of linear viscoelastic functions with frequency for oleogels prepared with 20 wt.% of ▶ 70:30 LSL/PVP electrospun nanofibers by adding **a** SDS, **b** Tween-20 and **c** CTAB surfactants at different concentration

to form oleogels. As can be observed in Fig. 6, nanofiber mats obtained by electrospinning from 70:30 LSL/PVP solutions were able to generate physically stable and though oleogels (Fig. 6a–d). However, the nanostructures obtained upon addition of surfactants (SDS, Tween-20 or CTAB) to a 90:10 LSL/PVP solution promote the formation of apparently thickened liquids or soft gels (see Fig. 6f–h), whereas the nanostructure obtained from the surfactant-free solution yields an unstable dispersion where a certain degree of separation can be appreciated (see Fig. 6e). In general, the formation of well-developed nanofiber mats, regardless the presence of beads or bundles, was required to noticeably structure oil. As previously reported [18], nanofiber mats are able to entrap castor oil more favorably in the porous network, thus enhancing the physical interactions between the oil and the LSL/PVP fibers. Figure 7 shows the influence of surfactant concentration on the rheological response of oleogels prepared with 70:30 LSL/PVP nanofibers. The evolution of the storage (G') and loss (G'') functions with frequency is concordant with the definition given by Almdal et al. [34] for solid-like gels and qualitatively similar in all cases. Differences of around one decade between both SAOS functions can be observed as well as small slopes of the G' and G'' vs. frequency plots. In contrast, gels prepared by dispersing 90:10 LSL/PVP nanofibers in castor oil exhibited rheological characteristics of soft gels (Fig. 8), with values of G' and G'' much lower to those shown in Fig. 7 and a tendency to crossover at high frequencies.

The values of the viscoelastic functions increased with surfactant addition. However, as can be seen in Fig. 7, nanofibers obtained from the surfactant-free solution provided values of both SAOS functions similar to those found for oleogels prepared with nanostructures resulting from solutions having small concentration of ionic surfactants (SDS and CTAB), i.e. around the CAC, whereas higher surfactant concentrations generally produced noticeable increments in the viscoelastic functions. Overall, higher values of SAOS functions correspond to oleogels stabilized with more uniform and compact nanofiber mats, like those obtained with Tween-20. Again, the fiber membrane obtained from the LSL/PVP solution containing 1 wt.% SDS showed a distinctive behavior, providing the oleogel with the highest viscoelastic functions, despite showing a higher average fiber diameter (see Fig. 4). On the contrary, the nanofiber templates obtained from solutions containing CTAB, which evinced some beaded fibers, generally displayed low values of the viscoelastic functions, particularly that prepared from the solution having 1 wt.% CTAB.

Tribological performance of oleogels structured with LSL/PVP nanofiber mats

To explore a potential lubricant application of these oleogels, the tribological performance was assessed in a ball-on-three-plate steel–steel tribological contact [27]. Figure 9 collects the friction coefficient values and average diameter of the resulting wear scars generated on the plates. As can be seen, all the oleogels

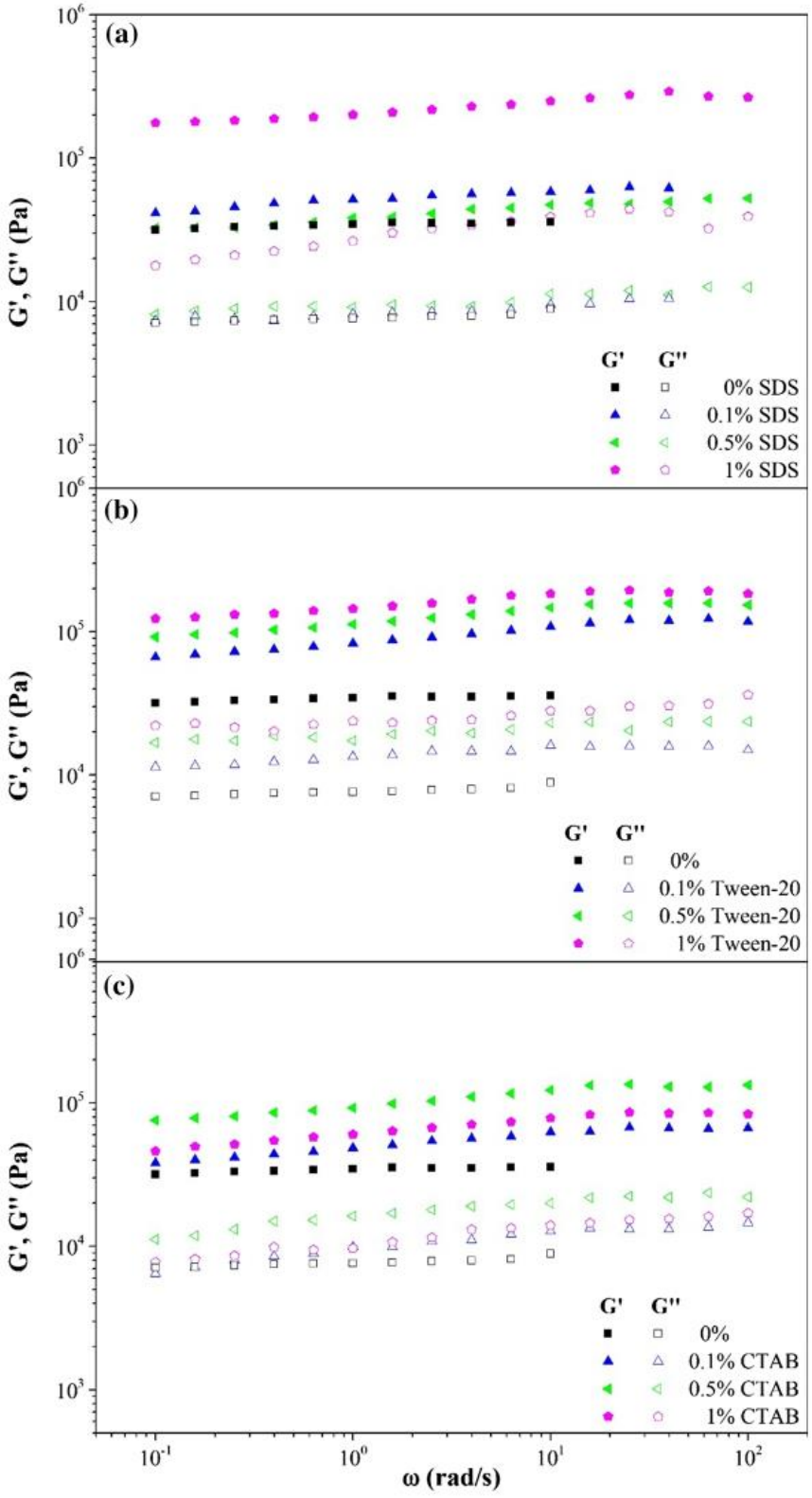
(a)
G', G'' (Pa)
G' G''
0% SDS
0.1% SDS
0.5% SDS
1% SDS
(b)
G', G'' (Pa)
G' G''
0%
0.1% Tween-20
0.5% Tween-20
1% Tween-20
(c)
G', G'' (Pa)
G' G''
0%
0.1% CTAB
0.5% CTAB
1% CTAB
ω (rad/s)

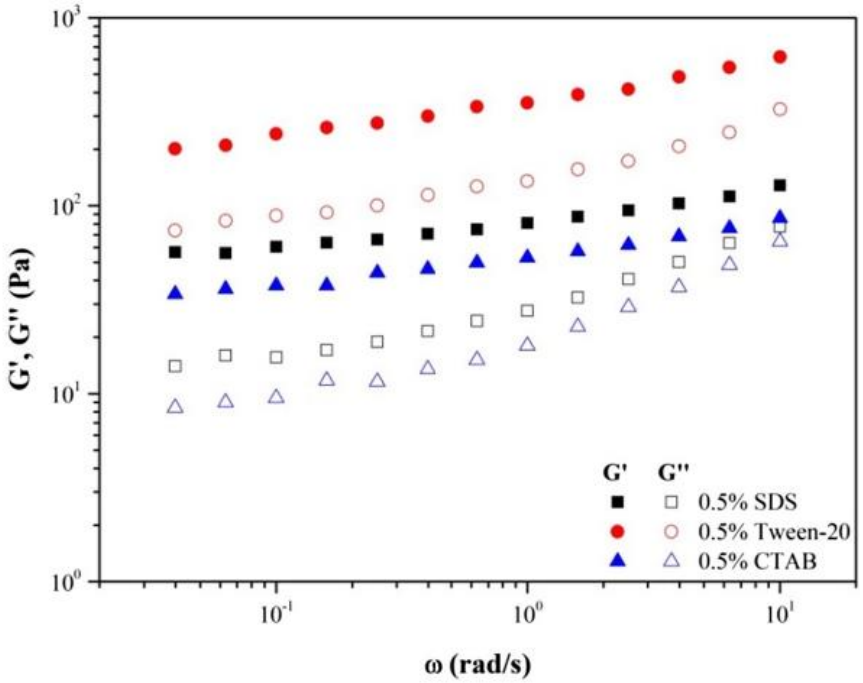

Fig. 8 Evolution of linear viscoelastic functions with frequency for oleogels prepared with 20 wt.% of 90:10 LSL/PVP electrospun nanostructures by adding 0.5% wt. surfactant

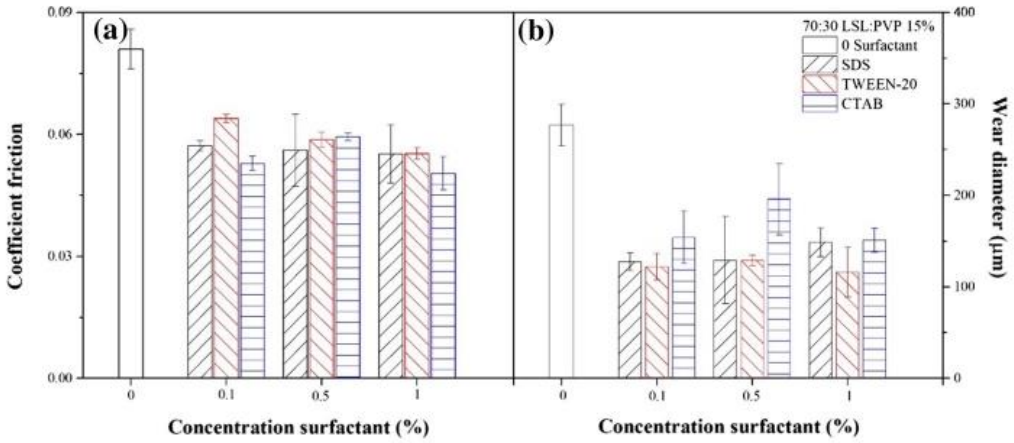

Fig. 9 Friction coefficient (**a**) and wear scar diameters (**b**), as a function of surfactant concentration, resulting when 70:30 LSL/PVP nanofiber-based oleogels were applied as lubricants in a tribological contact

prepared with nanofiber mats obtained by electrospinning from 70:30 LSL/PVP solutions containing surfactants provided excellent lubrication performance, with

extremely low values of the friction coefficient and wear scar diameters, generally much lower than those found when using conventional lubricating greases [35, 36] or chemically functionalized cellulose- and lignin-based oleogels [13, 36, 37] under similar conditions (i.e. friction coefficient values typically ranging from 0.07 to 0.12). Moreover, the addition of surfactants to the electrospun solution is beneficial since significantly lower values of both friction coefficient and wear scar diameters were obtained in comparison with those generated when using the oleogel prepared with the surfactant-free membrane. This result supports the idea that well-developed and more uniform nanofiber mats allow the oleogel to penetrate into the lubricating contact as a whole, promoting oil release once the nanostructure is stressed [18], at the same time that nanofibers may also prevent wear by increasing the film thickness. Regarding the kind of surfactant, no significant differences were found in the friction coefficient, but slightly larger wear scars were obtained when adding CTAB. These results are in agreement with the general opinion [38] that surfactants enhance the film formation of lubricants in a tribological contact, therefore imparting anti-wear properties.

Conclusions

Different nanostructures were produced by electrospinning from solutions of low-sulfonate lignin (LSL) and polyvinylpyrrolidone (PVP) in DMF, prepared at two different LSL/PVP weight ratios, 70:30 and 90:10, by adding variable concentrations (0–1 wt.%) of anionic (SDS), cationic (CTAB) and non-ionic (Tween-20) surfactants. 90:10 LSL/PVP solutions are Newtonian and the viscosity initially decreased with surfactant addition and then increased from a critical concentration in the case of ionic surfactants (SDS and CTAB), while viscosity slightly decreased initially and remained almost constant when adding the non-ionic surfactant (Tween-20). This behavior has been explained on the basis of different electrical and hydrophobic surfactant-lignin and surfactant-PVP interactions. In general, the increase in viscosity is especially favored by the formation of surfactant-polymer complexes above the critical aggregation concentration (CAC), which determines the onset of surfactant-polymer interaction. CAC was determined through the variation of the surface tension with surfactant concentration being very similar for all the surfactants studied, ranging from 0.08 to 0.12 wt.% For a 70:30 LSL/PVP weight ratio, solutions showed a non-Newtonian flow response and the viscosity always increased with surfactant concentration above 0.01 wt%, regardless of the type of surfactant, suggesting that the cooperative associations among lignin, PVP and surfactant are dominated by the PVP-surfactant interactions.

The addition of surfactants to 70:30 LSL/PVP solutions yields more compact and uniform fiber mats with a higher amount of junctions and generally reducing the average diameter of the nanofibers and the number of beads. However, beaded fibers are apparent when adding CTAB, even at 1 wt.%, whereas thick fibers and/or bundles of fibers were found in nanofiber mats containing 1 wt.% SDS. This fact suggests that surfactant-polymer complexes favored by ionic surfactants

cause a certain degree of agglomeration to some extent producing beaded fibers and/or bundles. In contrast, highly homogeneous and almost bead-free fiber mats were obtained from solutions containing high contents of Tween-20. On the other hand, nanofiber mats were not obtained with 90:10 LSL/PVP solutions but different nanostructures composed of electrosprayed particles eventually connected by thin filaments or particle clusters.

Nanostructures obtained upon addition of surfactants (SDS, Tween-20 or CTAB) to a 90:10 LSL/PVP solutions were able to form soft gels with the appearance of thickened liquids, while nanofiber mats obtained by electrospinning from 70:30 LSL/PVP solutions generated strong oleogels at 20% wt. concentration. In general, SAOS viscoelastic functions slightly increased with the surfactant concentration. In addition, these oleogels also showed excellent lubrication performance in a tribological contact, yielding extremely low values of the friction coefficient and wear, generally much lower than those found when using conventional lubricating greases. Moreover, the addition of surfactants to the electrospun solution significantly lowers both friction and wear in comparison with the oleogel prepared with surfactant-free nanofiber mats.

Overall, the addition of small amounts of surfactant to LSL/PVP solutions improves electrospinnability as well as the ability of resulting nanofiber mats to structure castor oil, resulting oleogels with enhanced rheological and tribological properties, which can drive potential applications as lubricants.

Acknowledgements This work is part of a research project (RTI2018-096080-B-C21) funded by MCIN/AEI/10. 13039/ 501100011033 and by "ERDF A way of making Europe." The financial support is gratefully acknowledged.

Funding Open Access funding provided by Universidad de Huelva / CBUA, thanks to the CRUE-CSIC agreement with Springer Nature.

Declarations

Conflict of interest The authors declare that there is no actual or potential conflict of interest in relation to this article.

References

1. Soni S, Agarwal M (2014) Lubricants from renewable energy sources—a review. Green Chem Lett Rev 7(4):359–382

2. Sadh PK, Duhan S, Duhan JS (2018) Agro-industrial wastes and their utilization using solid state fermentation: a review. Bioresour Bioprocess 5(1):1–15
3. Dachowski R, Kostrzewa P (2016) The use of waste materials in the construction industry. Procedia Eng 161:754–758
4. Kwek SY, Awang H (2021) Utilization of industrial waste materials for the production of lightweight aggregates: a review. J Sustain Cem Mater 10(6):353–381
5. Panchal TM, Patel A, Chauhan DD, Thomas M, Patel JV (2017) A methodological review on biolubricants from vegetable oil based resources. Renew Sustain Energy Rev 70:65–70
6. Carvajal JC, Gómez Á, Cardona CA (2016) Comparison of lignin extraction processes: economic and environmental assessment. Bioresour Technol 214:468–476
7. Pelaez-Samaniego MR, Yadama V, Garcia-Perez M, Lowell E, Zhu R, Englund K (2016) Interrelationship between lignin-rich dichloromethane extracts of hot water-treated wood fibers and high-density polyethylene (HDPE) in wood plastic composite (WPC) production. Holzforschung 70(1):31–38
8. Thakur VK, Thakur MK (2015) Recent advances in green hydrogels from lignin: a review. Int J Biol Macromol 72:834–347
9. Ragauskas AJ, Beckham GT, Biddy MJ, Chandra R, Chen F, Davis MF, Davison BH, Dixon RA 4, Gilna P, Keller M, Langan P, Naskar AK, Saddler JN, Tschaplinski TJ, Tuskan GA, Wyman CE (2014) Lignin valorization: improving lignin processing in the biorefinery. Science 344: 6185
10. Cecutti C, Agius D (2008) Ecotoxicity and biodegradability in soil and aqueous media of lubricants used in forestry applications. Bioresour Technol 99(17):8492–8496
11. Núñez N, Martín-Alfonso JE, Valencia C, Sánchez MC, Franco JM (2012) Rheology of new green lubricating grease formulations containing cellulose pulp and its methylated derivative as thickener agents. Ind Crops Prod 37(1):500–507
12. Gallego R, Arteaga JF, Valencia C, Díaz MJ, Franco JM (2015) Gel-like dispersions of hmdi-cross-linked lignocellulosic materials in castor oil: toward completely renewable lubricating grease formulations. ACS Sustain Chem Eng 3(9):2130–2141
13. Delgado MA, Cortés-Triviño E, Valencia C, Franco JM (2020) Tribological study of epoxide-functionalized alkali lignin-based gel-like biogreases. Tribol Int 146:106231
14. Cortés-Triviño E, Valencia C, Franco JM (2017) Influence of epoxidation conditions on the rheological properties of gel-like dispersions of epoxidized kraft lignin in castor oil. Holzforschung 71(10):777–784
15. Borrero-López AM, Martín-Sampedro R, Ibarra D, Valencia C, Eugenio ME, Franco JM (2020) Evaluation of lignin-enriched side-streams from different biomass conversion processes as thickeners in bio-lubricant formulations. Int J Biol Macromol 162:1398–1413
16. Borrero-López AM, Blánquez A, Valencia C, Hernández M, Arias ME, Eugenio ME, Fillat U, Franco JM (2018) Valorization of soda lignin from wheat straw solid-state fermentation: production of oleogels. ACS Sustain Chem Eng 6(4):5198–5205
17. Borrero-López AM, Blánquez A, Valencia C, Hernández M, Arias ME, Franco JM (2019) Influence of solid-state fermentation with Streptomyces on the ability of wheat and barley straws to thicken castor oil for lubricating purposes. Ind Crops Prod 140:111625
18. Borrego M, Martín-Alfonso JE, Sánchez MC, Valencia C, Franco JM (2021) Electrospun lignin-PVP nanofibers and their ability for structuring oil. Int J Biol Macromol 180:212–221
19. Kumar N, Tyagi R (2015) Analysis of the interactions of *Polyvinylpyrrolidone* with conventional anionic and dimeric anionic surfactant. J Dispers Sci Technol 36(11):1601–1606
20. Wang SC, Wei TC, Bin CW, Tsao HK (2004) Effects of surfactant micelles on viscosity and conductivity of poly(ethylene glycol) solutions. J Chem Phys 120(10):4980–4988
21. Jia L, Qin XH (2013) The effect of different surfactants on the electrospinning poly(vinyl alcohol) (PVA) nanofibers. J Therm Anal Calorim 112(2):595–605
22. Fang W, Yang S, Yuan TQ, Charlton A, Sun RC (2017) Effects of various surfactants on alkali lignin electrospinning ability and spun fibers. Ind Eng Chem Res 56(34):9551–9559
23. Araújo ES, Nascimento MLF, de Oliveira HP (2013) Influence of triton X-100 on PVA fibres production by the electrospinning technique. Fibres Text East Eur 100(4):39–43
24. Kriegel C, Kit KM, McClements DJ, Weiss J (2009) Electrospinning of chitosan-poly(ethylene oxide) blend nanofibers in the presence of micellar surfactant solutions. Polymer 50(1):189–200
25. Wang S-Q, He J-H, Xu L (2008) Non-ionic surfactants for enhacing electrospinability and for the preparation of electrospun nanofibers. Polym Int 57:1079–1082

26. Quinchia LA, Delgado MA, Franco JM, Spikes HA, Gallegos C (2012) Low-temperature flow behaviour of vegetable oil-based lubricants. Ind Crops Prod 37(1):383–388
27. Heyer P, Laüger J (2009) Correlation between friction and flow of lubricating greases in a new tribometer device. Lubr Sci 21(6):253–268
28. Wongsasulak S, Kit KM, McClements DJ, Yoovidhya T, Weiss J (2007) The effect of solution properties on the morphology of ultrafine electrospun egg albumen–PEO composite fibers. Polymer 48(2):448–457
29. Chari K, Antalek B, Lin MY, Sinha SK (1994) The viscosity of polymer-surfactant mixtures in water. J Chem Phys 100(7):5294–5300
30. Holmberg K, Jönsson B, Kronberg B, Lindman B (2003) Surfactants and polymers in aqueous solution. Wiley, New York, pp 39–66
31. Kriegel C, Arrechi A, Kit K, McClements DJ, Weiss J (2008) Fabrication, functionalization, and application of electrospun biopolymer nanofibers. Crit Rev Food Sci Nutr 48(8):775–797
32. Dallmeyer I, Ko F, Kadla JF (2010) Electrospinning of technical lignins for the production of fibrous networks. J Wood Chem Technol 30(4):315–329
33. Dallmeyer I, Ko F, Kadla JF (2014) Correlation of elongational fluid properties to fiber diameter in electrospinning of softwood kraft lignin solutions. Ind Eng Chem Res 53(7):2697–2705
34. Almdal K, Dyre J, Hvidt S, Kramer O (1993) Towards a phenomenological definition of the term "gel." Polym Gels Networks 1(1):5–17
35. Sánchez R, Valencia C, Franco JM (2014) Rheological and tribological characterization of a new acylated chitosan-based biodegradable lubricating grease: a comparative study with traditional lithium and calcium greases. Tribol Trans 57(3):445–454
36. Gallego R, Cidade T, Sánchez R, Valencia C, Franco JM (2016) Tribological behaviour of novel chemically modified biopolymer-thickened lubricating greases investigated in a steel-steel rotating ball-on-three plates tribology cell. Tribol Int 94:652–660
37. Cortés-Triviño E, Valencia C, Delgado MA, Franco JM (2019) Thermo-rheological and tribological properties of novel bio-lubricating greases thickened with epoxidized lignocellulosic materials. J Ind Eng Chem 80:626–632
38. Pogosian AK, Martirosyan TR (2007) Impact of surfactant structure on the tribological properties of bentonite-based greases. J Tribol 129(4):920–922

4. ARTICLE 3

Developing electrospun ethylcellulose nanofibrous webs: an alternative approach for structuring castor oil

María Borrego, José E. Martín-Alfonso*, M. Carmen Sánchez, Concepción Valencia, José M. Franco

* Pro2TecS – Chemical Product and Process Technology Research Center, Department of Chemical Engineering and Materials Science, Universidad de Huelva, ETSI, Campus de "El Carmen", 21071, Huelva, Spain.

Published in:

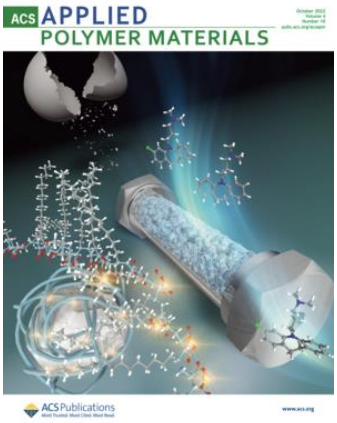

Publishing company: ACS

Editor-in-Chief: Kirk S. Schanze

Volume 4, Issue 10, pp 7217−7227

Year: 2022

ISSN: 2637-6105

DOI: https://doi.org/10.1021/acsapm.2c01090

Impact factor (2022): 5.0

JCR Journal rank: 16/86 in Polymer Science

4.1. Resumen

El objetivo de este estudio es estudiar la fabricación de nanofibras de etilcelulosa (EC) por electrohilado y examinar su capacidad de estructuración de aceites vegetales.

En primer lugar, se evaluó el efecto de la concentración de las disoluciones poliméricas en la morfología de las nanoestructuras preparando disoluciones desde el 2% hasta un 14 % p/p. El aumento de la concentración indujo un cambio en la morfología de las membranas obtenidas que se atribuye a una competencia entre la tensión superficial y la viscosidad. Para conseguir una disolución polimérica electrospinable se necesita superar un umbral de concentración conocido cómo concentración crítica de entrelazamiento (C_e), la cual define la transición entre el régimen de concentración semidiluido no-entrelazado y el régimen semidiluido entrelazado. En este caso al superar una concentración en torno a un 8% p/p se consiguieron fibras homogéneas sin defectos.

Por otra parte, otro de los parámetros evaluado ha sido el peso molecular de la EC, que afecta de forma directa a la viscosidad de la disolución y determina el cambio morfológico de las membranas desarrolladas. Para un mismo disolvente a 4, 8 y 12 % p/p se disolvió EC con diferentes pesos moleculares, i.e. 45 cP (EC1), 100 cP (EC2) y 300 cP (EC3). Por una parte, el aumento del peso molecular aumentó el diámetro de las fibras obtenidas y originó un descenso de la C_e y de la concentración crítica para un correcto electrohilado, conforme a la proporcionalidad $2.5C_e$. En definitiva, pesos moleculares mayores inducen a una mejora en la electrospinabilidad, lo que conduce a mayores diámetros y nanofibras más homogéneas y sin defectos.

Asimismo, se evaluó el papel de diferentes disolventes binarios en disoluciones de EC2 al 10% en THF/DMF (1/1), THF/DMAc (1/1), acetona/DMF (1/2), acetona/DMAc (1/2) y ácido acético. Debido a su baja constante dieléctrica y su momento

dipolar, además de un punto de ebullición más alto, el ácido acético no es capaz de desarrollar fibras sino una membrana compacta. Se observó que los diámetros medios de las nanofibras disminuyen al aumentar la constante dieléctrica y el momento dipolar de los disolventes, la viscosidad y el punto de ebullición. Las constantes dieléctricas más elevadas provocan mayores fuerzas de repulsión, las cuáles son responsables del estiramiento del jet, y mayores fuerzas electrostáticas, responsables de llevar el jet al colector.

Las redes de EC se dispersaron en aceite de ricino de forma que aquellas nanofibras obtenidas a partir de la concentración crítica de entrelazamiento dieron lugar a dispersiones físicamente estables a temperatura ambiente. En cambio, las membranas con combinaciones de fibras y partículas presentan una respuesta reológica predominantemente líquida. Aquellas físicamente estables, además presentaron una buena reversibilidad térmica y una adecuada respuesta tribológica, mejor que aquellos oleogeles de EC preparados por gelificación térmica. En definitiva, las membranas electrohiladas de EC se presentan cómo una buena alternativa a los espesantes de aceites vegetales.

ACS APPLIED POLYMER MATERIALS

pubs.acs.org/acsapm Article

Developing Electrospun Ethylcellulose Nanofibrous Webs: An Alternative Approach for Structuring Castor Oil

M. Borrego, J. E. Martín-Alfonso,* C. Valencia, María del Carmen Sánchez Carrillo, and J. M. Franco

Cite This: ACS Appl. Polym. Mater. 2022, 4, 7217−7227 Read Online

ACCESS | Metrics & More | Article Recommendations | Supporting Information

ABSTRACT: The development of environment-friendly natural polymer gel-like dispersions in oil media, with functional properties, in terms of formulation design and synthesis protocol, is still a cutting-edge research area for many applications. The aim of this work was to study the manufacture of electrospun ethylcellulose (EC) nanofibrous webs and to examine their usage to thicken vegetable oils as an alternative approach. The role of concentration, molecular weight (M_w), and binary solvent systems on the electrospinnability of EC and subsequently on the rheological properties of EC nanofiber dispersions in castor oil was investigated. It was observed that, for each M_w, defect-free nanofibers were produced above a critical concentration, corresponding to about 2.5 the entanglement concentration (C_e). The average fiber diameter increased with both M_w and EC concentrations. Dielectric constant and dipole moment of binary solvent systems influenced the morphology of the EC nanofiber web. The morphology of the micro- and nanoarchitectures generated played a key role in the physical stabilization and rheological behavior of electrospun EC dispersions. The storage modulus (G') of EC dispersions was correlated with both the spinning solution concentration and average fiber diameter. Furthermore, electrospun EC nanofiber dispersions were compared with EC oleogels obtained by traditional thermogelation from thermorheological and tribological points of view. Overall, this work proposes an efficient and innovative approach to produce bio-based oleogel-like dispersions with great potential in different sectors such as pharmaceuticals, food, or lubricants.

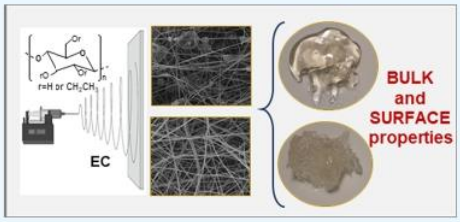

KEYWORDS: *ethylcellulose, electrospinning, entanglement network, gel-like dispersion, rheology*

1. INTRODUCTION

The design and development of electrospun nanofibers and their nanofibrous webs from natural polymers have attracted significant attention over several years to obtain bio-based materials with unique functional properties. These new nanoarchitectures could ideally drive a "smart material" for several engineering applications, such as biotechnology (tissue engineering, controlled/sustained release, etc.), food industry, membranes/filters, textiles, and so on.[1−5] In particular, cellulose and its derivatives have found profound applications in several engineering fields due to their biocompatibility and biodegradability characteristics.[6] Being the most abundant polymer on earth, cellulose is widely distributed over a variety of sources, including plants, algae, tunicates, and some bacteria such as *Acetobacter xylinum*.[7] Cellulose derivatives like methylcellulose, ethylcellulose, cellulose acetate, or carboxymethyl cellulose could be used to design functional nanofibers to provide a feasible approach to produce nanostructured porous materials with promising functionalities, flexibility, renewability, and biodegradability.[8,9] Ethylcellulose (EC) is a nonionic linear polysaccharide chemically derived from cellulose by ethylation. EC is composed of cellulose backbones with partial substitution of hydrogen hydroxyl end groups by ethyl groups,[10] and due to its nontoxicity, high flexibility, thermoplasticity, and film-forming ability, it is widely used in food, pharmaceutical, and biomedical applications.[11] In recent times, the development of functional nanocomposites of cellulose derivatives, and particularity from ethylcellulose, for different applications has drawn attention within the research community.[12−14] However, the potential of ethylcellulose to develop nanofibers with desired architectures via electrohydrodynamic processing has not been sufficiently explored. Electrospinning is a handy and cost-effective technique that uses an electric field to distort a droplet of a polymeric solution by inducing repulsion between the polymeric chains, thus overcoming the surface tension and allowing a jet to be formed while the solvent is evaporated,[15] eventually resulting in the formation of polymer fibers with diameters ranging from 2 nm to several micrometers using polymer solutions of both natural and synthetic polymers. This process offers unique capabilities to produce natural nanofibers with controllable pore structures.[16] Depending on the solution properties, mainly surface tension, rheology, and electrical conductivity, influ-

Received: June 25, 2022
Accepted: August 23, 2022
Published: September 8, 2022

enced by polymer concentration, and operating parameters (voltage, distance between the tip and collector, flow rate, ambient humidity, and temperature), either electrospinning or electrospraying will occur, thereby producing fibers or particles, respectively, with different architectures. Electrospinning is able to produce a range of nanostructures with different shapes and sizes; particles, beaded fibers, smooth fibers, and ribbons, depending on both solution physicochemical properties and operating parameters, make them favorable candidates to be used in a wide range of applications. The electrospinnability of ethylcellulose has been addressed in a few previous works.[17−19] Wu et al. discussed the effect of a mixed solvent of tetrahydrofuran (THF)/dimethylacetamide (DMAc) on the surface morphology and diameter distribution of ethylcellulose fibers and found that, using the binary solvent, the diameter of the fibers was thinner and the diameter distribution was narrower than when using either of the two solvents.[17] Park et al. studied the morphological and surface changes of electrospun EC fibers when using various solvents (THF and DMAc) and their ratios. Regular holes were formed on the surface of the fiber from pure THF and 80 wt % THF in DMAc, while a smooth surface was observed for the pure DMAc and 80:20 wt % DMAc ratio in THF.[18] Recently, Crabbe-Mann et al. investigated the influence of the EC concentration in ethanol/water at 80:20 (v/v) solutions on their electrospinnability and found that the morphological changes from particles with tails to thick fibers were charted from 17 to 25 wt % solutions.[19] These results indicated that the solvent type and biopolymer concentration remarkably affected the electrospinning process and the morphology of generated nanofibers.

On the other hand, oil structuring using sustainable thickeners has attracted great interest in both the industry and the academia in recent years, not only in food applications as a promising strategy for fat replacement[20] but also in the field of pharmaceuticals[21] and lubricants.[22] Oleogels are soft materials, consisting of a single self-assembling structuring agent, called gelator, or a combination of different thickener molecules able to form an entanglement network, which traps the oil into its micro- and/or nanostructure. The mechanical and rheological properties of oleogels depend on the interactions among their components (gelators, oils, additives, etc.) and the gelation mechanisms. Only a few biopolymers are able to gel oils by the formation of supramolecular structures through physical entanglements or chemical cross-linking among polymer chains.[23,24] Among them, EC is considered the only direct oil gelator to date able to generate physically viscoelastic gels in edible oils. The physical gelation of oils with EC is achieved by increasing the polymer/oil mixture temperature above the biopolymer glass transition (∼140 °C) and subsequently cooling down to room temperature, the so-called thermogelation mechanism. EC-based oleogels have shown potential in many applications such as the replacement of fats in foods,[25] heat resistance agents in chocolates,[26] oil binding agents in bakery products,[27] and as the basis for cosmetic pastes.[28] As previously mentioned, the strategy pursued for oil structuring, in all of these cases, involves a thermogelation mechanism. Besides, other indirect pathways to gel oils using hydrophilic biopolymers have been proposed, such as the so-called foam-templated[29] and emulsion-templated[30,31] approaches or stepwise solvent-exchange routes,[32,33] resulting in porous structures where oil can be adsorbed or entrapped. However, these procedures do not allow us to totally control or tune the self-assembled network formed by EC. Hence, the search for other more suitable approaches to incorporate EC nanostructures into an oil phase, aiming to create tailor-made three-dimensional networks that can likely give rise to oleogels with tunable functional properties, could be ideally welcomed for many applications. In this context, this work proposes an alternative approach to develop physically stable gel-like dispersions based on electrospun ethylcellulose nanofibrous webs and castor oil. Taking into account these considerations, the specific objectives of this work were (i) to study the role of the biopolymer concentration, molecular weight, and binary solvent systems on the electrospinnability of ethylcellulose solutions and (ii) to explore the ability of the different micro- and nanoarchitectures generated to structure castor oil by analyzing the rheological and tribological properties.

2. EXPERIMENTAL SECTION

2.1. Materials. Three commercially available ethylcellulose samples (48% ethoxy content) with different viscosity values (EC_1: 45 cP, EC_2: 100 cP, EC_3: 300 cP) purchased from Merck Sigma-Aldrich were used as spinning polymers as received. The higher the EC viscosity, the higher the molecular weight (M_w) is. Hence, M_w of the different EC samples were 3.9×10^4 (EC_1), 6.9×10^4 (EC_2), and 8.2×10^4 (EC_3) g/mol, and polydispersity indices were as follows: 1.60, 1.15, and 1.09.[34] The solvents used were acetone (Ac, purity 99.5%), dimethylformamide (DMF, purity 99.8%), dimethylacetamide (DMAc, purity 99.8%), tetrahydrofuran (THF, purity 99.0%), and acetic acid (AA, purity ≥99%). All solvents were supplied by Sigma-Aldrich and used as received without any purification. The main physical properties of these solvents are collected in Table S1 of the Supporting Information. Castor oil (viscosity: 0.55 Pa s, density: 0.958 g/mL, at 25 °C, Guinama, Spain) was stored at room temperature (23 °C), in a dark area, and used as vegetable oil to prepare different dispersions.

2.2. Preparation of Spinning Solutions and Rheological Characterization. The influence of EC concentration and molecular weight was investigated using a 1:1 THF/DMAc solvent system. EC was dissolved, at 40 °C, under magnetic stirring (300 rpm) for 2 h, to obtain solutions with concentrations ranging from 1.5 to 14 wt %. Then, the role of solvent systems was then studied for the most promising EC concentration. Homogeneous polymer solutions were prepared by dissolving EC_2 in different solvent systems: 1:1 THF/DMF, 1:1 THF/DMAc, 1:2 acetone/DMF, 1:2 acetone/DMAc, and acetic acid using the same protocol. All samples were centrifuged for 10 min at 3000 rpm and filtered to check that there were not solids in the solution. Viscous flow measurements of EC solutions were carried out at 23 °C, using an ARES controlled-strain rheometer (Rheometric Scientific, U.K.) equipped with a Couette geometry (internal radius 16 mm, external radius 17 mm, cylinder length 33.35 mm), in a shear rate range of 1−500 s^{-1}. At least two replicates were performed on fresh samples.

2.3. Electrospinning of EC Solutions and Morphological Characterization. The electrospinning device was constructed using a high-voltage power supply (Spellman High Voltage Electronics Corporation), a syringe with a blunt metal needle, a syringe pump (KD Scientific Pump Company), and a grounded aluminum foil collector. The EC solution was fed through the needle tip by a syringe pump at a flow rate of 0.8 mL/h (tip diameter ≈ 0.6 mm). Nanostructures were produced at a tip-to-target distance of 12 cm and an applied voltage of 20 kV. All of the electrospinning experiments were carried out at 23 °C with a humidity of 45%. The morphology of the electrospun fiber webs was examined using a scanning electron microscopy (FlexSEM 1000 II, Hitachi, Japan) after sputtering the samples with gold under vacuum. All SEM experiments were carried out at an accelerating voltage of 10 kV.

2.4. Manufacture of Dispersions of EC Electrospun Nanofiber Webs in Castor Oil and Their Rheological and

https://doi.org/10.1021/acsapm.2c01090
ACS Appl. Polym. Mater. 2022, 4, 7217−7227

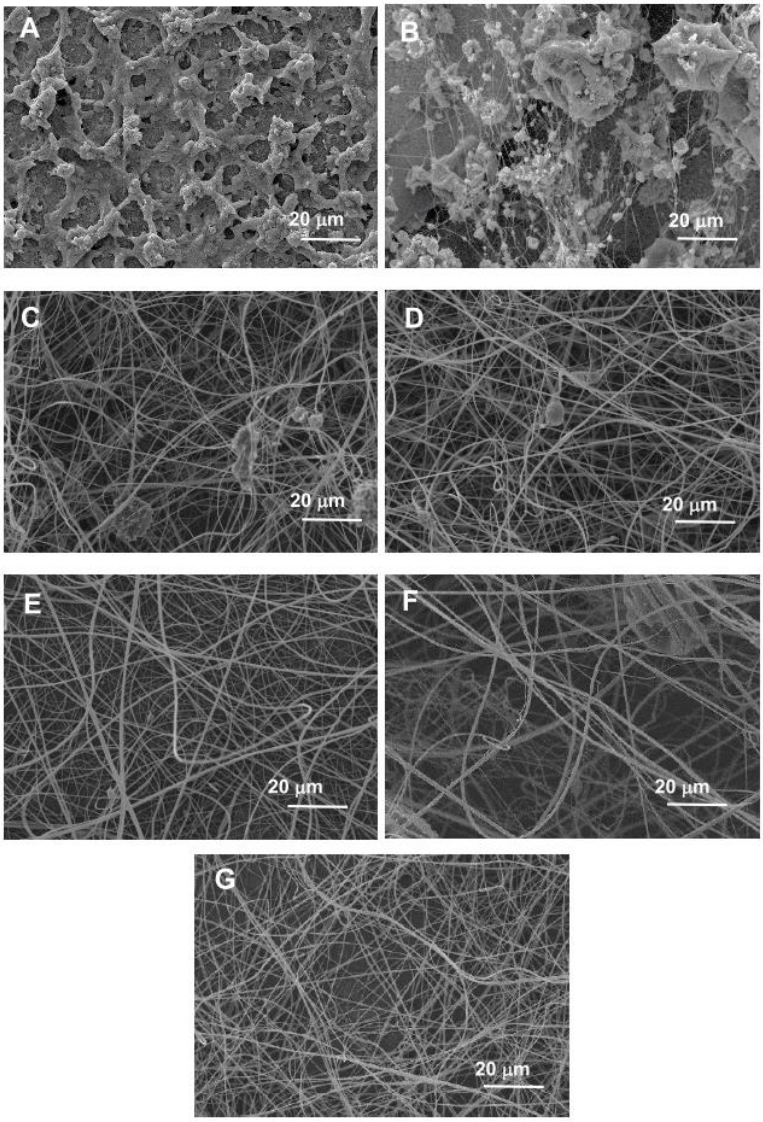

Figure 1. SEM micrographs of electrospun nanostructures obtained from ethylcellulose (EC_2) solutions in 1:1 THF/DMAc at different concentrations: (A) 2 wt %, (B) 4 wt %, (C) 6 wt %, (D) 8 wt %, (E) 10 wt %, (F) 12 wt %, and (G) 14 wt %.

Tribological Characterization. Electrospun EC nanofibrous webs were dispersed in castor oil, once placed in an open vessel, using an RW-20 mixer by IKA (Germany) coupled with an anchor impeller geometry. Selected electrospun EC nanostructures were dispersed at 15−20 wt % concentrations at room temperature (~23 °C) for 24 h (see Scheme S1 in the Supporting Information). This procedure involves two steps: first, ethylcellulose nanostructures are obtained via electrospinning and then the nanostructures are dispersed in the castor oil medium to promote the formation of a three-dimensional network. For comparison purposes, EC oleogels were prepared using a magnetic hot plate at a temperature of 150 °C under continuous stirring at 100 rpm until a homogeneous solution was achieved (~4 h). Samples were rheologically characterized with a controlled-stress rheometer Physica MCR-501 (Anton Paar, Austria) using a serrated parallel plate to avoid possible slip phenomena (25 mm diameter; 1 mm gap). A variety of rheological measurements were performed including steady-state flow tests and small-amplitude oscillatory shear (SAOS) measurements like amplitude, frequency, and temperature sweeps. All measurements were done under isothermal conditions (23 °C), except for obviously temperature ramps. The steady shear flow tests were performed by applying stepped shear rate ramps from 10^{-2} to 100 s^{-1}. A long enough data acquisition time was established, at each shear rate, to ensure the achievement of steady-state flow conditions. Frequency sweeps to determine the mechanical spectra were carried out over a 3×10^{-2}−10^{2} rad/s frequency range, and temperature sweep tests were performed at 0.628 rad/s and a heating rate of 5 °C/min from 25 to 125 °C. Both temperature and frequency sweep tests were performed within the linear viscoelastic regime. The friction coefficient of electrospun EC dispersions and oleogels was measured in a ball-on-three-plates tribological cell coupled with the same rheometer. The three lower plates (made from 1.4301 steel) were fixed through the sample holder forming 45° to the rotating axis, and the upper ball (made from 1.4401 steel) was placed on them with a preset normal load applied. The friction coefficient was obtained by applying a normal load of 30 N and a constant rotational speed of 50 rpm during 600 s at 23 °C. This test was repeated four times to obtain an accurate average friction coefficient.

3. RESULTS AND DISCUSSION

3.1. Electrospinnability of Ethylcellulose Solutions.

3.1.1. Effect of Ethylcellulose Concentration on Electro-

https://doi.org/10.1021/acsapm.2c01090
ACS Appl. Polym. Mater. 2022, 4, 7217−7227

spinning. To study the influence of the solution concentration on nanostructure morphology, EC_2 (100 cP) solutions in 1:1 THF/DMAc were prepared with concentrations in the range of 1.5−14 wt %. Figure 1 displays SEM micrographs of the EC_2 electrospun fiber mats collected using different biopolymer concentrations. The results show that not a really fibrous nanostructure but a kind of network composed of clusters of particles was obtained with the 2 wt % EC_2 solution. The particle formation indicates insufficient chain entanglements. Hence, the study was not extended to concentrations below 2 wt % EC_2. On increasing the biopolymer concentration to 4 wt %, nanofibers were produced to some extent although many defects and particles were still present. Above 8 wt %, defect-free fibers could be collected. The change in morphology with increasing concentration must be attributed to a competition between surface tension and viscosity. It is well known that to obtain uniform ejection of the charged jet in electrospinning, a solution with a minimum level of polymer concentration is required to exceed an extensive molecular entanglement like a prerequisite for the formation of a stable and continuous jet. This concentration is called the critical entanglement concentration (C_e). If the viscosity of the solution is too low, a continuous stream of the charged jet cannot be formed, as the charged jet experiences instability leading to the formation of droplets; this is called electrospraying.[35] Conversely, if the viscosity of the solution is too high, the continuous flow of the polymer liquid from the nozzle tip will be prevented. As a result, there is a processing window in terms of the concentration range within which polymer solutions are electrospinnable and beyond that discrete particles are likely to be formed. The critical entanglement concentration, C_e, defines the transition from the semidilute nonentangled to the semidilute entangled regimes. To determine C_e, viscous flow tests of EC_2 solutions were carried out. All of the systems exhibited a Newtonian behavior, and, obviously, the viscosity increased when the EC_2 concentration increased from 0.010 to 29.7 Pa·s in the 1.5−12 wt % concentration range, as can be observed in the Supporting Information (Figure S1). The concentration dependence of the specific viscosity ($\eta_{sp}=(\eta_p - \eta_{sol})/\eta_{sol}$, where η_p is the polymer solution viscosity and η_{sol} is the solvent viscosity) for EC_2 solutions in 1:1 THF/DMAc is also displayed in the Supporting Information (Figure S2). According to the method proposed by Colby et al.,[36] which involves the quantification of the concentration dependence of the specific viscosity of linear polymer solutions in good solvents, there are several different (power-law) scaling factors related to the dependences of the specific viscosity upon the polymer concentration in the different concentration regimes. For neutral linear polymers in a good solvent, the specific viscosity is represented as $\eta_{sp} \sim C^{1.25}$ in the semidilute nonentangled regime and as $\eta_{sp} \sim C^{3.75}$ in the semidilute entangled domain. For solutions below 3 wt % EC_2, it was found that $\eta_{sp} \sim C^{1.3}$, which is consistent with the theoretical prediction for semidilute nonentangled solutions. Above 4 wt % EC_2, $\eta_{sp} \sim C^{3.5}$, characteristic of semidilute entangled solutions. The change in slope occurs between 3 and 4 wt % (marked at $C_e \approx 3.4$), which delimits both regimes. As shown by the SEM micrographs in Figure 1, semidilute nonentangled solutions produce clusters of particles, while semidilute entangled solutions produce fibers with increased uniformity when qualitatively compared to nonentangled solutions; concentrations above 8 wt % EC_2 produces totally uniform fibers. The solution at a 4 wt % EC2 concentration, close to the estimated C_e, as discussed above, produces a hybrid architecture with beaded thin fibers in combination with clusters of particles. In this regard, Tang et al.,[37] who studied the electrospinnability of poly(vinyl alcohol) (PVA) nanofibers, determined that the critical concentration to spin bead-free nanofibers was ~2.5 times greater than the entanglement molecular weight concentration, C_e. In this case, this proportion provides a critical concentration of 8.5 wt % to achieve totally bead-free nanofibers, which is in agreement with the experimental observations. In addition, to investigate the electrospinnability of EC_2 solutions, the relationship between the average fiber diameter and the specific viscosity is displayed in Figure 2. The data points of the solutions that could be

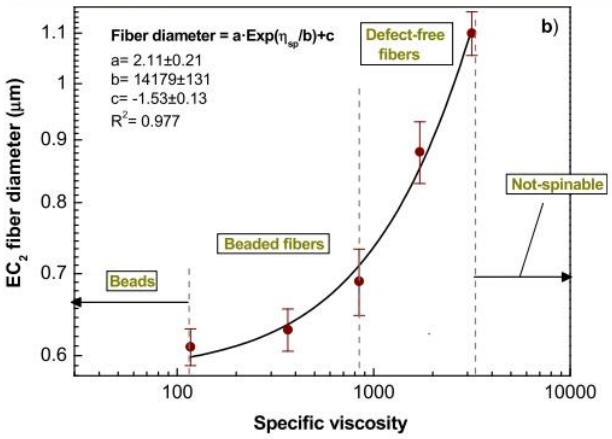

Figure 2. Effect of the specific viscosity of EC_2 solutions on the electrospun average fiber diameter and electrospinnability.

clearly electrospun into beaded or bead-free fibers are shown in the figure, and an exponential relationship was observed between the fiber diameter and the specific viscosity.

3.1.2. Effect of Ethylcellulose Molecular Weight on Electrospinning. As has been noted previously, the viscosity of the spinning solution is closely related to the morphology of the fibers obtained, one of the determining parameters directly influencing the viscosity of the solution being the polymer molecular weight (M_w). Viscosity influences the concentration regimes; therefore, the choice of the molecular weight determines, together with other parameters, the morphological changes. To study the effects of the molecular weight, solutions of ethylcellulose with different M_w values, i.e., 45 cP (EC_1), 100 cP (EC_2), and 300 cP (EC_3), were prepared to attain concentrations of 4, 8, and 12 wt %, respectively. To the best of our knowledge, the influence of the ethylcellulose molecular weight on the morphology of electrospun nanostructures has never been reported. As can be observed in Figure 3, EC with higher molecular weight (EC_3) produced defect-free fibers at a concentration of 8 wt %, and beaded fibers at 4 wt %. However, for EC with a lower molecular weight (EC_1), it was necessary to increase the concentration of the solution until 12 wt % to achieve bead-free electrospun fiber mats and even some embedded particles are eventually detected (see Figure 4G). In addition, for the same concentrations, the higher EC molecular weight, the larger average fiber diameter was. According to these results, uniform electrospun fiber mats were achieved above a minimum critical concentration, which depends on the EC molecular weight. This certain EC critical concentration for a 45 cP EC was above 12 wt %, whereas for

https://doi.org/10.1021/acsapm.2c01090
ACS Appl. Polym. Mater. 2022, 4, 7217−7227

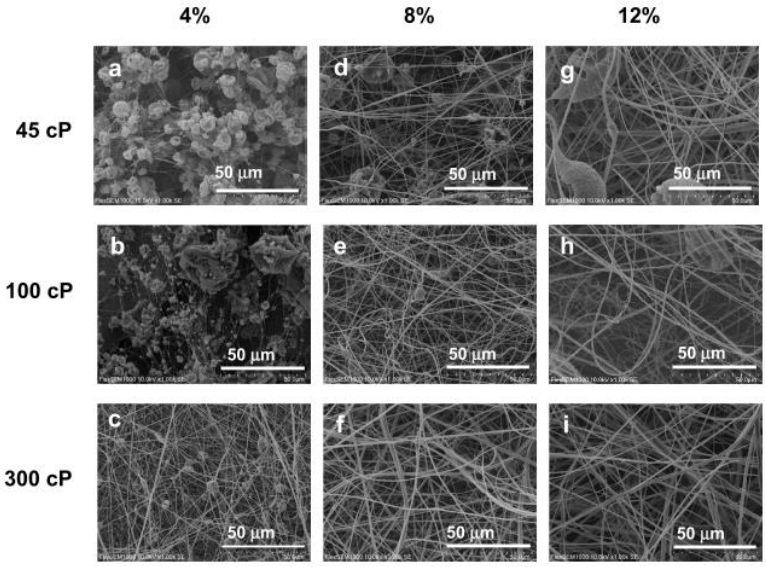

Figure 3. Effect of ethylcellulose molecular weights (45, 100, and 300 cP) on the morphology of electrospun nanostructures: 4 wt % (a–c), 8 wt % (d–f), and 12 wt % (g–i).

the 300 cP EC, it was below 8 wt %. Or, from another perspective, to obtain morphological appearance and fiber diameters similar to those of the nanostructures obtained with the spinning solution of high molecular weight (EC_3, 300 cP) at a concentration of 4 wt %, the concentration of the EC_1 (45 cP; $M_w \sim 2$ times lower) solution had to be increased to 8 wt %. The critical entanglement concentration (C_e) values determined from specific viscosity vs. EC concentration plots, for each of the molecular weights, were estimated to be 4.3, 3.4, and 2.7 wt % for EC_1, EC_2, and EC_3, respectively (Figure S3 in the Supporting Information). According to these C_e values, and considering the ~2.5 proportionality previously discussed, for the lowest molecular weight, an EC concentration of around 11 wt % would be needed to obtain bead-free nanofibers; however, if the EC molecular weight was increased to 100 and 300 cP, the concentration required would be reduced to 8.5 and 6.5 wt %, respectively, which is approximately in agreement with the experimental morphological observations (Figure 3). Therefore, increasing the molecular weight in the EC solutions increases the molecular entanglement of the biopolymer and improves the electrospinnability, which leads to larger fiber diameters and more homogeneous electrospun defect-free nanofiber mats.

3.1.3. Effect of Solvent Systems on Electrospinning. To determine the optimal solvent systems for EC electrospinning, several EC_2 spinning solutions at 10 wt % concentration in 1:1 THF/DMF, 1:1 THF/DMAc, 1:2 acetone/DMF, 1:2 acetone/DMAc, and acetic acid were electrospun. Figure 4 shows the SEM micrographs of the EC electrospun nanofiber mats in these mixed solvents and their average fiber diameters. As can be observed, at this EC2 concentration, all solvent systems studied were found to produce a sufficient quantity of bead-free fibers to form homogeneous electrospun fiber mats, with the exception of acetic acid (AA) that does not allow fibers to be obtained but a compact morphology instead (see Figure 4E). This fact is probably related to its relatively low dielectric constant and dipole moment compared to the other mixed solvents, combined with its higher boiling point (>100 °C) (see Supporting Information Table S1). In this case, the charged jets could not be dried enough before being collected on a grounded target. This result is in very good accordance with the literature findings, where AA was reported to be the less favorable solvent for cellulose acetate, yielding no uniform electrospun mats.[38] Comparing the binary solvent systems, both the THF-based and the acetone-based binary solvents are adequate to determine the effect of solvents on the morphology of electrospun fiber mats. According to the physicochemical properties of solvents (see Table S1), if THF was replaced by acetone in the binary system, the dielectric constant and dipole moment will be remarkably increased, while the density, surface tension, viscosity, and boiling point will be decreased. As may be observed in Figure 4, uniform nanofiber mats were collected when using all of the binary solvent systems studied; however, it was found that the average fiber diameters decreased when the dielectric constant and dipole moment of the solvents increased and the viscosity and boiling point of the solvents decreased, i.e., acetone-based binary solvents. Chuangchote et al. found a similar correlation between the dielectric constant and dipole moment of the solvent and resulting fiber diameters for the electrospinning of poly(vinyl pyrrolidone) in different alcohol solutions (methanol, ethanol, and 2-propanol),[39] whereas Lee et al. found that the solvent dielectric constant is one of the key properties in the electrospinning process.[40] Solvents with higher dielectric constants lead to greater Coulombic repulsion forces, which are responsible for the stretching of the charged jet, and electrostatic forces, which are responsible for carrying the charged jet to the collector. In this sense, the dielectric constant and dipole moment of the binary solvent systems investigated played an influential role in the morphological features of EC nanofibers. However, despite this, the differences found in the diameter of fibers cannot be considered very relevant. In general, the appearance of the electrospun fiber web obtained with these binary solvent systems was somewhat heterogeneous, exhibiting some beaded fibers and/or eventual embedded particles, except for the THF/DMAc solvent system.

https://doi.org/10.1021/acsapm.2c01090
ACS Appl. Polym. Mater. 2022, 4, 7217–7227

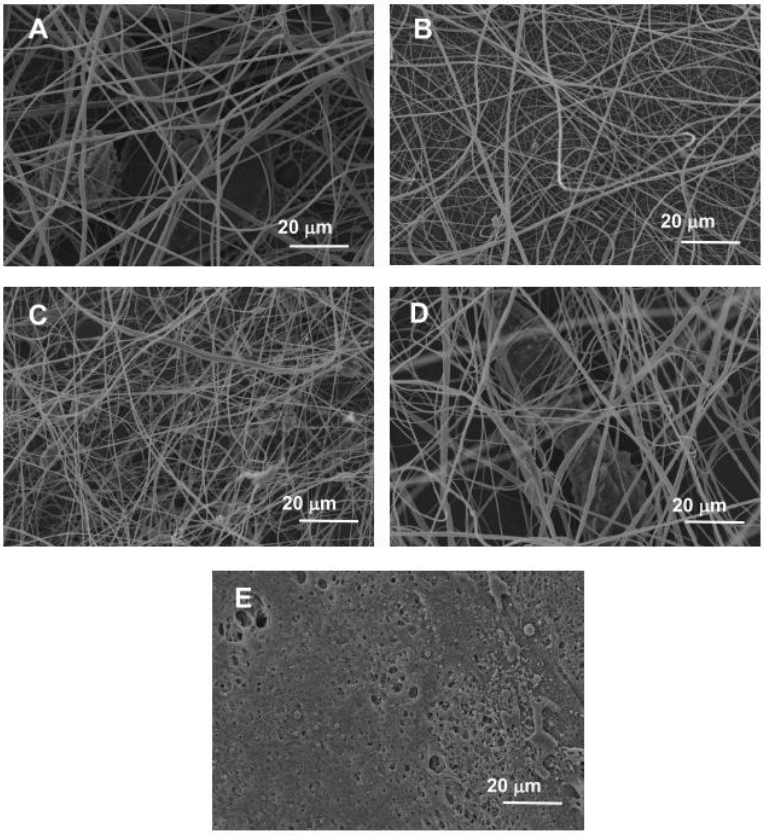

Samples	Fiber mean diameter* (μm)
(A) THF:DMF (1:1)	1.77±0.61
(B) THF:DMAc (1:1)	1.68±0.33
(C) DMF:Ac (2:1)	1.02±0.71
(D) DMAc:Ac (2:1)	1.45±0.71
(E) Acetic acid	-

Figure 4. Effect of solvent systems on the morphology of electrospun nanostructures. SEM micrographs obtained from 10 wt % ethylcellulose (EC_2) solutions in (A) THF/DMF, (B) THF/DMAc, (C) DMF/acetone, (D) DMAc/acetone, and (E) acetic acid. The table collects the average mean fiber diameters obtained from these pictures.

3.2. EC Electrospun Nanofiber Dispersions in Castor Oil. To study the ability of different EC electrospun structures obtained to form physically stable dispersions, the micro- and nanostructures were mixed with castor oil at 20 wt % using the methodology described in the Experimental Section. The structures were selected from EC spinning solutions at concentrations ranging from 4 to 12 wt % and the three molecular weights (EC_1, EC_2, and EC_3). Nanostructures obtained with spinning solutions below 4 wt %, i.e., essentially not well-developed nanofiber webs, provided physically unstable dispersions.

3.2.1. Rheological Properties. The evolution of the storage (G') and loss (G'') moduli with frequency for dispersions formulated with EC nanostructures is shown in Figure 5. In most cases, the mechanical spectra of all samples show a typical weak gel-like response with G' values higher than those of G''. As can be seen, the evolution of both moduli with frequency depends on the EC molecular weight and, especially, on the spinning polymer concentration. In addition, dispersions formulated with nanostructures obtained from solutions containing 4 wt % EC with lower molecular weights (EC_1 and EC_2) display a viscoelastic fluid response ($\tan \delta = G''/G' > 1$). G' and G'' values increased with the spinning solution concentration and EC molecular weight. Nevertheless, an exception was found for the dispersion of EC_3 (300 cP) nanofibrous web obtained from the solution with the highest concentration, where a decrease in the viscoelastic functions was observed. This behavior could be attributed to the strong H-bonds among the long chains of EC_3 molecules that inheritably keep the molecules in their own conformation, hindering the entry of oil molecules into the EC_3 network during the dispersion manufacture. Figure 6 illustrates the influence of nanofiber morphology on the linear viscoelastic response of the resulting dispersions formulated with EC_2. Figure 6a displays the evolution of the storage modulus obtained from the mechanical spectrum at 1 rad/s, G_1', as a function of the spinning polymer concentration and fiber diameter. As can be observed, G_1' increases with both spinning

https://doi.org/10.1021/acsapm.2c01090
ACS Appl. Polym. Mater. 2022, 4, 7217−7227

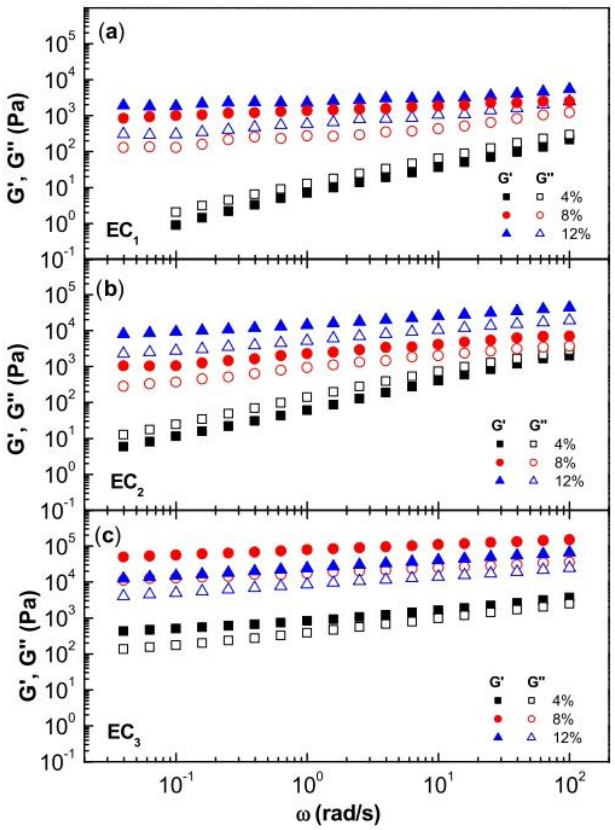

Figure 5. Evolution of the storage, G' (filled symbols), and loss, G'' (open symbols), moduli with frequency for dispersions of ethylcellulose electrospun nanofibrous webs in castor oil, as a function of the concentration in the spinning solution and the ethylcellulose molecular weight of the biopolymer: (a) 45 cP, (b) 100 cP, and (c) 300 cP.

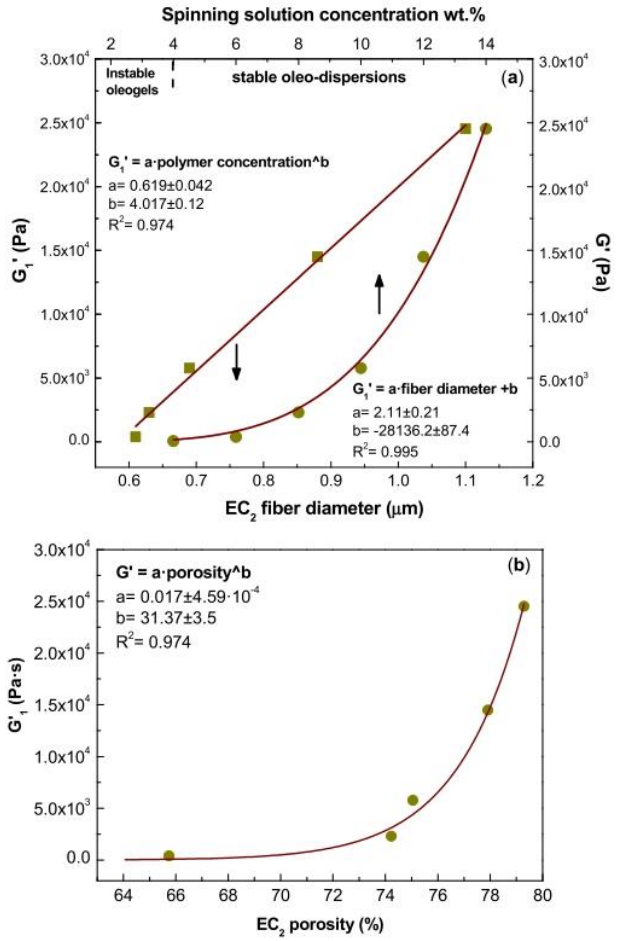

Figure 6. Evolution of the storage modulus, at 1 rad/s (G_1'), as a function of (a) the spinning solution concentration and average fiber diameter and (b) nanostructure porosity for dispersions of ethylcellulose (EC_2) electrospun nanofibrous webs in castor oil.

polymer concentration and fiber diameter and evolves potentially and linearly, respectively, in the experimental ranges studied. The influence of the porosity of electrospun nanostructures on the viscoelastic behavior of derived dispersions is also illustrated in Figure 6b. As can be observed, G_1' increases potentially with the porosity, which could be a consequence of a spongier nanostructure with a higher effective specific surface area to retain the oil. These results could be related to the wetting behavior of the electrospun EC nanostructures. As is known, the capacity of some modified cellulose-based products to retain or absorb oils is closely related to the physicochemical properties of the surface.[41] The results could also be corroborated through the physical appearance of the different oleo-dispersions (see Figure S4 of the Supporting Information). Thus, these empirical correlations allow estimating the physical stability and linear viscoelastic response of the oleo-dispersions from the nanoarchitecture (fiber size and porosity) of electrospun fiber webs and, indirectly, from the intrinsic properties of EC solutions. The viscous flow behavior of EC_2 electrospun nanofiber dispersions in castor oil was also studied, and the evolution of the apparent viscosity with shear rate is shown in Figure 7 as a function of the concentration of the spinning solution. The viscosity of the EC electrospun nanofiber dispersions increases monotonically with the spinning solution concentration (i.e., with fiber diameter) by 2.5 orders of magnitude at low shear

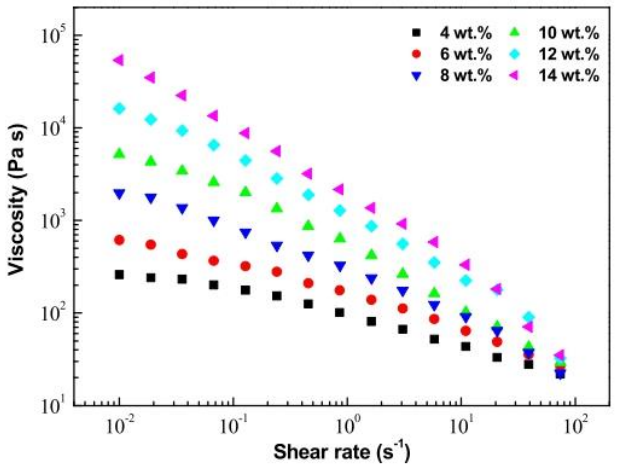

Figure 7. Evolution of the apparent viscosity with shear rates for dispersions formulated with ethylcellulose nanostructures obtained from spinning solutions having different EC_2 concentrations.

rates when the concentration was modified from 4 to 14 wt %. All of the dispersions exhibited a shear-thinning flow behavior that is more pronounced as the concentration of the spinning

https://doi.org/10.1021/acsapm.2c01090
ACS Appl. Polym. Mater. 2022, 4, 7217−7227

solution increases. The resistance of the entangled fiber network to flow is relatively strong at small shear rates and becomes weaker at high shear rates due to a reorientation and/or breakdown of fibers. Dispersions with higher spinning solution concentrations (12 and 14 wt %) exhibited fracture in the sample at high shear rates (>30 s^{-1}).

The impact of the concentration of dispersed EC electrospun nanofibers on SAOS tests was also investigated. Figure 8

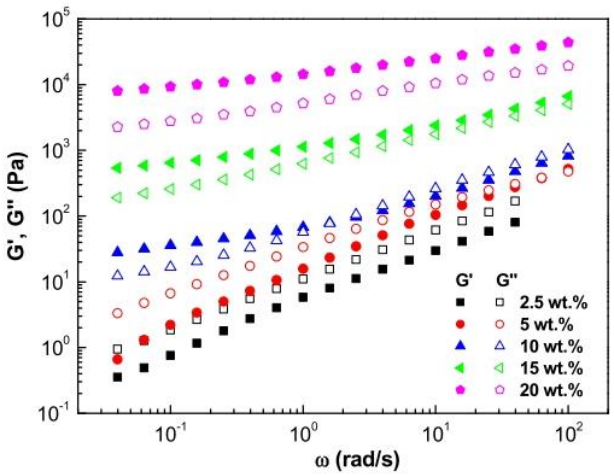

Figure 8. Evolution of the storage, G' (filled symbols), and loss, G'' (open symbols), moduli with frequency for dispersions of ethylcellulose (EC_2) electrospun nanofibrous webs in castor oil as a function of the nanofiber concentration.

displays the evolution of the viscoelastic functions of EC_2 electrospun nanofiber dispersions in castor oil as a function of concentration. As can be seen, for lower thickener concentrations (2.5−10 wt %), liquid-like viscoelastic responses were obtained, where both G' and G'' markedly increased with frequency and G'' values lay above those of G' until reaching a crossover at a certain frequency, which decreased with the nanofiber concentration. The reciprocal of the crossover frequency allows the terminal relaxation time to be estimated, the increase in the terminal relaxation time being a clear indication of the progressive relevance of the elastic response as nanofiber concentration was increased. On the other hand, dispersions with higher EC_2 electrospun nanofiber concentrations (15 and 20 wt %) evinced weak gel-like viscoelastic properties with a predominance of the storage modulus (G') over the loss modulus (G'') in the frequency range studied and much lower frequency dependence of both moduli. This change in rheological response could be attributed to a higher degree of interactions among adjacent EC fibers.[42]

Moreover, temperature sweep tests in the linear viscoelastic regime were performed on a selected EC_2 electrospun nanofiber dispersion, at 15 wt %, and compared with those performed on the respective EC_2 oleogel prepared by applying the typical thermogelation mechanism, i.e., by solubilizing EC_2 at 140 °C and cooling down to room temperature. These temperature sweep tests aim to analyze more deeply the thermorheological response of oleogel-like samples processed with different approaches. The test was carried out as a three-cycle experiment, which includes one heating to 125 °C, cooling down to 25 °C, and an additional second heating stage to 125 °C, to assess the thermoreversibility of the microstructural networks. Figure 9 displays the evolution of the linear viscoelastic moduli (G' and G'') with temperature for

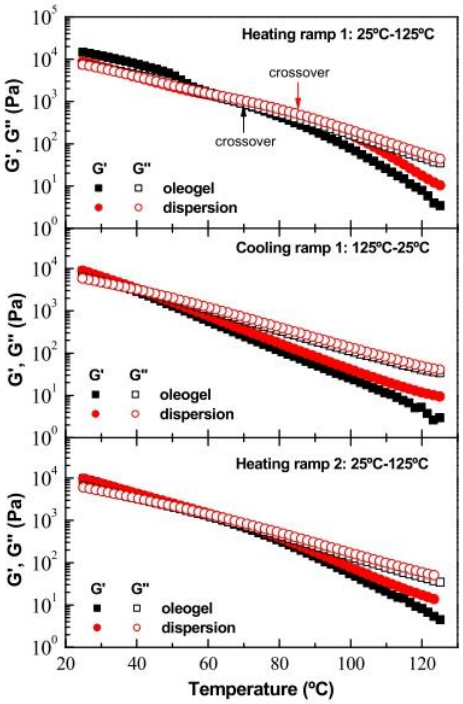

Figure 9. Evolution of the storage, G' (filled symbols), and loss, G'' (open symbols), moduli with temperature for a selected dispersion of ethylcellulose (EC_2) electrospun nanofibrous web in castor oil when applying a three-step heating−cooling−heating cycle as compared with that shown for the oleogel prepared by thermogelation (EC_2 concentration: 15 wt %).

both the EC_2 electrospun nanofiber dispersion and the equivalent oleogel. As can be observed, in the first heating, at low temperatures, the storage modulus (G') is higher than the loss modulus (G'') and both moduli gradually decreased when the temperature increased until a crossover was reached, and then G'' became higher than G'. The decrease in the linear viscoelastic moduli reflects a rearrangement and partial disruption of the entanglement network by heating, mainly due to a weakening of physical interactions, mostly hydrogen bonds.[43] This decrease is more pronounced for oleogel than for nanofiber dispersion. This fact could be attributed to the sol−gel transition of the network in the sample.[44] Interestingly, a clear influence of the processing protocol on the values of the crossover temperature can be observed. EC_2 electrospun nanofiber dispersion displayed a crossover temperature of about 15 °C higher than oleogel. Upon cooling and second heating, thermal reversibility was observed in both samples, with values of the linear viscoelastic moduli slightly higher for the dispersion and similar crossover points for both samples, which otherwise were shifted to lower temperatures. Therefore, according to these results, EC_2 electrospun nanofiber dispersions withstand medium−high temperatures similarly or better than the oleogel and displayed good thermal reversibility. The faster weakening of the conventional oleogel structure during the first heating reflects a more fragile nature of this network, which can disrupt more easily than the percolation network of electrospun nanofibers. After the first

https://doi.org/10.1021/acsapm.2c01090
ACS Appl. Polym. Mater. 2022, 4, 7217−7227

heating cycle, thermally induced rearrangements of both networks are very similar.

3.2.2. Tribological Properties. Finally, to explore one possible industrial application of these samples (nanofiber dispersion and conventional oleogel) as environment-friendly semisolid lubricant formulations, the friction coefficient was assessed in a ball-on-plate steel−steel tribological contact. Table 1 collects the stationary values of the friction coefficient and the corresponding average diameter of wear scars generated during the friction experiments. Both samples showed a satisfactory tribological response. Thus, the friction coefficient values were comparable to those obtained under similar conditions with a multipurpose lithium semisolid lubricant,[45] as well as with other gel-like dispersions based on synthetic polymers previously proposed as bio-based lubricants.[46] Interestingly, the EC_2 electrospun nanofiber dispersion used as a lubricant provided an extraordinarily low friction coefficient value and smaller wear scars than that obtained with the conventional oleogel. This fact could be attributed to the different entanglement networks achieved by both methods. In this sense, the electrospun nanofiber percolation network seems to have a greater ability to release the lubricating oil into the tribological contact, thereby improving the frictional and wear behavior.

Table 1. Values of the Friction Coefficient and Average Diameter of Wear Scars Obtained with Both a Selected Dispersion of Ethylcellulose (EC_2) Electrospun Nanofibrous Web in Castor Oil and the Equivalent Oleogel Prepared by Thermogelation When Acting as Lubricants in a Tribological Contact (EC_2 Concentration: 15 wt %)

sample	friction coefficient	wear scar diameter (μm)
ethylcellulose electrospun nanofiber dispersion	$0.075 \pm 2.5 \times 10^{-3}$	359.7 ± 18.3
oleogel (from thermogelation)	$0.110 \pm 1.4 \times 10^{-3}$	433.1 ± 24.1

4. CONCLUSIONS

Nanofibrous webs of ethylcellulose (EC) were successfully produced via electrospinning and validated for structuring castor oil. The morphology of EC nanostructures can be modulated by modifying the properties of the spinning solution, including EC concentration and molecular weight, and solvent. Particle networks and/or hybrid nanostructures comprised of thin fibers in combination with clusters of particles were collected from solutions with EC concentrations below or around the critical entanglement concentration (C_e), while defect-free nanofibers were produced when the concentration was increased to about 2.5 times C_e regardless of the EC molecular weight. An increase in both EC molecular weight and concentration improves electrospinnability resulting in a higher number of entanglements in the nanofibrous web and larger average fiber diameters. The physicochemical properties of binary solvent systems, especially dielectric constant and dipole moment, play an important role in the morphology of EC nanofiber webs. Among all of the solvent systems employed, THF/DMAc provides the most homogeneous nanofiber mats and the best electrospinning performance. EC nanofibrous webs obtained from solutions above C_e are able to form physically stable gel-like dispersions by simply mixing them in castor oil, at room temperature, for nanofiber concentrations above 15 wt %. Instead, liquid-like viscoelastic dispersions were obtained at nanofiber concentrations of 2.5−10 wt %. In addition, the morphology of the nanoarchitectures generated exerted a great impact on the rheological behavior of the resulting dispersions. Typical gel-like behavior was exhibited by dispersions of homogeneous and defect-free nanofibrous webs, while structures based on combinations of beaded fibers and particles give rise to predominantly liquid-like rheological responses. EC electrospun nanofiber dispersions in castor oil display very good thermal reversibility and better thermorheological and tribological behavior than conventional EC oleogels prepared by thermogelation. Overall, the electrospinning of ethylcellulose nanofibrous webs can be proposed as an alternative approach for structuring vegetable oils, which may have great importance in a diverse range of applications in fields such as lubricants, food, and pharmaceuticals.

■ ASSOCIATED CONTENT

Supporting Information

The Supporting Information is available free of charge at https://pubs.acs.org/doi/10.1021/acsapm.2c01090.

Manufacturing process of EC gel-like dispersions (Scheme S1); viscous flow curves of ethylcellulose (EC2) solutions in 1:1 THF/DMAc as a function of concentration (Figure S1); specific viscosity versus concentration plot for ethylcellulose (EC2) solutions in 1:1 THF/DMAc (Figure S2); specific viscosity versus concentration plots for ethylcellulose solutions in 1:1 THF/DMAc for different ethylcellulose molecular weights (Figure S3); physical appearance of oleodispersions formulated with ethylcellulose nanostructures obtained from spinning solutions having different EC2 concentrations: (a) 4 wt %, (b) 6 wt %, (c) 8 wt %, (d) 10 wt %, (e) 12 wt %, and (f) 14 wt % (Figure S4); and physical properties of the solvents used to prepare binary solvent systems for electrospinning of ethylcellulose (Table S1) (PDF)

■ AUTHOR INFORMATION

Corresponding Author

J. E. Martín-Alfonso − *Department of Chemical Engineering and Materials Science, Campus de "El Carmen", University of Huelva, Chemical Product and Process Technology Research Center (Pro2TecS), 21071 Huelva, Spain;* orcid.org/0000-0003-3180-7838; Email: jose.martin@diq.uhu.es

Authors

M. Borrego − *Department of Chemical Engineering and Materials Science, Campus de "El Carmen", University of Huelva, Chemical Product and Process Technology Research Center (Pro2TecS), 21071 Huelva, Spain*

C. Valencia − *Department of Chemical Engineering and Materials Science, Campus de "El Carmen", University of Huelva, Chemical Product and Process Technology Research Center (Pro2TecS), 21071 Huelva, Spain;* orcid.org/0000-0002-9197-4606

María del Carmen Sánchez Carrillo − *Department of Chemical Engineering and Materials Science, Campus de "El Carmen", University of Huelva, Chemical Product and Process Technology Research Center (Pro2TecS), 21071 Huelva, Spain*

J. M. Franco − *Department of Chemical Engineering and Materials Science, Campus de "El Carmen", University of Huelva, Chemical Product and Process Technology Research Center (Pro2TecS), 21071 Huelva, Spain;* orcid.org/0000-0002-3165-394X

Complete contact information is available at: https://pubs.acs.org/10.1021/acsapm.2c01090

Notes

The authors declare no competing financial interest.

■ ACKNOWLEDGMENTS

This work was supported by MCIN/AEI/10.13039/501100011033, "ERDF-A way of making Europe" (grant number: RTI2018-096080-BC21), and FEDER European Programme and Junta de Andalucía/EPIT2020-UHU (grant numbers: PY20_00751 and UHU202029).

■ REFERENCES

(1) Sencadas, V. Energy harvesting applications from poly(ε-caprolactone) electrospun membranes. *ACS Appl. Polym. Mater.* **2020**, *2*, 2105−2110.
(2) Golba, B.; Kalaoglu-Altan, O. I.; Sanyal, R.; Sanyal, A. Hydrophilic cross-linked polymeric nanofibers using electrospinning: imparting aqueous stability to enable biomedical applications. *ACS Appl. Polym. Mater.* **2022**, *4*, 1−17.
(3) Baji, A.; Truong, V. K.; Gangadoo, S.; Yin, H.; Chapman, J.; Abtahi, M.; Oopath, S. V. Durable antibacterial and antifungal hierarchical silver-embedded poly(vinylidene fluoride-co-hexafluoropropylene) fabricated using electrospinning. *ACS Appl. Polym. Mater.* **2021**, *3*, 4256−4263.
(4) Wang, S.; Shi, K.; Tripathi, A.; Chakraborty, U.; Parsons, G. N.; Khan, S. A. Designing intrinsically microporous polymer (pim-1) microfibers with tunable morphology and porosity via controlling solvent/nonsolvent/polymer interactions. *ACS Appl. Polym. Mater.* **2020**, *2*, 2434−2443.
(5) Liu, L.; Xu, W.; Ding, Y.; Agarwal, S.; Greiner, A.; Duan, G. A review of smart electrospun fibers toward textiles. *Compos. Commun.* **2020**, *22*, No. 100506.
(6) Joseph, B.; Sagarika, V. K.; Sabu, C.; Kalarikkal, N.; Thomas, S. Cellulose nanocomposites: Fabrication and biomedical applications. *J. Bioresour. Bioprod.* **2020**, *5*, 223−237.
(7) Blessy, J.; Hanna, J. M.; Sabu, T. N. K. Nanocellulose: Health Care Applications. In *Encyclopedia of Polymer Applications*, Mishra, M., Ed.; CRC Press: Boca Raton, 2018; pp 1829−1852.
(8) Schuhladen, K.; Raghu; Swathi, N. V.; Liverani, L.; Neščáková, Z.; Boccaccini, A. R. Production of a novel poly(ε-caprolactone)-methylcellulose electrospun wound dressing by incorporating bioactive glass and Manuka honey. *J. Biomed. Mater. Res., Part B* **2021**, *109*, 180−192.
(9) Shi, D.; Wang, F.; Lan, T.; Zhang, Y.; Shao, Z. Convenient fabrication of carboxymethyl cellulose electrospun nanofibers functionalized with silver nanoparticles. *Cellulose* **2016**, *23*, 1899−1909.
(10) Martín-Alfonso, J. E.; Nuñez, N.; Valencia, C.; Franco, J. M.; Díaz, M. J. Formulation of new biodegradable lubricating greases using ethylated cellulose pulp as thickener agent. *J. Ind. Eng. Chem.* **2009**, *15*, 818−823.
(11) Xiao, M.; Wan, L.; Corke, H.; Yan, W.; Ni, X.; Fang, Y.; Jiang, F. Characterization of konjac glucomannan-ethyl cellulose film formation via microscopy. *Int. J. Biol. Macromol.* **2016**, *85*, 434−441.
(12) Davidovich-Pinhas, M.; Co, E. D.; Barbut, S.; Marangoni, A. G. Physical structure and thermal behavior of ethylcellulose. *Cellulose* **2015**, *22*, 2137.
(13) Liu, Y.; Deng, L.; Zhang, C.; Feng, F.; Zhang, H. Tunable Physical Properties of Ethylcellulose/Gelatin Composite Nanofibers by Electrospinning. *J. Agric. Food Chem.* **2018**, *66*, 1907−1915.
(14) Niu, B.; Zhan, L.; Shao, P.; Xiang, N.; Sun, P.; Chen, H.; Gao, H. Electrospinning of zein-ethyl cellulose hybrid nanofibers with improved water resistance for food preservation. *Int. J. Biol. Macromol.* **2020**, *142*, 592−599.
(15) Muñoz, V.; Buffa, F.; Molinari, F.; Hermida, L. G.; García, J. J.; Abraham, G. A. Electrospun ethylcellulose-based nanofibrous mats with insect-repellent activity. *Mater. Lett.* **2019**, *253*, 289−292.
(16) Bhardwaj, N.; Kundu, S. C. Electrospinning: A fascinating fiber fabrication technique. *Biotechnol. Adv.* **2010**, *28*, 325−347.
(17) Wu, X.; Wang, L.; Yu, H.; Huang, Y. Effect of solvent on morphology of electrospinning ethyl cellulose fibers. *J. Appl. Polym. Sci.* **2005**, *97*, 1292−1297.
(18) Park, J. Y.; Han, S. W.; Lee, I. H. Preparation of electrospun porous ethyl cellulose fiber by THF/DMAc binary solvent system. *J. Ind. Eng. Chem.* **2007**, *13*, 1002−1008.
(19) Crabbe-Mann, M.; Tsaoulidis, D.; Parhizkar, M.; Edirisinghe, M. Ethyl cellulose, cellulose acetate and carboxymethyl cellulose microstructures prepared using electrohydrodynamics and green solvents. *Cellulose* **2018**, *25*, 1687−703.
(20) Martins, A. J.; Vicente, A. A.; Cunha, R. L.; Cerqueira, M. A. Edible oleogels: An opportunity for fat replacement in foods. *Food Funct.* **2018**, *9*, 758−773.
(21) Balasubramanian, R.; Sughir, A. A.; Damodar, G. Oleogel: A promising base for transdermal formulations. *Asian J. Pharm.* **2012**, *6*, 1−9.
(22) Martín-Alfonso, J.; Martín-Alfonso, M. J.; Franco, J. M. Tunable rheological-tribological performance of "green" gel-like dispersions based on sepiolite and castor oil for lubricant applications. *Appl. Clay Sci.* **2020**, *192*, No. 105632.
(23) Suzuki, M.; Hanabusa, K. Polymer organogelators that make supramolecular organogels through physical cross-linking and self-assembly. *Chem. Soc. Rev.* **2010**, *39*, 455−463.
(24) Patel, A. R. A colloidal gel perspective for understanding oleogelation. *Curr. Opin. Food Sci.* **2017**, *15*, 1−7.
(25) Marangoni, A. G. Polymer Gelation of Oils. WO Patent WO2010/1430662010.
(26) Marangoni, A. G. Chocolate Compositions Containing Ethylcellulose. WO Patent WO2012/0662772010.
(27) Cattaruzza, A.; Radford, S.; Marangoni, A. G. Dough Products Comprising Ethylcellulose and Exhibiting Reduced Oil Migration. WO Patent WO2012/0662772012.
(28) Marangoni, A. G. Thixotropic Compositions. WO Patent WO2012/0716512012.
(29) Patel, A. R.; Schatteman, D.; Lesaffer, A.; Dewettinck, K. A foam-templated approach for fabricating organogels using a water-soluble polymer. *RSC Adv.* **2013**, *3*, 22900−22903.
(30) Patel, A. R.; Cludts, N.; Sintang, M. D. B.; Lewille, B.; Lesaffer, A.; Dewettinck, K. Polysaccharide-based oleogels prepared with an emulsion-templated approach. *ChemPhysChem* **2014**, *15*, 3435−3439.
(31) Wijaya, W.; Van der Meeren, P.; Dewettinck, K.; Patel, A. R. High internal phase emulsion (HIPE)-templated biopolymeric oleofilms containing an ultra-high concentration of edible liquid oil. *Food Funct.* **2018**, *9*, 1993−1997.
(32) de Vries, A.; Hendriks, J.; van der Linden, E.; Scholten, E. Protein oleogels from protein hydrogels via a stepwise solvent exchange route. *Langmuir* **2015**, *31*, 13850−13859.
(33) de Vries, A.; Wesseling, A.; van der Linden, E.; Scholten, E. Protein oleogels from heat-set whey protein aggregates. *J. Colloid Interface Sci.* **2017**, *486*, 75−83.
(34) Sánchez, R.; Franco, J. M.; Delgado, M. A.; Valencia, C.; Gallegos, C. Thermal and mechanical characterization of cellulosic derivatives-based oleogels potentially applicable as bio-lubricating greases: Influence of ethyl cellulose molecular weight. *Carbohydr. Polym.* **2011**, *83*, 151−158.
(35) Saquing, C. D.; Tang, Ch.; Monian, B.; Bonino, Ch.A.; Manasco, J. L.; Eben Alsberg, E.; Khan, S. A. Alginate-polyethylene oxide blend nanofibers and the role of the carrier polymer in electrospinning. *Ind. Eng. Chem. Res.* **2013**, *52*, 8692−8704.

(36) Colby, R. H.; Fetters, L. J.; Funk, W. G.; Graessley, W. W. Effects of concentration and thermodynamic interaction on the viscoelastic properties of polymer solutions. *Macromolecules* **1991**, *24*, 3873−3882.
(37) Tang, C. A.; Ozcam, E.; Stout, B.; Khan, S. A. Effect of pH on protein distribution in electrospun PVA/BSA composite nanofibers. *Biomacromolecules* **2012**, *13*, 1269−1278.
(38) Liu, H.; Hsieh, Y.-L. Ultrafine fibrous cellulose membranes from electrospinning of cellulose acetate. *J. Polym. Sci., Part B: Polym. Phys.* **2002**, *40*, 2119−2129.
(39) Chuangchote, S.; Sagawa, T.; Yoshikawa, S. Electrospinning of poly(vinyl pyrrolidone): Effects of solvents on electrospinnability for the fabrication of poly(p-phenylene vinylene) and TiO_2 nanofibers. *J. Appl. Polym. Sci.* **2009**, *114*, 2777−2791.
(40) Lee, K. H.; Kim, H. Y.; Bang, H. J.; Jung, Y. H.; Lee, S. G. The change of bead morphology formed on electrospun polystyrene fibers. *Polymer* **2003**, *44*, 4029−4034.
(41) Wei, D. W.; Wei, H.; Gauthier, A. C.; Song, J.; Jin, Y.; Xiao, H. Superhydrophobic modification of cellulose and cotton textiles: Methodologies and applications. *J. Bioresour. Bioprod.* **2020**, *5*, 1−15.
(42) Yogev, S.; Mizrahi, B. Organogels as a delivery system for volatile oils. *ACS Appl. Polym. Mater.* **2020**, *2*, 2070−2076.
(43) Davidovich-Pinhas, M.; S Barbut, S.; Marangoni, A. G. The gelation of oil using ethyl cellulose. *Carbohydr. Polym.* **2015**, *117*, 869−878.
(44) Martins, A. J.; Cerqueira, M. A.; Fasolin, L. H.; Cunha, R. L.; Vicente, A. A. Beeswax organogels: Influence of gelator concentration and oil type in the gelation process. *Food Res. Int.* **2016**, *84*, 170−179.
(45) Martín-Alfonso, J.; López-Beltrán, F.; Valencia, C.; Franco, J. M. Effect of an alkali treatment on the development of cellulose pulp-based gel-like dispersions in vegetable oil for use as lubricants. *Tribol. Int.* **2018**, *123*, 329−336.
(46) Martín-Alfonso, J.; Franco, J. M. Ethylene-vinyl acetate copolymer (EVA)/sunflower vegetable oil polymer gels: Influence of vinyl acetate content. *Polym. Test.* **2014**, *37*, 78−85.

https://doi.org/10.1021/acsapm.2c01090
ACS Appl. Polym. Mater. 2022, 4, 7217−7227

5. ARTÍCULO 4

Impact of the morphology of electrospun lignin-ethyl cellulose nanostructures of their capacity to thicken castor oil

María Borrego, José E. Martín-Alfonso*, M. Carmen Sánchez, Concepción Valencia, José M. Franco

* Pro2TecS – Chemical Product and Process Technology Research Center, Department of Chemical Engineering and Materials Science, Universidad de Huelva, ETSI, Campus de "El Carmen", 21071, Huelva, Spain.

Published in:

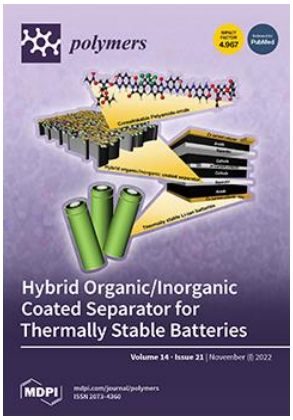

Publishing company: mdpi

Editor-in-Chief: QiangbingWei

Volume 14, Issue 21, pp 4741

Year: 2022

ISSN: 2073-4360

DOI: https://doi.org/10.3390/polym14214741

Impact factor (2022): 5.0

JCR Journal rank: 16/86 in Polymer Science

5.1. Resumen

En este artículo se describe una estrategia para formular geles a partir de la dispersión de nanofibras de lignina/etilcelulosa en aceite de ricino. Se prepararon disoluciones de lignina de bajo contenido en sulfonato (LSL) y etilcelulosa (EC) en una mezcla de THF:DMAc a diferentes concentraciones (8, 10 y 15 wt%) y relaciones en peso LSL:EC (50:50, 70:30 y 90:10) que se usaron cómo alimentación en el equipo de electrospinning con el fin de desarrollar nanofibras de estos polímeros. Las diferentes disoluciones fueron caracterizadas tanta fisicoquímica cómo reológicamente, y se relacionaron con las características morfológicas de las membranas. Posteriormente se estudió la capacidad para estructurar el aceite de ricino con el objetivo de desarrollar lubricantes biodegradables potenciales.

En cuanto a las propiedades fisicoquímicas, la adición de LSL conduce a un aumento de la conductividad eléctrica debido al carácter polar de la lignina. Del mismo modo, el aumento de la concentración de la disolución también produce una mayor conductividad eléctrica. Estos resultados sugieren que estas disoluciones se encuentran por debajo de la concentración crítica de entrelazamiento. Por otra parte, mayores relaciones en peso LSL:EC dan lugar a un descenso de la tensión superficial, lo cual supone una ventaja a la hora de formar fibras. En cuanto a la respuesta reológica, las disoluciones al 8 y 10 % p/p dan lugar a una respuesta Newtoniana, con una viscosidad aparente que disminuye con el contenido de LSL.

Al aumentar la concentración de la disolución se detecta una transición en la morfología de las nanoestructuras, desde partículas conectadas por filamentos finos a fibras bien formadas y uniformes. Lo mismo ocurre al disminuir la relación en peso LSL:EC. Se observó que aquellas disoluciones que forman membranas homogéneas con

fibras desarrolladas regulares son fluidos con alta conductividad y que presentan propiedades extensionales con un tiempo de relajación de al menos 30 ms. El tamaño del diámetro de dichas fibras depende de la concentración de la disolución y del contenido de LSL, lo cual está asociado a las propiedades reológicas de la disolución. Así, estructuras de nanofibras con pequeños diámetros y/o presencia de partículas se forman a partir de disoluciones con propiedades extensionales nulas y/o baja viscosidad.

Las membranas obtenidas con disoluciones al 15 % p/p se dispersaron en aceite de ricino a diferentes concentraciones (10, 20 y 30 % p/p). Todas presentaron una buena capacidad de retención de aceite y formaron geles estables físicamente. Los resultaron confirmaron que las nanoestructuras de fibras homogéneas mejoran la interacción fase continua-fase dispersa mientras que oleo-dispersiones formadas por agregados de nanofibras con partículas dan lugar a dispersiones de aspecto líquido. Las nanoestructuras dispersas a concentraciones de un 30 % p/p dan lugar a funciones viscoelásticas dinámicas que muestran una respuesta tipo-gel. Sin embargo, a concentraciones menores, mostraron una respuesta de gel débil, al igual que cuando se reduce la relación en peso EC:LSL la concentración de la disolución de alimentación. Los geles desarrollados se evaluaron tribológicamente. En todos los casos se produjo un desgaste entre las superficies con surcos rugosos y profundos, lo cual sugiere un mecanismo de desgaste predominantemente por abrasión. No obstante, los tamaños de la huella de desgaste obtenidos fueron ligeramente menores que los obtenidos con grasas comerciales, con valores del coeficiente de fricción similares, y muy inferiores a los obtenidos con aceite de ricino sin estructurar.

En definitiva, en este trabajo se valida de forma satisfactoria el uso de etilcelulosa cómo polímero coadyuvante para mejorar la electrospinabilidad de la lignina. Las

membranas resultantes de LSL:EC dispersadas en aceite de ricino impartieron propiedades reológicas y tribológicas adecuadas para proponer estas oleo-dispersiones cómo potenciales grasas lubricantes ecológicas.

polymers

MDPI

Article

Impact of the Morphology of Electrospun Lignin/Ethylcellulose Nanostructures on Their Capacity to Thicken Castor Oil

María Borrego, José E. Martín-Alfonso *, Concepción Valencia, M. Carmen Sánchez and José M. Franco

Chemical Product and Process Technology Research Center (Pro2TecS), Department of Chemical Engineering and Materials Science, ETSI, Campus de "El Carmen", University of Huelva, 21071 Huelva, Spain
* Correspondence: jose.martin@diq.uhu.es

Abstract: This study reports on a novel strategy for manufacturing thickened gel-like castor oil formulations by dispersing electrospun lignin/ethylcellulose nanostructures. These thickened formulations were rheologically and tribologically evaluated with the aim of being proposed as alternative ecofriendly lubricating greases. Low-sulfonate kraft lignin (LSL) and ethylcellulose (EC) were dissolved in a DMAc:THF mixture at different concentrations (8, 10, and 15 wt.%) and LSL:EC ratios (50:50, 70:30, and 90:10) and subjected to electrospinning. The resulting electrospun nanostructures were morphologically characterized. EC acting as the cospinning polymer improved both LSL spinnability and the oil structuring ability. Solutions with a high lignin content achieved microsized particles connected by fibrils, whereas solutions with a high EC content (50:50 ratio) and LSL/EC total concentration (10 and 15 wt.%) yielded beaded or bead-free nanofibers, due to enhanced extensional viscoelastic properties and nonNewtonian characteristics. The gel-like properties of electrospun nanostructure dispersions in castor oil were strengthened with the nanostructure concentration and the EC:LSL ratio, as a result of the formation of a more interconnected fiber network. The oleodispersions studied exhibited a satisfactory frictional response in a tribological contact, with friction coefficient values that were comparable to those achieved with traditional lithium-lubricating greases.

Keywords: lignin; ethylcellulose; electrospinning; nanostructure; dispersion; rheology

Citation: Borrego, M.; Martín-Alfonso, J.E.; Valencia, C.; Sánchez, M.C.; Franco, J.M. Impact of the Morphology of Electrospun Lignin/Ethylcellulose Nanostructures on Their Capacity to Thicken Castor Oil. *Polymers* **2022**, *14*, 4741. https://doi.org/10.3390/polym14214741

Academic Editor: Qiangbing Wei

Received: 25 September 2022
Accepted: 31 October 2022
Published: 5 November 2022

1. Introduction

Biopolymer-based micro- and nanofibers are increasingly being introduced into different types of materials and formulations for a wide range of applications owing to their outstanding properties, such as high specific surface area, high porosity, and superior stiffness and tensile strength as compared to conventional fibers, and ease of functionalization [1]. Filtration in environmental and energy fields [2], food packaging [3], catalysis [4], biomedical [5], and many others [6,7] are included among the wide range of applications. Different methods are available to generate polymeric micro- and nanofibers at present, for instance, phase separation [8], drawing [9,10], template synthesis [11], self-assembly [12], and electrospinning [13]. Among all of them, electrospinning may be considered the simplest one for nanofiber production. Electrospinning has emerged as a simple and cost-effective method to produce nanofibers from a variety of polymer sources. As is well known, electrospinning refers to the formation of fibers from a polymer solution, which is ejected from a thin spinneret located between two electrodes with opposite polarity electrical charges [14], one placed onto the spinneret and the other onto a fiber collector. The charged solution jet evaporates on its way to the collector typically to form an arrangement of nonwoven fibers. The potential difference may be modified to achieve the required morphology, depending on the physicochemical properties of the solution, i.e., electrical conductivity, surface tension, and viscosity [15]. Electrospinning processing parameters, such as electrodes spacing, voltage, humidity, volumetric feed flow, and needle diameter, may also be tuned to control solvent evaporation, preventing fibers from melting or failing

to form [6,16]. A wide variety of biopolymers, such as proteins, polysaccharides, and lignocellulosic biomass components, have been used to produce renewable nanofibers [17,18] with tailored functional properties that can be achieved by controlling the intermolecular interactions among polymeric molecules.

Lignocellulosic biomass is basically composed of cellulose, hemicellulose, and lignin as the main structural biopolymers. Lignin is especially interesting as it is composed of aromatic structures, which have the potential to replace aromatic polymers and fine chemicals of industrial interest [19,20]. The primary structure of lignin is formed by copolymerized three main phenylpropane monomers, i.e., sinapyl, coniferyl, and *p*-coumaryl alcohols [21]. Roughly, 50 million tons of residual lignin are annually produced by the paper industry, but only ~2% has been commercially employed in low-value chemicals, such as dispersants, adhesives, or surfactants [22,23]. Electrospinning of pure lignin is challenging due to its structural complexity and variability of the composition, according to the different processes and different biomass resources, which cause a potential lack of molecular entanglement, leading to a failure in fiber formation [24]. Aiming to overcome these problems, several polymers, such as polyvinyl acetate (PVA) [25,26], poly ethylene oxide (PEO) [27,28], polyhydroxybutyrate (PHB) [29], polycaprolactone (PCL) [30,31], polylactic acid (PLA) [32], and polyvinylpyrrolidone (PVP) [33] have been incorporated to lignin solutions in order to improve their electrospinnability. Most of the studies conducted to date were focused on blends of lignin with synthetic polymers, which might be expected to behave differently from blends with other natural polymers or derived from these, such as ethylcellulose. The production of ethylcellulose electrospun micro- or nanostructures, rather than with synthetic polymers, may also be interesting from the point of view of compatibility with nonpolar fluids because of their hydrophobic–oleophilic character [34], which could give rise to porous structures where oils can be adsorbed or entrapped, and therefore to stimulate and promote oil structuring.

Oil structuring is generally referred to as oleogelation and is applied to obtain soft and semisolid oil-based products [35]. The use of thickening agents to form gels from vegetable oils has been extensively studied [36,37] in the last years. With continuous growth in this field, different thickeners and vegetable oils have been explored to produce oleogels. The performances, applications, and properties of oleogels depend on the nature of their components (vegetable oil/gelator) and the microstructure (kind of assembly, crystal structure, morphology, crystallinity, etc.) achieved during the manufacturing process [38]. In the most common oleogelation process, the gelator molecules led to the formation of oleogel through the direct dispersion method. This process generally involves mixing gelators in the vegetable oil at a temperature higher than their melting point. This step is followed by a cooling step where a three-dimensional network formation occurs that entraps the oil. Other indirect methods to obtain gel oils have been proposed, such as the so-called foam-templated [39] and emulsion-templated [40] approaches or stepwise solvent-exchange [41] routes, yielding porous nanostructures where oil can be adsorbed or entrapped. However, most of these methods are tedious and very time- and/or energy-consuming. Thus, alternative strategies for oleogelation and oil structuring might attract great interest in several engineering domains and products, such as pharmaceuticals, food industry, and lubricants. In particular, in the lubricant field, obtaining oleogels from natural and renewable components is challenging in terms of the substitution of products derived from petrochemicals.

Taking into account these considerations, this study reports a novel strategy for manufacturing gel-like oleo-dispersions based on electrospun lignin/ethylcellulose nanostructures and castor oil. First, the electrospinnability of low-sulfonate lignin solutions in a DMAc:THF solvent was evaluated using ethylcellulose as a cospinning polymer. The morphological properties of the nanostructures were related to the physicochemical properties of the solutions. Then, the nanostructures were used as thickening agents to promote the structuring of castor oil, assessing the rheological and tribological properties of these gel-like dispersions aiming to explore their potential as lubricants.

2. Materials and Methods

2.1. Materials

Softwood low-sulfonate kraft lignin (LSL, Mw: ~10 kDa) and ethylcellulose (EC, Mw: ~82 kDa, 48% ethoxyl) from Merck Sigma-Aldrich (Taufkirchen, Germany) were used as base materials for the preparation of the electrospun structures. *N*,*N*-dimethylacetamide (DMAc, purity ≥99.8%) and tetrahydrofuran (THF, purity ≥99.0%) from Sigma-Aldrich were used as solvents to prepare LSL/EC solutions. Castor oil (211 cSt at 40 °C) was supplied by Guinama (Valencia, Spain) and used to prepare the oleo-dispersions.

2.2. Preparation and Characterization of Polymer Solutions for Electrospinning

LSL/EC biopolymers were dissolved in a DMAc:THF (1:1 wt/wt) blend to attain 8, 10, and 15 wt.% total concentrations, modifying the LSL:EC ratio (50:50, 70:30, and 90:10). This binary solvent was selected on the basis of the proper ability to solve EC for electrospinning purposes studied in a previous work [42]. First, EC solutions were prepared by magnetic stirring (300 rpm) in the DMAc:THF binary solvent during 2 h, at 40 °C. Then, LSL was added to the EC solution and left under agitation for 24 h. Finally, solutions were transferred to centrifuge tubes and centrifuged at 3000 rpm for 10 min to remove any remaining impurities from the solution.

Physicochemical characterization of the polymeric solutions was carried out by means of electrical conductivity, surface tension, and shear and extensional viscosity measurements.

Electrical conductivity of LSL:EC solutions was tested in a Crison (GLP 31) conductivity meter (Crison, Barcelona, Spain). The measurements were performed at 23 °C and reported after five times replication.

Surface tension of the different solutions was measured using a dynamic Wilhelmy plate tensiometer Sigma 703D (Biolin Scientific, Beijing, China) at 20 °C and repeated five times.

Measurements of shear viscosity were performed at 23 °C in an ARES-controlled strain rheometer (Rheometric Scientific, Leatherhead, UK) using a conventional coaxial cylinder geometry (32 mm inner diameter, 2 mm gap, 33.35 mm length) in a 0.03-300 s^{-1} shear rate range. Some LSL/EC solutions exhibited a non-Newtonian response, where the shear rate dependence of viscosity was described well by the Williamson model ($R^2 < 0.995$):

$$\eta = \frac{\eta_0}{1 + \left(k \cdot \dot{\gamma}\right)^m} \quad (1)$$

where η is the non-Newtonian viscosity; $\dot{\gamma}$ is the shear rate; η_0 is the zero-shear-rate-limiting viscosity; m is the parameter related to the slope of the shear-thinning region, and k is the constant whose inverse coincides with the shear rate for which $\eta = \eta_0/2$.

Extensional viscosity of solutions was measured using the CaBER-1 capillary break-up extensional rheometer (ThermoHaake, Karlsruhe, Germany). The break-up of the fluid filament after stretching and the filament diameter vs. time evolution were measured with a laser micrometer. To perform tests, 6 mm parallel plates were set at an initial plate separation of 1 mm (h_0). Then, a given strain was suddenly imposed to create a filament separating the plates from their initial distance h_0 to their final separation h_f = 10.0 mm within 40 ms at a constant separating speed. Once the fluid filament was formed between the plates, it drained through capillary action depending on the elastic relaxation time of the fluid. The extensional rheological properties were indirectly deduced from the evolution of the filament diameter with time, and the extensional viscosity was quantified as:

$$\eta_{ext} = \frac{\sigma}{\left(-\frac{dD(t)}{dt}\right)} \quad (2)$$

where η_{ext} is the extensional viscosity; σ is the surface tension of the polymer solution; D is the diameter of the filament, and t is the time. Three replicates of each extensional test were performed on fresh samples.

2.3. Electrospinning Process

LSL/EC solutions were electrospun using an in-house electrospinning apparatus, consisting of a high-voltage power supply (Spellman, Hauppauge, NY, USA), a syringe with a blunt metal needle, a syringe pump (KD Scientific Inc.; Holliston, MA, USA, and an electrically grounded collector. The LSL/EC solutions were pumped at a specified speed (0.8 mL/h) through the needle tip while applying a high voltage (20 kV). Tip-to-target distance was 12 cm, and tip diameter was ≈ 0.6 mm. All the electrospinning experiments were carried out at room temperature (~ 23 °C) and relative humidity (~ 55%).

2.4. Morphological Characterization of Nanostructures

The morphology of LSL/EC nanostructures was observed in a FlexSEM 1000 II microscope (Hitachi, Tokyo, Japan) at an accelerating voltage of 20 kV. Each sample was coated with gold for analysis. The average diameters of the obtained electrospun fiber mats were determined by using image-analytical software (Image J; NIMH, Bethesda, MD, USA).

2.5. Preparation and Characterization of Dispersions of Electrospun Nanostructures in Castor Oil

LSL:EC nanostructures produced by electrospinning were dispersed in castor oil using an open vessel with an anchor impeller geometry at room temperature (~23 °C) and a rotation speed of 60 rpm during 60 min, at different concentrations of (10, 20, and 30 wt.%). Then, the dispersions were stored at least 24 h to carry out the rheological and tribological characterizations. The homogeneity of the resulting dispersions was verified through optical observations and digital photos.

Rheological characterization of oleo-dispersions was conducted in a Rheoscope controlled-stress rheometer (ThermoHakee, Karlsruhe, Germany), using roughened stainless steel parallel plate geometries (20 and 35 mm, 1 mm gap). Small-amplitude oscillatory shear (SAOS) tests were performed inside the linear viscoelastic region, in a frequency range comprised between 0.03 and 100 rad/s. Stress sweep tests were previously performed to determine the linear viscoelastic regime. At least two replicates were conducted for every sample. The tribological performance of the oleo-dispersions was investigated in a tribological cell coupled to a MCR-501 rheometer (Anton Paar, Graz, Austria) consisting of a 6.35 mm diameter steel ball rotating on three 45°-inclined rectangular steel plates, on which the samples to be tested as lubricants were spread. Constant normal load and rotational speed of 30 N and 30 min^{-1}, respectively, were applied for 10 min. Testing time was long enough to achieve stationary values of the friction coefficient. At least five replicates were made for each oleo-dispersion sample. The wear scars produced on the steel plates were analyzed using a BX51 microscope (Olympus, Tokyo, Japan), from which the mean diameters were determined.

3. Results and Discussion

3.1. Physicochemical Properties of LSL:EC Solutions

The electrical conductivity, surface tension, and shear and extensional rheological properties of the LSL:EC solutions in DMAc:THF were measured, and the results are shown in Table 1. As can be observed, EC (LSL-free) solutions displayed very low values of electrical conductivity (33.53–30.81 μS/cm), and this property increased with the total polymer concentration, but particularity with the LSL content. This fact could be related to the polar character of lignin, due to the presence of phenolic and aliphatic hydroxyl and carboxyl groups as well as substructures based on β-O-4′alkyl ethers in its chemical structure [19]. In addition, the increase in conductivity with the LSL concentration suggests that these solutions are below the concentration at which the macromolecules start to overlap (overlap concentration), delimiting the transition between the dilute and semidilute regime, from which the conductivity decreases due to the reduced mobility of the entangled polymeric molecules [43]. Moreover, the higher the lignin proportion in the blend, the lower the surface tension of the LSL:EC solutions (see Table 1). A similar behavior was found by Ago et al. [26] for lignin–PVA blends and by Borrego et al. [44] for lignin/PVP–surfactant

mixtures. This fact could represent a positive point with respect to the fiber-forming ability of LSL:EC solutions. However, the balance with the other important properties, such as viscosity and electrical conductivity, should be taken into account in the right fiber formation.

Figure 1a shows the viscosity curves for solutions with 10 and 15 wt.% total concentrations and variable LSL:EC ratios. According to the experimental results of shear rheology, most of the solutions containing 8 and 10 wt.% total concentrations of the LSL:EC blends showed Newtonian behavior throughout the whole shear rate range studied, with apparent viscosity values that decreased with the LSL content. It is well known that the three-dimensional structural network of lignin particles is composed of aromatic monolignols, and these molecular units are not able to easily produce physical entanglements like linear polymers, such as EC. Thus, an increase in LSL content resulted in lower viscosity values of the LSL:EC solutions. However, at a higher LSL:EC concentration (15 wt.%, except for the 90:10 LSL:EC ratio) the shear flow response became shear thinning, with a tendency to reach a Newtonian plateau at low shear rates (at around 0.1 s^{-1}). The shear rate dependence of viscosity fitted the Williamson model (see Figure 1a) well, and the parameters obtained from the fitting to this model are shown in Table 1. As can be observed, the η_0 and shear-thinning character (m) decrease as the LSL content increases, while k values increase.

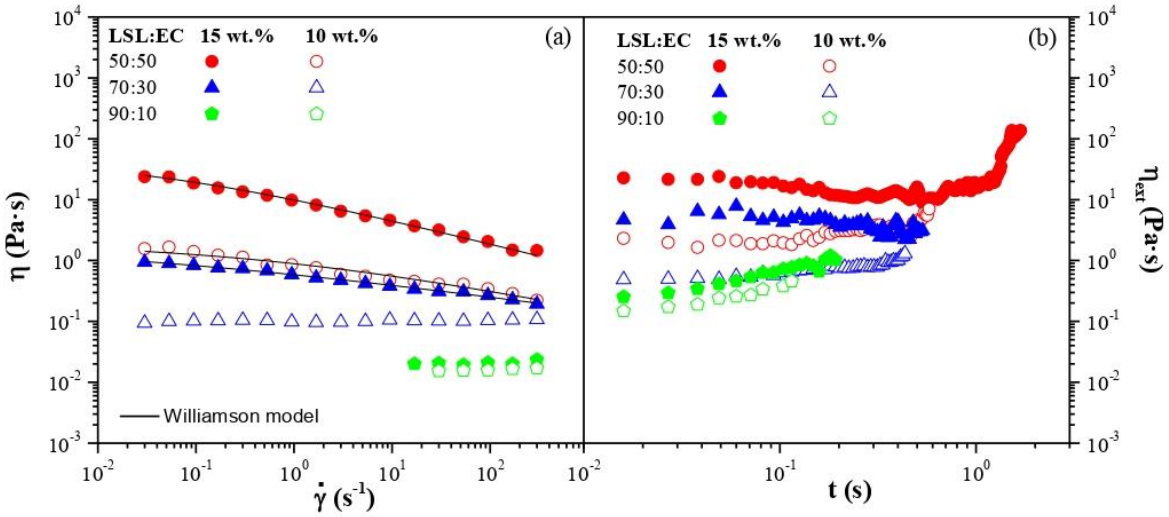

Figure 1. (**a**) Viscous flow curve of LSL:EC solutions in DMAc:THF to 15 and 10 wt.% total concentration. Solid lines represent fits to the Williamson model with the parameters given in Table 1 and (**b**) Extensional viscosity as a function of time.

Table 1. Electrical conductivity, surface tension, and shear and extensional viscosity of LSL:EC solutions in THF:DMAc.

Concentration (%.wt)	LSL:EC Ratio (%)	Electrical Conductivity, s (μS/cm)	Surface Tension, (mN/m)	Newtonian Viscosity, η (Pa·s)	η_o (Pa·s)	k (s)	m (-)	Extensional Viscosity $\eta_{ext,o}$ (Pa·s)	D_o (mm)	Relaxation time, λ (ms)	A (-)
8%	0:100	33.53 ($\pm 2.5\ 10^{-1}$)	32.91 ($\pm 6.0\ 10^{-1}$)	1.48 ($\pm 2\ 10^{-1}$)	-	-	-	-	-	-	-
	50:50	75.01 ($\pm 2.3\ 10^{-1}$)	28.21 ($\pm 1.0\ 10^{-1}$)	1.2×10^{-1} ($\pm 3\ 10^{-2}$)	-	-	-	-	-	-	-
	70:30	103.63 ($\pm 2.1\ 10^{-1}$)	29.26 ($\pm 7.0\ 10^{-1}$)	4.8×10^{-2} ($\pm 1\ 10^{-2}$)	-	-	-	-	-	-	-
	90:10	108.20 ($\pm 1.0\ 10^{-1}$)	28.89 ($\pm 1.5\ 10^{-1}$)	4.5×10^{-3} ($\pm 3\ 10^{-4}$)	-	-	-	-	-	-	-
10%	0:100	32.01 ($\pm 2.6\ 10^{-1}$)	32.51 (± 1.1)	-	5.9	36.2	0.31	14.9	2.75	143	0.6
	50:50	98.27 ($\pm 6.5\ 10^{-1}$)	28.86 ($\pm 4.0\ 10^{-1}$)	-	1.4	1.95	0.32	3.14	1.87	57	0.7
	70:30	110.17 ($\pm 1.2\ 10^{-1}$)	29.67 ($\pm 1.3\ 10^{-1}$)	1.4×10^{-1} ($\pm 9\ 10^{-2}$)	-	-	-	0.49	1.68	32	0.9
	90:10	127.27 ($\pm 4.1\ 10^{-1}$)	28.74 ($\pm 2.5\ 10^{-1}$)	1.2×10^{-2} ($\pm 5\ 10^{-3}$)	-	-	-	0.14	0.14	6	124.7
15%	0:100	30.81 ($\pm 3.0\ 10^{-1}$)	31.71 ($\pm 9.0\ 10^{-1}$)	-	419.1	0.81	0.79	223.4	4.97	-	-
	50:50	90.97 ($\pm 4.6\ 10^{-1}$)	27.46 ($\pm 8.0\ 10^{-1}$)	-	24.7	30.43	0.41	53.99	3.27	96	0.3
	70:30	148.21 ($\pm 3.0\ 10^{-1}$)	25.73 ($\pm 7.0\ 10^{-1}$)	-	0.9	54.54	0.22	2.72	1.33	32	0.4
	90:10	292.67 ($\pm 4.2\ 10^{-1}$)	20.35 (± 1.3)	2.3×10^{-2} ($\pm 6\ 10^{-3}$)	-	-	-	0.25	1.51	7	2.1

Regarding the extensional rheology, the extensional viscosity of solutions with 8 wt.% total LSL:EC concentration and that containing 10 wt.% polymers at a 10:90 LSL:EC ratio could not be experimentally measured since the filament ruptured immediately after imposing the stretching strain as a result of their poor elastic properties. Nevertheless, the extensional properties of the LSL:EC solutions with higher concentrations were satisfactorily assessed. Since capillary extensional processes are inherently transient phenomena, the extensional viscosity continuously increases when moving from the coiled to stretched states [45]. A convenient parameter accounting for the whole filament thinning process is the characteristic relaxation time (λ). For a polymer solution, the decay of the filament diameter $D(t)$ respecting the initial value D_0, i.e., just after imposing the strain, can be described as [46]:

$$\frac{D(t)}{D_0} = A\, exp\left(-\frac{t}{3\lambda}\right) \quad (3)$$

where λ is the relaxation time, and A is the fitting parameter, which is proportional to the elastic modulus. The characteristic relaxation time λ was extracted from the fitting of the experimental $D(t)$ vs. time data to Equation (3), and the resulting values are shown for each LSL:EC solution in Table 1 as well as the values of the fitting parameter A. The transient extensional viscosity can be calculated directly from the diameter decay according to:

$$\eta_{ext} = -\frac{\sigma}{dD(t)/dt} \quad (4)$$

The extensional viscosity is displayed as a function of time in Figure 1b. As can be seen, the extensional viscosity values are constant for a very short time scale and subsequently increase monotonically until filament breakup. The short time-limiting extensional viscosity values ($\eta_{ext,0}$) are also provided in Table 1. As expected, both the characteristic relaxation time and the apparent extensional viscosity increase with the total LSL:EC concentration and decrease by increasing the LSL:EC ratio.

3.2. Electrospinnability of LSL:EC Solutions

Figure 2 displays the SEM images of the morphology of the resulting LSL:EC nanostructures obtained by electrospinning for different LSL:EC weight ratios (50:50, 70:30, and 90:10 wt/wt) and total polymer concentrations (8, 10, and 15 wt.%), respectively. As can be clearly inferred from SEM images (Figure 2), the composition of the spinning solutions had a significant impact on the morphology of the resulting nanostructures. For a given LSL:EC solution concentration, a transition from microsized particles connected by fibrils to well-developed electrospun fiber networks was obtained by decreasing the LSL:EC weight ratio in the solution. Therefore, increasing the solution concentration and relatively decreasing the amount of LSL yielded a progressive transformation in the morphology of electrospun structures from agglomerated particles to a bead-on-string architectures or even almost bead-free nanofibers (see, for instance, Figure 2c). Regarding the relationship between the physicochemical properties of the LSL:EC solutions and the nanostructure morphology, it may be deduced that polymer solutions from which nanofibers that largely dominate the morphology are produced should preferentially be conductive, shear-thinning fluids and display extensional properties with relaxation times of at least around 30 ms. As we know, physicochemical properties of lignin solutions play a key role in achieving uniform fiber mats via electrospinning. According to Aslanzadeh et al. [27], a certain polymer fraction above the critical overlap concentration is required to obtain bead-free uniform nanofibers. On the other hand, Dallmayer et al. [28] reported the influence of the extensional properties of kraft lignin/PEO solutions, which were improved by increasing either the lignin concentration or the PEO/lignin ratio. Our results are in agreement with these findings. Bead-free fibers were obtained from the solution with the highest LSL/EC concentration (15 wt.%) and the lowest LSL:EC ratio (50:50), showing enhanced extensional properties. Moreover, nanofiber formation was favored when polymer solutions showed shear-thinning behavior, as a result of the easier filament stretching at the high spinning flow rate imposed. Table 2

shows the average fiber diameters of the obtained electrospun nanostructures. The average diameter of the nanofibers was in the range of 0.12–0.23 μm. In general, the diameter of the electrospun nanofibers slightly depended on both the polymer concentration and the LSL:EC weight ratio. Thinner nanofibers were obtained as the content of LSL increased or total polymer concentration decreased, which is also correlated with the number of beads or particles produced. As mentioned above, this fact can be associated with the poor rheological properties of the LSL-rich solutions (low viscosity and low or negligible elastic relaxation times), together with probable excessive conductivity, which favor higher elongation forces leading to a thinner fiber formation and/or fiber break-up.

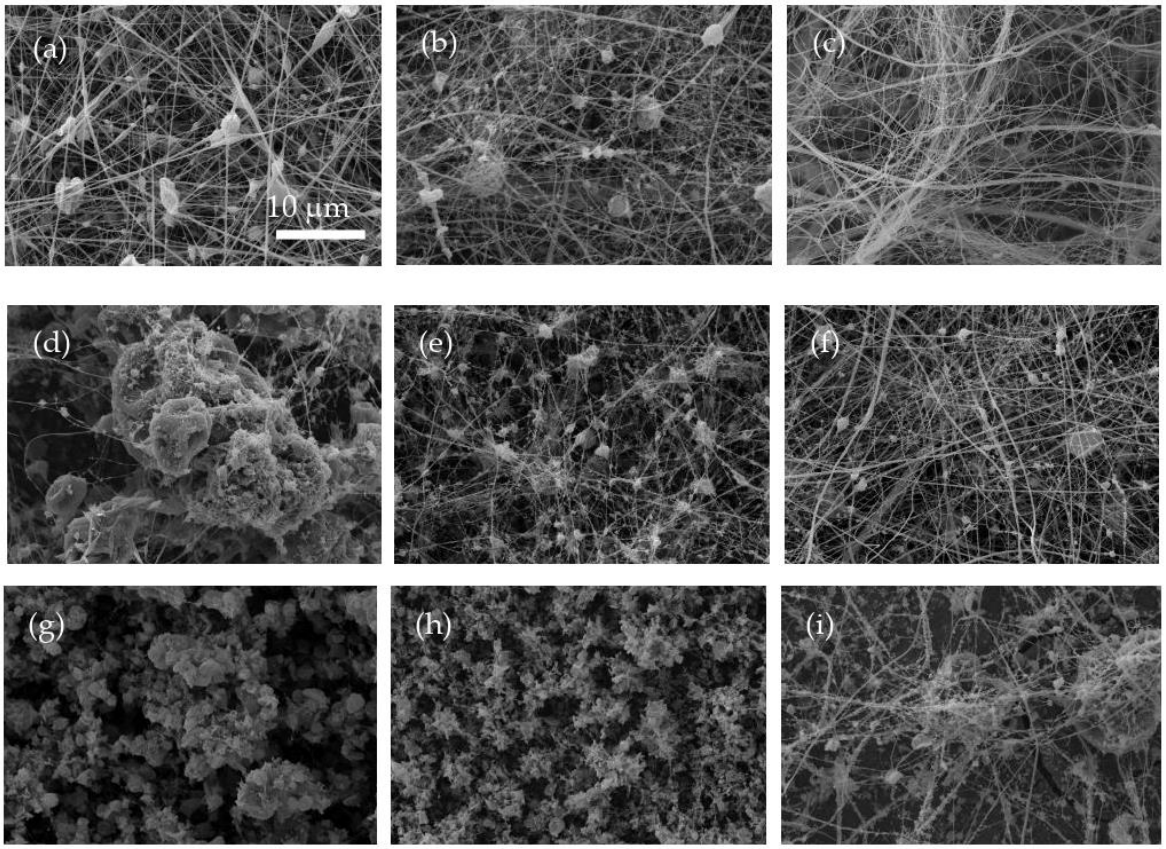

Figure 2. SEM images of electrospinning obtained from LSL:EC solutions at different concentrations and LSL:EC ratios: 50:50 LSL:EC ratio (**a**) 8% wt., (**b**) 10% wt, (**c**) 15% wt, 70:30 LSL:EC ratio, (**d**) 8% wt., (**e**) 10% wt., (**f**) 15% wt., 90:10 LSL:EC ratio, (**g**) 8% wt., (**h**) 10% wt, and (**i**) 15% wt.

Table 2. Average fiber diameter values in the LSL/EC-electrospun nanostructures obtained.

Systems		Fiber Diameter (μm)
8%	50:50	$0.17 \pm 5.7\ 10^{-2}$
	70:30	Beads
	90:10	Beads
10%	50:50	$0.19 \pm 3.4\ 10^{-2}$
	70:30	$0.12 \pm 4.1\ 10^{-2}$
	90:10	Beads
15%	50:50	$0.23 \pm 5.2\ 10^{-2}$
	70:30	$0.22 \pm 4.8\ 10^{-2}$
	90:10	$0.15 \pm 1.1\ 10^{-1}$

3.3. Rheological and Tribological Properties of Dispersions of Electrospun Nanostructures in Castor Oil

In order to study the ability of the electrospun nanostructures to form gel-like oleo-dispersions, selected LSL:EC nanostructures obtained from the most concentrated solutions (15 wt.% total concentration of LSL/EC) were dispersed in castor oil by applying gentle mechanical agitation at different concentrations. For this study, these nanostructures were selected, since other electrospun samples, especially those obtained from the most diluted solutions (8 wt.%) and with a high LSL content, formed unstable dispersions in which phase separation was evidenced just after blending the components. Figure 3 shows the physical appearance of the LSL:EC nanostructures of different LSL:EC weight ratios (50:50, 70:30, and 90:10) dispersed in castor oil at several concentrations (10, 20, and 30 wt.%). As can be observed, all the nanostructures have a good oil-binding capacity and are physically stable against phase separation. However, the oleo-dispersion formulated with a higher LSL:EC ratio at 10 wt.% evidences signs of oil separation (see Figure 3c). These results confirm that homogeneous nanostructures largely dominated by nanofibers improved the interaction continuous phase–dispersed phase, giving rise to physically stable oleo-dispersions with a gel-like appearance. On the contrary, structures formed by particles or randomly distributed aggregates of particles interconnected by fibrils, led to unstable and/or slightly thickened liquid-like dispersions. Similar results were found for lignin/PVP nanostructures [33].

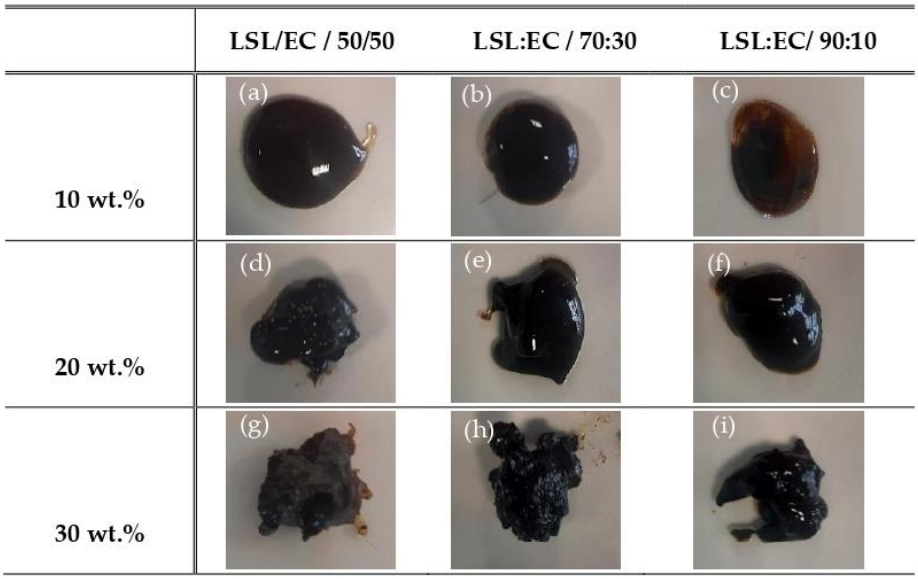

Figure 3. Physical appearance of LSL/EC nanostructures of different LSL:EC ratios (50:50, 70:30, 90:10) dispersed in castor oil at several concentrations (10, 20, and 30 wt.%).

Figures 4 and 5 display the evolution of SAOS functions, i.e., the storage (G') and loss (G") moduli and loss tan (tan δ), with frequency, within the linear viscoelastic range, for selected oleo-dispersions as a function of the LSL:EC nanostructure concentration (Figure 4) and the LSL:EC ratio (Figure 5). As can be seen, oleo-dispersions formulated with a higher nanostructure concentration (30 wt.%) or 50:50 LSL:EC ratio showed a typical gel-like behavior where $G' > G''$ in the frequency range studied (tan $\delta < 1$), where G' and G" are only slightly dependent on ω [47]. However, a different behavior was found for dispersions with lower concentrations and higher LSL:EC ratios, since a crossover between G' and G" at a high frequency occurred, and higher values of tan δ are observed. This crossover point corresponds to the end of the plateau region and to the beginning of the transition zone of the relaxation spectrum and decreased as the nanostructure concentration and EC content decreased. These results are indicative of a weaker gel-like response where a

reduction in the extension of the plateau region takes place by lowering these variables. Similar mechanical spectra were obtained for oleo-dispersions formulated with electrospun ethylcellulose nanostructures [42].

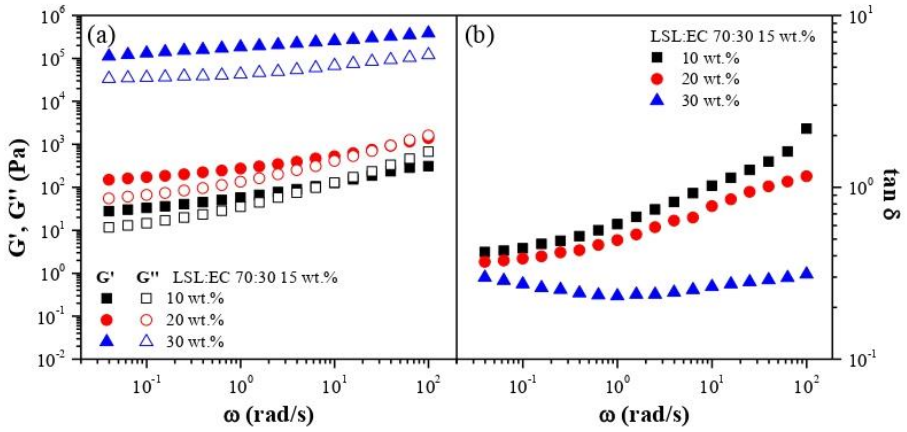

Figure 4. Frequency dependence of (**a**) the storage and loss moduli and (**b**) the loss tangent for oleo-dispersions formulated with the same nanostructure (70:30/LSL:EC ratio) at different concentrations.

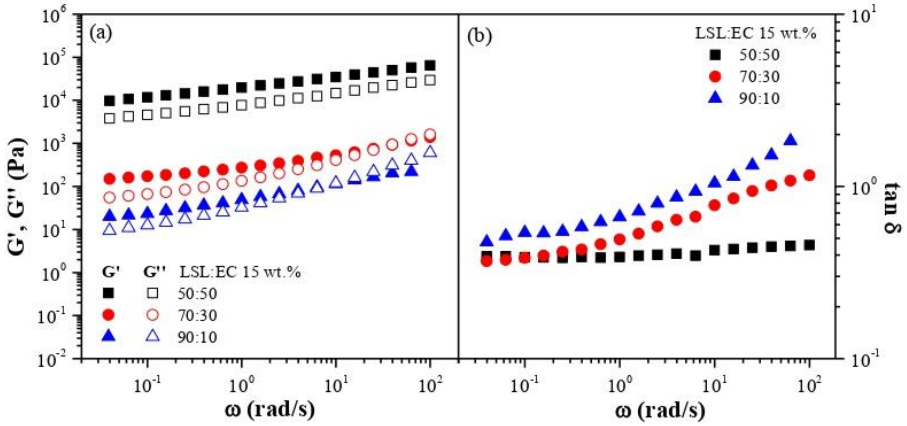

Figure 5. Frequency dependence of (**a**) the storage and loss moduli and (**b**) the loss tangent for oleo-dispersions formulated with nanostructures differing in the LSL:EC ratio (20 wt.% nanostructure concentration).

Aiming to explore the capacity of these oleo-dispersions based on the LSL/EC nanostructures and castor oil to act as semisolid lubricants, the tribological performance was evaluated in a ball-on-plates steel–steel tribological contact. The wear marks obtained on the plates after performing the tribological tests, i.e., after 10 min, are presented in Figure 6, and the corresponding average values of wear scar diameters and stationary friction coefficients are shown in Table 3. As can be observed, the contact surfaces of steel plates are damaged in all cases, and the rounded worn surfaces show a rather rough trace and deep furrows along the sliding direction (see Figure 6), suggesting a predominant abrasion wear mechanism. A decrease in the nanostructure concentration increased the wear scar size. Increasing the LSL:EC above 50:50 also tends to increase wear. These wear scar sizes were slightly lower than obtained with commercial mineral oil-based lithium grease [48]. On the contrary, very similar values of the friction coefficient, around 0.086 ± 0.008, were obtained in all cases, comparable to those found when using traditional lithium-lubricating greases or other gel-like dispersions based on synthetic polymers previously proposed as lubricants [49]. These results may be related to the rheological behavior, i.e., softer oleo-

dispersions yield higher wear scar values, while oleo-dispersions formulated with higher nanostructure concentrations and a low LSL content exhibiting enhanced gel strength and significantly reduced wear. On the other hand, the friction coefficient values of these electrospun LSL:EC nanofiber-thickened oil formulations are comparable to that obtained for pure castor oil under similar conditions; however, the addition of nanofibers significantly improves the wear reduction [50].

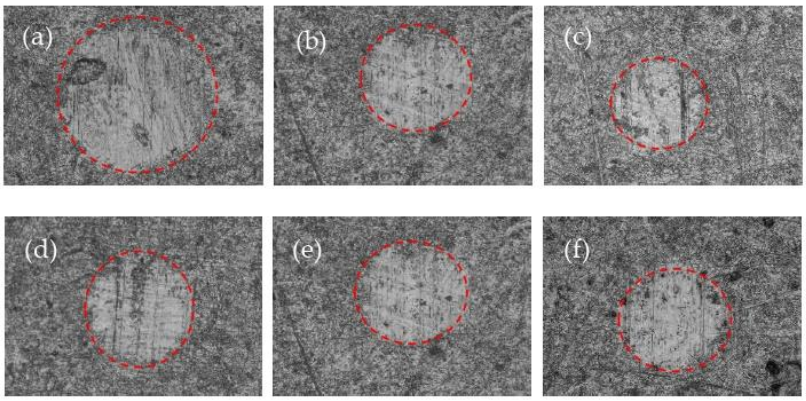

Figure 6. Wear scar micrographs of the lubricated plates with oleo-dispersions formulated with 70:30 LSL:EC nanostructures at different concentrations (**a**) 10 wt.%, (**b**) 20 wt.%, and (**c**) 30 wt.% and different LSL:EC ratios (**d**) 50:50, (**e**) 70:30, and (**f**) 90:10 and 20 wt.% nanostructure concentrations.

Table 3. Average values of the friction coefficient and wear scar diameters obtained with the dispersions of LSL:EC nanostructures in castor oil acting as lubricants.

Concentration (wt%)	Ratio LSL:EC	Nanostructure Concentration (wt%)	Friction Coefficient (-)	Wear Scar Diameter (μm)
15%	50:50	1020	$0.088 \pm 2.2\ 10^{-3}$ $0.077 \pm 3.7\ 10^{-3}$	225 ± 12.1 228 ± 14.4
	70:30	10 20 30	$0.094 \pm 5.1\ 10^{-3}$ $0.088 \pm 1.5\ 10^{-3}$ $0.082 \pm 1.9\ 10^{-3}$	259 ± 42.3 252 ± 8.3 208 ± 39.8
	90:10	20 30	$0.089 \pm 4.6\ 10^{-3}$ $0.081 \pm 5.2\ 10^{-3}$	250 ± 24.9 201 ± 6.1
Castor oil			$0.071 \pm 2.9\ 10^{-3}$	523 ± 13.6

4. Conclusions

In this work, electrospun nanostructures of low-sulfonate kraft lignin (LSL)/ethylcellulose (EC) were successful fabricated via electrospinning. EC was used as a cospinning polymer to improve the spinning stability and the fiber quality. The role of the spinning solution concentration and the LSL:EC ratio were systematically investigated. The morphology of the nanostructures obtained is specially influenced by the rheological properties of the solution, which depend on the total LSL/EC concentration and the LSL:EC ratio. Electrospun architectures composed of nanoparticles or microsized particles connected by fibrils were generated from solutions with lower LSL/EC concentrations and/or higher LSL:EC ratios. On the contrary, beaded fibers or uniform fiber networks were achieved by increasing the solution concentration and/or decreasing the LSL:EC ratio. This fact was mainly attributed to the shear and extensional rheological properties of LSL/EC solutions. In this sense, nanofiber-dominated morphologies were achieved from LSL/EC solutions with shear-thinning characteristics and relaxation times of at least 30 ms. Uniform fiber mats with some beads randomly distributed were obtained from the solutions with the

lower LSL:EC ratios and higher LSL/EC concentrations, such as those having 15% wt. concentration and a 70:30 LSL:EC ratio or a 10% wt. concentration and a 50:50 LSL:EC ratio. Electrospun LSL/EC nanostructures formed by beaded nanofibers were able to form stable oleo-dispersions in castor oil, whereas structures characterized by nanoparticles or microsized particles connected by fibrils yielded unstable oleo-dispersions with a partial separation of phases. In general, the oleo-dispersions studied exhibited gel-like viscoelastic properties, with a crossover between G'' and G' in the medium–high frequency ranges studied, associated with the end of the plateau region, which was found for dispersions with higher LSL:EC ratios and lower nanostructure concentrations. On the contrary, a high nanostructure concentration and/or low LSL/EC ratio produced oleo-dispersions with higher gel stiffness that showed an extended plateau region in the mechanical spectrum. Thus, the viscoelastic properties of these oleo-dispersions may be tailored by modifying the nanostructure concentration and the LSL:EC ratio, according to the morphology of the nanostructure network achieved by electrospinning. The oleo-dispersions also demonstrated adequate tribological performance to be potentially applied as sustainable lubricating greases.

Author Contributions: M.B.: conceptualization, methodology, formal analysis, and data curation. J.E.M.-A.: conceptualization, methodology, validation, resources, funding acquisition, supervision, and writing. C.V.: conceptualization, validation, and formal analysis. M.C.S.: conceptualization, validation, and formal analysis. J.M.F.: conceptualization, methodology, validation, resources, funding acquisition, supervision, and writing. All authors have read and agreed to the published version of the manuscript.

Funding: This work was supported by MCIN/AEI/10.13039/501100011033, by "ERDF—A way of making Europe" (grant number: RTI2018-096080-BC21) and by Junta de Andalucía/EPIT2020-UHU (grant numbers: PY20_00751 and UHU202029) by the FEDER European Programme.

Institutional Review Board Statement: Not applicable.

Informed Consent Statement: Not applicable.

Data Availability Statement: Not applicable.

Conflicts of Interest: The authors declare no conflict of interest.

References

1. Wang, X.; Nakane, K. Preparation of polymeric nanofibers via immersion electrospinning. *Eur. Polym. J.* **2020**, *134*, 109837. [CrossRef]
2. Dai, Y.; Liu, W.; Formo, E.; Sun, Y.; Xia, Y. Ceramic nanofibers fabricated by electrospinning and their applications in catalysis, environmental science, and energy technology. *Polym. Adv. Technol.* **2011**, *22*, 326–338. [CrossRef]
3. Zhang, C.; Li, Y.; Wang, P.; Zhang, H. Electrospinning of nanofibers: Potentials and perspectives for active food packaging. Compr. *Rev. Food Sci. Food Saf.* **2020**, *19*, 479–502. [CrossRef] [PubMed]
4. Li, S.; Cui, Z.; Li, D.; Yue, G.; Liu, J.; Ding, H.; Gao, S.; Zhao, Y.; Wang, N.; Zhao, Y. Hierarchically structured electrospinning nanofibers for catalysis and energy storage. *Compos. Commun.* **2019**, *13*, 1–11. [CrossRef]
5. Agarwal, S.; Wendorff, J.H.; Greiner, A. Use of electrospinning technique for biomedical applications. *Polymer* **2008**, *49*, 5603–5621. [CrossRef]
6. Xue, J.; Wu, T.; Dai, Y.; Xia, Y. Electrospinning and electrospun nanofibers: Methods, materials, and applications. *Chem. Rev.* **2019**, *119*, 5298–5415. [CrossRef] [PubMed]
7. Liu, H.; Gough, C.R.; Deng, Q.; Gu, Z.; Wang, F.; Hu, X. Recent Advances in Electrospun Sustainable Composites for Biomedical, Environmental, Energy, and Packaging Applications. *Int. J. Mol. Sci.* **2020**, *21*, 4019. [CrossRef] [PubMed]
8. Deka, M.; Nath, A.K.; Kumar, A. Ionic conduction and phase separation studies in PEO–P(VdF–HFP)–LiClO4–dedoped polyaniline nanofiber composite polymer electrolytes—I. *Indian J. Phys.* **2010**, *84*, 1299–1305. [CrossRef]
9. Sehaqui, H.; Ezekiel Mushi, N.; Morimune, S.; Salajkova, M.; Nishino, T.; Berglund, L.A. Cellulose Nanofiber Orientation in Nanopaper and Nanocomposites by Cold Drawing. *ACS Appl. Mater. Interfaces* **2012**, *4*, 1043–1049. [CrossRef]
10. Jao, D.; Beachley, V.Z. Continuous dual-track fabrication of polymer micro-/nano-fibers based fibers based on direct drawing. *ACS Macro Lett.* **2019**, *8*, 588–595. [CrossRef]
11. Feng, L.; Li, S.H.; Zhai, J.; Song, Y.L.; Jiang, L.; Zhu, D.B. Template based synthesis of aligned polyacrylonitrile nanofibers using a novel extrusion method. *Synth. Met.* **2003**, *135*, 817–818. [CrossRef]

12. Sun, F.; Chen, L.; Ding, X.F.; Xu, L.; Zhou, X.; Wei, P.; Liang, J.F.; Luo, S.Z. High–resolution insights into the stepwise self–assembly of nanofiber from bioactive peptides. *J. Phys. Chem.* **2017**, *121*, 7421–7430. [CrossRef] [PubMed]
13. Li, D.; Xia, Y. Electrospinning of nanofibers: Reinventing the wheel. *Adv. Mater.* **2004**, *16*, 1151–1170. [CrossRef]
14. Yarin, A.L.; Koombhongse, S.; Reneker, D.H. Taylor cone and jetting from liquid droplets in electrospinning of nanofibers. *J. Appl. Phys.* **2001**, *90*, 4836–4846. [CrossRef]
15. Haider, A.; Haider, S.; Kang, I.K. A comprehensive review summarizing the effect of electrospinning parameters and potential applications of nanofibers in biomedical and biotechnology. *Arab. J. Chem.* **2018**, *11*, 1165–1188. [CrossRef]
16. Huang, Z.M.; Zhang, Y.Z.; Kotaki, M.; Ramakrishna, S. A review on polymer nanofibers by electrospinning and their applications in nanocomposites. *Compos. Sci. Technol.* **2003**, *63*, 2223–2253. [CrossRef]
17. Mendes, A.C.; Stephansen, K.; Chronakis, I.S. Electrospinning of food proteins and polysaccharides. *Food Hydrocoll.* **2017**, *68*, 53–68. [CrossRef]
18. Ahn, Y.; Lee, S.H.; Kim, H.J.; Yang, Y.H.; Hong, J.H.; Kim, Y.-H.; Kim, H. Electrospinning of lignocellulosic biomass using ionic liquid. *Carbohydr. Polym.* **2012**, *88*, 395–398. [CrossRef]
19. Ragauskas, A.J.; Beckham, G.T.; Biddy, M.J.; Chandra, R.; Chen, F.; Davis, M.F.; Davison, B.H.; Dixon, R.A.; Gilna, P.; Keller, M.; et al. Lignin valorization: Improving lignin processing in the biorefinery. *Science* **2014**, *344*, 6185. [CrossRef]
20. Laurichesse, S.; Avérous, L. Chemical modification of lignins: Towards biobased polymers. *Prog. Polym. Sci.* **2014**, *39*, 1266–1290. [CrossRef]
21. Zhao, W.; Simmons, B.; Singh, S.; Ragauskas, A.; Cheng, G. From lignin association to nano-/micro-particle preparation: Extracting higher value of lignin. *Green Chem.* **2016**, *18*, 5693–5700. [CrossRef]
22. Sen, S.; Patil, S.; Argyropoulos, D.S. Thermal properties of lignin in copolymers, blends, and composites: A review. *Green Chem.* **2015**, *17*, 4862–4887. [CrossRef]
23. Laskar, D.D.; Yang, B.; Wang, H.; Lee, J. Pathways for biomass-derived lignin to hydrocarbon fuels. *Biofuels Bioprod. Biorefin.* **2013**, *7*, 602–626. [CrossRef]
24. Dallmeyer, I.; Ko, F.; Kadla, J.F. Electrospinning of technical lignins for the production of fibrous networks. *J. Wood Chem. Technol.* **2010**, *30*, 315–329. [CrossRef]
25. Lai, C.; Zhou, Z.; Zhang, L.; Wang, X.; Zhou, Q.; Zhao, Y.; Wang, Y.; Wu, X.F.; Zhu, Z.; Fong, H. Free-standing and mechanically flexible mats consisting of electrospun carbon nanofibers made from a natural product of alkali lignin as binder-free electrodes for high-performance supercapacitors. *J. Power Sources* **2014**, *247*, 134–141. [CrossRef]
26. Ago, M.; Okajima, K.; Jakes, J.E.; Park, S.; Rojas, O.J. Lignin-based electrospun nanofibers reinforced with cellulose nanocrystals. *Biomacromolecules* **2012**, *13*, 918–926. [CrossRef] [PubMed]
27. Aslanzadeh, S.; Ahvazi, B.; Boluk, Y.; Ayranci, C. Morphologies of electrospun fibers of lignin in poly(ethylene oxide)/N,N dimethylformamide. *J. Appl. Polym. Sci.* **2016**, *133*, 44. [CrossRef]
28. Dallmeyer, I.; Ko, F.; Kadla, J.F. Correlation of elongational fluid properties to fiber diameter in electrospinning of softwood kraft lignin solutions. *Ind. Eng. Chem. Res.* **2014**, *53*, 2697–2705. [CrossRef]
29. Kai, D.; Chong, H.M.; Chow, L.P.; Jiang, L.; Lin, Q.; Zhang, K.; Zhang, H.; Zhang, Z.; Loh, X.J. Strong and biocompatible lignin/poly (3-hydroxybutyrate) composite nanofibers. *Compos. Sci. Technol.* **2018**, *158*, 26–33. [CrossRef]
30. Wang, J.; Tian, L.; Luo, B.; Ramakrishna, S.; Kai, D.; Loh, X.J.; Yang, I.H.; Deen, G.R.; Mo, X. Engineering PCL/lignin nanofibers as an antioxidant scaffold for the growth of neuron and Schwann cell. *Colloids Surf. B Biointerfaces* **2018**, *169*, 356–365. [CrossRef]
31. Kai, D.; Zhang, K.; Jiang, L.; Wong, Z.H.; Li, Z.; Zhang, Z.; Loh, X.J. Sustainable and antioxidant lignin-polyester copolymers and nanofibers for potential healthcare applications. *ACS Sustain. Chem. Eng.* **2017**, *5*, 6016–6025. [CrossRef]
32. Kai, D.; Ren, W.; Tian, L.; Lin Chee, P.; Liu, Y.; Ramakrishna, S.; Loh, X.J. Engineering poly (lactide)-lignin nanofibers with antioxidant activity for biomedical application. *ACS Sustain. Chem. Eng.* **2016**, *4*, 5268–5276. [CrossRef]
33. Borrego, M.; Martín-Alfonso, J.E.; Sánchez, M.C.; Valencia, C.; Franco, J.M. Electrospun lignin-PVP nanofibers and their ability for structuring oil. *Int. J. Biol. Macromol.* **2021**, *180*, 212–221. [CrossRef] [PubMed]
34. Martín-Alfonso, J.E.; Núñez, N.; Valencia, C.; Franco, J.M.; Díaz, M.J. Formulation of new biodegradable lubricating greases using ethylated cellulose pulp as thickener agent. *J. Ind. Eng. Chem.* **2011**, *17*, 818–823. [CrossRef]
35. Pernetti, M.; van Malssen, K.F.; Flöter, E.; Bot, A. Structuring of edible oils by alternatives to crystalline fat. *Curr. Opin. Colloid Interface Sci.* **2007**, *12*, 221–231. [CrossRef]
36. Co, E.D.; Marangoni, A.G. Organogels: An alternative edible oil-structuring method. *J. Am. Oil Chem. Soc.* **2012**, *89*, 749–780.
37. Singh, A.; Auzanneau, F.-I.; Rogers, M.A. Advances in edible oleogel technologies–A decade in review. *Int. Food Res. J.* **2017**, *97*, 307–317. [CrossRef]
38. Zetzl, A.K.; Gravelle, A.J.; Kurylowicz, M.; Dutcher, J.; Barbut, S.; Marangoni, A.G. Microstructure of ethylcellulose oleogels and its relationship to mechanical properties. *Food Struct.* **2014**, *2*, 27–40. [CrossRef]
39. Patel, A.R.; Schatteman, D.; Lesaffer, A.; Dewettinck, K. A foam-templated approach for fabricating organogels using a water-soluble polymer. *RSC Adv.* **2003**, *3*, 22900–22903. [CrossRef]
40. Wijaya, W.; Van der Meeren, P.; Dewettinck, K.; Patel, A.R. High internal phase emulsion (HIPE)-templated biopolymeric oleofilms containing an ultra-high concentration of edible liquid oil. *Food Funct.* **2018**, *9*, 1993–1997. [CrossRef]
41. De Vries, A.; Wesseling, A.; van der Linden, E.; Scholten, E. Protein oleogels from heat-set whey protein aggregates. *J. Colloid Interface Sci.* **2017**, *486*, 75–83. [CrossRef] [PubMed]

42. Borrego, M.; Martín-Alfonso, J.E.; Valencia, C.; Sánchez, M.C.; Franco, J.M. Developing electrospun ethylcellulose nanofibrous webs: An alternative approach for structuring castor oil. *ACS Appl. Polym. Mater.* **2022**, *4*, 7217–7227. [CrossRef]
43. Rubio-Valle, J.F.; Sánchez, M.C.; Valencia, C.; Martín-Alfonso, J.E.; Franco, J.M. Electrohydrodynamic processing of pvp-doped kraft lignin micro- and nano-structures and application of electrospun nanofiber templates to produce oleogels. *Polymers* **2021**, *13*, 2206. [CrossRef] [PubMed]
44. Borrego, M.; Martín-Alfonso, J.E.; Sánchez, M.C.; Valencia, C.; Franco, J.M. Influence of surfactants on the electrospinnability of lignin-PVP solutions and subsequent oil structuring properties of nanofber mats. *Polym. Bull.* **2022**. [CrossRef]
45. Anna, S.L.; McKinley, G.H.; Nguyen, D.A.; Sridhar, T.; Muller, S.J.; Huang, J.; James, D.F. An interlaboratory comparison of measurements from filament-stretching rheometers using common test fluids. *J. Rheol.* **2001**, *45*, 83–114. [CrossRef]
46. Arnolds, O.; Buggisch, H.; Sachsenheimer, D.; Willenbacher, N. Capillary breakup extensional rheometry (CaBER) on semi-dilute and concentrated polyethyleneoxide (PEO) solutions. *Rheol. Acta* **2010**, *49*, 1207–1217. [CrossRef]
47. Gorbacheva, S.N.; Yadykova, A.Y.; Ilyin, S.O. Rheological and tribological properties of low-temperature greases based on cellulose acetate butyrate gel. *Carbohydr. Polym.* **2021**, *272*, 118509. [CrossRef]
48. Gallego, R.; Cidade, T.; Sánchez, R.; Valencia, C.; Franco, J.M. Tribological behaviour of novel chemically modified biopolymer-thickened lubricating greases investigated in a steel-steel rotating ball-on-three plates tribology cell. *Tribol. Int.* **2016**, *94*, 652–660. [CrossRef]
49. Martín-Alfonso, J.E.; Franco, J.M. Ethylene-vinyl acetate copolymer (EVA)/sunflower vegetable oil polymer gels: Influence of vinyl acetate content. *Polym. Test.* **2014**, *37*, 78–85. [CrossRef]
50. Delgado, M.A.; Cortés-Triviño, E.; Valencia, C.; Franco, J.M. Tribological study of epoxide-functionalized alkali lignin-based gel-like biogreases. *Tribol. Int.* **2020**, *146*, 106231. [CrossRef]

6. ARTÍCULO 5

Assessment of the tribological performance of electrospun lignin nanofibrous web-thickened bio-based greases in a nanotribometer

María Borrego, E. Kuhn**, José E. Martín-Alfonso, José M. Franco *

* Pro2TecS – Chemical Product and Process Technology Research Center, Department of Chemical Engineering and Materials Science, Universidad de Huelva, ETSI, Campus de "El Carmen", 21071, Huelva, Spain.

** Laboratory of Machine Elements and Tribology, Department of Mechanical Engineering and Production, Faculty of Engineering Technology and Computer Science, Hamburg University of Applied Sciences (HAW-Hamburg), Berliner Tor 21, 20099 Hamburg, Germany.

Published in:

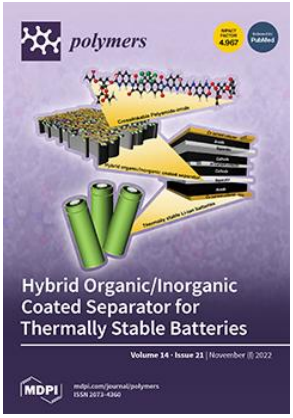

Publishing company: MDPI

Editor-in-Chief: Shirley Chiang

Volume 13, Issue 21, pp: 2852

Year: 2023

ISSN: 2079-4991

DOI: https://doi.org/10.3390/nano13212852

Impact factor (2022): 5.3

JCR Journal rank: 39/160 in Applied Physics; 110/334 in Materials Science, Multidisciplinary.

6.1. Resumen

En este trabajo se ha estudiado el comportamiento tribológico de grasas lubricantes modelo, desarrolladas a partir de nanofibras de lignina obtenidas mediante electrospinning, seleccionadas de los trabajos discutidos en los capítulos precedentes, que incluyen EC o PVP como polímeros de co-spinning, en un nanotribómetro.

Se demostró que la morfología de las fibras ejerce gran impacto sobre la fricción y el desgaste de las superficies a lubricar. Cómo ya se ha discutido anteriormente, la morfología depende de la concentración de la disolución de alimentación y de la relación en peso LSL:polímero de co-spinning. Se seleccionaron diferentes membranas con morfología diversa, desde partículas aglomeradas, a las típicas fibras con partículas (BOAS), hasta estructuras enteramente dominadas por nanofibras.

Un aumento de la concentración de la nanoestructura (es decir de espesante) produce un aumento significativo del coeficiente de fricción. En cuanto al efecto de la fuerza normal aplicada, se confirmó que los ensayos se realizaron en condiciones de lubricación mixta.

Un aumento en la proporción del polímero coadyuvante, especialmente si es el PVP, disminuye el coeficiente de fricción, del mismo modo que la concentración de la disolución de la alimentación. Esto sugiere que nanoestructuras más homogéneas y predominante formadas por fibras son capaces de liberar el aceite de forma más constante y sostenida en el tiempo. Por otra parte, la presencia de lignina, en especial en membranas particuladas o BOAS resultan abrasivas y afecta negativamente al desgaste de la superficie de contacto, dando lugar también a una mayor fricción. En definitiva, reducir la presencia de microesferas es un objetivo para conseguir grasas menos abrasivas.

Con el fin de relacionar la morfología con el comportamiento tribológico se estudiaron parámetros relacionados con la misma, cómo la porosidad y el diámetro medio de las fibras. En las redes de lignina estudiadas el número de partículas está inversamente correlacionado con el diámetro y es proporcional a la porosidad. Pequeños diámetros de fibras y alta porosidad están se encuentran predominantemente en estructuras dominadas por partículas o morfologías dispuestas por BOAS con una gran cantidad de microesferas. Por el contrario, diámetros mayores están relacionados con membranas más homogéneas y dominadas por fibras las cuáles tienden a reducir el coeficiente de fricción.

En cuanto al desgaste, el diámetro de las fibras no parece influir significativamente, pero la porosidad sí aparece como un factor importante a tener en cuenta. Cuanto mayor es la porosidad de la membrana mayor fricción y desgaste en las superficies se produce. Estos resultados se pueden explicar mediante dos hipótesis:

1- Las nanofibras pueden penetrar en el contacto más fácilmente que las partículas aumentando el espesor de la capa de lubricante, evitando mejor el desgaste.
2- Si algunas partículas de lignina son capaces de penetrar en el contacto, éstas son más abrasivas, debido a su tamaño, y aumentan el desgaste cómo consecuencia de la interacción con las superficies de contacto.

En resumen, se concluyó que las membranas de lignina electrohiladas pueden utilizarse como espesantes efectivos para desarrollar grasas lubricantes biodegradables. Las propiedades tribológicas de las mismas se ven ampliamente afectadas por la morfología de estas membranas. Se consiguieron menores valores del coeficiente de fricción y grasas menos abrasivas cuando las membranas son homogéneas sin presencia

de perlas o BOAS, lo cuál se favorece cuando se reduce la proporción lignina:polímero de co-spinning, o bien, cuando aumentamos la concentración de la disolución. Por lo tanto, membranas homogéneas constituidas por nanofibras dan lugar a biolubricantes capaces de retener el aceite de ricino pero liberarlo satisfactoriamente por acción de la carga normal, proporcionando así una reposición constante al contacto lubricado.

nanomaterials

MDPI

Article

Assessment of the Tribological Performance of Electrospun Lignin Nanofibrous Web-Thickened Bio-Based Greases in a Nanotribometer

María Borrego [1], Erik Kuhn [2], José E. Martín-Alfonso [1] and José M. Franco [1,*]

[1] Chemical Product and Process Technology Research Center (Pro2TecS), Department Chemical Engineering and Materials Science, Escuela Técnica Superior de Ingeniería (ETSI), Campus de "El Carmen", University of Huelva, 21071 Huelva, Spain; maria.borrego@diq.uhu.es (M.B.); jose.martin@diq.uhu.es (J.E.M.-A.)

[2] Laboratory of Machine Elements and Tribology, Department of Mechanical Engineering and Production, Faculty of Engineering Technology and Computer Science, Hamburg University of Applied Sciences (HAW-Hamburg), Berliner Tor 21, 20099 Hamburg, Germany; erik.kuhn@haw-hamburg.de

* Correspondence: franco@uhu.es

Abstract: The tribological performance of novel bio-based lubricating greases thickened with electrospun lignin nanostructures was investigated in a nanotribometer using a steel–steel ball-on-disc configuration. The impact of electrospun nanofibrous network morphology on friction and wear is explored in this work. Different lignin nanostructures were obtained with electrospinning using ethylcellulose or PVP as co-spinning polymers and subsequently used as thickeners in castor oil at concentrations of 10–30% wt. Friction and wear generally increased with thickener concentration. However, friction and wear decreased when using homogeneous bead-free nanofiber mats (with higher fiber diameter and lower porosity) rather than nanostructures dominated by the presence of particles or beaded fibers, which was favored by reducing the lignin:co-spinning polymer ratio.

Keywords: bio-based lubricating greases; electrospinning; friction; lignin; nanofiber; wear

Citation: Borrego, M.; Kuhn, E.; Martín-Alfonso, J.E.; Franco, J.M. Assessment of the Tribological Performance of Electrospun Lignin Nanofibrous Web-Thickened Bio-Based Greases in a Nanotribometer. *Nanomaterials* **2023**, *13*, 2852. https://doi.org/10.3390/nano13212852

Academic Editors: Csaba Balázsi, Md Abdul Maleque and Md Mustafizur Rahman

Received: 25 September 2023
Revised: 16 October 2023
Accepted: 26 October 2023
Published: 27 October 2023

1. Introduction

The main purpose of lubrication is the reduction in energy losses caused by friction in machine elements and wear minimization, thus prolonging the reliability and service life of mechanical components and equipment [1]. In addition, in the case of lubricating greases, the rheological characteristics imparted by the thickener microstructure make this particular lubricant especially appropriate in some applications where decreasing leakage and the frequency of lubrication are desired, especially in hermetic or hard-to-reach contacts, or when vibrations and fluctuations with temperature and loads must be minimized [2]. Moreover, lubricating greases act as effective seals against contaminants, such as particles and water [3].

As extensively reported by Lugt and co-workers [4–7], the lubrication mechanism of greases is extremely complex and affected by many factors such as the inherent complex rheological properties of greases, geometry of the lubricated contacts and components and the different coexisting shear and extension rates internally achieved. In most cases, grease lubrication involves the mixed or elastohydrodynamic (EHL) lubrication regimes, where the film is not only determined by the lubricant properties. Although several aspects are still under discussion, it is generally accepted that the grease lubrication mechanism is mainly governed by the replenishment of the lubricant into the contact and the oil bleeding ability, i.e., the capacity of the grease microstructure to release oil [8–10]. In this sense, the grease microstructure would act as a sponge that replenishes the lubricated contact with the bled oil once submitted to an external load [8,9,11]. Different models considering the morphology of grease microstructure and/or thickener particle geometry have been reported [9,12]. However, it is also generally assumed that the thickener exerts a significant

impact in grease lubrication, not only acting as a reservoir for the oil but penetrating into the contact and affecting the film thickness, either thickening the bled oil or as isolated particles, eventually influencing friction and wear [1,13–17]. Both effects, the oil bleeding ability and thickener penetration, are largely determined by the grease microstructure imparted by the thickener, which may be also influenced by its mechanical degradation [18–20]. Therefore, the correct elucidation of grease microstructure, as well as the effect of shearing on this, is essential to understanding the lubrication mechanisms [17,21,22].

On the other hand, as a consequence of environmental awareness, there is a widespread concern in the lubricant industry to replace petroleum-based components with others, biodegradable or obtained from natural resources. Thus, the number of scientific and technical research related to the development of biolubricants from natural resources has increased accordingly over the last two decades, as can be deduced from the vast number of review papers recently published on this topic [23–27]. In the case of lubricating greases, since the main component is the base oil and preserving the functionality associated with thickener microstructure is essential for proper lubrication, the main initiatives to achieve biodegradable formulations have been focused on the replacement of traditional mineral oils with vegetable-derived oils or glycerol esters, while maintaining metallic thickeners in the formulation [23,28,29]. However, given that the thickener content in greases can vary between 3% and 40% by weight, and that the thickeners with the best technical performance and most widely used in industry are metal soaps and polyureas, especially lithium soaps, there is a clear need to develop new renewable thickening agents that may provide adequate technical performance. In addition, the importance of lithium in other more demanding and priority applications like batteries and the supply constraints associated with this scarce resource must be taken into account. Therefore, the development of bio-based thickeners obtained from natural and renewable polymers, making them technologically efficient, represents an environmentally friendly alternative to metal soaps and synthetic polymers derived from the petrochemical industry (polyurea, polyurethanes, polypropylene, etc.) that are not biodegradable and/or require highly toxic or polluting production processes. Unfortunately, the oil structuring ability of biopolymers such as cellulose and chitosan derivatives or lignocellulosic components is very limited due to their polar chemical nature. Only very few biopolymers, like ethylcellulose, are able to gel oils directly by the formation of supramolecular structures [30] but still exhibit serious drawbacks as effective thickeners in lubricant formulations [31].

In previous investigations, different strategies involving chemical modifications of biopolymers to reduce their polarity and enhance oil affinity [32] or to induce oil structuration via chemical crosslinking with isocyanate or epoxide reactive groups [33,34] have been proposed. Three-dimensional structural networks that perfectly mimic the grease microstructure provided by lithium soaps, were for instance achieved with lignocellulose modified with diisocyanates [33]. Nevertheless, these chemical modifications usually require chemicals, solvents and/or catalysts that make the synthesis of biopolymeric thickeners and the subsequent oil structuring process relatively complex and not entirely environmentally friendly, despite the fact the final product is. Very recently, we demonstrated that nanostructures generated with electrospinning from non-modified biopolymers can be proposed as effective oil structuring agents [35,36]. The high porosity, small size and high surface/volume ratio of nanofibrous webs are able to induce the formation of three-dimensional networks with a superior capacity to promote physical interactions between the oil and the nanofibers stabilizing the colloidal system through the formation of a percolation network.

Lignin is an attractive biopolymer due to the fact that is considered a waste or low-value by-product resulting from different biorefinery processes, which has been previously employed to produce oil thickening agents via chemical crosslinking [37]. However, producing lignin nanofibers using electrospinning is particularly challenging as a consequence of its chemical structure and relatively low molecular weight [38], and often requires the use of a co-spinning polymer [35,39]. However, non-uniform nanostructures

typically obtained with lignins, consisting of particles or globules distributed along the filaments, which have come to be called BOAS (beads-on-a-string) [40,41] or weakly mixed particle–fiber nanostructures might also be appropriate for lubricating purposes, in terms of an easy oil release, i.e., oil bleeding [36]. The aim of this work is to investigate the tribological performance of novel bio-based lubricating greases, thickened with different electrospun lignin nanostructures, in a ball-on-disc nanotribometer by addressing the impact of the electrospun network morphology on friction and wear. A nanotribometer was selected because of its sensitivity in measuring weak effects due to small variations in thickener nanostructures.

2. Materials and Methods

2.1. Materials

A softwood low-sulphonate lignin (LSL) from Merck Sigma-Aldrich (St. Louis, MO, USA) (M_w: ~10,000 g/mol) was used as the main polymer to produce structural networks using electrospinning and subsequently thicken castor oil (viscosity: 0.55 Pa·s, density: 0.958 g/mL, at 25 °C) supplied by Guinama (Valencia, Spain). High molecular weight ethyl cellulose (EC, $M_w = 8.2 \times 10^4$ g/mol) and polyvinylpyrrolidone (PVP, M_w: ~ 3.6×10^5 g/mol) purchased from Merck Sigma-Aldrich, were used as co-spinning polymers. Tetrahydrofuran (THF, purity 99.0%), dimethylacetamide (DMAc, 99.8% purity) and dimethylformamide (DMF, 99.8% purity), also supplied by Sigma-Aldrich (St. Louis, MO, USA), were used as solvents.

2.2. Electrospinning of Lignin Solutions

Solutions of LSL/EC in a DMAc:THF (1:1 *w*/*w*) binary solvent system were prepared at 10 and 15% wt. total concentration by modifying the LSL:EC ratio (50:50, 70:30 and 90:10), under agitation at 40 °C for 24 h, using a magnetic stirrer, at 500 rpm, on a hot plate. LSL/PVP solutions were similarly prepared in DMF at 10% wt. total concentration at the same weight ratios (50:50, 70:30 and 90:10). These solutions were used as feed for electrospinning in a device constructed using a high-voltage power supply (Spellman High Voltage Electronics Corporation, Hauppauge, NY, USA), a syringe with a blunt metal needle, a syringe pump (KD Scientific Pump Company, Holliston, MA, USA) and a grounded aluminum foil collector. The polymeric solution was fed through the needle tip with a syringe pump at a flow rate of 0.8–2 mL/h (tip diameter ≈ 0.6 mm). Nanostructures were produced at a tip-to-target distance of 12 cm and an applied voltage of 12–20 kV. All the electrospinning experiments were carried out at 23 °C (±2 °C) with a relative humidity of 45% (±5%). The relative humidity was roughly controlled by inserting a dehumidifier containing a saturated $Mg(NO_3)_2$ solution in the electrospinning chamber.

The morphology of the resulting electrospun fiber webs was examined using scanning electron microscopy (FlexSEM 1000 II, Hitachi, Tokyo, Japan) after sputtering the samples with gold under vacuum. SEM experiments were carried out at accelerating voltages of 10–20 kV. The FIJI ImageJ analysis software (version 1.52p, 2019) was used to analyze the SEM pictures. Random observations were carried out at the same magnification to determine the average diameter of particles and fibers and the porosity of the electrospun nanostructure by adjusting the contrast of the micrographs.

2.3. Preparation of Bio-Based Greases with Electrospun Lignin Nanostructures

Electrospun lignin nanostructures obtained using electrospinning were used to thicken castor oil by simply dispersing the solid collected from the electrospinning device under gentle mechanical agitation (60 rpm, during 60 min) using an anchor impeller geometry at room temperature (~23 °C). Electrospun lignin nanostructures were incorporated at three different concentrations (10, 20 and 30%). These dispersions were stored at room temperature and rest conditions for at least 24 h to assess physical stability, i.e., no phase separation, previously to carry out the rheological and tribological characterization. Only the dispersion of nanostructures formed with 90:10 LSL/co-spinning polymer ratios ob-

tained from solutions at 10% wt. evinced a certain degree of oil separation after several days. The oil separation ability was studied using centrifugation. Approximately 0.7 g of each selected sample was centrifuged in a Sorvall ST8 (Thermo Fisher Scientific, Waltham, MA, USA) centrifuge at 16,000 rpm (equivalent to 24,328$\times$ g) for 30 min, and the amount of separated oil was subsequently weighed.

2.4. Tribological Characterization

The tribological performance of the model greases thickened with electrospun lignin nanostructures was investigated in a ball-on-disc CSM nanotribometer (Peseux, Switzerland). The set-up basically consists of a static ball, which is fixed to a cantilever to avoid rolling, and a movable disc, which is stressed by applying a normal force. A fiber-optic sensor measures the deflection of the cantilever in the radial direction to determine the frictional force. A more detailed description of the equipment and experimental setup can be found elsewhere [42]. All tests were carried out in the rotational mode under pure sliding motion (sliding speed: 40 mm·s^{-1}) in a steel–steel (115CrV3, hardness 22.72 HRC) ball-on-disc configuration, using a 1 mm diameter ball. Three normal loads (400, 700 and 900 mN, corresponding to 1.60, 1.93 and 2.10 GPa Hertzian pressures, respectively) were applied during a test duration of 20 min. The examined greases were applied to the disc surface prior to the start of each test without manual relubrication during the test. Each test was replicated ten times on the same track at room temperature (21 $\pm$ 1 °C). The dimensions of the wear grooves on the steel plates created after the ten repetitions of the test were quantified using the white light interferometry technique using a Zygo Nexview apparatus (Middlefield, OH, USA) and Zygo Mx software (version 7.1.0.4, 2017). The wear volume values reported hereunder correspond to a groove length of 100 μm. Obviously, wear also occurs to some extent on the balls. However, wear marks in the 1 mm balls were small, and the results did not discriminate between the different greases. Therefore, wear data of the ball surface have not been considered.

2.5. Rheological Characterization

Model greases were rheologically characterized using a MARS controlled-stress rheometer (ThermoHakee, Uhingen, Germany), using serrated parallel plate (20 and 35 mm; 1 mm gap) geometries to avoid possible slip effects. Viscous flow tests were performed, at 25 °C, by applying stepped shear rate ramps from 0.02 to 300 s^{-1}. At least two replicates of each test were performed.

3. Results and Discussion

3.1. Morphology of Electrospun Lignin Nanostructures

The morphology of LSL/EC nanostructures subsequently used to thicken castor oil largely depends on the concentration of the feeding solution and the LSL:EC ratio, as illustrated in Figure 1. As can be seen, an evolution from agglomerated submicrometric electrosprayed particles to the typical BOAS (beads-on-a-string) structure dominated by nanofibers was found when increasing the solution concentration or decreasing the LSL:EC ratio. The lower the LSL:EC ratio, the lower the number of beads that appear in the nanofibrous web. Finally, when feeding the electrospinning chamber with a solution having high concentration and a low LSL:EC ratio, i.e., 15% wt. and 50:50 LSL:EC ratio, bead-free nanofiber webs were obtained (see Figure 1F). Different lignin nanostructures were also obtained using PVP as a co-spinning polymer and modifying the LSL:PVP weight ratio in the feeding solution. As can be observed in Figure 2, a similar evolution in the morphology was detected when increasing the amount of PVP in the nanostructure, although generally, more homogeneous nanofiber mats and a lower amount of particle beads were detected when replacing EC with PVP as the co-spinning polymer (compare, for instance, Figure 2B,C with Figure 1C,E, respectively, for the same feeding solution concentration and electrospinning conditions). Further details on the relationship between

the physicochemical properties of the lignin solutions and the morphology of the resulting nanostructures can be found elsewhere [35].

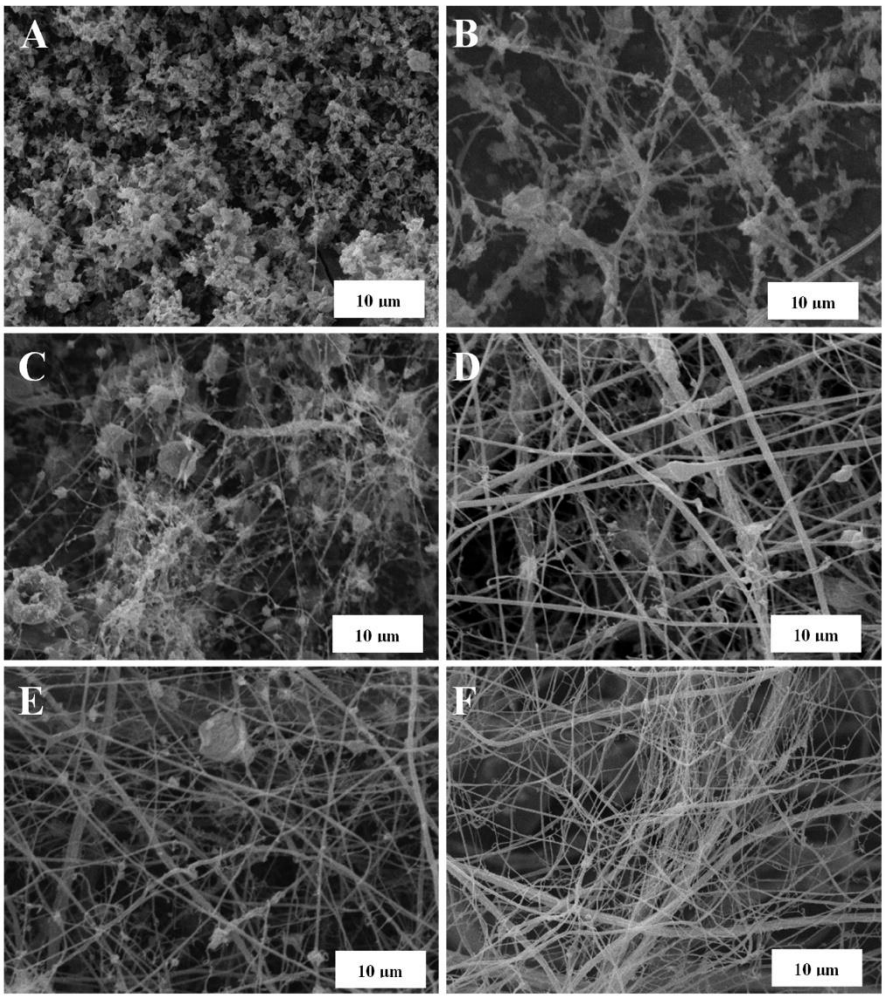

Figure 1. SEM images of electrospun LSL/EC nanostructures obtained with different LSL:EC ratios and concentrations of the feeding solution: (**A**) 90:10, 10% solution concentration, (**B**) 90:10, 15% solution concentration, (**C**) 70:30, 10% solution concentration, (**D**) 70:30, 15% solution concentration, (**E**) 50:50, 10% solution concentration and (**F**) 50:50, 15% solution concentration.

3.2. Rheological Behavior of Electrospun Nanostructure-Thickened Lubricating Greases

The electrospun lignin nanostructures described above were used to thicken castor oil, aiming to impart gel-like characteristics and obtain model bio-based greases. Regardless of the thickener concentration and the LSL:co-spinning polymer ratio, all greases showed a similar shear-thinning response with a tendency to reach a constant high shear-rate limiting viscosity. Experimental viscous flow curves were satisfactorily fitted ($R^2 < 0.995$) to the Sisko model:

$$\eta = K\dot{\gamma}^{n-1} + \eta_\infty \quad (1)$$

where η is the non-Newtonian viscosity, $\dot{\gamma}$ is the shear rate, K and n are the consistency and flow indexes, respectively, and η_∞ is the high shear-rate limiting viscosity. Table S1 in the Supplementary Materials collects the values of Sisko parameters obtained from the fits. In general, K and η_∞ values clearly increased with the thickener concentration, i.e., the content of electrospun nanostructures, and decreased with the LSL:co-spinning

polymer ratio, whereas n generally decreases with increasing the thickener concentration or the co-spinning polymer proportion. Figures S1 and S2 in the Supplementary Materials illustrate the effect of both these compositional variables on the viscous flow curves of the bio-greases studied. According to the morphological characteristics of the electrospun nanostructures, the more homogeneous and well-developed nanofiber mats and the lower amount of particle beads, the higher the viscosity of the colloidal dispersion, reflected in higher K and η_∞ values.

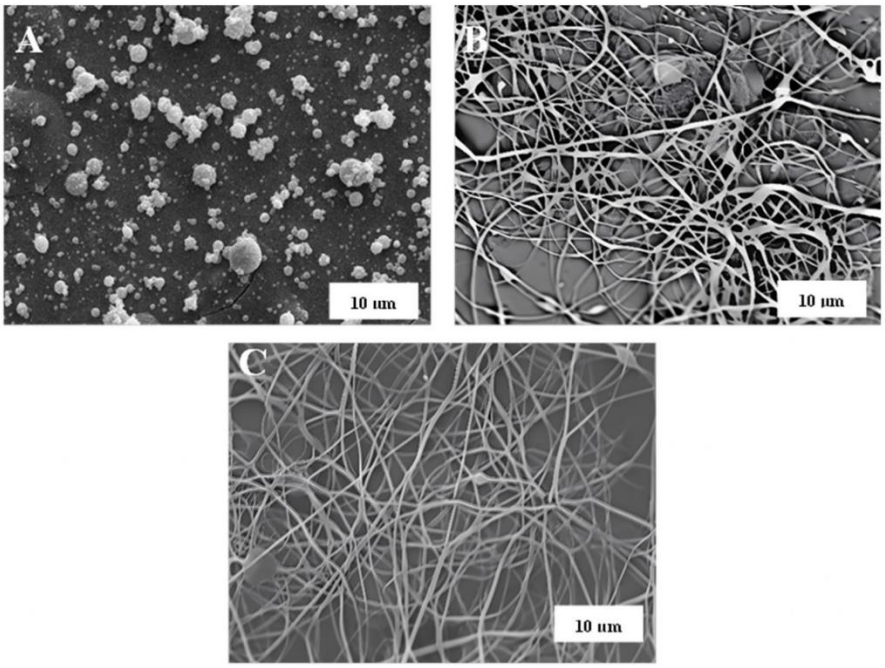

Figure 2. SEM Images of electrospun LSL/PVP nanostructures obtained with different LSL:PVP ratios: (**A**) 90:10, (**B**) 70:30 and (**C**) 50:50 (feeding solution concentration: 10% wt.).

3.3. Influence of Concentration on the Tribological Properties of Electrospun Nanostructure-Thickened Lubricating Greases

Electrospun lignin nanostructures were dispersed in castor oil at three different concentrations (10, 20 and 30% wt.), and the resulting greases were tested in a steel–steel ball-on-disc nanotribometer. Figure 3 shows the values of the friction coefficient, measured at different normal forces, using greases thickened with the 70:30 LSL:EC nanostructure as the lubricant. In general, it is worth noting a significant increase in the friction coefficient with the nanostructure concentration, which is more evident at high normal force. Moreover, the friction coefficient is not significantly affected by the normal force when using a low thickener concentration or slightly increases with this at higher concentrations, which confirms that the experiments were conducted under mixed lubrication conditions. Furthermore, the friction coefficient values obtained when using these novel greases as lubricants are significantly higher than those obtained with the nanofiber-free base oil (see the values in Table S2). This is a well-known result in the mixed lubrication regime since friction is caused by both the contact between the surface asperities and by the contribution of the lubricant, which, in the case of greases, includes the internal friction of the microstructure.

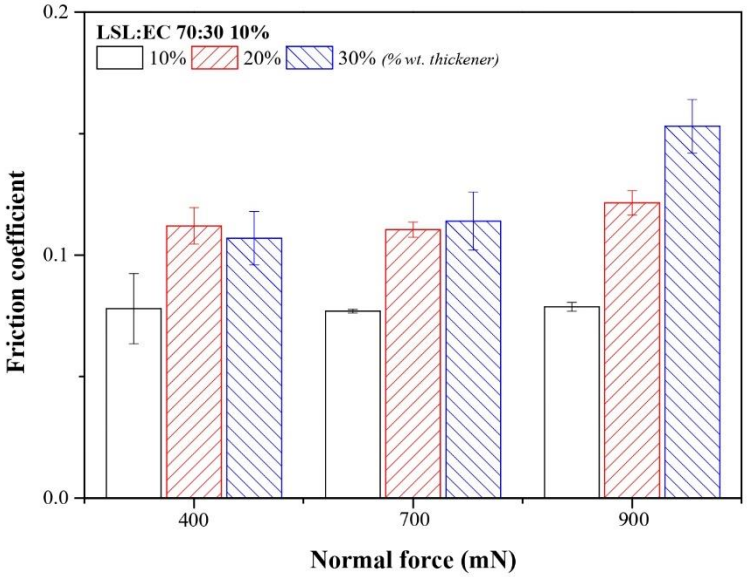

Figure 3. Friction coefficient values obtained with lubricating greases thickened with the 70:30 LSL/EC electrospun nanostructure at different concentrations (10%, 20% and 30% wt.).

Aiming to explain the influence of lignin nanostructure concentration on the friction coefficient, two phenomena must be taken into account. As extensively discussed by Gonçalves et al. [13,43,44], the friction coefficient values typically increase with a decrease in the entrainment speed, which is related to the grease replenishment into the contact. The contact replenishment capacity is probably reduced by increasing the thickener concentration as a result of a significantly increased grease consistency (see rheological parameters in Table S1 in the Supplementary Materials). The oil bleeding ability is generally dampened by increasing the thickener concentration since the three-dimensional network entraps the oil more effectively [12,13]. For selected samples, Table S3 in the Supplementary Materials shows that after centrifugation oil separation is favored by decreasing thickener concentration. On the other hand, the penetration of the thickener into the contact increases the film thickness and must reduce the friction coefficient [14,44], as it must occur when reducing the normal force applied (see Figure 3). However, the increase in nanostructure concentration does not seem to favor the thickener penetration or, if this penetration occurs, it does not exert a friction reduction. It must be taken into account that lignin, especially particles or beads, is somewhat abrasive and may negatively affect the mating surface, contributing to increased friction and wear, similar to what happens with debris particles or contaminants in the tribological contact [45]. The effects of the normal force under mixed conditions and the possible penetration of lignin nanofibers into the contact were also elucidated by analyzing the wear tracks on the plates measured using interferometry. Figure 4 shows the effect of thickener concentration on the evolution of both the wear groove volume and the average wear width as a function of the applied normal force. As can be seen, wear is not noticeably influenced by lignin concentration at the lowest normal force (400 mN), but significantly increases with this for higher normal forces, when the lubrication mechanism seems to be mainly governed by the oil bleeding ability. A similar thickener concentration influence on friction and wear was previously reported when using epoxidized lignin [46] or nanosized montmorillonite [47] as thickeners in castor oil or cellulose acetate butyrate in acetyl tributyl citrate and triethyl citrate media, respectively [48,49].

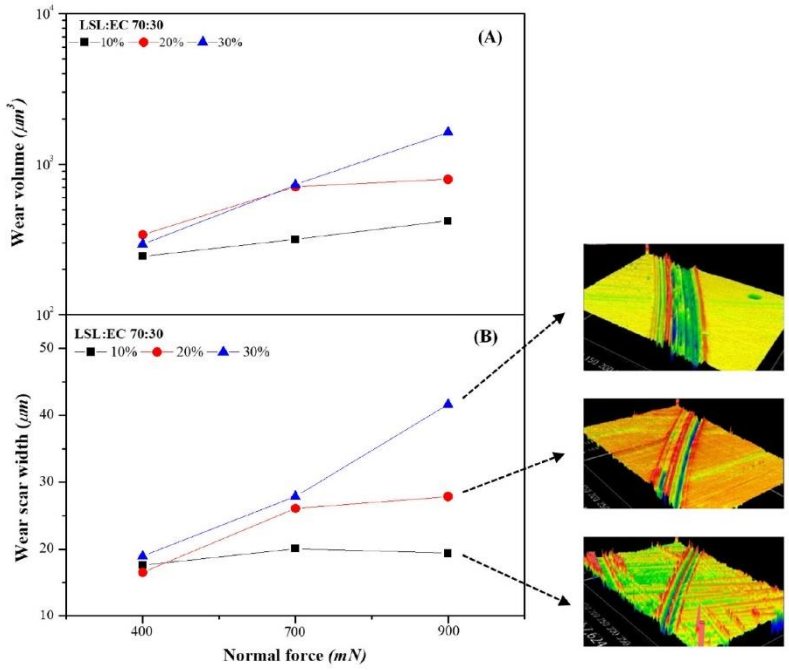

Figure 4. Evolution of the average scar wear volume (**A**) and wear width (**B**) with the normal force applied when using lubricating greases thickened with the 70:30 LSL/EC electrospun nanostructure (10% wt. feeding solution) at different concentrations (10%, 20% and 30% wt.).

3.4. Influence of the LSL:EC Ratio on the Tribological Properties of Electrospun Nanostructure-Thickened Lubricating Greases

Figure 5 shows the values of the friction coefficient obtained for the three normal forces applied when using bio-based greases thickened with LSL/EC nanostructures, at 20% wt., as a function of the LSL:EC ratio (50:50, 70:30 and 90:10) and the initial feeding solution concentration (10 and 15% wt.). As previously discussed, the morphology of the electrospun nanostructures largely depends on these variables and also strongly affects the friction behavior of the resulting greases, as shown in Figure 5. The friction coefficient generally decreases when increasing both the concentration of the feeding solution to the electrospinning chamber and the EC proportion in the nanostructures. These results suggest that more homogeneous and fiber-dominated mats are able to more steadily release the oil entrapped in the three-dimensional network, facilitating a regular replenishment in the contact, rather than nanostructures with the prevalence of particles or beads inserted in the fibers where the oil is much more readily separated (see oil separation data in Table S3 for selected samples). In general, the contact replenishment capacity of greases thickened with LSL/EC nanostructures differing in the LSL:EC ratio at the same concentration (20% wt.) seems not to be very different, being the morphological characteristics that govern the tribological performance. In fact, the wear scar volume produced in the steel plates was also significantly reduced when using more homogeneous and fiber-dominated electrospun nanofibrous webs as thickeners (see Figure 6), i.e., when increasing the EC proportion, which produced more viscous greases. On the other hand, the achievement of bead-free nanofiber webs, or, at least, a significant reduction in the number of beads, must also minimize the negative contribution of lignin particles in the tribological contact.

Finally, the friction coefficient values obtained using only castor oil as a lubricant (i.e., the nanofiber-free base oil) are only slightly lower (see Table S2) than those found with fiber-dominated uniform nanostructures (lower values in Figure 5), which supports the idea that friction reduction is mainly driven by a steady oil release from the nanofiber webs.

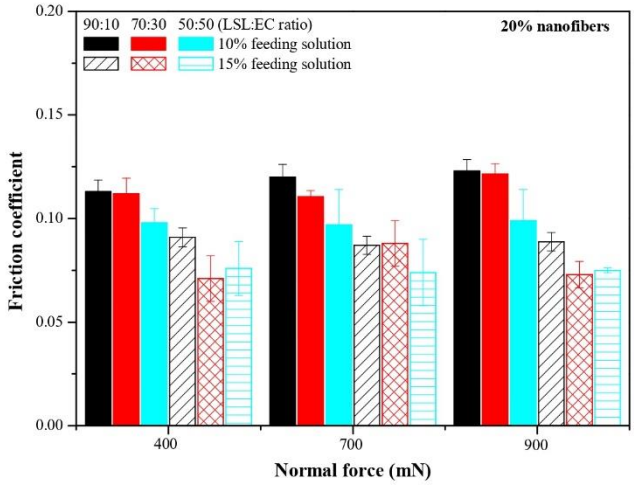

Figure 5. Friction coefficient values obtained with lubricating greases thickened with LSL/EC electrospun nanostructures differing in the LSL:EC weight ratio (thickener concentration 20% wt.).

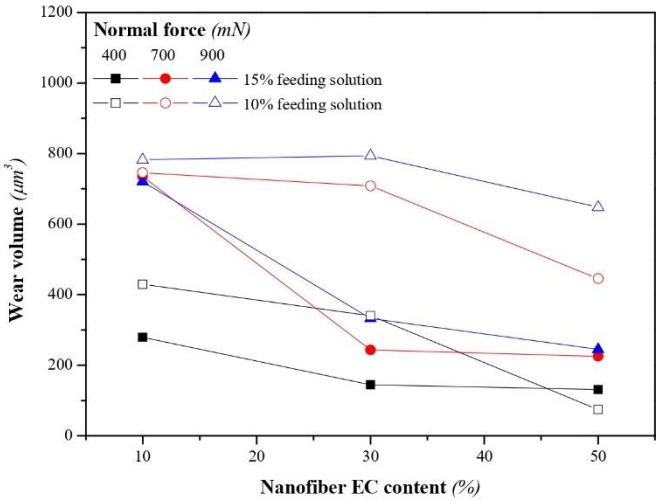

Figure 6. Wear volume produced when using lubricating greases thickened with LSL/EC electrospun nanostructures differing in the LSL:EC weight ratio (thickener concentration: 20% wt.).

3.5. Influence of the Co-Spinning Polymer on the Tribological Properties of Electrospun Nanostructure-Thickened Lubricating Greases

As above mentioned, when replacing EC with PVP as a co-spinning polymer, more homogeneous lignin nanofiber webs with a decreased amount of beads were generally obtained. Figure 7 illustrates the impact of replacing the co-spinning polymer on the friction and wear response of the resulting greases thickened with the electrospun nanostructures. As may be seen, the LSL/PVP nanostructures, under the same electrospinning processing conditions (70:30 LSL:co-spinning polymer ratio, 10% feeding solution) and thickener concentration (20% wt.), provide better lubrication performance to the greases in terms of lower friction coefficient values and reduced dimensions of wear grooves. Again, the lowest friction coefficient values are very similar to those obtained with neat castor oil (Table S2). Particularly, lower friction values were measured using greases containing 10% wt. of LSL/PVP-based nanostructures (see Figure S3 in the Supplementary Materials), where again, increasing the amount of the co-spinning polymer, PVP in this case, proved to be beneficial.

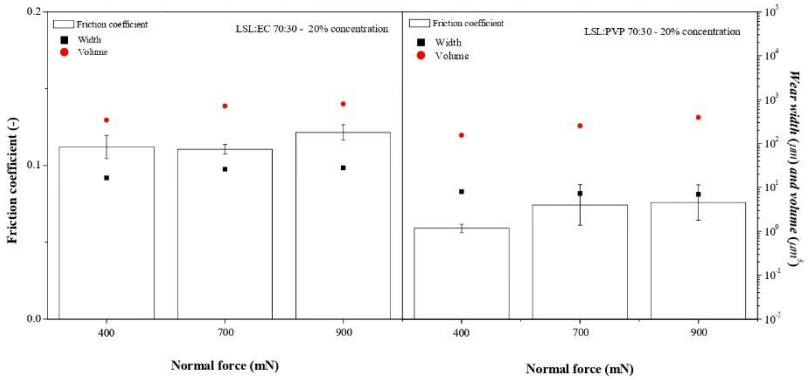

Figure 7. Comparison of the values of the friction coefficient and wear width and volumes obtained with lubricating greases thickened with LSL/EC and LSL/PVP electrospun nanostructures for the same LSLS:co-spinning polymer ratio (70:30 *w*/*w*) and concentration (20%).

3.6. Effect of Morphological Parameters on the Friction and Wear Behavior of Electrospun Nanostructure-Thickened Lubricating Greases

Aiming to better elucidate the role of electrospun nanostructure morphology on the tribological response of the resulting greases, some structural parameters such as the average fiber diameter and the nanostructure porosity were calculated from SEM observations and further correlated with the friction coefficient and dimensions of the wear grooves. Although the number of nanoparticles and beads in the electrospun nanostructures is actually an influencing parameter, in these particular lignin webs, it is inversely correlated with fiber diameter, whereas it is proportional to the network porosity. Therefore, electrospun nanostructures with low values of fiber diameters and high porosity are either generally dominated by nanoparticles or composed of BOAS morphologies with a significant number of beads.

Figure 8 shows the evolution of the friction coefficient with fiber diameter for greases thickened with LSL/EC nanofibrous webs at the three different concentrations studied. As can be seen, nanostructures with larger average fiber diameters tend to reduce friction in any case. As mentioned, it must be taken into account that smaller fiber diameters are also generally associated with the presence of beads in the nanostructure, whereas larger diameters correspond to more homogeneous and fiber-dominated webs. On the contrary, no significant influence of fiber diameter on wear mark dimensions was evinced.

Even more relevant is the influence of the nanostructure porosity. High porosity is one of the most striking characteristics of the electrospun lignin networks used as thickener agents, which roughly ranges from 50 to 70%, as well as their ability to adsorb or entrap vegetable oils in the voids (see for instance refs. [35,36]). As can be seen in Figure 9, the friction coefficient and the wear scar volume increase with the porosity of the electrospun lignin network. In particular, the friction coefficient correlates linearly with the porosity of the LSL/EC nanofibrous web regardless of the normal force applied in the experimental range analyzed (see linear fit in Figure 9B). In principle, these results may seem unexpected since highly porous networks should facilitate oil release and the replenishment of the lubricated contact. However, it must be taken again into account that, in this case, the more porous electrospun networks correspond to nanostructures dominated by the presence of particles or BOAS. Therefore, two possible and compatible hypotheses must be considered. On the one hand, nanofibers may penetrate into the contact more easily than particles, increasing the film thickness and preventing wear. On the contrary, lignin particles find it more difficult to come into the tribological contact due to their size and are probably accumulated at the inlet zone, particularly under pure sliding conditions, and the bled oil inversely flows under a pressure gradient, causing inlet starvation and more severe wear. On the other hand, although not so porous, a well-developed and homogeneous fibrous

network is able to retain but also release oil by the action of an external load more steadily, acting as a sponge and favoring a gradual replenishment of the lubricated contact.

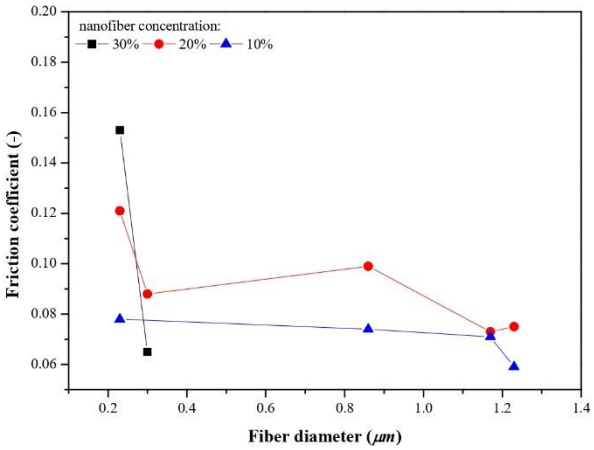

Figure 8. Evolution of the friction coefficient with the nanofiber diameter for greases thickened with LSL/EC electrospun nanofibrous webs at different concentrations (normal force applied: 900 mN).

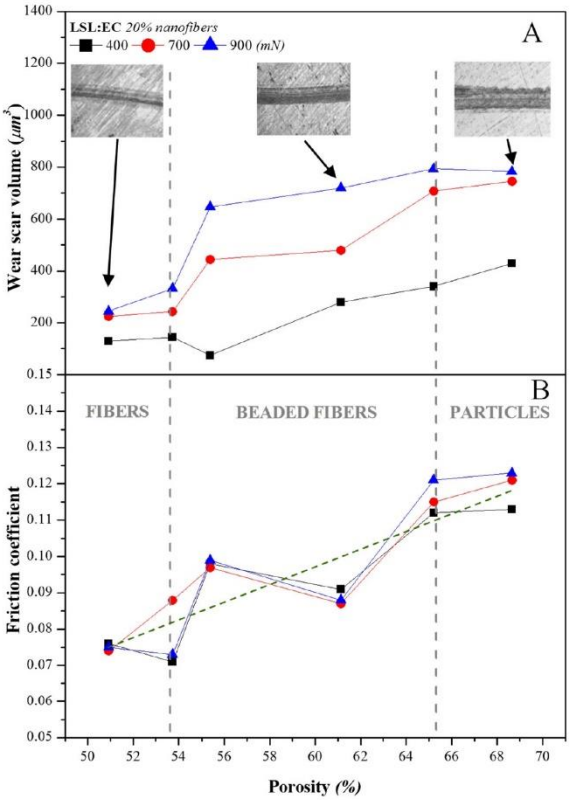

Figure 9. Evolution of (**A**) the wear scar volume and (**B**) the friction coefficient with the porosity of LSL/EC electrospun nanofibrous webs used to thicken greases (20% nanofiber concentration). The green dotted line in (**B**) corresponds to a linear fit $y = -0.05 + 0.02x$ ($R^2 = 0.879$), considering all experimental values regardless of the normal load applied.

4. Conclusions

Electrospun lignin nanostructures obtained using EC or PVP as co-spinning polymers were able to form stable gel-like colloidal dispersions in castor oil at concentrations between 10 and 30% wt. through the formation of percolation networks and can be satisfactorily proposed as cost-effective and renewable thickeners for bio-based lubricating grease formulations.

Friction and wear investigated in a nanotribometer using a steel–steel ball-on-disc configuration was reduced when using lubricating greases thickened with homogeneous bead-free nanofiber mats rather than nanostructures dominated by the presence of particles or beaded fibers. Obtaining homogeneous nanofibrous webs using electrospinning was favored by reducing the lignin:co-spinning polymer ratio or by increasing the concentration of the polymeric feeding solution, yielding larger average fiber diameters and lower porosity values.

The use of PVP as a co-spinning polymer resulted in nanofibrous webs with enhanced friction and wear performance in comparison with ethylcellulose, although ethylcellulose also provided good results at high proportions, and it is preferred in terms of renewability.

In general, according to the experimental results, it may be concluded that well-developed uniform fibrous lignin networks having larger average fiber diameters and lower porosity are able to retain but satisfactorily release the castor oil by the action of the normal load, thus providing a steady replenishment of the lubricated contact.

The lowest friction coefficient values obtained with these well-developed nanofiber webs are very similar to those found with castor oil, which supports the idea that a steady oil release is the main mechanism governing the anti-friction properties of these bio-based greases. Moreover, it was hypothesized that nanofibers are able to better penetrate into the tribological contact much more easily than lignin particles or beaded fibers and thus better prevent wear.

Finally, friction and wear generally increased with thickener concentration, especially at the higher normal loads applied, which must be attributed to a decrease in both the oil release and the contact replenishment capacity as a consequence of the increased viscosity.

Supplementary Materials: The following supporting information can be downloaded at: https://www.mdpi.com/article/10.3390/nano13212852/s1. Figure S1: Viscosity vs. shear rate plots for lubricating greases thickened with (a) 70:30 LSL/EC and (b) 70:30 LSL/PVP electrospun nanostructures at different concentrations (10%, 20% and 30% wt.); Figure S2: Viscosity vs. shear rate plots for lubricating greases thickened with LSL/EC electrospun nanostructures differing in the LSL:EC weight ratio (thickener concentration 20% wt.); Table S1: Values of the Sisko model parameters obtained from fitting the viscous flow curves of greases thickened with electrospun nanostructures to Equation (1); Table S2: Friction coefficient values obtained using castor oil as the lubricant; Table S3: Oil separation after centrifugation for selected greases thickened with different electrospun LSL:EC nanostructures; Figure S3: Values of the friction coefficient obtained with lubricating greases thickened with LSL/PVP electrospun nanostructures with different LSL:PVP ratios (10% nanofiber concentration).

Author Contributions: M.B.: conceptualization, methodology, investigation, formal analysis and data curation. E.K.: conceptualization, methodology, investigation, validation, resources and supervision. J.E.M.-A.: conceptualization, methodology, investigation, validation and supervision. J.M.F.: conceptualization, methodology, investigation, validation, resources, funding acquisition, supervision and writing. All authors have read and agreed to the published version of the manuscript.

Funding: This work is part of a research project (PID2021-125637OB-I00) funded by MCIN/AEI/10.13039/501100011033 and by "ERDF A way of making Europe" (EU). The financial support is gratefully acknowledged.

Data Availability Statement: The data presented in this study are available upon request from the corresponding author.

Conflicts of Interest: The authors declare no conflict of interest.

References

1. Fan, X.; Li, W.; Li, H.; Zhu, M.; Xia, Y.; Wang, J. Probing the effect of thickener on tribological properties of lubricating greases. *Tribol. Int.* **2018**, *118*, 128–139. [CrossRef]
2. Lugt, P.M. A review on grease lubrication in rolling bearings. *Tribol. Trans.* **2009**, *52*, 470–480. [CrossRef]
3. Baart, P.; Lugt, P.M.; Prakash, B. Contaminant migration in the vicinity of a grease lubricated bearing seal contact. *J. Tribol.* **2011**, *133*, 41801. [CrossRef]
4. Lugt, P.M. *Grease Lubrication in Rolling Bearings*; John Wiley & Sons: Hoboken, NJ, USA, 2013.
5. Lugt, P.M. Modern advancements in lubricating grease technology. *Tribol. Int.* **2016**, *97*, 467–477. [CrossRef]
6. Lugt, P.M.; Velickov, S.; Tripp, J.H. On the chaotic behavior of grease lubrication in rolling bearings. *Tribol. Trans.* **2009**, *52*, 581–590. [CrossRef]
7. Cen, H.; Lugt, P.M. Film thickness in a grease lubricated ball bearing. *Tribol. Int.* **2019**, *134*, 26–35. [CrossRef]
8. Cousseau, T.; Björling, M.; Graça, B.; Campos, A.; Seabra, J.; Larsson, R. Film thickness in a ball-on-disc contact lubricated with greases, bleed oils and base oils. *Tribol. Int.* **2012**, *53*, 53–60. [CrossRef]
9. Saatchi, A.; Shiller, P.J.; Eghtesadi, S.A.; Liu, T.; Doll, G.L. A fundamental study of oil release mechanism in soap and non-soap thickened greases. *Tribol. Int.* **2017**, *110*, 333–340. [CrossRef]
10. Cen, H.; Lugt, P.M. Replenishment of the EHL contacts in a grease lubricated ball bearing. *Tribol. Int.* **2020**, *146*, 106064. [CrossRef]
11. Scarlett, N. Use of grease in rolling bearings. *Proc. Inst. Mech. Eng. Part A* **1967**, *182*, 585–593.
12. Baart, P.; van der Vorst, B.; Lugt, P.M.; van Ostayen, R.A.J. Oil-bleeding model for lubricating grease based on viscous flow through a porous microstructure. *Tribol. Trans.* **2010**, *53*, 340–348. [CrossRef]
13. Gonçalves, D.; Graça, B.; Campos, A.V.; Seabra, J.; Leckner, J.; Westbroek, R. On the film thickness behaviour of polymer greases at low and high speeds. *Tribol. Int.* **2015**, *90*, 435–444. [CrossRef]
14. Cen, H.; Lugt, P.M.; Morales-Espejel, G. On the film thickness of grease-lubricated contacts at low speeds. *Tribol. Trans.* **2014**, *57*, 668–678. [CrossRef]
15. Cousseau, T.; Graça, B.; Campos, A.V.; Seabra, J.H.O. Influence of grease rheology on thrust ball bearings friction torque. *Tribol. Int.* **2012**, *46*, 106–113. [CrossRef]
16. Couronné, I.; Vergne, P.; Mazuyer, D.; Truong-Dinh, N.; Girodin, D. Nature and properties of the lubricating phase in grease lubricated contact. *Tribol. Trans.* **2003**, *46*, 37–43. [CrossRef]
17. Cyriac, F.; Lugt, P.M.; Bosman, R.; Padberg, C.J.; Venner, C.H. Effect of thickener particle geometry and concentration on the grease EHL film thickness at medium speeds. *Tribol. Lett.* **2016**, *61*, 18. [CrossRef]
18. Rezasoltani, A.; Khonsari, M.M. Mechanical degradation of lubricating grease in an EHL line contact. *Tribol. Int.* **2017**, *109*, 541–551. [CrossRef]
19. Zhou, Y.; Bosman, R.; Lugt, P.M. A model for shear degradation of lithium soap grease at ambient temperature. *Tribol. Trans.* **2018**, *61*, 61–70. [CrossRef]
20. Zhou, Y.; Bosman, R.; Lugt, P.M. An Experimental Study on Film Thickness in a Rolling Bearing for Fresh and Mechanically Aged Lubricating Greases. *Tribol. Trans.* **2019**, *62*, 557–566. [CrossRef]
21. Roman, C.; Valencia, C.; Franco, J.M. AFM and SEM assessment of lubricating grease microstructures: Influence of sample preparation protocol, frictional working conditions and composition. *Tribol. Lett.* **2016**, *63*, 20. [CrossRef]
22. Paszkowski, M.; Olsztynska-Janus, S. Grease thixotropy: Evaluation of grease microstructure change due to shear and relaxation. *Ind. Lubric. Tribol.* **2014**, *66*, 223–237. [CrossRef]
23. Panchal, T.M.; Patel, A.; Chauhan, D.D.; Thomas, M.; Patel, J.V. A methodological review on bio-lubricants from vegetable oil based resources. *Renew Sust. Energ. Rev.* **2017**, *70*, 65–70. [CrossRef]
24. Syahir, A.Z.; Zulkifli, N.W.M.; Masjuki, H.H.; Kalam, M.A.; Alabdulkarem, A.; Gulzar, M.; Khuong, L.S.; Harith, M.H. A review on bio-based lubricants and their applications. *J. Clean. Prod.* **2017**, *168*, 997–1016. [CrossRef]
25. Singh, Y.; Farooq, A.; Raza, A.; Mahmood, M.A.; Jain, S. Sustainability of a non-edible vegetable oil based bio-lubricant for automotive applications: A review. *Process Saf. Env. Prot.* **2017**, *111*, 701–713. [CrossRef]
26. Zainal, N.A.; Zulkifli, N.W.M.; Gulzar, M.; Masjuki, H.H. A review on the chemistry, production, and technological potential of bio-based lubricant. *Renew Sust. Energ. Rev.* **2018**, *82*, 80–102. [CrossRef]
27. Kumar Kurre, S.; Yadav, J. A review on bio-based feedstock, synthesis, and chemical modification to enhance tribological properties of biolubricants. *Ind. Crops Prod.* **2023**, *193*, 116122. [CrossRef]
28. Adhvaryu, A.; Sung, C.; Erhan, S.Z. Fatty acids and antioxidant effects on grease microstructures. *Ind. Crops Prod.* **2005**, *21*, 285–291. [CrossRef]
29. Thampi, A.D.; Alokkan, D.; Biju, G.; Sasidharan, B.; Rani, S. Influence of grease formulation parameters on the tribological property of rice bran oil based lubricating grease. *J. Am. Oil Chem. Soc.* **2021**, *98*, 769–778. [CrossRef]
30. Davidovich-Pinhas, M.; Barbut, S.; Marangoni, A.G. The gelation of oil using ethyl cellulose. *Carbohydr. Polym.* **2015**, *117*, 869–878. [CrossRef]
31. Martín-Alfonso, J.E.; Núñez, N.; Valencia, C.; Franco, J.M.; Díaz, M.J. Formulation of new biodegradable lubricating greases using ethylated cellulose pulp as thickener agent. *J. Ind. Eng. Chem.* **2011**, *17*, 818–823. [CrossRef]
32. Sánchez, R.; Alonso, G.; Valencia, C.; Franco, J.M. Rheological and TGA study of acylated chitosan gel-like dispersions in castor oil: Influence of acyl substituent and acylation protocol. *Chem. Eng. Res. Des.* **2015**, *100*, 170–178. [CrossRef]

33. Gallego, R.; Arteaga, J.F.; Valencia, C.; Díaz, M.J.; Franco, J.M. Gel-like dispersions of HMDI-cross-linked lignocellulosic materials in castor oil: Toward completely renewable lubricating grease formulations. *ACS Sustain. Chem. Eng.* **2015**, *3*, 2130–2141. [CrossRef]
34. Cortes-Triviño, E.; Valencia, C.; Delgado, M.A.; Franco, J.M. Thermo-rheological and tribological properties of novel biolubricating greases thickened with epoxidized lignocellulosic materials. *J. Ind. Eng. Chem.* **2019**, *80*, 626–632. [CrossRef]
35. Borrego, M.; Martín-Alfonso, J.E.; Sánchez, M.C.; Valencia, C.; Franco, J.M. Electrospun lignin-PVP nanofibers and their ability for structuring oil. *Int. J. Biol. Macromol.* **2021**, *180*, 212–221. [CrossRef] [PubMed]
36. Rubio-Valle, J.F.; Valencia, C.; Sánchez, M.C.; Martín-Alfonso, J.E.; Franco, J.M. Oil structuring properties of electrospun Kraft lignin/cellulose acetate nanofibers for lubricating applications: Influence of lignin source and lignin/cellulose acetate ratio. *Cellulose* **2023**, *30*, 1553–1566. [CrossRef]
37. Borrero-López, A.M.; Valencia, C.; Ibarra, D.; Ballesteros, I.; Franco, J.M. Lignin-enriched residues from bioethanol production: Chemical characterization, isocyanate functionalization and oil structuring properties. *Int. J. Biol. Macromol.* **2022**, *195*, 412–423. [CrossRef]
38. Dallmeyer, I.; Ko, F.; Kadla, J.F. Electrospinning of technical lignins for the production of fibrous network. *J. Wood Chem. Technol.* **2010**, *30*, 315–329. [CrossRef]
39. Dallmeyer, I.; Ko, F.; Kadla, J.F. Correlation of elongational fluid properties to fiber diameter in electrospinning of softwood kraft lignin solutions. *Ind. Eng. Chem. Res.* **2014**, *53*, 2697–2705. [CrossRef]
40. Oliveira, M.S.N.; Yeh, R.; McKinley, G.H. Iterated stretching, extensional rheology and formation of beads-on-a-string structures in polymer solutions. *J. Non-Newton. Fluid Mech.* **2006**, *137*, 137–148. [CrossRef]
41. Aslanzadeh, S.; Ahvazi, B.; Boluk, Y.; Ayranci, C. Morphologies of electrospun fibers of lignin in poly(ethylene oxide)/N.,N dimethylformamide. *J. Appl. Polym. Sci.* **2016**, *133*, 44172. [CrossRef]
42. Fiedler, M.; Kuhn, E.; Franco, J.M.; Litters, T. Tribological properties of greases based on biogenic base oils and traditional thickeners in sapphire-steel contact. *Tribol. Lett.* **2011**, *44*, 293–304. [CrossRef]
43. Gonçalves, D.; Pinho, S.; Graça, B.; Campos, A.V.; Seabra, J. Friction torque in thrust ball bearings lubricated with polymer greases of different thickener content. *Tribol. Int.* **2016**, *96*, 87–96. [CrossRef]
44. Gonçalves, D.; Graça, B.; Campos, A.V.; Seabra, J. On the friction behaviour of polymer greases. *Tribol. Int.* **2016**, *93*, 399–410. [CrossRef]
45. Nikas, G.K. An advanced model to study the possible thermomechanical damage of lubricated sliding–rolling line contacts from soft particles. *J. Tribol.* **2001**, *123*, 828–841. [CrossRef]
46. Delgado, M.A.; Cortes-Triviño, E.; Valencia, C.; Franco, J.M. Tribological study of epoxide-functionalized alkali lignin-based gel-like biogreases. *Tribol. Int.* **2020**, *146*, 106231. [CrossRef]
47. Martín-Alfonso, J.E.; Martín-Alfonso, M.J.; Valencia, C.; Cuberes, M.T. Rheological and tribological approaches as a tool for the development of sustainable lubricating greases based on nano-montmorillonite and castor oil. *Friction* **2021**, *9*, 415–428. [CrossRef]
48. Gorbacheva, S.N.; Yadykova, A.Y.; Ilyin, S.O. Rheological and tribological properties of low-temperature greases based on cellulose acetate butyrate gel. *Carbohydr. Polym.* **2021**, *272*, 118509. [CrossRef]
49. Ilyin, S.O.; Gorbacheva, S.N.; Yadykova, A.Y. Rheology and tribology of nanocellulose-based biodegradable greases: Wear and friction protection mechanisms of cellulose microfibrils. *Tribol. Int.* **2023**, *178*, 108080. [CrossRef]

Chapter 5: Conclusions

Conclusions

This section collects the main conclusions derived from the experimental results:

1. Low-sulfonate lignin in combination with PVP or ethyl cellulose produce uniform nanofibers mats or beaded nanofibers (BOAS) via electrospinning with ability for structuring castor oil.
2. Controlling the rheological and physicochemical properties of the spinning solutions is essential for tailoring the morphology of electrospun mats. Solutions with low polymer concentrations and/or high lignin proportion generally exhibit Newtonian behaviour and poor extensional properties, yielding heterogeneous membranes typically composed of particles or beaded thin fibers (BOAS). On the contrary uniform and homogenous nanofiber mats were achieved from solutions with high polymer concentrations and/or lower lignin:co-spinning polymer ratios.
3. The addition of low concentrations of surfactants improved the electrospinnability and leads to a reduction in both the number of beads and fiber diameter, provided that the critical aggregation concentration is exceeded. These fibers produce stable oleogels that reduce friction and wear values compared to the surfactant-free counterparts.
4. Electrospun ethyl cellulose solutions generally produced well-developed nanofiber mats with excellent oil structuring ability when the solution concentration is higher than 2.5 times the critical entanglement concentration. An increase in ethyl cellulose molecular weight improves the electrospinnability, reducing this critical concentration. Derived oleogels obtained upon dispersion of ethyl cellulose nanofibers exhibit good thermal reversibility, better than those oleogels prepared by the traditional thermal gelling process.

5. Solvents with higher dielectric constants lead to higher repulsive forces, resulting in enhanced jet stretching and higher electrostatic forces, thus decreasing the average diameter of nanofibers.
6. The morphology of electrospun nanostructures plays a crucial role in structuring castor oil and stabilizing the gel-like dispersions. Homogeneous and defect-free nanofibers impart and enhanced gel-like behaviour, whereas BOAS nanostructures generally provide liquid-like or softer viscoelastic responses.
7. The viscoelastic properties of electrospun lignin-derived oleogels can be modulated by modifying the spinning solution concentration, the lignin:co-spinning polymer ratio and the concentration of the nanostructures in castor oil.
8. In terms of tribological performance, friction and wear are reduced by dispersing homogeneous nanofibers in castor oil, rather than nanostructures composed of microspheres or beaded nanofibers. PVP as co-spinning polymer provides a higher reduction of both friction and wear than ethyl cellulose, despite ethyl cellulose also performs well as co-spinning polymer of lignin.
9. In general, friction and wear decrease with increasing nanofiber diameter, and reducing the number of beads and porosity. It is hypothesized that nanofibers are able to penetrate better into the tribological contact being much less abrasive than lignin particles or beaded fibers.
10. Overall, electrospun nanofibers developed from lignin in combination with another polymer possess oil structuring capabilities, giving rise to gel-like oleo-dispersions with suitable rheological and tribological properties which allows to propose them as potential bio-based lubricating greases.

Conclusiones

En esta sección se recoge las principales conclusiones derivadas de los resultados experimentales:

1. La lignina de bajo sulfonato en combinación con PVP o etilcelulosa produce nanofibras uniformes o nanofibras con partículas (BOAS) mediante electrospinning con capacidad para estructurar el aceite de ricino.
2. El control de las propiedades reológicas y fisicoquímicas de las disoluciones de electrohilado es esencial para adecuar la morfología de las membranas resultantes. Las disoluciones con bajas concentraciones de polímero y/o alta proporción de lignina presentan generalmente un comportamiento Newtoniano y escasas propiedades extensionales, dando lugar a membranas heterogéneas compuestas generalmente por partículas o fibras finas en forma BOAS. Por el contrario, se obtuvieron membranas de nanofibras uniformes y homogéneas a partir de disoluciones con altas concentraciones de polímero y/o menores proporciones de lignina:polímero de cohilado.
3. La adición de bajas concentraciones de tensioactivos mejora la electrospinnabilidad y conduce a una reducción tanto del número de microesferas como del diámetro de las fibras, siempre que se supere la concentración crítica de agregación. Estas fibras producen oleogeles estables que reducen los valores de fricción y desgaste en comparación con sus homólogas sin tensioactivos.
4. Las disoluciones de etilcelulosa electrohiladas produjeron, en general, membranas de nanofibras bien desarrolladas con una excelente capacidad de estructuración del aceite cuando la concentración de la disolución es superior a 2,5 veces la concentración crítica de entrelazamiento. Un aumento del peso molecular de la

etilcelulosa mejora la electrospinabilidad, reduciendo esta concentración crítica. Los oleogeles derivados obtenidos a partir de la dispersión de nanofibras de etilcelulosa presentan una buena reversibilidad térmica, mejor que los oleogeles preparados mediante el proceso tradicional de gelificación térmica.

5. Los disolventes con constantes dieléctricas más altas dan lugar a fuerzas repulsivas más altas, lo que provoca un mayor estiramiento del jet de electrohilado, disminuyendo así el diámetro medio de las nanofibras.
6. La morfología de las nanoestructuras electrohiladas desempeña un papel crucial en la estructuración del aceite de ricino y en la estabilización de las dispersiones tipo gel. Las nanofibras homogéneas y sin defectos confieren y mejoran el comportamiento de gel, mientras que las nanoestructuras tipo BOAS generalmente proporcionan respuestas de líquido viscoelástico o del gel débil.
7. .Las propiedades viscoelásticas de los oleogeles derivados de la lignina electrohilada pueden modularse modificando la concentración de la disolución de electrohilado, la relación lignina:polímero de cohilado y la concentración de las nanoestructuras en el aceite de ricino.
8. En términos de rendimiento tribológico, la fricción y el desgaste se reducen dispersando nanofibras homogéneas en aceite de ricino, en lugar de nanoestructuras compuestas de microesferas o BOAS. El PVP como polímero de cohilado proporciona una mayor reducción tanto de la fricción como del desgaste que la etilcelulosa, a pesar de que la etilcelulosa también funciona bien como polímero de cohilado de la lignina.
9. En general, la fricción y el desgaste disminuyen al aumentar el diámetro de la nanofibra y reducir el número de microesferas y la porosidad. Se sostiene la

hipótesis de que las nanofibras son capaces de penetrar mejor en el contacto tribológico siendo mucho menos abrasivas que las partículas de lignina o las fibras con partículas (BOAS).

10. En definitiva, las nanofibras electrohiladas desarrolladas a partir de lignina, en combinación con otro polímero, poseen capacidad de estructuración del aceite, dando lugar a oleo-dispersiones tipo gel con propiedades reológicas y tribológicas adecuadas que permiten proponerlas como potenciales grasas lubricantes de base biológica.

List of figures & tables

1. List of Figures

Chapter 2: State of the art

Figure 1. Chemical structure of cellulose 23

Figure 2. Main structural unit that form the hemicelluloses 24

Figure 3. Lignin constituent monomers a) coniferyl alcohol, b) sinapyl alcohol and c) p-coumaryl alcohol 25

Figure 4. Lignin structure 26

Figure 5. Schematic diagram of electrospinning equipment assembly 35

Figure 6. Nanofibers of polymeric material developed by electrospinning 36

Figure 7. SEM photographs nanofibers electrospun under different electrical potentials 37

Figure 8. Average fiber diameter vs applied voltage 38

Figure 9. SEM images of the electrospun nanofibers at various flow rates 39

Figure 10. Taylor Cone formation 39

Figure 11. Average diameter of nanofiber for different needle-tip-to-collector 40

Figure 12. SEM images of nanofiber morphology depending on viscosity 41

Figure 13. a) Traditional horizontal layout of the technique b) vertical layout of the technique 42

Figure 14. Coaxial electrospinning system 43

Figure 15. Traditional layout of the forcespinning method 44

Figure 16. Mechanism of the fiber formation by means of forcespinning 45

Figure 17. AFM micrographs for selected commercial lubricating greases 52

Figure 18. Thermorgheological behaviour of commercial fats 56

Figure 19. Coefficients of friction of functionalized greases 56

Figure 20. Evolution of SAOS functions with frequency for chitin-based oleogel formulations, at 25ºC 58

Figure 21. Shear-thinning behaviour in lubricating greases a) effect of thickener concentration b) effect of oil viscosity 59

Figure 22. Frequency dependence of the storage (G') and loss (G'') moduli of selected lubricating greases samples 60

Figure 23. Schematic of a tribological system 61

Figure 24. Mechanical properties of a tribological system 61

Figure 25. Stribeck curve of a lubricated contact 62

Chapter 3: Materials and methods.

Figure 26. A structural model of a technical kraft lignin fragment 83

Figure 27. Structure of polyvinylpyrrolidone 84

Figure 28. Structure of ethylcellulose 84

Figure 29. SDS structure 85

Figure 30. CTAB structure 85

Figure 31. Tween-20 structure 86

Figure 32. Doxa Microfluids electrospinning equipment 89

Figure 33. Sigma 703D tensiometer 91

Figure 34. Controlled shear rate rheometer 91

Figure 35. CaBER rheometer 92

Figure 36. Rheoscope controlled strain rheometer (Thermo Haake) 93

Figure 37. ARES II controlled deformation rheometer 94

Figure 38. Schematic set-up tribology accessory in side and top views. Torque and normal force applied by the rheometer are indicated by arrows 94

Figure 39. Interferometer Zygo neoview 95

Figure 40. Olympus Bx51 Optical microscope 96

Figure 41. CSM nanotribometer 97

Figure 42. Scanning Electron Microscope JSM-5410 97

Figure 43. Thermogravimetric balance TGA model Q50 98

2. List of Tables

Chapter 2: State of the art

Table 1. Chemical components of lignocellulosic materials 22

Table 2. Commercial lignin types according to origin 27

Table 3. Common organic solvents of commercial lignins 28

Table 4. Commercial lignin eutectic solvents 30

Table 5. Polymer nanofiber processing techniques 32

Table 6. Advantages and disadvantages of nanofibers processing techniques 33

Table 7. Studies on the processing of biopolymers and biocompatible polymers using electrohydrodynamic techniques, including solvents and range of solution concentration 50

Table 8. Electrospun lignin together with their copolymer 51

Table 9. Typical composition of traditional lubricants 53

Table 10. Composition of biodegradable lubricating greases 54

Table 11. Results of thermogravimetric analysis of biodegradable lubricating Greases 57

Table 12. Characteristic TGA parameters of the studied oleogel formulations based on isocyanate-functionalized chitin and chitosan 58

Chapter 3: Materials and methods

Table 13. Fatty acids compositions of castor oil 87

Table 14. Process parameters 88

ANNEX I

1. List of articles that make up this Doctoral Thesis

- M. Borrego; José E. Martín-Alfonso; M.Carmen Sánchez; Concepción Valencia; José M. Franco. Electrospun lignin-PVP nanofibers and their ability for structuring oil. International Journal of Biological Macromolecules 2021, 180, 212-221, https://doi.org/10.1016/j.ijbiomac.2021.03.069.
- M. Borrego; José E. Martín-Alfonso; M.Carmen Sánchez; Concepción Valencia; José M. Franco. Influence of surfactants on the electrospinability of lignin-PVP solutions and subsequent oil structuring properties of nanofibers mats. Polymer Bulletin 2023, 80, 6885-6904, https://doi.org/10.1007/s00289-022-04382-0.
- M. Borrego; José E. Martín-Alfonso; M.Carmen Sánchez; Concepción Valencia; José M. Franco. Developing electrospun ethylcellulose nanofibrous webs: an alternative approach for structuring castor oil. ACS Applied Polymer Materials 2022, 4, 7217-7227. https://doi.org/10.1021/acsapm.2c01090.
- M. Borrego; José E. Martín-Alfonso; M.Carmen Sánchez; Concepción Valencia; José M. Franco. Impact of the morphology of electrospun lignin/Ethylcellulose nanostructures on their capacity to thicken Castor Oil. Polymers 2022, 14, 4741, https://doi.org/10.3390/polym14214741.
- M. Borrego; Erik Kuhn; José E. Martín-Alfonso; José M. Franco. Assessment of the tribological performance of electrospun lignin nanofibrous web-thickened bio-based greases in a nanotribometer. Nanomaterials 2023, 13, 2852, https://doi.org/10.3390/nano13212852.

2. Contributions to congresses and conferences derived from this Doctoral Thesis..

- Title of the contributions: Impact of lignin-solvent interactions on the performance on electrohydrodynamic techniques.

  Type of contribution: Poster

  Congress: Engineering, Environment and Materials in process industry.

  City: Bosnia and Herzegovina

  Opening date: 17/03/2021

  Closing date: 19/03/2021

  Authors: María Borrego Algarra; José María Franco Gómez, José Enrique Martín Alfonso, Concepción Valencia Barragán, María del Carmen Sánchez.

- Title of the contributions: Development of lignin-PVP micro-and nano-structures by electrospinning and their thickening capacity in oil media.

  Type of contribution: Poster

  Congress:International conference on Minerals, Metallurgy and Materials.

  Opening date: 22/03/2021

  Closing date: 23/03/2021

  Authors: María Borrego Algarra; José María Franco Gómez, José Enrique Martín Alfonso, Concepción Valencia Barragán, María del Carmen Sánchez.

- Title of the contributions: Rheology-electrospinning relationship of nanofibers based on ethylcellulose and the role of solvents and molecular weight.

  Type of contribution: Poster

  Congress:Annual European Rheology Conference.

  City: Seville.

Opening date: 26/04/2022

Closing date: 28/04/2022

Authors: María Borrego Algarra; José María Franco Gómez, José Enrique Martín Alfonso, Concepción Valencia Barragán, María del Carmen Sánchez.

- Title of the contributions: Oil structuring properties of electrospn lignin-PVP nanofiber mats: Influence of surfactant addition to the electrospun solution

  Congress:XXXVIII Reunión Bienal de la Sociedad Española de Química.

  Type of contribution: Poster

  City: Granada.

  Opening date: 27/06/2022

  Closing date: 30/04/2022

  Authors: María Borrego Algarra; José María Franco Gómez, José Enrique Martín Alfonso, Concepción Valencia Barragán, María del Carmen Sánchez.

- Title of the contributions: Tribological behaviour of biolubricantes based on nanofibers developed by electrospinning.

  Type of contribution: Oral Presentation.

  Congress: 17th Arnold Tross Colloquium.

  City: Granada.

  Opening date: 10/06/2022

  Closing date: 10/06/2022

  Authors: María Borrego Algarra; José María Franco Gómez, José Enrique Martín Alfonso.